

# Long-term evolutionary dynamics on graphs

*Space voyages exploring new stars*

Dissertation in fulfillment of the requirements for the degree  
*Doctor rerum naturalium*  
of the Faculty of Mathematics and Natural Sciences  
at the Christian-Albrechts University of Kiel

Submitted by

Nikhil Sharma

Department of Theoretical Biology,  
Max Planck Institute for Evolutionary Biology, Plön.

Kiel, 2023

**First examiner:** Prof. Dr. Arne Traulsen,  
Department of Theoretical Biology,  
MPI for Evolutionary Biology, Plön, Germany.

**Second examiner:** Prof. Dr. Sören Christensen,  
Department of Mathematics,  
CAU, Kiel, Germany.

**Additional examiner:** Prof. Dr. Tal Dagan,  
Institute for General Microbiology,  
CAU, Kiel, Germany.

**Chairperson:** Prof. Dr. Regina Scherließ,  
Department of Pharmaceutics and Biopharmaceutics,  
CAU, Kiel, Germany.

**Date of defense:** 12.12.2023

*Dedicated to family and friends*

# Abstract

Evolutionary dynamics in well-mixed populations have been studied quite extensively. While the respective studies provide a good starting point for a mathematical analysis, populations in the wild are rarely well-mixed. Natural populations often come with spatial structures, resulting in dynamics different from the well-mixed case. Therefore, it is crucial to understand evolution on spatial structures. To this end, we use the framework of evolutionary graph theory, where nodes represent asexually reproducing entities, and links define the neighborhood of nodes.

First, we develop a model to study population structures adapting to a single-peaked fitness landscape. The mutation rates are considered very low, making the mutation-selection dynamics sequential. Surprisingly, a structure with a poor ability to fix beneficial mutants outcompetes the well-mixed population in the long run by achieving higher fitness. This result is explained by the structure's ability to reject disadvantageous mutants more efficiently. Subsequently, we discovered that this phenomenon occurs in the majority of randomly generated spatial structures. Consequently, it is not only the beneficial mutant regime that is relevant for adaptive evolution, but the deleterious mutant regime is equally important.

Birth-death models are frequently employed to understand the interplay of natural selection and genetic drift in evolving populations. While it is known that the so-called Birth-death and death-Birth updating leads to different evolutionary outcomes on spatial structures, the choice of individual moving to vacant sites also considerably affect the dynamics. We observed that allowing parent individuals to replace dead individuals yields substantially different results as compared to the default choice of offspring replacing the dead individuals. This observation led to the identification of a new class of graphs, namely amplifiers of fixation, where a structure exhibits a higher probability of fixation than the complete graph, regardless of the mutant's



fitness. Notably, one of the example graphs has a non-zero probability of fixation for deleterious mutants, even when the population size tends to infinity. This finding contradicts the intuition from the previous studies on structured and well-mixed populations, where the probability of fixation for deleterious mutants diminishes for large population sizes.

Furthermore, another category of graphs, known as amplifiers of selection, generally exhibits a longer fixation time than the complete graph, making them more restrictive to the weak mutation approximation. Upon examining high mutation rate dynamics, we observed that the self-looped amplifiers of selection, which achieve higher fitness in the low mutation rate regime, actually attain lower fitness than the well-mixed population and suppressors of selection. This suggests that amplifiers of selection may not be a reliable choice for structures adapting better than the well-mixed population.

Finally, to experimentally validate our results obtained from the one-node-one-individual framework, a theoretical extension to structured metapopulations is required. We provide a mapping between the network of individuals and the network of demes that can be utilised to transfer the one-node-one-individual results to the metapopulation level.

# Kurzfassung

Evolutionäre Dynamiken in gut durchmischten Populationen wurden intensiv erforscht. Während die entsprechenden Studien ein guter Ausgangspunkt sind, sind reale Populationen selten gut durchmischt. Natürliche Populationen sind oft räumlich strukturiert, was zu einer Dynamik führt, die sich von dem gut durchmischten Fall unterscheidet. Daher ist es entscheidend, die Evolution in räumlichen Strukturen zu verstehen. Zu diesem Zweck verwenden wir Modelle der evolutionären Graphentheorie, wobei Knoten asexuell reproduzierende Einheiten darstellen und Kanten die Nachbarschaft der Knoten definieren.

Zunächst entwickeln wir ein Modell, um Populationen zu studieren, die sich an eine Fitnesslandschaft mit einem eindeutigen Maximum anpassen. Die Mutationsraten werden als sehr niedrig angenommen, wodurch die Mutations-Selektions-Dynamik sequenziell wird. Überraschenderweise übertrifft eine Struktur mit geringer Fähigkeit, vorteilhafte Mutanten zu fördern, langfristig die gut durchmischte Population durch Erreichen einer höheren Fitness. Dieses Ergebnis wird durch die Fähigkeit der Struktur erklärt, nachteilige Mutanten effizienter auszusortieren. Später entdeckten wir, dass dieses Phänomen in der Mehrheit der zufällig generierten räumlichen Strukturen auftritt. Daher ist nicht nur das Regime der vorteilhaften Mutanten für die adaptive Evolution relevant, sondern das Regime der schädlichen Mutanten ist ebenso wichtig.

Modelle von Geburts- und Todesprozessen werden häufig verwendet, um das Zusammenspiel von natürlicher Selektion und genetischem Drift in sich entwickelnden Populationen zu verstehen. Während bekannt ist, dass eine unterschiedliche Reihenfolge von Geburts- und Todesereignissen zu verschiedenen evolutionären Ergebnissen in räumlichen Strukturen führt, beeinflusst die Wahl des Individuums, welches an freie Standorte zieht, die Dynamik ebenfalls erheblich. Wir haben festgestellt, dass es deutlich unterschiedliche

Ergebnisse liefert, wenn Elternindividuen tote Individuen ersetzen, im Vergleich zu dem Fall, in dem Nachkommen die toten Individuen ersetzen. Diese Beobachtung führte zur Identifizierung einer neuen Klasse von Graphen, nämlich Verstärkern der Fixierung. Ein solcher Graph weist eine höhere Wahrscheinlichkeit der Fixierung auf als der vollständige Graph, unabhängig von der Fitness des Mutanten. Bemerkenswerterweise hat einer der Beispielpergraphen eine strikt positive Wahrscheinlichkeit der Fixierung für schädliche Mutanten, selbst wenn die Populationsgröße gegen unendlich geht. Dieses Erkenntnis widerspricht der Annahme, die typischerweise in gut durchmischten Studien gemacht wird, wo die Wahrscheinlichkeit der Fixierung für schädliche Mutanten für große Populationsgrößen abnimmt.

Des Weiteren weist eine andere Kategorie von Graphen, bekannt als Verstärker der Selektion, im Allgemeinen eine längere Fixierungszeit als der vollständige Graph auf. Für diese Graphen ist die Annahme schwacher Mutationen noch restriktiver. Bei der Untersuchung der Dynamik bei hohen Mutationsraten stellten wir fest, dass die Verstärker der Selektion mit Schlingen, die im Regime mit niedriger Mutationsrate einen höheren Fitnessgrad erreichen, tatsächlich einen niedrigeren Fitnessgrad als die gut durchmischte Population und Unterdrücker der Selektion erreichen. Dies legt nahe, dass Verstärker der Selektion möglicherweise keine zuverlässige Wahl für bessere Anpassung sind.

Abschließend ist zur experimentellen Validierung unserer aus dem Ein-Individuum-Ein-Knoten-Modell gewonnenen Ergebnisse eine theoretische Erweiterung auf strukturierte Metapopulationen erforderlich. Wir stellen eine Zuordnung zwischen Netzwerken von Individuen und Netzwerken von Populationen her, die dazu genutzt werden kann, die Ergebnisse des Ein-Individuum-Ein-Knoten-Modells auf die Metapopulationsebene zu übertragen.

# Contents

<b>Abstract</b>	<b>1</b>
<b>Kurzfassung</b>	<b>3</b>
<b>1 Introduction</b>	<b>7</b>
<b>2 Suppressors of fixation can increase fitness beyond amplifiers of selection</b>	<b>17</b>
<b>3 On the role of deleterious mutant regime in steering long-term evolution</b>	<b>29</b>
3.1 Introduction . . . . .	30
3.2 Update mechanisms in graph structured populations . . . . .	33
3.3 Short time scales: Fixation dynamics . . . . .	36
3.3.1 The star graph . . . . .	36
3.3.2 Random graphs . . . . .	40
3.4 Long time scales: Mutation-selection balance . . . . .	43
3.4.1 The star graph . . . . .	46
3.4.2 Random graphs . . . . .	50
3.5 Discussion . . . . .	52
3.5.1 Exact formula for the fixation probability of a mutant on the star graph under dB and Bd updating . . . . .	54
3.5.2 Matrix approach to compute fixation probability on a random graph . . . . .	57
3.5.3 Long-term evolution on regular graphs . . . . .	61
3.5.4 Reversibility . . . . .	64
3.5.5 Standard deviation in the steady-state fitness distribution . . . . .	66

3.5.6	Long-term evolution on discrete fitness space . . . . .	68
3.5.7	Criterion for a graph to have higher steady-state fitness than the complete graph . . . . .	69
3.5.8	Effects of deleterious mutants on the initial phase of the long-term dynamics . . . . .	73
3.5.9	Amplifier of fixation and suppressor of fixation in a metapopulation model . . . . .	75
<b>4</b>	<b>Self-loops: friends or foes?</b>	<b>78</b>
<b>5</b>	<b>Categorising update rules for network structured metapopulations</b>	<b>111</b>
<b>6</b>	<b>Discussion</b>	<b>129</b>
	<b>Author contributions</b>	<b>138</b>
	<b>Acknowledgements</b>	<b>139</b>
	<b>Declaration</b>	<b>141</b>
	<b>Bibliography</b>	<b>142</b>

# Chapter 1

## Introduction

Biological systems often exhibit spatial structures. Spatial structures are ubiquitous; ranging from cancer cells [1, 2, 3] to biofilms in bacteria [4, 5], colonic crypts in the intestine [6, 7] to seed dispersal in forest ecosystems [8], gene networks in a cell [9] to social networks and epidemics [10]. The presence of spatial structure can substantially influence the outcomes of eco-evolutionary dynamics. Therefore, it is crucial to have a toolbox for analysing spatial systems.

In this thesis, we explore the role of spatial structures in evolutionary dynamics. Early population genetics work typically assumes a well-mixed population [11]. However, some past studies have explored the role of spatial structures [12, 13, 14, 15, 16, 17]. These early investigations mainly focused on symmetric structures, which, compared to a well-mixed population, did not considerably impact the steady-state results. This is where evolutionary graph theory (EGT) comes into play, enabling the study of evolution on arbitrary spatial structures that need not be symmetric [18, 19]. EGT offers a versatile approach where a spatially structured population is represented by a graph, with nodes (vertices) representing asexually reproducing entities.

In EGT, nodes interact with their neighbors, and the neighborhood of a node is determined by the links (edges) connecting it to other nodes. These links can be directed and weighted, meaning that the weight of the link directed from node  $i$  to node  $j$  can differ from the link directed from node  $j$  to node  $i$  ( $w_{ij} \neq w_{ji}$ ). In the language of graph theory, a well-mixed population is represented by the complete graph, where each node is connected to every other node with links of equal propensity, see Fig. 1.1. The precise form of the interactions between a node and its neighbors is determined by an update

rule. As an example, we consider the Moran Birth-death (Bd) update rule [19, 20]. Under the Moran Bd updating, an individual at node  $i$  is selected to reproduce with a probability proportional to its fitness  $f_i$ . The population is assumed to be constant throughout the dynamics. Consequently, to maintain constant population size an individual dies. A random node  $j$  neighboring node  $i$  is chosen to die with a probability proportional to the weight of the link directed from node  $i$  to  $j$ . The offspring of the parent individual at node  $i$  then replaces the individual at node  $j$ , see Fig. 1.2 for illustration. The first letter of the shorthand Bd represents a birth event, whereas the second letter denotes a death event. The uppercase B signifies that natural selection operates in the birth event, while the lowercase d represents the neutral nature of the death event. In this way, a variety of Moran update rules exist based on the orderings of birth and death events and the events where selection operates [21, 22]— Bd, bd, bD, Db, dB, BD and DB.

Other frameworks also used to investigate spatial structures include reaction-diffusion systems [23], patch models [24, 25], and interacting particle systems [26]. Notably, different frameworks can yield qualitatively different results within a given parameter range. While the theories of reaction-diffusion systems and interacting particle systems primarily deal with regular structures, EGT takes a step forward by not only accounting for the discrete nature of individuals but also addressing non-regular structures.

The original formulation of EGT aims to study the interplay of natural selection and genetic drift in spatially structured populations. This is achieved by investigating the fixation probability of a mutant on graphs. In general, the fixation probability of a mutant depends on the node where it initially appears [27]. A mutant initialisation scheme, which is a probability distribution spanning all nodes of the graph, determines which nodes are more likely to receive an initial mutant. A common example is the uniform mutant initialisation ( $\mathcal{U}$ ) where every node is equally likely to be initialised with the mutant. Temperature initialisation ( $\mathcal{T}$ ) in another example where the initial mutant appear on a node  $i$  with probability proportional to node's temperature,  $\sum_j w_{ji}$  [28].

When a mutant emerges in a population, assuming the mutation rate to be very low, there are two possible outcomes for the mutant: either it takes over the entire population—mutant fixation—, or it goes extinct—mutant extinction [29], refer to Fig. 1.3 for illustration. The discrete nature of individuals makes the fixation dynamics a stochastic process. To elucidate the stochastic nature of fixation dynamics, we briefly sketch the derivation of

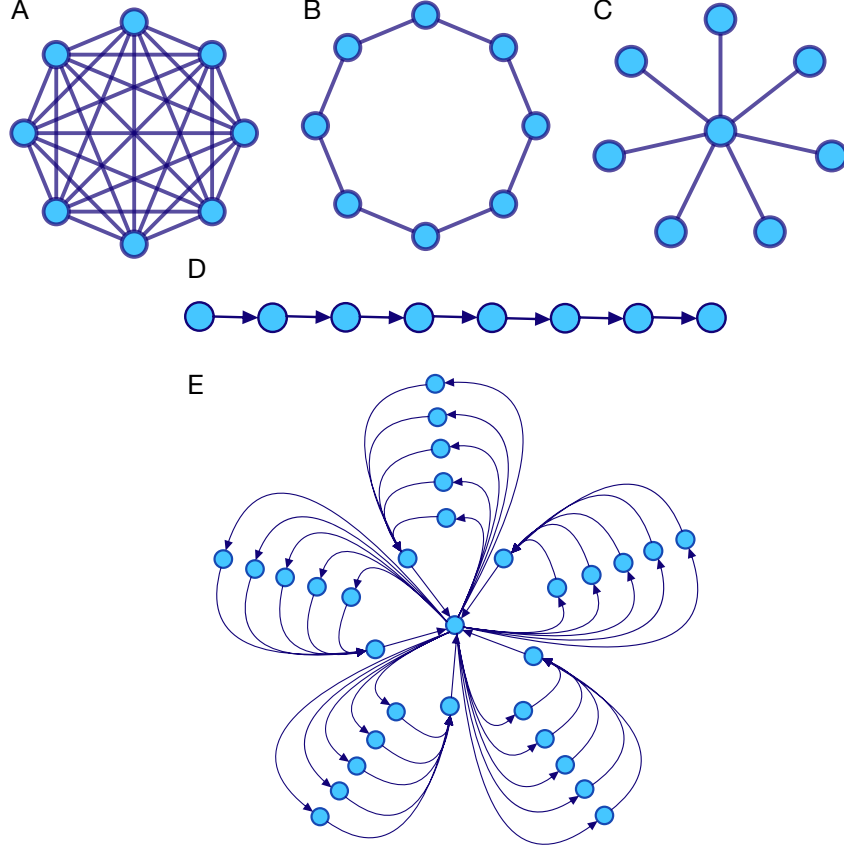


Figure 1.1: **Popular graphs in evolutionary graph theory.** A. The complete graph, AKA the well-mixed population, B. The cycle graph, C. The star graph, D. The directed line, and E. The superstar graph.

fixation probability for the complete graph. For a detailed description, refer to [19, 30]. The fixation probabilities for a population satisfy,

$$\begin{aligned} \Phi_i &= T_i^- \Phi_{i-1} + (1 - T_i^- - T_i^+) \Phi_i + T_i^+ \Phi_{i+1}, \quad \text{for } 1 \leq i \leq N, \\ \Phi_0 &= 0 \quad \text{and,} \quad \Phi_N = 1. \end{aligned} \quad (1.1)$$

Here  $\Phi_i$  is the probability that the mutant-type fix in the population when initialised with  $i$  copies.  $T_i^+$  is the probability of making a forward transition from the state with  $i$  mutants to the state with  $i + 1$  mutants, whereas  $T_i^-$  is the probability of making a backward transition from the state with  $i$  mutants to the state with  $i - 1$  mutants. Solving Eq. 1.1 for the fixation



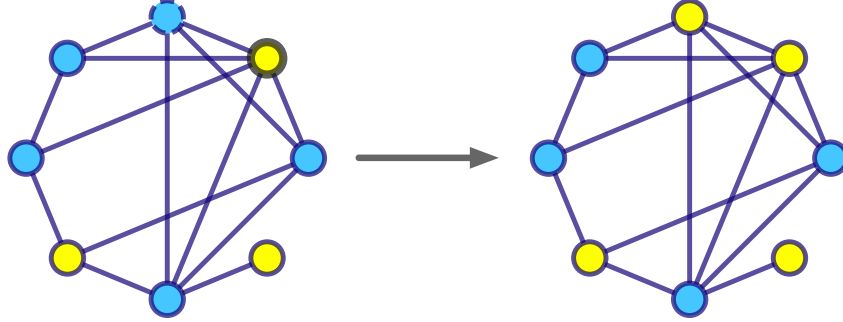


Figure 1.2: **Moran Birth-death updating.** An illustration of the Moran Birth-death (Bd) process is depicted here, showcasing a population composed of two types of individuals: yellow and blue, each with potentially distinct fitness values. The first step involves selecting an individual with the probability proportional to its fitness for reproduction. In the given illustration, it is a yellow individual encircled within a thick grey line. This is followed by the death of a randomly chosen neighbor, indicated by the blue individual encircled with a dashed line. The update process concludes when the yellow offspring replaces the blue individual chosen for replacement.

probability when started with a single mutant,  $\Phi_1$ , gives

$$\Phi_1 = \frac{1}{1 + \sum_{k=1}^{N-1} \prod_{j=1}^k \gamma_j}, \quad (1.2)$$

with  $\gamma_i = \frac{T_i^-}{T_i^+}$ .

For the well-mixed population, the fixation probability of a mutant given by Eq. 1.2 is exact. For the Moran Bd process on the complete graph, we have

$$T_i^+ = \frac{f' i}{f' i + f(N-i)} \cdot \frac{N-i}{N-1} \quad \text{and,} \quad T_i^- = \frac{f(N-i)}{f' i + f(N-i)} \cdot \frac{i}{N-1}, \quad (1.3)$$

with  $f'$  denoting the mutant's fitness and  $f$  denoting the wild-type fitness. The ratio of transition probabilities  $\gamma_i$  simplifies to,

$$\gamma_i = \frac{f}{f'} \quad \text{for } 1 \leq i \leq N-1. \quad (1.4)$$

Plugging this back into Eq. 1.2 gives us the fixation probability for the complete graph under Bd updating,

$$\Phi_C(f', f) = \frac{1 - \frac{f}{f'}}{1 - \left(\frac{f}{f'}\right)^N}. \quad (1.5)$$

Note that for the complete graph the fixation probability does not depend on the mutant initialisation scheme because of the symmetry of the graph. Using the definition of selection coefficient,  $s = \frac{f' - f}{f}$ , the formula in Eq. 1.5

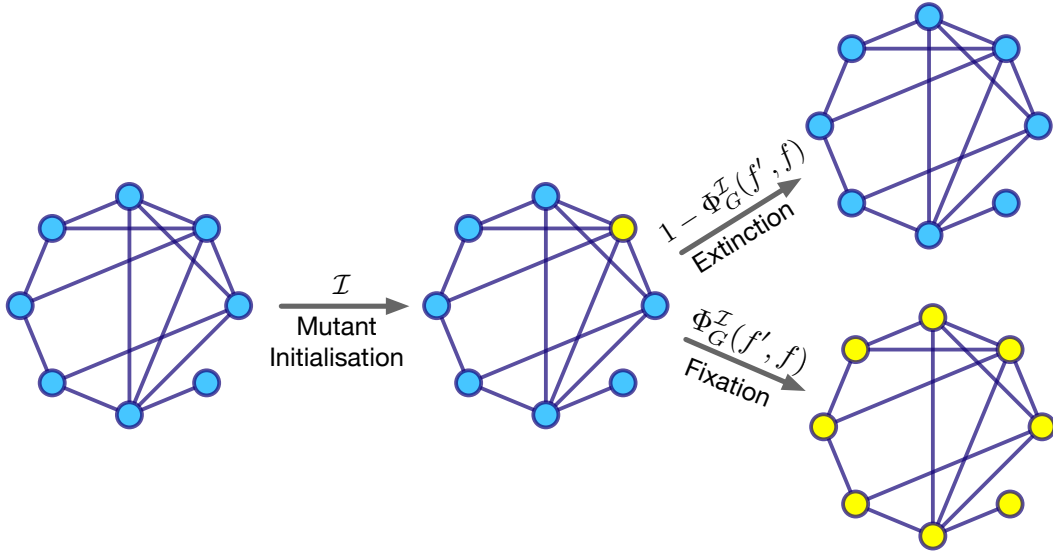


Figure 1.3: **Mutant initialisation and fixation.** In the process of fixation, first a mutant (shown in yellow) appears in homogenous population. Depending on the mutant initialisation  $\mathcal{I}$ , the initial mutant is more likely to appear on some nodes. After that, the mutant either fixes or gets extinct. Overall, the probability of fixation depends on the underlying spatial structure (the graph), the population size, the node where the initial mutant appears, the update rule, and the relative fitness of the mutant.

can be approximated by the fixation probability formula derived by Kimura

using diffusion approximation [31, 32],

$$\begin{aligned}
\Phi_C(f', f) &= \frac{1 - \frac{1}{1+s}}{1 - \left(\frac{1}{1+s}\right)^N}, \\
&\underset{s \ll 1}{\approx} \frac{1 - (1-s)}{1 - ((1-s))^N}, \\
&\approx \frac{1 - e^{-s}}{1 - e^{-sN}}.
\end{aligned} \tag{1.6}$$

In the first decade of EGT, the Moran Bd and dB updating with uniform mutant initialisation scheme was the most commonly investigated cases. Based on the fixation probability of mutants, three main categories of graphs emerged: amplifiers of selection, suppressors of selection and isothermal graphs.

- An amplifier of selection is a graph that has a higher probability of fixing advantageous mutants and a lower probability of fixing deleterious mutations than the complete graph. Mathematically, a graph  $G$  is an amplifier of selection if  $\Phi_G^{\mathcal{I}}(f', f) < \Phi_C(f', f)$  for  $f' < f$  and  $\Phi_G^{\mathcal{I}}(f', f) > \Phi_C(f', f)$  for  $f' > f$ .
- Conversely, a suppressor of selection is a graph with a lower probability of fixing advantageous mutants and a higher probability of fixing deleterious mutations compared to the complete graph. That is, a graph  $G$  is a suppressor of selection if  $\Phi_G^{\mathcal{I}}(f', f) > \Phi_C(f', f)$  for  $f' < f$  and  $\Phi_G^{\mathcal{I}}(f', f) < \Phi_C(f', f)$  for  $f' > f$ .
- An isothermal graph is a graph where all the nodes have equal in-temperature (sum of all the weights flowing into a node). Under Bd updating, an isothermal graph has the same fixation probability as the complete graph, that is,  $\Phi_G^{\mathcal{I}}(f', f) = \Phi_C(f', f)$  for all  $f'$ . An example of an isothermal graph is the cycle graph.

The star graph is a well-known example of an amplifier of selection under Bd updating with uniform initialisation. The fixation probability for the star

graph is [18],

$$\Phi_{\star}^{\mathcal{U}}(f', f) \approx \frac{1 - \left(\frac{f}{f'}\right)^2}{1 - \left(\frac{f}{f'}\right)^{2N}}. \quad (1.7)$$

For the star graph, the amplification factor is two. That is, the fixation probability of a mutant with relative fitness  $r$  on the star graph is the same as that of a mutant with relative fitness  $r^2$  in a well-mixed population. An amplifier of selection can also amplify selection strongly. A strong amplifier of selection ensures the fixation of a beneficial mutant with certainty, regardless of the relative fitness advantage. In other words, strong amplifiers have an amplification factor that tends to infinity. The superstar is a popular example of a strong amplifier [18, 33, 34, 35, 36], see Fig. 1.1. Conversely, a directed line is a suppressor of selection under Bd updating, with fixation probability equal to  $1/N$  regardless of the mutant's fitness.

But how common are the amplifiers and suppressors of selection? Hindersin and Traulsen [37] found that most small graphs are amplifiers of selection under Moran Bd updating and suppressors of selection under Moran dB updating with uniform initialisation. However, amplifiers of selection have gained more attention than other graph categories due to their ability to accelerate the pace of evolution. This phenomenon primarily holds true under very low mutation rates [38]. As mutation rates increase, the time to fixation also becomes an important factor. For higher mutation rates, both fixation probability and fixation time contribute in determining the rate of evolution [39]. Moreover, graphs amplifying selection tend to have higher fixation times [22] decreasing the effective rate of evolution [40]. Consequently, research efforts are devoted to identifying structures with a higher probability of fixing advantageous mutants, while maintaining marginally close fixation times to complete graphs [41].

While this thesis primarily focuses on constant selection, it is important to highlight the huge field of frequency-dependent selection on graphs [42, 43]. In frequency-dependent selection, an individual's fitness depends on the state of the population, and thus constantly changes with the population's composition. For games played on graphs, an individual's fitness is determined by its neighborhood. A quantity of interest for games of graphs is the evolution of cooperation [44, 45, 46]. The usual idea is to look for scenarios— combi-

nation of graphs, update rules, initialisation and games— where cooperation can be boosted. Additionally, a substantial body of research has explored the concept of mutation-selection balance on graphs focusing on conditions that lead to cooperation prevailing in equilibrium. Refer to the review by Nowak et al. [47] for more details and references.

Recently, Yagoobi et al. [48] explored mutation-selection balance on spatial graphs with mutations considered among two types of individuals. In this thesis, we investigate evolutionary dynamics on spatial structures adapting on a continuous fitness landscape. For this we primarily focus on the star-like graphs. There are two reasons for this choice. First, the exact analytical expressions for the fixation probability on the star graph are known [49, 50, 51]. Second, the star graph exhibits a high degree of variation in node degrees [52]. Therefore, if an evolutionary dynamics on the star graph do not considerably differ from the one on the complete graph, a random spatial structure is less likely to exhibit substantial differences. After studying evolution on the star graph, we extend our analysis to random graphs using numerical methods.

The star graph has a history with various combinations of update rules and mutant initialisations studied on it. The Moran Bd process with uniform initialisation was the first one to be investigated on the star graph [18]. Since then, the star graph is recognised as an example of an amplifier of selection [49, 51, 50]. However, the star graph fails to amplify selection if the initial mutant appears based on the temperature initialisation scheme, where the central node is more likely to receive the initial mutant [28]. Under temperature-initialised Bd updating, the star acts a suppressor of fixation, meaning it has a lower probability of fixing mutants regardless of their fitness value [53]. Similarly for uniform initialised dB updating, the star graph is a suppressor of selection [54]. In chapter three, we will see that the star graph is an amplifier of fixation— a graph with a higher probability of fixing mutants regardless of their fitness— under temperature initialised dB updating. Fig. 1.4 shows the fixation probability profiles corresponding to four main categories of graphs—amplifier of selection, suppressor of selection, amplifier of fixation and suppressor of fixation.

In the second chapter, we introduce a model for studying long-term evolutionary dynamics on spatial structures. Focusing on the low mutation rate regime, we observe that amplifiers of selection achieve higher fitness than well-mixed populations, while suppressors of selection achieve lower fitness, as expected. Surprisingly, suppressors of fixation— structures with a lower

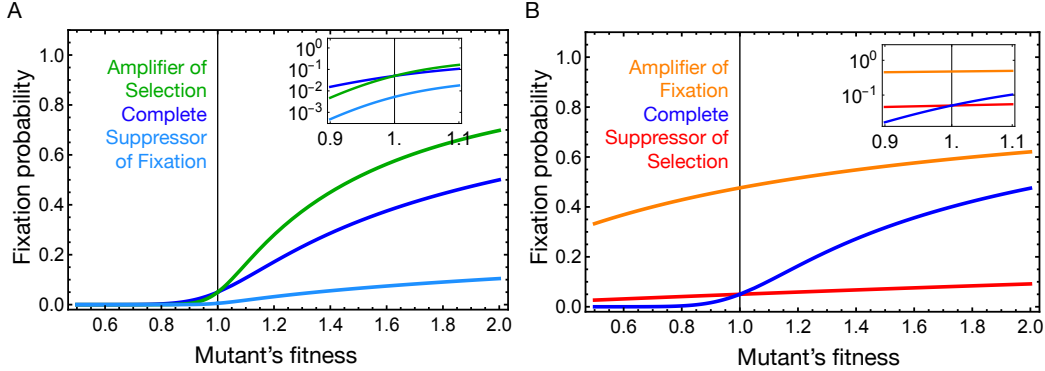


Figure 1.4: **Categories of graphs.** With the complete graph as a reference, based on the fixation probability of mutants four main categories of graphs are prominent in evolutionary graph theory. The widely recognised categories include amplifiers of selection (panel A) and suppressors of selection (panel B). Less discussed is the category of suppressors of fixation (panel A). In addition to these, a new category of graphs, detailed in chapter three, is the amplifier of fixation (panel B). The beneficial mutants have fitness greater than one whereas the deleterious mutants have fitness lower than one with wild-type's fitness equal to one.

probability of fixing mutations, regardless of their fitness— can attain higher fitness than the well-mixed population. In the third chapter, we discover a new category of graphs— amplifiers of fixation. This is achieved simply by allowing the parent individuals to replace the dead individuals, instead of the conventional choice of offspring replacing the dead individuals. We also find that the majority of random graphs are amplifiers of fixation under temperature-initialised dB updating, and suppressors of fixation under temperature-initialised Bd updating. To investigate the long-term evolution, we study the steady-states of Moran origin-fixation dynamics on various random graphs. To our surprise, we find that amplifiers of fixation, which are better at fixing beneficial mutations, attain lower fitness while suppressors of fixation, worse at fixing beneficial mutations, attain higher steady-state fitness than the complete graph.

In the fourth chapter, we find that for higher mutation rates (self-looped) amplifiers of selection attain lower fitness than the complete graph. On the other hand, suppressors of fixation outcompetes the complete graph, both

within and beyond the low mutation rate approximation. In chapter five, we move to network-structured metapopulations where each node is occupied by a deme. We categorise various update rules for metapopulations based on whether the migration occurs during a birth event. The outline for the thesis is present in Fig. 1.5.

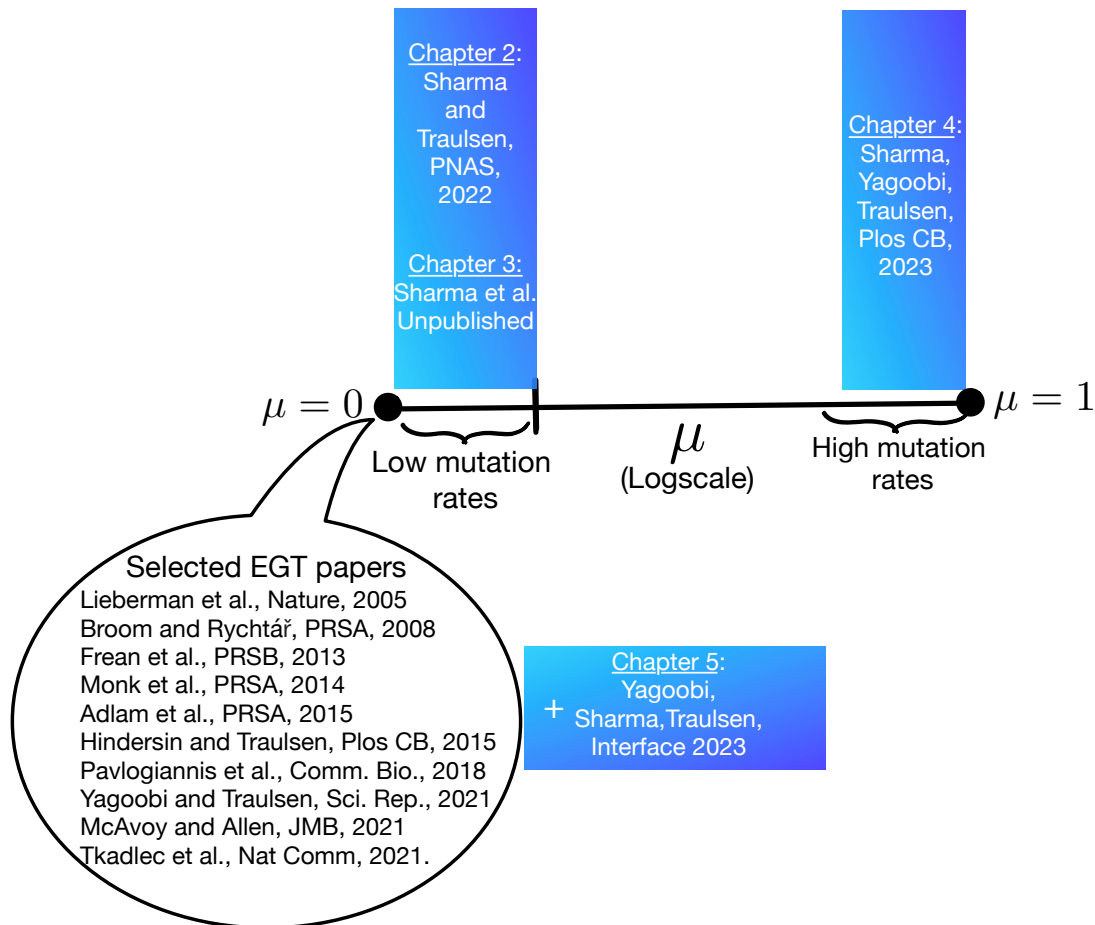


Figure 1.5: **Thesis layout.** Placing our work in the space of existing literature of EGT. While most of the literature focusses on fixation time scales, in this thesis we study the role of spatial structure in long-term dynamics with non-zero mutation rates.

## Chapter 2

# Suppressors of fixation can increase fitness beyond amplifiers of selection

The motivation behind this chapter is to move beyond the conventional fixation time scale analysis in EGT by allowing mutations to appear continuously. For that, we develop a model where long-term evolution is studied on spatially structured populations.

This chapter went through peer-review and is published in Proceedings of the National Academy of Sciences of the United States of America as: Sharma and Traulsen 2022, [53]—Suppressors of fixation can increase average fitness beyond amplifiers of selection. This manuscript version is made available under the CC-BY-NC-ND 4.0 license <https://creativecommons.org/licenses/by-nc-nd/4.0/> . The authors contributions are detailed at the end of the thesis.





# Suppressors of fixation can increase average fitness beyond amplifiers of selection

Nikhil Sharma<sup>a,1</sup> and Arne Traulsen<sup>a,1</sup>

Edited by Kenneth Wachtler, University of California, Berkeley, CA; received March 28, 2022; accepted August 3, 2022

Evolutionary dynamics on graphs has remarkable features: For example, it has been shown that amplifiers of selection exist that—compared to an unstructured population—increase the fixation probability of advantageous mutations, while they decrease the fixation probability of disadvantageous mutations. So far, the theoretical literature has focused on the case of a single mutant entering a graph-structured population, asking how the graph affects the probability that a mutant takes over a population and the time until this typically happens. For continuously evolving systems, the more relevant case is that mutants constantly arise in an evolving population. Typically, such mutations occur with a small probability during reproduction events. We thus focus on the low mutation rate limit. The probability distribution for the fitness in this process converges to a steady state at long times. Intuitively, amplifiers of selection are expected to increase the population's mean fitness in the steady state. Similarly, suppressors of selection are expected to decrease the population's mean fitness in the steady state. However, we show that another set of graphs, called suppressors of fixation, can attain the highest population mean fitness. The key reason behind this is their ability to efficiently reject deleterious mutants. This illustrates the importance of the deleterious mutant regime for the long-term evolutionary dynamics, something that seems to have been overlooked in the literature so far.

evolutionary graph theory | mutation-selection balance | low mutation rates | deleterious mutant regime

Understanding how spatial structures can affect evolutionary dynamics has been of interest to evolutionary biologists for a long time. More than a decade ago, a framework known as evolutionary graph theory was introduced (1). The primary quantity of interest has been the fixation probability of a mutant on graphs, which is the probability that a mutant with given fitness takes over the rest of the wild-type population (2–6).

Fixation probability is a central concept in evolutionary biology, as it determines the rate of evolution in the low mutation rate regime (7, 8). Spatial structure tweaks the strength of selection and genetic drift (9, 10). As a consequence, some graphs have higher probability of fixation than others for a mutant with a given fitness value. Of particular interest are those graphs that increase the fixation probabilities for advantageous mutants and decrease the fixation probabilities for disadvantageous mutants—so-called amplifiers of selection. While initially, amplifiers seemed to be special structures (1), it turned out that under Birth–death (Bd) updating, most random networks are amplifiers of selection (11).

However, fixation describes evolutionary dynamics only on a relatively short time scale. In the long run, additional mutants will arise, and the population will eventually reach a steady state in terms of fitness (12). A model that investigates such long evolutionary trajectories in graph-structured populations has been missing so far. This problem has been studied via a process where two types of individuals with fixed fitness values compete with each other, leading to a mutation–selection balance in the steady state (13), but not for the case of continuously arising mutations with a potentially infinite number of types. The neutrality counterpart of this problem has been investigated in ref. 14, where equilibrium properties are shown to be independent of the population structure.

In evolutionary graph theory, every node of a graph is an individual. If an individual produces an offspring, the offspring is placed in a neighboring node. We focus on undirected and unweighted graphs, where all neighboring nodes are chosen with the same probability. Graphs can be classified based on their fixation probability, as compared to that of the complete graph. The fixation probability of a mutant with fitness  $f'$  appearing in a population with fitness  $f$  on a complete network  $C$  (corresponding to a well-mixed population) is given by

$$\phi_C^I(f', f) = \phi_C(f', f) = \frac{1 - \frac{f}{f'}}{1 - \left(\frac{f}{f'}\right)^N}. \quad [1]$$

## Significance

Spatial structure can substantially affect evolutionary dynamics. These dynamics are usually studied through the fixation process of a single mutation. This allows one to classify structures, e.g., as amplifiers, which enhance the effect of selection. Here, we provide a model integrating the fixation process of single mutations into the long-term evolutionary dynamics, characterized by a balance between mutation and selection. Certain structures that do not perform well for single fixation events can perform very well at longer time scales due to their ability to reject deleterious mutants. This means that a structure can be improved by only increasing its ability to reject deleterious mutants—the increase of its ability to fix advantageous mutations is less central than previously thought.

Author affiliations: <sup>a</sup>Department of Evolutionary Theory, Max Planck Institute for Evolutionary Biology, 24306 Plön, Germany

Author contributions: N.S. and A.T. designed research; N.S. and A.T. performed research; N.S. contributed new reagents/analytic tools; N.S. and A.T. analyzed data; and N.S. and A.T. wrote the paper.

The authors declare no competing interest.

This article is a PNAS Direct Submission.

Copyright © 2022 the Author(s). Published by PNAS. This article is distributed under Creative Commons Attribution-NonCommercial-NoDerivatives License 4.0 (CC BY-NC-ND).

<sup>1</sup>To whom correspondence may be addressed. Email: nsharma@evolbio.mpg.de or traulsen@evolbio.mpg.de. Published September 6, 2022.

In this case, all nodes are equivalent, and it does not matter where the mutation occurs. In the general case, the fixation probability depends crucially upon the node where the mutant first arises (15). In Eq. 1,  $\mathcal{I}$  denotes this initialization scheme, according to which a mutant arises on the network. To be specific,  $\mathcal{I}$  is the probability distribution represented by a row vector of size  $N$  where element  $i$  is the probability with which a mutant arises at node  $i$  in a homogenous background. In the simplest case, this is a uniform probability—this case is typically referred to as uniform initialization.

Based on fixation probabilities and the initialization scheme, graphs typically fall into three categories (11):

- An amplifier of selection is a graph  $G$  that increases the fixation probability of an advantageous mutant and decreases the fixation probability of a disadvantageous mutant compared to a complete graph,  $\phi_G^{\mathcal{I}}(f', f) > \phi_C^{\mathcal{I}}(f', f)$  for  $f' > f$  and  $\phi_G^{\mathcal{I}}(f', f) < \phi_C^{\mathcal{I}}(f', f)$  for  $f' < f$ .
- A suppressor of selection is a graph  $G$  that decreases the fixation probability of an advantageous mutant and increases the fixation probability of a disadvantageous mutant compared to a complete graph,  $\phi_G^{\mathcal{I}}(f', f) < \phi_C^{\mathcal{I}}(f', f)$  for  $f' > f$  and  $\phi_G^{\mathcal{I}}(f', f) > \phi_C^{\mathcal{I}}(f', f)$  for  $f' < f$ .
- An isothermal graph is a graph  $G$  that has the same fixation probability as the complete graph,  $\phi_G^{\mathcal{I}}(f', f) = \phi_C^{\mathcal{I}}(f', f)$  for all  $f'$  and  $f$ . In particular, any graph where the number of links for each node is the same is an isothermal graph for uniform initialization [in the more general case of weighted graphs, where mutants are placed on neighboring nodes with different probabilities (16). For a structure to be an isothermal graph, every node should have equal temperature. The temperature of a node  $i$  is equal to the sum of the incoming link weights  $w_{ji}$ ,  $\sum_{j=1}^N w_{ji}$ ].

For later purposes, we introduce a fourth type (11, 17), suppressors of fixation:

- A suppressor of fixation is a graph  $G$  that reduces the fixation probability for both advantageous and disadvantageous mutants,  $\phi_G^{\mathcal{I}}(f', f) < \phi_C^{\mathcal{I}}(f', f)$  for all  $f' \neq f$ . These graphs are also called reducers of fixation (18).

The definition for isothermal networks has originally been defined for a uniform initialization scheme. In general, such a definition would depend on the details of the update rule (19). The classifications for amplifiers and suppressors above have also been developed for uniform mutant initialization. For other initialization schemes—for example, temperature initialization—the classifications become less straightforward, especially near neutrality (20).

## Model

In order to generate any evolutionary dynamics, we must choose an update mechanism. We focus on the Bd update rule, where, first, an individual is selected at random, but proportional to fitness. This individual produces an offspring, which is placed in one of the neighboring nodes. We assume that the offspring is mutated with a small probability  $\mu$  and identical to its parent with probability  $1 - \mu$ . The state of a population is represented by a fitness vector  $\mathbf{f} = (f_1, f_2, \dots, f_{N-1}, f_N)^T$ , where  $f_i$  is the fitness of an individual at node  $i$ . When an offspring is mutated, we choose

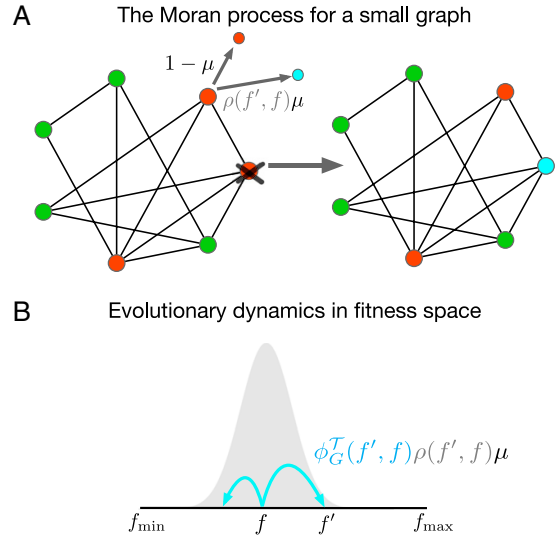


**Fig. 1.** Moran Birth-death (Bd) with continuous mutation on a graph. (A) The Moran Bd update mechanism with continuous mutation is shown for a small graph. An individual is selected to reproduce with probability proportional to its fitness. The offspring mutates with probability  $\mu$ , and its fitness  $f'$  is sampled from a distribution  $\rho(f', f)$ , where  $f$  is the parent's fitness. A neighboring individual is then chosen for death at random among the neighboring nodes, and the offspring is placed in the empty node. We work in the low mutation rate approximation where  $\mu$  is very small, such that only a single type is typically present in the population. (B) Evolutionary dynamics in fitness space. For low mutation rates, the evolutionary dynamics effectively becomes a biased random walk on the fitness space. The transition rates depend on the mutation rate  $\mu$ , the fitness distribution of the mutant offspring  $\rho(f', f)$  (shown in gray), and the fixation probabilities  $\phi_G^{\mathcal{I}}(f', f)$ .

its fitness  $f'$  from a continuous bounded distribution  $\rho(f', f)$ , where  $f$  is the parent's fitness and  $f_{\min} \leq f' \leq f_{\max}$  (Fig. 1A).

Instead of looking into the full evolutionary trajectory of the system, we focus only on the fitness distribution in the steady state. As this is difficult for arbitrary mutation rates, we concentrate on the low mutation rate regime here. In this regime, the entire population effectively moves as a point (most of the time) in the fitness space. Typically, every individual in a population has the same fitness. Thus, the state of the population can be labeled by a single fitness value,  $f$ . This is a good approximation if the time between two successive mutations is sufficiently high that a new mutant either gets extinct or takes over the entire population before the next mutation arises. Thus, our model describes sequential fixation (21) (Fig. 1B). We are mainly interested in the dynamics of probability density  $P_G(f, t)$ . One important observation is that mutations do not arise in all nodes with uniform probability, but mostly in those nodes that have more incoming links. This is captured by the idea of “temperature initialization” (20), where the probability that a mutation arises is proportional to the temperature of a node  $i$ ,  $\sum_{j=1}^N w_{ji}$ . In the case of unweighted networks,  $w_{ji} = 1$  if a link between  $j$  and  $i$  exists; otherwise,  $w_{ji} = 0$ . With this, we can write down the master equation of the corresponding jump process (22, 23),

$$\begin{aligned} \frac{\partial P_G(f, t)}{\partial t} = & \int df' \underbrace{\phi_G^{\mathcal{I}}(f, f') \rho(f, f') \mu}_{T_{f \leftarrow f'}} P_G(f', t) \\ & - \int df' \underbrace{\phi_G^{\mathcal{I}}(f', f) \rho(f', f) \mu}_{T_{f' \leftarrow f}} P_G(f, t), \quad [2] \end{aligned}$$

where  $T_{f' \leftarrow f}$  is the probability to change the population's fitness from  $f$  to  $f'$ .  $T_{f' \leftarrow f}$  is given by the product of the probability of mutation,  $\mu$ , the probability that a mutant with fitness  $f'$  arises,  $\rho(f', f)$ , and the probability that such a mutation, arising preferentially in nodes that are replaced often, reaches fixation,  $\phi_G^T(f', f)$  (where  $T$  denotes temperature initialization). The probability  $T_{f \leftarrow f'}$  is given by an equivalent argument.

The reason behind using fixation probability under temperature initialization is that the probability for a mutant to arise on a certain node during reproduction in a homogenous population is proportional to the temperature of that node (20). This follows from our assumption that during a birth event, it is always the offspring individual that replaces a neighboring individual. For the opposite case, where the parent individual replaces a neighboring individual and the offspring (potentially a mutant) individual stays at the focal node, the fixation probability for uniform initialization has to be used in Eq. 2 instead. The corresponding evolutionary dynamics on the fitness space is a biased random walk with transition rates  $T_{f' \leftarrow f}$  and  $T_{f \leftarrow f'}$ . To derive the steady state,  $P_G^*(f)$ , we start from the assumption of detailed balance (23),

$$\int df' T_{f \leftarrow f'} P_G^*(f') = \int df' T_{f' \leftarrow f} P_G^*(f). \quad [3]$$

This condition is fulfilled if we have  $T_{f \leftarrow f'} P_G^*(f') = T_{f' \leftarrow f} P_G^*(f)$  for all  $f, f'$ . From this, we obtain the steady state (23),

$$P_G^*(f) = \frac{1}{\int df' \frac{T_{f' \leftarrow f}}{T_{f \leftarrow f'}}} = \frac{1}{\int df' \frac{\phi_G^T(f', f)}{\phi_G^T(f, f')} \cdot \frac{\rho(f', f)}{\rho(f, f')}}. \quad [4]$$

If the mutant's fitness distribution  $\rho(f', f)$  only depends on the fitness distance between parent and offspring,  $\rho(f', f) = \rho(|f' - f|)$ , the population's steady-state statistics depends only on the fixation probabilities—in this case, the second factor cancels out. Furthermore, the steady-state probability density for the population's fitness is the same for all isothermal graphs, irrespective of the offspring mutational fitness distribution—the first factor is the same for all isothermal graphs, including the complete graph.

As an example, the steady-state distribution for the complete graph when mutant's fitness is sampled from the uniform distribution is

$$P_G^*(f) = \frac{N}{f_{\max}^N - f_{\min}^N} f^{N-1}. \quad [5]$$

See App. A for details. This steady-state statistics is exactly the same as derived in ref. 24. However, in ref. 24, the evolutionary dynamics was studied by using a nearest-neighbor jump process on a discretized state space. In our derivation of Eq. 5, at a given point in the dynamics, the population could jump to any arbitrary point of the fitness space. Yet, interestingly, we obtain the same steady-state distribution for the complete graph as derived in ref. 24, but for a different scenario.

To study mutation–selection balance on graphs, we choose the complete graph, the star graph, and the (weighted) star graph with self-loops, i.e., a star where every individual can also be replaced by its own offspring. Under temperature initialization, a complete graph is an isothermal graph. For finite  $N$ , the star is a suppressor of fixation (for  $N \rightarrow \infty$ , it becomes a suppressor of selection), and the star graph with self-loops is a piece-wise amplifier of selection (20) (only for  $N \rightarrow \infty$ , it becomes an amplifier in a strict sense) (Fig. 2 B and D). Adding self-loops and making edges

weighted can make the star graph an amplifier of selection for temperature initialization. According to ref. 25, for a structure to be an amplifier of selection, it should have a sufficient number of cold nodes (low-temperature nodes), where a mutant is less likely to get replaced by wild-type individuals and, thus, increasing the likelihood for a mutant to fix. The star graph (unweighted, without self-loops) indeed has many cold nodes, making it an amplifier of selection under uniform initialization (1) (Fig. 2 A and C). However, under the temperature initialization process, the initial mutant appears on the central node with high probability, as the central node has the highest temperature. Thus, the mutant is more likely to get extinct during the course of the dynamics, explaining its suppressing nature. By adding self-loops to the star graph with a larger weight, one decreases the temperature of the central node and increases the temperature of the leaves, thus increasing the likelihood for the leaf nodes to receive an initial mutant. This transformation facilitated via self-loops and weighted edges is the reason behind the amplifying nature of the self-looped star graph.

We use these graphs because exact expressions for the corresponding fixation probabilities are known (App. C). The fixation probabilities for these three graphs under uniform and temperature initialization are plotted as a function of the mutant's fitness in Fig. 2.

The microscopic Moran-Bd update is costly to simulate for low mutation rates, especially for large graphs. Thus, we use a coarse-grained description, where we focus on the changes arising from mutations. We use the following Monte Carlo-type algorithm (26, 27), which measures time steps in terms of mutational events:

- An initial fitness value  $f$  between  $f_{\min}$  and  $f_{\max}$  is assigned to each individual in a population on a graph  $G$ .
- At every time step, a mutant  $f'$  is drawn from a distribution  $\rho(f', f)$ .
- The fitness of the entire population is then updated to  $f'$  with probability  $\phi_G^T(f', f)$ . With probability  $1 - \phi_G^T(f', f)$ , it remains the same. Note that this step takes into account that mutants tend to arise in different places with different probabilities.
- The last two steps are repeated for a sufficiently long number of time steps until a mutation–selection balance is attained.

We use this algorithm to infer how mutation–selection balance is attained in our three spatial structures. In Fig. 3 A and B, the independent fitness trajectories, as well as the ensemble average fitness trajectory of the population, are plotted as a function of the number of mutations occurred.

## Results

The star with self-loops, an amplifier of selection, reaches the highest steady-state fitness in its mutation–selection balance (Fig. 3B). This is expected because, compared to the other graphs, the self-looped star graph is best at fixing beneficial mutants for temperature initialization. What is surprising is that the star graph, a suppressor of fixation with lower fixation probability for all fitness values of a mutant, attains not just higher steady-state fitness than the complete graph (and, thus, all isothermal graphs), but almost the same balance as the star with loops, an amplifier of selection. We also observe that, just like isothermal networks, the star graph with loops takes fewer mutations to reach the balance than the star graphs, which takes many more mutations to reach the steady

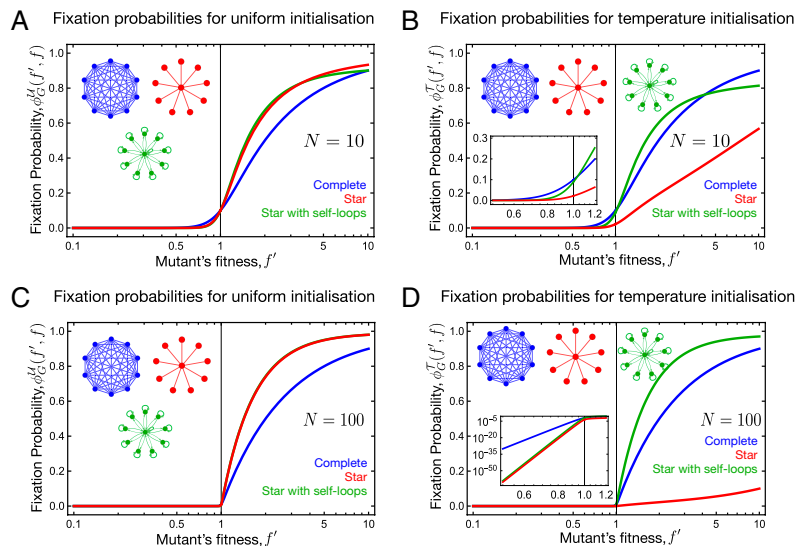


**Fig. 2.** Fixation probabilities for uniform and temperature initialization. (A) The fixation probabilities  $\phi_C^U(f', f)$  as functions of mutant's fitness  $f'$  with background fitness  $f = 1$  for uniform initialization  $\mathcal{U}$  for three graphs with  $N = 10$ : the complete graph, the star, and a weighted star with self-loops. For this initialization scheme, both the star and the star with loops are amplifiers of selection, and all fixation probabilities intersect at  $f' = f$  and  $\phi_C^U(f, f) = N^{-1}$ . (B) Fixation probabilities as in A, but for temperature initialization. Now, the star with self-loops is only a piecewise amplifier of selection, as it reduces the fixation probability for very large  $f'$ . The star is a suppressor of fixation and reduces the fixation probability for all mutant fitness values. Note that even under neutrality,  $f' = 1$ , the fixation probabilities are different. (C) Fixation probabilities as in A, but with  $N = 100$ . For large  $N$ , probabilities to fix deleterious mutants decrease, while they increase for the beneficial mutants. (D) For temperature initialization, a larger self-looped star graph amplifies selection for the entire fitness domain considered in the figure. On the other hand, even at  $N = 100$ , the star graph continues to be a suppressor of fixation; see D, *Inset* (Parameters: with  $n$  leaves, the weight of all the leaves' self-loops is  $1 - n^{-1}$ , and the weight for the center's self-loop is  $1 - n^{-2}$ . All the links directed from the center to leaves and vice versa have weights  $n^{-3}$  and  $n^{-1}$ , respectively).

state. In the subsequent sections, we will discuss these observations and give an explanation for them.

**Amplifiers Attain Higher Steady-State Fitness in Mutation-Selection Equilibrium.** Amplifiers of selection are better at fixing beneficial mutants and avoiding the fixation of deleterious mutants than isothermal graphs. They are expected to attain a higher steady-state fitness in the mutation-selection balance than isothermal graphs. We verify this expectation in Fig. 3 C and D, which shows the average steady-state fitness of the population for different population sizes. We consider two types of mutational fitness jump distribution, a uniform and a (truncated) Gaussian, centered around the parent's fitness. We observe that, regardless of the mutational fitness distribution, the star graph with loops attains a higher steady-state fitness than the complete graph for all considered population sizes. In *App. B*, we provide a formal proof that, for any mutational fitness distributions, amplifiers of selection have higher steady-state fitness than well-mixed populations and suppressors of selection. As a reference, by using Eq. 5, we derive the steady-state average fitness for the complete graph with uniform mutational fitness distribution,

$$\langle f \rangle_C^* = \frac{N}{N+1} \frac{f_{\max}^{N+1} - f_{\min}^{N+1}}{f_{\max}^N - f_{\min}^N}. \quad [6]$$

Thus, in the limit of large  $N$ ,  $\langle f \rangle_C^* \rightarrow f_{\max}$ . The steady-state fitness approaches the maximal possible value,  $\langle f \rangle^* \rightarrow f_{\max}$  for  $N \rightarrow \infty$ , for both the complete and the self-looped star graph. This is true for a general mutational fitness distribution, where there is always a finite probability to fix a beneficial mutation, and where the probability to fix a deleterious mutant goes to zero in the limit of  $N \rightarrow \infty$ . In fact,  $f_{\max}$  becomes an absorbing state for the evolutionary trajectories on the amplifiers of selection and the well-mixed population. Therefore, the fluctuations around

the steady state for these graphs also go to zero. This can be illustrated by studying the large- $N$  limit dynamics of the self-looped star graph and the complete graph. In the limit of  $N \rightarrow \infty$ , the fixation probability for the self-looped star under temperature initialization becomes  $1 - f^2/f'^2$  for any  $f' > f$  and 0 otherwise (*App. C*), whereas from Eq. 1, it follows that for the complete graph, the fixation probability becomes,  $1 - f/f'$  for  $f' > f$  and 0 otherwise. Hence, in the limit of  $N \rightarrow \infty$ , both of these graphs can only fix beneficial mutants, and, thus, the long-term mutation-selection dynamics gets absorbed at  $f_{\max}$ . This also leads to the conclusion that the self-looped star needs fewer mutations than the complete graph to reach  $f_{\max}$ . The large- $N$  analysis for the star graph (unweighted and without self-loops), however, is a bit subtle, as in the limit of  $N \rightarrow \infty$ , the fixation probability becomes zero for all possible pairs of mutant and background fitness values. For very large, but finite, *App. D*, we show that the steady-state average fitness for the star graph also converges to  $f_{\max}$ .

**Do Amplifiers Maximize Average Fitness?** The star graph with no self-loops, a suppressor of fixation, not only attains higher steady-state fitness in the mutation-selection balance than the complete graph, but almost the same steady-state fitness as the star with self-loops, an amplifier of selection, as shown in Fig. 3 C and D. In *App. D*, we show that even for very large  $N$ , the star graph continues to attain higher steady-state average fitness than the well-mixed population. There are two main factors that drive the steady-state fitness: 1) fixing beneficial mutants with high probability and 2) avoiding the fixation of deleterious mutants. As an amplifier of selection, the star with self-loops is superior in fixing beneficial mutants. But the star without self-loops is much better at avoiding the fixation of deleterious mutants (Fig. 2 B, *Inset*, and D, *Inset*). In this way, the star without self-loops

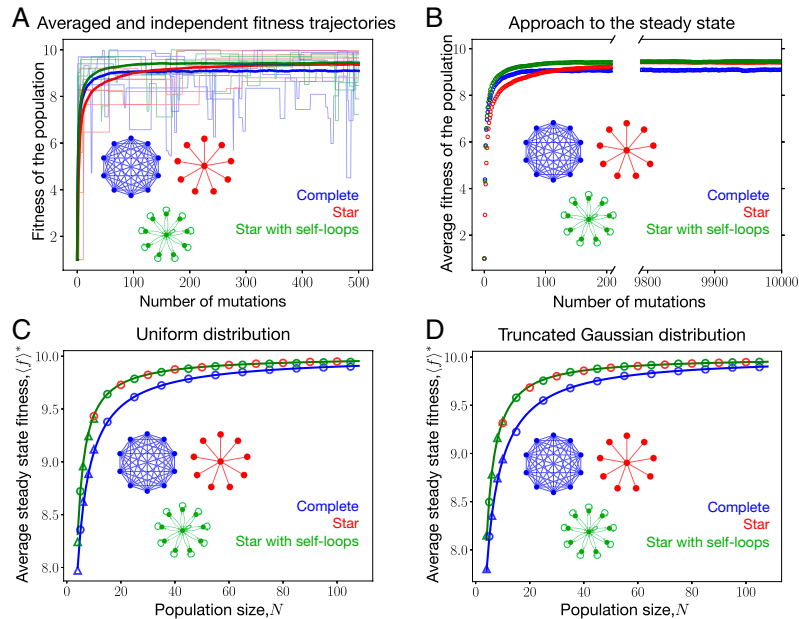


**Fig. 3.** Fitness trajectories and steady-state average fitness for different graphs. (A) The average fitness trajectories (in dark colors) for the complete graph, the star graph, and the self-looped star graph with a uniform mutational fitness distribution, starting from a population where every individual has fitness  $f = 1$ . For each graph, the average fitness trajectory is computed by performing an ensemble average over an ensemble of 2,000 independent realizations. In the background of A, five such independent realizations are shown (in light colors) for each graph. After reaching high fitness value, the fitness of the complete graphed population fluctuates more than the other two graphs. This is because after reaching higher fitness values, deleterious mutations become more likely to appear. The complete graph is worse at rejecting such deleterious mutants compared to other two graphs (Fig. 2 B, *Inset*, and D, *Inset*); it experiences more fluctuations. (B) Although the star is a suppressor of fixation, it attains the same steady-state fitness in the mutation–selection balance as the self-looped star graph. This is due to its better response to deleterious mutants (Fig. 2 B, *Inset*, and D, *Inset*). In C and D, steady-state fitnesses in the mutation–selection balance attained for the self-looped star graph (green) and complete graph (blue) as a function of population size are shown with uniform (C) and truncated (D) Gaussian mutational fitness distribution. The SD for the Gaussian distribution is chosen to be  $\sigma = 1$ . Solid lines are the numerical solutions of Eq. 4, and circles represent simulation points obtained using the Monte Carlo algorithm, while triangles correspond to microscopic Moran Bd simulations, which are feasible only for very small  $N$ . Regardless of the mutational fitness distribution, the self-looped star (an amplifier) always attains higher steady-state fitness in the mutation–selection balance than isothermal graphs for all (finite)  $N$ . Red circles correspond to the steady-state fitness attained by the star graph, a suppressor of fixation. From C and D, we find that even for large  $N$ , the star graph reaches almost the same steady-state fitness as that of the self-looped star graph. Parameters  $N = 10$ ,  $f_{\min} = 0.1$ , and  $f_{\max} = 10$ .

compensates for its lower fixation probabilities of beneficial mutants. Therefore, the fixation probability profile for deleterious mutants can contribute considerably to the long-term mutation–selection evolutionary dynamics. We expect this to be quite general, and not just restricted to the graphs that we have considered. We argue this in the following way: Let us take two amplifiers,  $A_1$  and  $A_2$ , and, without any loss of generality, assume that  $A_1$  is a better amplifier than  $A_2$ . That is,  $A_1$  is better in fixing advantageous mutants and avoiding the fixation of deleterious mutants than  $A_2$ . In that case, by the proof given in *App. B*, it follows that the average steady-state fitness of  $A_1$  is greater than the average steady-state fitness of  $A_2$ —i.e.,  $\langle f \rangle_{A_1}^* > \langle f \rangle_{A_2}^*$ . However, if  $A_2$  can be modified, along the lines of ref. 28, such that its fixation probability for deleterious mutants becomes much lower than  $A_1$ , the average steady-state fitness  $\langle f \rangle_{A_2}^*$  can exceed  $\langle f \rangle_{A_1}^*$ . But this compensation for lower fixation probabilities of beneficial mutants by decreasing the acceptance rate of deleterious mutants comes at a cost in terms of the time it takes to reach the steady state.

**Time to Reach the Steady State.** So far, we have studied the steady-state average fitness values for different graphs. Now, we discuss the time they take to reach their respective steady states. To estimate these times, we use the concept of mixing times (29). In a generic stochastic process, the probability distribution  $P_G(f)$

defined on a space  $\Omega$  changes with time before reaching its steady state. The mixing time can then be defined as the time when the distance of this evolving distribution to its steady state  $P_G^*(f)$  goes to zero. Formally, the mixing time  $t_{\text{mix}}$  is defined as the minimal time when the distance  $d(t)$  to the steady-state distribution is smaller than a threshold  $\varepsilon$ ,

$$t_{\text{mix}}(\varepsilon) = \min\{t : d(t) \leq \varepsilon\}, \quad [7]$$

where

$$d(t) = \frac{1}{2} \sum_{f \in \Omega} |P_G(f, t) - P_G^*(f)|. \quad [8]$$

In Fig. 4A, we find that the star graph, a suppressor of fixation, attains the same balance as the self-looped star, but takes many more mutations to reach the steady state than all other considered graphs. The mixing times for the complete and the self-looped star do not vary much with the population size. In fact, it decreases for the self-looped star with increasing  $N$ . This is because the self-looped star becomes a better amplifier for larger  $N$  (Fig. 2 B and D). Adaptation for the complete graph and the self-looped star graph is mostly governed by the fixation of beneficial mutants, which improves with large  $N$ . On the other hand, the adaptation for the star graph depends crucially on preventing the fixation of deleterious mutants, as it becomes less likely to



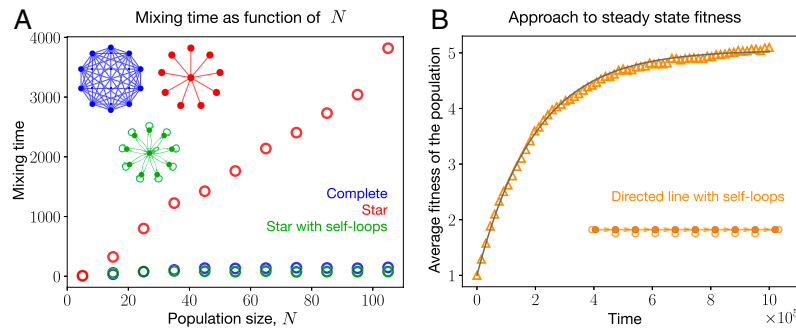


**Fig. 4.** Approach to the steady state. (A) Mixing time for various graphs as a function of population size  $N$  measured in number of mutations. Parameters are same as in Fig. 3C. Mixing times have been obtained by using the Monte Carlo algorithm. The star graph takes the longest to reach a steady state. This is because the star graph, especially for large  $N$ , has very small fixation probabilities, even for beneficial mutants, and, thus, more attempts to increase fitness are needed to reach the steady state (for the mixing time, we assume  $\varepsilon = \frac{1}{4}$  in Eq. 7). (B) Increase of average fitness on the directed line with self-loops. We compare Eq. 42 and the corresponding microscopic Moran Bd simulations. Parameters are the same as in Fig. 3, with a mutation probability  $\mu = 10^{-4}$ . We see a good agreement between simulations (orange symbols) and the analytical result (gray line). From App. E, we know that the relaxation time for single rooted graphs goes as  $\frac{N}{\mu T_r}$ . Substituting values for the parameters and the root temperature for the directed line with self-loops,  $T_r = \frac{1}{2}$ , we get the mixing time to be approximately  $2 \times 10^5$ . Here, the time is measured in terms of the number of Moran Bd steps. Although the simulation here is performed for the self-looped directed line, the same result is expected for any other single rooted (self-looped) graph, as long as  $\mu$  is sufficiently low. For more details, see App. E.

fix beneficial mutants with the increase in  $N$  (Fig. 2 B and D). Therefore, most mutations arising in this graph do not reach fixation. Another interesting observation is that for large  $N$ , the self-looped star graph has the smallest mixing time. This contrasts with the typical fixation probability and time relation, where larger fixation probability tends to correlate with higher fixation times (30–33). The mixing time is difficult to calculate for the general case. But for single rooted graphs with  $\phi_G^T \sim \frac{1}{N}$ , it can be computed efficiently. In fact, for single rooted graphs, the full temporal statistics can be computed (App. E). In Fig. 4B, we see a good agreement between the microscopic Moran Bd simulations performed for the self-looped directed line and the analytical expression for the average fitness trajectory (Eq. 42). We also verify that the self-looped directed line, a suppressor of selection, attains lower steady-state average fitness in the mutation–selection balance than the complete graph and the self-looped star graph. This is in accordance with App. B, where suppressors of selection are proved to attain lower steady-state fitness than the complete graph and amplifiers of selection.

**Gaussian Phenotype-Fitness Map.** Until now, the dynamics were considered in fitness space. However, in many cases, mutations occur on the level of an individual's phenotype. In that case, the state of a population is represented by a phenotype vector  $\mathbf{p} = (p_1, p_2, \dots, p_{N-1}, p_N)^T$ , where  $p_i$  is the phenotypic trait value of the individual at node  $i$ . The Moran Bd update still only takes the fitness of individuals into account. Therefore, a phenotype-fitness map  $f(\mathbf{p})$  is used to assign a fitness value to a phenotype. The fitness profile of the population can then be denoted by  $\mathbf{f}(\mathbf{p}) = (f(p_1), f(p_2), \dots, f(p_N))^T$ . Similar to the previous case, when an offspring is mutated, we choose its phenotype  $p'$  from a continuous bounded distribution  $\rho(p', p)$ , where  $p$  is the parent's phenotypic value and  $p_{\min} \leq p' \leq p_{\max}$ . In this way, the work presented so far is identical to what would be obtained by considering a linear phenotype-fitness map,  $f(\mathbf{p}) = \mathbf{p}$ . In this section, we study the dynamics of a nonmonotonic Gaussian phenotype-fitness map. In Fig. 5A, we show that the order of the steady-state fitness in mutation–selection balance for different graphs remains the same as that of the linear phenotype-fitness

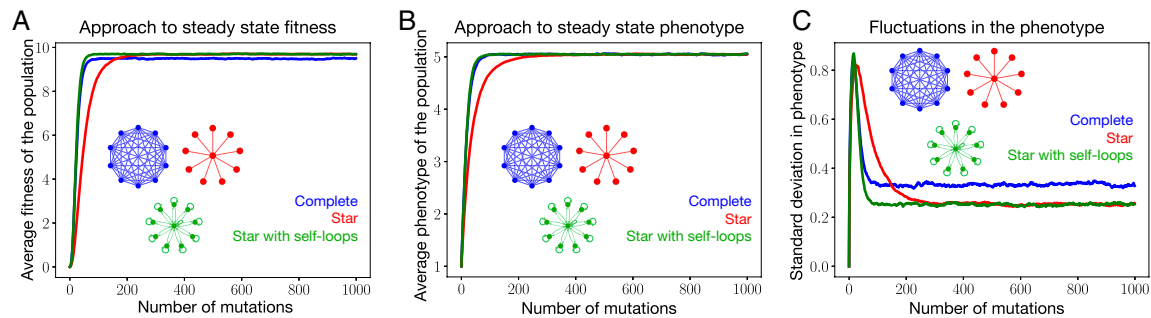


**Fig. 5.** Gaussian phenotype-fitness map: Fitness and phenotypic trajectories for different graphs. Here, we consider a Gaussian phenotype-fitness map,  $f(\mathbf{p}) = f_{\text{opt}} \exp(-\frac{(p - p_{\text{opt}})^2}{2\sigma_p^2})$ , where  $p_{\text{opt}}$  is the optimal phenotype, where the fitness is maximal and  $f(p_{\text{opt}}) = f_{\text{opt}}$ . (A) As in the case of a linear phenotype-fitness map, the star and the self-looped star have a higher state fitness than isothermal graphs. (B) All graphs converge to an average phenotype corresponding to the fitness maximum, but they have different fitness in steady state (A). The reason for this is differences in the fluctuations in steady state. (C) The SD of the phenotypes shows that the complete graph is more prone to fluctuations than the other two graphs. Parameters  $f_{\text{opt}} = 10$ ,  $p_{\text{opt}} = 5.05$ , and  $\sigma_p = 1$ , all other parameters are as in the previous figures, with  $\sigma = 0.5$  for the Gaussian mutational jump phenotype distribution.

map. It is interesting to note that the average steady-state phenotype for all the graphs is the same (Fig. 5B). Nevertheless, we see different steady-state average fitness values. Even though all graphs have the same steady-state phenotypic value, isothermal graphs are more prone to fluctuations and have a lower steady-state average fitness value (Fig. 5C). This happens again because the other two graphs are better in preventing the fixation of deleterious mutants. At long times, after reaching higher fitness values, populations are more likely to receive deleterious mutations than beneficial ones. Therefore, in the steady state, what determines fitness fluctuations of a population is its ability to reject deleterious mutants. In a nutshell, the steady-state fitnesses of graphs need not be same even when they have same phenotypes because the average of a function in general is not equal to the function of average, i.e.,  $\langle f(p) \rangle \neq f(\langle p \rangle)$ .

## Discussion

In evolutionary graph theory, evolutionary dynamics on graph structures has been studied in great detail. While the field has been mostly driven from the mathematical and computational community (1, 2, 19, 25, 32), partly driven by biological applications (17, 34, 35), now, there is increasing interest in applying these ideas to experimental systems in microbiology (36, 37).

The prospects of engineering a population structure that can optimize the chances to evolve certain mutations or to observe evolved population structures that minimize the evolution of mutations seem exciting, but these applications call for an extension of the field of evolutionary graph theory: Most applications implicitly assume that each node is a small population, and not all results carry over from graphs of individuals to graphs of subpopulations (38–41). In addition, the field has focused so far on fixation probability and fixation time (42–49).

This approach assumes that we can focus on the fate of a single mutant, but it can break down when mutations continuously arise, especially in graphs where the time to fixation or extinction is very high. Moreover, in the case where mutations continuously arise, one has to take into account where they arise. Thus, one needs to work with temperature initialization, where the definitions of amplifiers and suppressors of selection are less clear-cut.

We developed a model that takes such a continuous supply of mutations into account. We worked in the low mutation rate regime, where the fixation time of a mutant is much smaller than the average time between the two successive mutants. We found that the prevention of deleterious mutants from fixing can be more important than increasing the chances of advantageous mutants in order to obtain a higher steady-state fitness in the mutation–selection balance. In our case, the star, a suppressor of fixation for temperature initialization, beats isothermal graphs and attains almost the same balance as a self-looped star, an amplifier. The cause for this is the ability of the star graph to prevent deleterious mutants much better from fixing than isothermal graphs. The deleterious mutants regime is usually overlooked in the literature while studying fixation probabilities by using large- $N$  arguments. However, here, we have shown that the deleterious mutants regime is equally important, if not more, even for large  $N$ , as the beneficial mutants regime when studying long-term evolutionary dynamics.

Typically, amplifiers of selection also have a higher fixation time (25, 32, 33). Thus, one has to be careful that the assumption of small mutation rate is still fulfilled. When the fixation time becomes comparable to the average time between two successive mutations, one expects deviation from the low mutation rate approximation. On going beyond the weak mutation approximation, we found that the star continues to maintain higher

steady-state average fitness in the mutation–selection balance than the complete graph, while the self-looped star attains a lower steady-state average fitness than the complete graph outside the low mutation rate (*App. F*). Therefore, an amplifier of selection need not maximize fitness both inside and outside the low mutation rate regime. However, within the weak mutation rate regime, structures that allow more mutations to reach fixation will have a smaller mixing time—therefore, amplifiers of selection tend to have a lower mixing time until their steady-state fitness is reached.

Due to their ability to reach a high steady-state fitness, population structures that suppress selection could be much more interesting in applications than previously thought—suppressing selection may be as relevant as amplifying it. We have shown that in a situation where a dynamic, graph-structured population continuously evolves, the amplification of selection via the promotion of advantageous mutations does not necessarily imply a higher steady-state fitness. Instead, in such a process, one has to carefully consider also the fate of deleterious mutations, an issue that has so far not been in the focus of evolutionary graph theory.

## Appendix

**A. Steady State for the Complete Graph.** Here, we derive the mutation–selection balance steady-state statistics for the complete graph. To do so, we assume that the mutant's fitness is drawn from a uniform distribution defined over the domain  $[f_{\min}, f_{\max}]$ . Therefore, the general form of the steady-state fitness distribution, Eq. 4, reduces to

$$P_G^*(f) = \frac{1}{\int df' \frac{\phi_G^T(f', f)}{\phi_G^T(f, f')} \cdot 1} \quad [9]$$

By inserting the fixation probabilities for the complete graph in the above equation using Eq. 1, we obtain

$$P_G^*(f) = \frac{1}{\int df' \left(\frac{f'}{f}\right)^{N-1}} = \frac{f^{N-1}}{\int df' f'^{N-1}} = \frac{Nf^{N-1}}{f_{\max}^N - f_{\min}^N} \quad [10]$$

Using the above distribution, the steady-state average fitness in the mutation–selection balance for the complete graph takes the form,

$$\langle f \rangle_G^* = \int df f P_G^*(f) = \frac{N}{N+1} \frac{f_{\max}^{N+1} - f_{\min}^{N+1}}{f_{\max}^N - f_{\min}^N} \quad [11]$$

## B. Amplifiers of Selection Attain Higher Steady-State Fitness in Mutation–Selection Balance than Suppressors of Selection.

Here, we prove that amplifiers of selection attain higher steady-state fitness in their mutation–selection balance than suppressors of selection. We denote an arbitrary amplifier by  $A$  and an arbitrary suppressor by  $S$ . From the definitions of amplifiers and suppressors mentioned in the introduction, we have for every  $f' < f$  (and arbitrary initialization scheme  $\mathcal{I}$ )

$$\phi_A^{\mathcal{I}}(f, f') > \phi_S^{\mathcal{I}}(f, f'), \quad [12]$$

as well as

$$\phi_A^{\mathcal{I}}(f', f) < \phi_S^{\mathcal{I}}(f', f), \quad [13]$$

Combining these two inequalities, we get,

$$\frac{\phi_A^{\mathcal{I}}(f', f)}{\phi_A^{\mathcal{I}}(f, f')} < \frac{\phi_S^{\mathcal{I}}(f', f)}{\phi_S^{\mathcal{I}}(f, f')}. \quad [14]$$

Multiplying the above equation with  $\rho(f', f)/\rho(f, f')$ , followed by integrating over  $f'$  from  $f_{\min}$  to  $f$ , we obtain,

$$\int_{f_{\min}}^f df' \frac{\phi_A^T(f', f)}{\phi_A^T(f, f')} \cdot \frac{\rho(f', f)}{\rho(f, f')} < \int_{f_{\min}}^f df' \frac{\phi_S^T(f', f)}{\phi_S^T(f, f')} \cdot \frac{\rho(f', f)}{\rho(f, f')}. \quad [15]$$

Similarly, we find,

$$\int_f^{f_{\max}} df' \frac{\phi_A^T(f', f)}{\phi_A^T(f, f')} \cdot \frac{\rho(f', f)}{\rho(f, f')} > \int_f^{f_{\max}} df' \frac{\phi_S^T(f', f)}{\phi_S^T(f, f')} \cdot \frac{\rho(f', f)}{\rho(f, f')}. \quad [16]$$

By making use of the steady-state solution Eqs. 4 and 15, we find an inequality for probability density functions at the boundary  $f_{\max}$  of the fitness domain,

$$P_A^*(f_{\max}) > P_S^*(f_{\max}). \quad [17]$$

While Eq. 4 contains temperature-initialized fixation probabilities, the same expression follows for the steady-state statistics for any arbitrary initialization. As an example, instead of the mutations taking place during reproduction, they could appear spontaneously at any of the nodes. Eq. 4 would then contain uniform initialized fixation probabilities.

Similarly, at the fitness boundary  $f_{\min}$ , using Eqs. 4 and 16, we have,

$$P_A^*(f_{\min}) < P_S^*(f_{\min}). \quad [18]$$

The very same inequalities, [17] and [18], hold if  $A$  (amplifier) or  $S$  (suppressor) is replaced by  $C$  (complete).

Let us now first prove that amplifiers of selection attain higher steady-state fitness in mutation–selection balance than the complete graph. We take the case of an amplifier and the complete graph of the same size. The inequalities [17] and [18] imply that there exists a fitness,  $\hat{f}$ , such that,

$$P_A^*(\hat{f}) = P_C^*(\hat{f}). \quad [19]$$

For simplicity, here, we assumed that there is only one intersection point for the curves  $P_A^*(f)$  and  $P_C^*(f)$ . The proof, however, is not restricted to this assumption and can be extended to the general case where more than one intersection points are there. The main idea behind the proof is sketched in Fig. 6.

Let us define the  $P_A^*(f)$  as:

$$P_A^*(f) = \begin{cases} P_C^*(f) + \varepsilon_A^<(f), & \text{if } f \leq \hat{f} \\ P_C^*(f) + \varepsilon_A^>(f), & \text{otherwise.} \end{cases} \quad [20]$$

From the normalization condition of  $P_A^*(f)$  and  $P_C^*(f)$ , it follows that

$$\left| \int_{f_{\min}}^{\hat{f}} df \varepsilon_A^<(f) \right| = \int_{\hat{f}}^{f_{\max}} df \varepsilon_A^>(f). \quad [21]$$

We are interested in the difference of mean fitness in the steady state,

$$\langle f \rangle_A^* - \langle f \rangle_C^* = \underbrace{\int_{f_{\min}}^{\hat{f}} df f \varepsilon_A^<(f)}_{\Gamma_1} + \underbrace{\int_{\hat{f}}^{f_{\max}} df f \varepsilon_A^>(f)}_{\Gamma_2}. \quad [22]$$

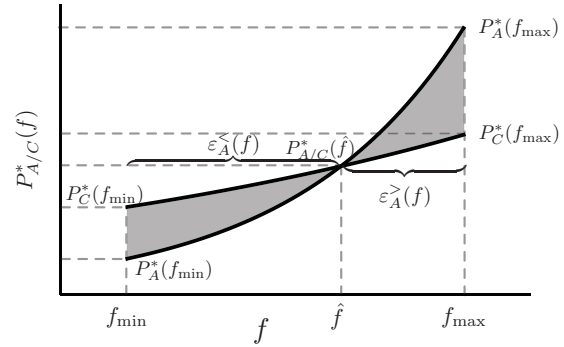


**Fig. 6.** Sketch for the proof. Here, we sketch the main idea behind the proof that the average fitness of an amplifier of selection exceeds that of a suppressor of selection or the complete graph in the steady state. Without any loss of generality, we take the case of an amplifier  $A$  and the complete graph  $C$ . The proof starts by first computing the order of  $P_{A/C}^*(f)$  at the fitness boundaries  $f_{\min}$  and  $f_{\max}$ . It turns out that  $P_A^*(f_{\min}) < P_C^*(f_{\min})$  and  $P_A^*(f_{\max}) > P_C^*(f_{\max})$ . This implies that there exists a fitness point  $\hat{f}$ , where these probability densities intersect.  $P_A^*$  is then decomposed as the sum of  $P_C^*$  and the functions  $\varepsilon_A^< / >$  (Eq. 20). By using the normalization conditions for  $P_C^*$  and the properties of functions  $\varepsilon_A^< / >$  (Eq. 21), we prove that amplifiers of selection attain higher steady-state fitness than the well-mixed population and, by extension, the suppressors of selection.

The first term in the above equation is negative,  $\Gamma_1 < 0$ , while the second term is positive,  $\Gamma_2 > 0$ . In the following, we show that the magnitude of the term  $\Gamma_1$  is less than the term  $\Gamma_2$ . Taking  $\Gamma_1$ , we find that

$$|\Gamma_1| < \hat{f} \left| \int_{f_{\min}}^{\hat{f}} df \varepsilon_A^<(f) \right|. \quad [23]$$

Similarly,

$$\hat{f} \int_{\hat{f}}^{f_{\max}} df \varepsilon_A^>(f) < \Gamma_2. \quad [24]$$

Now, because

$$\hat{f} \left| \int_{f_{\min}}^{\hat{f}} df \varepsilon_A^<(f) \right| = \hat{f} \int_{\hat{f}}^{f_{\max}} df \varepsilon_A^>(f), \quad [25]$$

using inequalities [23] and [24], we find  $|\Gamma_1| < \Gamma_2$ . Therefore, at last, we have

$$\langle f \rangle_A^* > \langle f \rangle_C^*. \quad [26]$$

Following the same procedure, one can show that  $\langle f \rangle_C^* > \langle f \rangle_S^*$ . This implies that  $\langle f \rangle_A^* > \langle f \rangle_S^*$  for all amplifiers of selection  $A$  and suppressors of selection  $S$ .

**C. Fixation Probability for the Weighted Self-Looped Star Graph under Temperature Initialization.** In this section, we introduce the weighted self-looped star graph that has been used throughout the main text. It is defined by the weighted adjacency matrix

$$\mathbf{w} = \begin{pmatrix} 1 - \delta & \frac{\delta}{n} & \frac{\delta}{n} & \cdots & \frac{\delta}{n} \\ \lambda & 1 - \lambda & 0 & \cdots & 0 \\ \vdots & \vdots & \ddots & \ddots & \vdots \\ \lambda & 0 & \cdots & 1 - \lambda & 0 \\ \lambda & 0 & \cdots & 0 & 1 - \lambda \end{pmatrix}, \quad [27]$$



with  $0 < \lambda \leq 1$  and  $0 < \delta \leq 1$ . Here,  $w_{ij}$  is the weight of the link directed from the node  $i$  to node  $j$ , with the center being the node 0. The fixation probability under temperature initialization for this graph has been derived by using the techniques of martingales (3, 20) and is given by

$$\phi_{G_{n+1}(\lambda, \delta)}^T(f', f) = \frac{1 - \left(\frac{f'}{f}\right)^2}{n\lambda\frac{f'}{f} + \delta} \frac{1}{n+1} \times \frac{n^3(1-\lambda)\lambda^2 + n^2\lambda\delta\left(\frac{f'}{f} + \lambda\right) + n\lambda\delta\left(\frac{f'}{f} + \delta\right) + (1-\delta)\delta^2}{\left(n\lambda\frac{f'}{f} + \delta\right)\left(\frac{\delta\frac{f'}{f} + n\lambda}{\delta\frac{f'}{f} + n\lambda\left(\frac{f'}{f}\right)^2}\right)^n - \frac{f'}{f}\left(\delta\frac{f'}{f} + n\lambda\right)}, \quad [28]$$

where  $G_{n+1}(\lambda, \delta)$  denotes the weighted self-looped star graph with  $n$  leaves. In the limit of  $n \rightarrow \infty$ , when  $\lambda$  and  $\delta$  are independent of  $n$ , Eq. 28 becomes,

$$\lim_{n \rightarrow \infty} \phi_{G_{n+1}(\lambda, \delta)}^T(f', f) = \begin{cases} \left(1 - \left(\frac{f'}{f}\right)^2\right)(1-\lambda), & \text{if } f' > f, \\ 0 & \text{otherwise.} \end{cases} \quad [29]$$

We use two versions of this weighted graph by first setting  $\lambda = \delta = 1$  in the above equation that results in the unweighted star graph, which, however, is a suppressor in the limit  $n \rightarrow \infty$  under temperature initialization. This is reflected by  $\lim_{n \rightarrow \infty} \phi_{G_{n+1}(\lambda=1, \delta=1)}^T(f', f) = 0$  for all  $f'$  and  $f$ . Setting instead  $\lambda = \frac{1}{n}$  and  $\delta = \frac{1}{n^2}$  followed by taking the infinite population size limit of Eq. 28 yields a structure that is an amplifier for  $n \rightarrow \infty$ . That is,

$$\lim_{n \rightarrow \infty} \phi_{G_{n+1}(\lambda, \delta)}^T(f', f) = \begin{cases} 1 - \left(\frac{f'}{f}\right)^2, & \text{if } f' > f, \\ 0 & \text{otherwise.} \end{cases} \quad [30]$$

**D. Large- $N$  Steady-State Fitness Statistics of the Simple Star Graph.** Here, we derive the steady-state statistics for the star graph (without self-loops, unweighted) for large, but finite,  $n$  ( $= N - 1$ ) under temperature initialization. To do so, we work with the uniform mutational offspring fitness distribution. In that case, from Eq. 4, we know that the steady-state fitness distribution of a graph depends only on the fixation probabilities. Therefore, to derive the steady-state distribution for the star graph in the limit of large  $n$ , we first approximate the temperature-initialized fixation probability,  $\phi_{G_{n+1}(\lambda=1, \delta=1)}^T(f', f)$ . Unless specified, we use the shorthand  $G_{n+1}$  to denote a star graph (without self-loops, unweighted) with  $n$  leaves. To approximate the fixation probability, we first set  $\lambda = 1$  and  $\delta = 1$  and then perform a Taylor expansion of Eq. 28 around  $1/n = 0$ , leading to

$$\phi_{G_{n+1}}^T(f', f) = \begin{cases} \frac{\left(\frac{f'}{f}-1\right)\left(1+\frac{f'}{f}\right)^2}{n\left(\frac{f'}{f}\right)^2} + \mathcal{O}\left(\frac{1}{n^2}\right), & \text{if } f' > f, \\ \frac{\left(1-\frac{f'}{f}\right)\left(1+\frac{f'}{f}\right)^2}{n\left(\frac{f'}{f}\right)^2} \left(\frac{f'}{f}\frac{n\frac{f'}{f}+1}{\left(\frac{f'}{f}+n\right)}\right)^n \\ + \mathcal{O}\left(\frac{1}{n^2}\right), & \text{if } f' \leq f. \end{cases} \quad [31]$$

Thus, for large  $N$ ,  $\phi_{G_{n+1}}^T(f', f) \sim 1/n$ , which makes the star graph a suppressor of selection under temperature initialization

for infinite  $n$ . This is in accordance with the infinite  $n$  limit of  $\phi_{G_{n+1}(\lambda=1, \delta=1)}^T(f', f)$  that we saw in the previous section.

To make use of the approximated fixation probability shown in Eq. 31, we write the denominator appearing in the steady-state distribution (Eq. 4) as

$$\int_{f_{\min}}^{f_{\max}} df' \frac{\phi_{G_{n+1}}^T(f', f)}{\phi_{G_{n+1}}^T(f, f')} = \int_{f_{\min}}^f df' \underbrace{\frac{\phi_{G_{n+1}}^T(f', f)}{\phi_{G_{n+1}}^T(f, f')}}_{\Gamma_3} + \int_f^{f_{\max}} df' \underbrace{\frac{\phi_{G_{n+1}}^T(f', f)}{\phi_{G_{n+1}}^T(f, f')}}_{\Gamma_4}. \quad [32]$$

Notice that the  $1/n$  scaling of the fixation probabilities responsible for the suppression of selection for a large-sized star graph drops out in both the integrands. Putting it differently, the steady-state fitness decreasing contribution coming from the poor beneficial mutant fixation profile has been compensated by the deleterious mutant fixation profile. As a side remark, the steady-state statistics for a general graph  $G$  is invariant under the scaling of the fixation profile  $\phi_G^T$  by any  $n$ -dependent bounded function  $g(n)$ , i.e.,  $P_G^*[g\phi_G^T] = P_G^*[\phi_G^T]$ .

Now, for the integrand  $\Gamma_3$ ,  $f' \leq f$ , whereas for  $\Gamma_4$ ,  $f' > f$ . The integrand  $\Gamma_3$  can be simplified as,

$$\begin{aligned} \Gamma_3 &= \frac{\frac{(1-\frac{f'}{f})(1+\frac{f'}{f})^2}{n\left(\frac{f'}{f}\right)^2} \left(\frac{f'}{f}\frac{n\frac{f'}{f}+1}{\left(\frac{f'}{f}+n\right)}\right)^n}{\frac{(1-\frac{f'}{f})(1+\frac{f'}{f})^2}{n\frac{f'}{f}}} \\ &= \left(\frac{f'}{f}\right)^{n-1} \left(\frac{n\frac{f'}{f}+1}{\frac{f'}{f}+n}\right)^n \\ &= \left(\frac{f'}{f}\right)^{2n-1} \left(\frac{1+\frac{f}{nf'}}{1+\frac{f'}{nf}}\right)^n \\ &\approx \left(\frac{f'}{f}\right)^{2n-1} \exp\left(\frac{f}{f'} - \frac{f'}{f}\right), \end{aligned} \quad [33]$$

where in the last line, we have used the limit definition of the exponential function by assuming large  $n$ ,  $\exp(x) \approx (1 + \frac{x}{n})^n$  for large  $n$ . Furthermore, if we assume  $f, f' \ll n$ , the dominant contribution to the integrand  $\Gamma_3$  then comes from the  $n$  dependent term, and, thus,  $\Gamma_3$  simplifies to

$$\Gamma_3 \approx \left(\frac{f'}{f}\right)^{2n-1}. \quad [34]$$

Similarly,  $\Gamma_4$  takes the form,

$$\Gamma_4 \approx \left(\frac{f'}{f}\right)^{2n-1}. \quad [35]$$

Since the integrands  $\Gamma_3$  and  $\Gamma_4$  are identical, Eq. 32 reduces to

$$\begin{aligned} \int_{f_{\min}}^{f_{\max}} df' \frac{\phi_{G_{n+1}}^T(f', f)}{\phi_{G_{n+1}}^T(f, f')} &= \int_{f_{\min}}^{f_{\max}} df' \left(\frac{f'}{f}\right)^{2n-1} \\ &= \frac{f_{\max}^{2n} - f_{\min}^{2n}}{2n} \frac{1}{f^{2n-1}}. \end{aligned} \quad [36]$$

This gives us the steady-state fitness distribution for the star graph in the large- $n$  limit,

$$P_{G_{n+1}}^*(f) = \frac{2n}{f_{\max}^{2n} - f_{\min}^{2n}} f^{2n-1}. \quad [37]$$

With this, we can now compute the average steady-state fitness for the star graph in the large- $n$  limit,

$$\begin{aligned} \langle f \rangle_{G_{n+1}}^* &= \int df f P_{G_{n+1}}^*(f) \\ &= \frac{2n}{f_{\max}^{2n} - f_{\min}^{2n}} \int_{f_{\min}}^{f_{\max}} df f \cdot f^{2n-1} \\ &= \frac{2n}{2n+1} \frac{f_{\max}^{2n+1} - f_{\min}^{2n+1}}{f_{\max}^{2n} - f_{\min}^{2n}} \\ &\approx f_{\max}, \end{aligned} \quad [38]$$

where in the last line, we have again made use of the large- $n$  approximation. Therefore, the steady-state average fitness for the star graph asymptotes to  $f_{\max}$  for large population size. In Fig. 3C, we have seen that for small  $n$ , the star graph attains higher steady-state average fitness in the mutation-selection balance than the complete graph. To see if this holds for large  $n$  as well, we study the quantity  $\langle f \rangle_{G_{n+1}}^* - \langle f \rangle_C^*$ .

$$\begin{aligned} \langle f \rangle_{G_{n+1}}^* - \langle f \rangle_C^* &= \frac{2n}{2n+1} \frac{f_{\max}^{2n+1} - f_{\min}^{2n+1}}{f_{\max}^{2n} - f_{\min}^{2n}} \\ &\quad - \frac{n+1}{n+2} \frac{f_{\max}^{n+2} - f_{\min}^{n+2}}{f_{\max}^{n+1} - f_{\min}^{n+1}} \\ &= \frac{f_{\max}}{2n} + \mathcal{O}\left(\frac{1}{n^2}\right). \end{aligned} \quad [39]$$

Because  $\frac{f_{\max}}{2n} > 0$ , in the large- $n$  limit, the star graph—a suppressor of fixation—attains higher steady-state average fitness in the mutation-selection balance than the complete graph.

**E. Mixing Time for Single Rooted Graphs.** For any one-rooted network with self-loops, we can use Eq. 2 to find an exact expression for the full temporal statistics,  $P_G(f, t)$ , when mutational fitness jump distribution is uniform. To do so, we first note that the fixation probabilities become independent of fitness values,  $\phi_G^T(f, f') = \phi_G^T(f', f) = \frac{T_r}{N}$ , where  $T_r$  is the temperature of the root node. Substituting the fixation probabilities in Eq. 2, and using the normalization condition for  $P_G(f', t)$ , we obtain a first-order ordinary differential equation for  $P_G(f, t)$  in time,

$$\frac{\partial P_G(f, t)}{\partial t} = \frac{\mu T_r}{N} \left( \frac{1}{f_{\max} - f_{\min}} - P_G(f, t) \right). \quad [40]$$

Solving this equation, we obtain

$$P_G(f, t) = \frac{1}{f_{\max} - f_{\min}} - \left( \frac{1}{f_{\max} - f_{\min}} - P_G(f, 0) \right) e^{-\frac{\mu T_r t}{N}}. \quad [41]$$

From this expression, we find that in the limit  $t \rightarrow \infty$ , the dynamics for a single rooted graph becomes completely random. That is, at long times, a population spends equal time in all the fitness states. On comparing with Eq. 7, we find that the mixing time—i.e., the number of mutations required to reach the steady-state—for these graphs scales as  $\frac{N}{T_r \mu}$ .

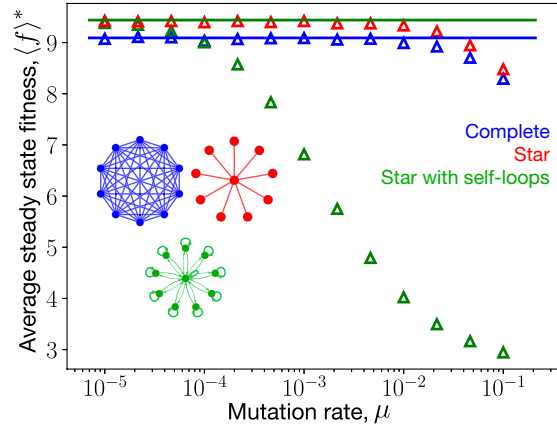


**Fig. 7.** Deviation from the low mutation rate approximation. Using the Moran Bd simulations, the average steady-state fitness attained in the mutation-selection balance is plotted as a function of mutation rate, which is identical to the mutation probability with a single Moran Bd update step as the unit of time. Parameters are the same as those of Fig. 3. We observe that the self-looped star is much more restrictive to low mutation approximation than the other two graphs. The reason for this is its much higher fixation time. On the other hand, for the star graph, the low mutation approximation is valid in a similar regime as for the complete graph. Again, this is due to its fixation time being the same order as the complete graph under temperature initialization. Outside the weak mutation regime, the star continues to maintain higher steady-state average fitness, while the steady-state fitness for the self-looped star graph, an amplifier of selection, falls rapidly.

As a result, the mixing time for a single rooted graph can be modulated by changing the temperature of the root node. Moreover, the average fitness for the case of a single-rooted graph (root with self-loops) with temperature  $T_r$  can be found using Eq. 41,

$$\langle f(t) \rangle_G = \frac{f_{\max} + f_{\min}}{2} - \left( \frac{f_{\max} + f_{\min}}{2} - \langle f(0) \rangle_G \right) e^{-\frac{\mu T_r t}{N}}. \quad [42]$$

In the limit  $t \rightarrow \infty$ , the average fitness converges to the average of the fitness domain. We also note that the steady state for single rooted graphs (with self-loops) is independent of the choice of phenotype-fitness map—simply because the fixation probability for these graphs does not depend on fitness.

**F. Deviation from the Low Mutation Rate Approximation.** The weak mutation approximation works well if the time between two successive mutation events is much longer than the average time it takes for the fixation or extinction of a mutant. Thus, there exists an upper bound for the mutation rate, above which the dynamics starts showing deviation from the weak mutation approximation. For the case of an evolutionary game in a well-mixed population, this upper bound for the mutation rate is derived in ref. 50. The validity of the low mutation rate approximation depends not only on the mutation rates, but also the fixation time. Previous studies have indicated that, compared to the complete graph, the graphs with higher fixation times call for lower mutation rates for this approximation to hold (25, 31, 33). Here, we verify these predictions. In Fig. 7, we find that, compared to the complete graph, the self-looped star graph is very restrictive to the low-mutation-rate approximation. On the other hand, in the star graph, a suppressor of fixation, the threshold mutation rate value for the deviation from the low mutation rate approximation is similar to the complete graph. This may be unexpected, as for uniform

initialization, the fixation time for the star graph is an order of magnitude higher than for the complete graph. However, here, we are dealing with temperature-initialized sequential dynamics, where the fixation time for the star graph becomes almost the same as that of the complete graph, at least for small population sizes, while the fixation times for self-looped star remains much higher. Also, the star not only attains a higher steady-state average fitness than the complete graph under the weak mutation approximation, but also outside the weak mutation regime. In contrast, the self-looped star graph, an amplifier of selection, performs poorly outside the weak mutation rate regime by attaining lower steady-state

average fitness than the complete graph. Therefore, in general, an amplifier of selection does not maximize fitness.

**Data, Materials, and Software Availability.** Code to reproduce figures and underlying data (Mathematica files/Jupyter notebooks) has been deposited in GitLab ([https://gitlab.gwdg.de/mpievolbio-sci/DynamicsOnGraphs\\_LowMutationRate.git](https://gitlab.gwdg.de/mpievolbio-sci/DynamicsOnGraphs_LowMutationRate.git)) (51).

**ACKNOWLEDGMENTS.** We are grateful to the members of the Evolutionary Theory department and the Dynamics of Social Behavior group for continuous discussions. We thank Carsten Fortmann-Grote for assistance with computer cluster usage.

1. E. Lieberman, C. Hauert, M. A. Nowak, Evolutionary dynamics on graphs. *Nature* **433**, 312–316 (2005).
2. M. Broom, J. Rychtář, B. Stadler, Evolutionary dynamics on small-order graphs. *J. Interdiscip. Math.* **12**, 129–140 (2009).
3. T. Monk, P. M. P. Green, Martingales and fixation probabilities of evolutionary graphs. *Proc. R. Soc. A Math. Phys. Eng. Sci.* **470**, 20130730 (2014).
4. L. Hindersin, B. Wu, A. Traulsen, J. García, Computation and simulation of evolutionary game dynamics in finite populations. *Sci. Rep.* **9**, 6946 (2019).
5. Y. P. Kuo, C. Nombela-Arrieta, O. Carja, A theory of evolutionary dynamics on any complex spatial structure. *bioRxiv* [Preprint] (2021). <https://www.biorxiv.org/content/10.1101/2021.02.07.430151v1>. Accessed 10 July 2022.
6. J. Tkadlec, A. Pavlogiannis, K. Chatterjee, M. A. Nowak, Limits on amplifiers of natural selection under death-birth updating. *PLOS Comput. Biol.* **16**, e1007494 (2020).
7. M. Kimura, Evolutionary rate at the molecular level. *Nature* **217**, 624–626 (1968).
8. D. M. McCandlish, C. L. Epstein, J. B. Plotkin, Formal properties of the probability of fixation: Identities, inequalities and approximations. *Theor. Popul. Biol.* **99**, 98–113 (2015).
9. M. A. Nowak, *Evolutionary Dynamics: Exploring the Equations of Life* (Harvard University Press, Cambridge, MA, 2006).
10. S. Gaiotto, J. Arranz, A. Traulsen, Invasion and effective size of graph-structured populations. *PLOS Comput. Biol.* **14**, e1006559 (2018).
11. L. Hindersin, A. Traulsen, Most undirected random graphs are amplifiers of selection for birth-death dynamics, but suppressors of selection for death-birth dynamics. *PLOS Comput. Biol.* **11**, e1004437 (2015).
12. D. L. Hartl, C. H. Taubes, Towards a theory of evolutionary adaptation. *Genetica* **102–103**, 525–533 (1998).
13. S. Yagoobi, H. Yousefi, K. A. Samani, Mutation-selection stationary distribution in structured populations. *Phys. Rev. E* **98**, 042301 (2018).
14. A. McAvoy, B. Adlam, B. Allen, M. A. Nowak, Stationary frequencies and mixing times for neutral drift processes with spatial structure. *Proc. R. Soc. A Math. Phys. Eng. Sci.* **474**, 20180238 (2018).
15. T. Antal, S. Redner, V. Sood, Evolutionary dynamics on degree-heterogeneous graphs. *Phys. Rev. Lett.* **96**, 188104 (2006).
16. M. Newman, *Networks* (Oxford University Press, Oxford, UK, 2018).
17. L. Hindersin, B. Werner, D. Dingli, A. Traulsen, Should tissue structure suppress or amplify selection to minimize cancer risk? *Biol. Direct* **11**, 41 (2016).
18. B. Allen *et al.*, Fixation probabilities in graph-structured populations under weak selection. *PLOS Comput. Biol.* **17**, e1008695 (2021).
19. K. Kaveh, N. L. Komarova, M. Kohandel, The duality of spatial death-birth and birth-death processes and limitations of the isothermal theorem. *R. Soc. Open Sci.* **2**, 140465 (2015).
20. B. Adlam, K. Chatterjee, M. A. Nowak, Amplifiers of selection. *Proc. R. Soc. A Math. Phys. Eng. Sci.* **471**, 20150114 (2015).
21. D. M. McCandlish, A. Stoltzfus, Modeling evolution using the probability of fixation: History and implications. *Q. Rev. Biol.* **89**, 225–252 (2014).
22. C. W. Gardiner, *Handbook of Stochastic Methods, Springer Series in Synergetics*, vol. 13 (Springer, Berlin, ed. 3, 2004).
23. N. van Kampen, *Stochastic Processes in Physics and Chemistry* (North Holland, Amsterdam, 2007).
24. G. Sella, A. E. Hirsh, The application of statistical physics to evolutionary biology. *Proc. Natl. Acad. Sci. U.S.A.* **102**, 9541–9546 (2005).
25. J. Tkadlec, A. Pavlogiannis, K. Chatterjee, M. A. Nowak, Fast and strong amplifiers of natural selection. *Nat. Commun.* **12**, 4009 (2021).
26. J. H. Gillespie, A simple stochastic gene substitution model. *Theor. Popul. Biol.* **23**, 202–215 (1983).
27. H. A. Orr, The genetic theory of adaptation: A brief history. *Nat. Rev. Genet.* **6**, 119–127 (2005).
28. A. Pavlogiannis, J. Tkadlec, K. Chatterjee, M. A. Nowak, Construction of arbitrarily strong amplifiers of natural selection using evolutionary graph theory. *Commun. Biol.* **1**, 71 (2018).
29. D. A. Levin, Y. L. Peres, E. Wilmer, *Markov Chains and Mixing Times* (American Mathematical Society, Providence, RI, 2009).
30. C. Hadjichrysanthou, M. Broom, J. Rychtář, Evolutionary games on star graphs under various updating rules. *Dyn. Games Appl.* **1**, 386–407 (2011).
31. M. Frean, P. B. Rainey, A. Traulsen, The effect of population structure on the rate of evolution. *Proc. Biol. Sci.* **280**, 20130211 (2013).
32. M. Möller, L. Hindersin, A. Traulsen, Exploring and mapping the universe of evolutionary graphs identifies structural properties affecting fixation probability and time. *Commun. Biol.* **2**, 137 (2019).
33. J. Tkadlec, A. Pavlogiannis, K. Chatterjee, M. A. Nowak, Population structure determines the tradeoff between fixation probability and fixation time. *Commun. Biol.* **2**, 138 (2019).
34. J. Cairns, Mutation selection and the natural history of cancer. *Nature* **255**, 197–200 (1975).
35. M. Nowak, F. Michor, Y. Iwasa, The linear process of somatic evolution. *Proc. Natl. Acad. Sci. U.S.A.* **100**, 14966–14969 (2003).
36. P. P. Chakraborty, L. R. Nemzer, R. Kassen, Experimental evidence that metapopulation structure can accelerate adaptive evolution. *bioRxiv* [Preprint] (2021). <https://www.biorxiv.org/content/10.1101/2021.07.13.452242v1>. Accessed 10 July 2022.
37. S. van Vliet, C. Hauert, K. Fridberg, M. Ackermann, A. Dal Co, Global dynamics of microbial communities emerge from local interaction rules. *PLOS Comput. Biol.* **18**, e1009877 (2022).
38. G. W. Constable, A. J. McKane, Population genetics on islands connected by an arbitrary network: An analytic approach. *J. Theor. Biol.* **358**, 149–165 (2014).
39. B. Allen *et al.*, Transient amplifiers of selection and reducers of fixation for death-birth updating on graphs. *PLOS Comput. Biol.* **16**, e1007529 (2020).
40. S. Yagoobi, A. Traulsen, Fixation probabilities in network structured meta-populations. *Sci. Rep.* **11**, 17979 (2021).
41. L. Marrec, I. Lamberti, A. F. Bitbol, Toward a universal model for spatially structured populations. *Phys. Rev. Lett.* **127**, 218102 (2021).
42. A. McAvoy, B. Allen, Fixation probabilities in evolutionary dynamics under weak selection. *J. Math. Biol.* **82**, 14 (2021).
43. T. Monk, Martingales and the fixation probability of high-dimensional evolutionary graphs. *J. Theor. Biol.* **451**, 10–18 (2018).
44. M. Askari, K. A. Samani, Analytical calculation of average fixation time in evolutionary graphs. *Phys. Rev. E Stat. Nonlin. Soft Matter Phys.* **92**, 042707 (2015).
45. B. Ottino-Löffler, J. G. Scott, S. H. Strogatz, Takeover times for a simple model of network infection. *Phys. Rev. E* **96**, 012313 (2017).
46. D. Hathcock, S. H. Strogatz, Fitness dependence of the fixation-time distribution for evolutionary dynamics on graphs. *Phys. Rev. E* **100**, 012408 (2019).
47. T. Monk, A. van Schaik, Wald's martingale and the conditional distributions of absorption time in the Moran process. *Proc. Math. Phys. Eng. Sci.* **476**, 20200135 (2020). Correction in: *Proc. Math. Phys. Eng. Sci.* **476**, 20200731 (2020).
48. Y. P. Kuo, O. Carja, Evolutionary graph theory beyond pairwise interactions: Higher-order network motifs shape times to fixation in structured populations. *bioRxiv* [Preprint] (2021). <https://www.biorxiv.org/content/10.1101/2021.06.26.450017v1>. Accessed 10 July 2022.
49. T. Monk, A. van Schaik, Martingales and the fixation time of evolutionary graphs with arbitrary dimensionality. *R. Soc. Open Sci.* **9**, 220011 (2022).
50. B. Wu, C. S. Gokhale, L. Wang, A. Traulsen, How small are small mutation rates? *J. Math. Biol.* **64**, 803–827 (2012).
51. N. Sharma, A. Traulsen, *DynamicsOnGraphs\_LowMutationRate*. GitLab. [https://gitlab.gwdg.de/mpievolbiosci/DynamicsOnGraphs\\_LowMutationRate.git](https://gitlab.gwdg.de/mpievolbiosci/DynamicsOnGraphs_LowMutationRate.git). Deposited 9 July 2022.

## Chapter 3

# On the role of deleterious mutant regime in steering long-term evolution

In Chapter 2, we found an example where the graph, despite being a suppressor of fixation could achieve higher fitness than the well-mixed population. This serves as the first instance where the deleterious mutant regime can significantly influence the long-term evolution. In this chapter, we aim to determine whether the results from the previous chapter were a special case. If not, it would imply that the role of the deleterious mutant regime is much more general than what the studies on well-mixed populations tend to ignore.

The work in this chapter was carried out in collaboration with Suman G. Das (University of Bern), Joachim Krug (University of Cologne), and Arne Traulsen. We are currently awaiting final confirmation from all co-authors regarding the manuscript draft. The submission to a scientific journal is planned accordingly. Detailed information about the authors' contributions can be found at the end of the thesis.

## Abstract

Birth-death models have long been employed to understand the interplay of genetic drift and natural selection in evolving populations. While well-mixed populations are insensitive to the choice of the individual type for replacement—parent or offspring—this choice strongly influences the evolutionary outcomes for spatially structured populations. Moving parent individuals to vacant sites gives rise to new update rules, leading to new fixation categories for spatial graphs. We discover a new category of graphs, amplifiers of selection, where a structure has a higher probability of fixation for mutants than the well-mixed population, regardless of its fitness value. Under death-Birth updating with parents moving to vacant sites, the star graph is an amplifier of fixation. For very large population sizes, the fixation probability to fix deleterious mutants on the star graph converges to a non-zero value, contradicting the result from well-mixed populations where the probability goes to zero. Additionally, most random graphs are amplifiers of fixation for death-Birth updating, with parent individuals replacing dead individuals. Conversely, most random graphs are suppressors of fixation—graphs with lower fixation probability for mutants than the well-mixed population regardless of their fitnesses—for Birth-death updating with offspring replacing dead individuals. When subjected to long-term evolution, amplifiers of fixation, despite being more efficient at fixing beneficial mutants, attain lower fitness than the well-mixed population, whereas suppressors attain higher fitness despite their inferior ability to fix beneficial mutants. These surprising findings can be explained by their deleterious mutant regime. Therefore, the deleterious mutant regime is equally crucial as the beneficial mutant regime for adaptive evolution.

## 3.1 Introduction

Spatial structures can substantially impact the evolution of a population [1, 26, 2, 55]. Understanding the role of spatial structures in evolutionary biology is crucial and demands moving beyond the commonly assumed well-mixed populations [11]. Evolutionary graph theory provides a platform where spatially structured populations are modelled as graphs [18], with each node representing asexually reproducing individuals and the links defining the interaction neighbourhood of nodes. In this framework, a complete graph rep-

resents a well-mixed population where each node interacts with every other node with equal propensity. Fixation probability and fixation time are two intensively studied observables in evolutionary graph theory. Fixation probability of a mutant denotes the probability of the mutant taking over the population of wild-types [31, 19, 56, 57], while fixation time represents the duration it takes for this process to occur [58, 59, 30, 60]. Unlike fixation probability, fixation time of a mutant is a random variable with a specific distribution, and the quantity of interest generally is the average fixation time [61].

Fixation probability is an important quantity in evolutionary biology, as it determines the rate of evolution [38, 62, 39]. During a fixation dynamics, two key evolutionary forces are at play— natural selection and genetic drift. Spatial structures possess the ability to modulate the strength of these forces. With the well-mixed population serving as the reference, structures that amplify the strength of selection are termed amplifiers of selection (*AoS*), while those that suppress it are referred to as suppressors of selection (*SoS*) [18, 19]. An *AoS* is a graph that has a higher probability of fixing beneficial mutants and a lower probability of fixing deleterious mutants compared to the complete graph. On the other hand, a *SoS* is a graph that has a lower probability of fixing beneficial mutants and a higher probability of fixing deleterious mutants.

In general, graphs can be weighted and directed [63, 36, 41]. This means that an individual may not interact with its neighbor as strongly as the neighbor interacts with the focal individual. In this work, we focus on unweighted and undirected graphs. The precise form of the interactions among individuals is determined by an update rule. The commonly studied update rules in evolutionary graph theory are the Moran Birth-death (Bd) and the Moran death-Birth (dB) [20, 21]. The shorthand Bd indicates that the birth event precedes the death event. The uppercase B suggests that selection operates during the birth event, while the lowercase d represents the neutral nature of the death event. This offers various choices for the birth-death updates [64]. The fixation probability of a mutant on a graph depends crucially on the update rule [65]. In Ref. [37], it was found that for Bd updating, most of the small random graphs are *AoS*, whereas under dB updating, most of the random graphs are *SoS*.

Not only the update rules, but also the node where the mutant initially appears substantially affects the fixation probability. Mutant initialisation schemes determine the likelihood for a node to be initialised with the mutant.

Two well-known schemes are uniform mutant initialisation and temperature mutant initialisation [28]. Under uniform mutant initialisation, every node is equally likely to be initialised with the mutant. For temperature initialisation, the initial mutant appears on nodes with higher turnover rates. The star graph is an *AoS* under Moran Bd updating with uniform mutant initialisation. However, for temperature initialisation, the star graph is a suppressor of fixation (*SoF*)—a graph with lower probability of fixing a mutant than the well-mixed population, regardless of the mutant’s fitness.

Recently, a few studies went beyond the fixation time scales and explored mutation-selection balance on graphs [48, 66]. When the uniform initialised star graph (an *AoS*) was subjected to long-term mutation-selection dynamics, it achieved a higher average steady-state fitness compared to the complete graph [53]. This outcome was anticipated because an *AoS* is more efficient at fixing beneficial mutants and preventing the fixation of deleterious mutants. Surprisingly, the temperature initialised star graph, despite being a *SoF*, not only attained a higher fitness than the complete graph but also the same as the uniform initialised star graph. This surprising result can be explained by the temperature initialised star graph’s efficient ability to reject deleterious mutants, compensating for its inability to fix beneficial mutants. To our knowledge, this is the only known example so far where the deleterious mutant regime has the potential to influence long-term evolution. But how common are *SoFs* for temperature initialised Bd updating? Do all of *SoFs* attain higher fitness than the complete graph despite having lower probabilities of fixing advantageous mutants? What about dB updating? Does the deleterious mutant regime play any significant role for dB long-term dynamics? We explore all of these questions here.

The structure of this paper is outlined as follows. We begin by establishing a connection between update rules and mutant initialisation schemes. These schemes naturally arise from the choice of individuals moving to vacant nodes— either the parent-type offspring or the mutant offspring. Subsequently we study the star graph and Erdős-Rényi random graphs at short-term fixation time scales, considering various update rules. Notably, we observe that the star graph acts as an amplifier of fixation (*AoF*) under temperature initialised dB updating with a higher probability of fixing mutants compared to the complete graph, regardless of the fitness value. Similarly, we find that most of the small random graphs are *AoFs* under temperature initialised dB updating and *SoFs* under temperature initialised Bd updating. Additionally, we study the star graph and random graphs under long-term

mutation-selection dynamics. Surprisingly, despite being *SoFs*, most of the random graphs achieve higher fitness than the complete graph for temperature initialised Bd updating whereas, most of the random graphs attain lower fitness for temperature initialised dB updating despite being *AoFs*.

### 3.2 Update mechanisms in graph structured populations

When working with spatial structures, the choice of update rule substantially affects the dynamics. An evolutionary update rule is not just about the order of the birth and death events and the choice of event(s) where selection operates, but also the process by which new mutations appear in the population.

The mutant initialisation scheme  $\mathcal{I}$  denotes the probability distribution with which an initial mutant appears on a node,  $p = (p_0, p_1, \dots, p_{N-1})$ . For example, in the uniform mutant initialisation scheme  $\mathcal{U}$ , we have  $p_i = 1/N$  for all nodes  $i$ , i.e., a mutant appears in every node with the same probability. Similarly, for the temperature initialisation scheme  $\mathcal{T}$ , the probability for a node to receive an initial mutant is proportional to the temperature (sum of incoming/outgoing weight) of the node.

As an example for temperature initialisation, let us focus on the Moran Birth-death (Bd) update rule with the offspring moving to another site [28]: First an individual is selected with probability proportional to its fitness to give birth to an offspring. The offspring either resembles its parent with probability  $1 - \mu$  or is a mutant with probability  $\mu$ . Then the offspring takes over the node of a random neighboring individual chosen to die. Therefore, in a population where every individual has the same fitness, the first mutant is more likely to appear on nodes with higher in-degree. To be specific, the probability that a mutant appears in a node is the in-temperature,  $\mathcal{T}^{\text{in}}$ . More formally, the probability that the initial mutant appears on a node  $i$  of a homogenous population is equal to,

$$\begin{aligned} p_i &= \frac{1}{N} \sum_{j \in \mathcal{N}_i} \frac{a_{ji}}{\sum_{k \in \mathcal{N}_j} a_{jk}}, \\ &= \frac{1}{N} \mathcal{T}_i^{\text{in}}. \end{aligned} \tag{3.1}$$



Here,  $a_{lm}$  is an element of the adjacency matrix  $\mathbf{A}$  with value equal to 1 if there is link directed from node  $l$  to  $m$ , 0 otherwise.  $\mathbf{A}$  is a symmetric matrix for undirected graphs.  $\mathcal{N}_i$  is a set containing neighbors of node  $i$ . For further examples for this update mechanism, see also Refs. [67, 68].

So far, we assumed that the offspring moves to a neighboring node while the parent remains at its position, see Fig. 3.1 A. To denote this, we use the shorthand  $\text{Bd}^o$  where the superscript represent the offspring moving to a vacant site. With the same assumption, for death-Birth updating  $\text{dB}^o$ , the mutant initialisation is uniform: The probability that an initial mutant appears in node  $i$  under  $\text{dB}^o$  updating is equal to  $1/N$ .

However, a priori there is no reason why the offspring individual moves and not the parent. To explore other possibilities, we consider the case where the parent moves to the neighboring node and the offspring stays at the original node, see Fig. 3.1 B. These update rules will be denoted by the superscript  $p$ . The probability that the initial mutant under  $\text{dB}^p$  arises in node  $i$  is

$$\begin{aligned} p_i &= \frac{1}{N} \sum_{j \in \mathcal{N}_i} \frac{a_{ij}}{\sum_{k \in \mathcal{N}_j} a_{kj}}, \\ &= \frac{1}{N} \mathcal{T}_i^{\text{out}}. \end{aligned} \tag{3.2}$$

This means that the mutant initialisation for  $\text{dB}^p$  updating with parent-type offspring moving to a vacant node is out-temperature initialised. For unweighted and undirected graphs  $\mathcal{T}^{\text{in}} = \mathcal{T}^{\text{out}}$ . For weighted graphs, in the definitions of  $\mathcal{T}^{\text{in}}$  and  $\mathcal{T}^{\text{out}}$ , all elements of the adjacency matrix must be replaced with the elements of the weight matrix,  $\mathbf{W}$ . Note that for the complete graph the choice of individual moving to vacant node is irrelevant due to the symmetry of the graph.

In the literature, it has been suggested that for dB updating temperature initialisation does not exist [54]. This is true when the offspring individuals moves to a neighbouring node. But when we instead assume that the parent moves, we obtain the temperature initialised dB update. Moreover, for  $\text{Bd}^p$  updating with the parent moving to the vacant node recovers the uniform mutant initialisation.

Tab. 3.1 C lists the combination of update rules and the choice of individual moving to vacant site leading to different mutant initialisation schemes.

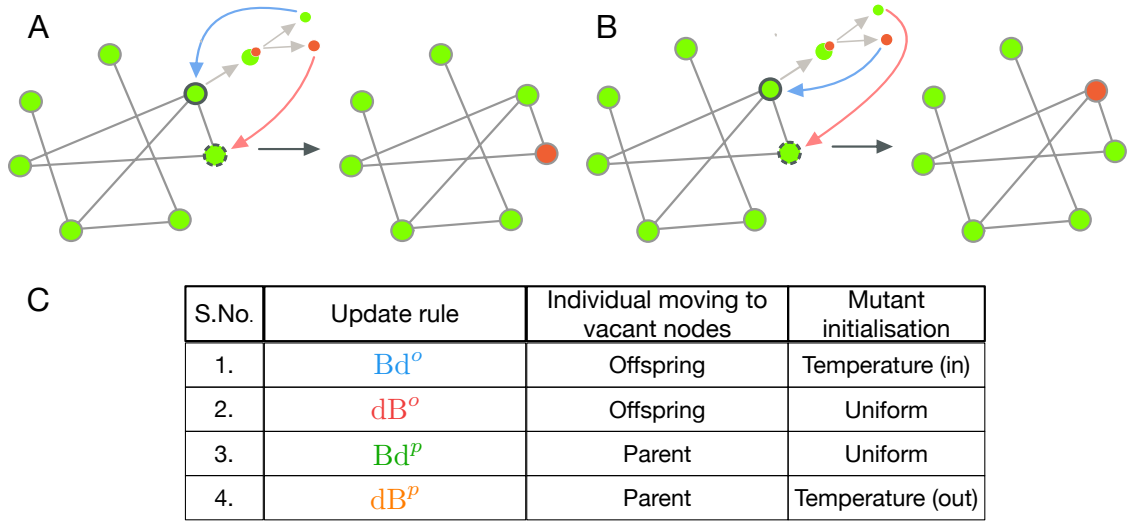


**Figure 3.1: Type of individuals moving to vacant sites and mutant initialisation schemes.** Mutant initialisation scheme, the likelihood that the initial mutant appears on a given node in a homogenous fitness background, comes out automatically from the evolutionary update rule. The choice of individual, wild-type (green) or mutant (red), moving to vacant node additionally contributes in deciding the mutant initialisation. This is shown via panels A and B. Additionally, an individual chosen for birth is encircled by solid line while the one chosen for death is encircled by dashed line. The birth event results in two offspring. During mutation, one offspring is a wild-type (parent) and the other one is a mutant. In panel A, the mutant offspring moves to the death site. For the  $Bd$  updating, the resulting initialisation scheme is temperature initialised— equivalent to  $Bd^o$ , and for  $dB$  updating, it is uniform initialised— equivalent to  $dB^o$ . Similarly, in panel B the parent-type offspring moves to the vacant node while the mutant offspring resides at the birth site. Parent-type offspring moving to vacant site leads to uniform initialised  $Bd$ , equivalent to  $Bd^p$  and temperature initialised  $dB$  update rule, equivalent to  $dB^p$ . Tab. C lists the combinations of update rule and the choice of individual moving to vacant site.

### 3.3 Short time scales: Fixation dynamics

In evolutionary graph theory, the typical focus is on the fixation probability of a mutant. The fixation probability of a mutant on a given graph depends crucially on the node where it first appears. To make this explicit, we denote  $\phi_{G,i}(f', f)$  as the fixation probability of a mutant with fitness  $f'$  in a wild-type population of fitness  $f$  on a graph  $G$  starting from node  $i$ . Again, the mutant does not arise in every node  $i$  with the same probability  $p_i$ . The average fixation probability of a mutant on graph  $G$  is

$$\Phi_G^{\mathcal{I}}(f', f) = \sum_{i=0}^{N-1} p_i \cdot \phi_{G,i}(f', f). \quad (3.3)$$

Here  $\mathcal{I}$  is the mutant initialisation scheme, which arises from the update rule, as discussed above.

Next, we study fixation probabilities on the star graph and random graphs for different update rules.

#### 3.3.1 The star graph

The star graph has been intensively studied in evolutionary graph theory, as it is highly inhomogeneous but still analytical tractable [52]. The Moran Bd process was intensively studied on the star graph in [18]. Since then the star graph is popularly known as the prime example of an *AoS* for uniform mutant initialisation which can even be solved exactly [49, 51] for various update rules including the ones that have not been discussed here like bD, Db [50]. However, the star graph fails to amplify selection if the initial mutant appears as per temperature initialisation scheme where leaves are more likely to receive the initial mutant [28]. Under temperature initialised Bd updating, the star is instead a *SoF* [53], see Fig 3.2 A and a *SoS* for uniform initialised dB updating [54], see Fig 3.2 B.

So far the star graph was not studied for the temperature initialised dB updating, because this requires the assumption that the parent moves instead of the offspring.

For the dB update rule, the fixation probability for a mutant with fitness

$f'$  in the background fitness  $f$  in a complete graph is

$$\Phi_C^{\mathcal{I}}(f', f) = \Phi_C(f', f) = \frac{N-1}{N} \frac{1 - \frac{f}{f'}}{1 - \left(\frac{f}{f'}\right)^{N-1}}. \quad (3.4)$$

It the limit of large  $N$  this becomes equal to the Bd fixation probability [19]. Also, because of the symmetry of the complete graph, the fixation probability is independent of the mutant initialisation scheme,  $\mathcal{I}$ . This is true for other regular graphs as well. Now using the approach of recursive relations [50], in App. 3.5.1 we derive the fixation probability of a mutant under dB updating on the star graph. When the mutant initially placed on the center node, its fixation probability is

$$\phi_{\text{dB}, \star}^{\bullet}(f', f) = \frac{N-1}{N \left(1 + \frac{N-2}{1+(N-1)\frac{f'}{f}}\right)}. \quad (3.5)$$

Here star symbol denotes the star graph. The filled circle in the superscript of  $\phi_{\star}^{\bullet}$  indicates that the initial mutant is at the center node. Similarly, the fixation probability for a mutant initially placed on a leaf node is,

$$\phi_{\text{dB}, \star}^{\circ}(f', f) = \frac{\frac{f'}{f}}{\left(N-2 + 2\frac{f'}{f}\right) \left(1 + \frac{N-2}{1+(N-1)\frac{f'}{f}}\right)}. \quad (3.6)$$

From Eq. 3.5 and 3.6, we can compute the temperature initialised fixation probability of a mutant on the star graph under dB updating (equivalent to  $\text{dB}^p$ ),

$$\Phi_{\text{dB}, \star}^{\mathcal{T}}(f', f) = \frac{(N-1)\phi_{\text{dB}, \star}^{\bullet}(f', f) + \phi_{\text{dB}, \star}^{\circ}(f', f)}{N}. \quad (3.7)$$

From Eq. 3.7, we find that the star graph amplifies selection under temperature initialised dB updating, see Fig. 3.2 B. But it does so in a peculiar way. The probability to fix advantageous mutants on the star graph is higher than the well-mixed population. But the fixation probability for deleterious mutants is also higher than the fixation probability on the complete graph, contrary to the original definition of  $AoS$  where the probability to fix deleterious mutant is lower [18]. Therefore, it represents a new category of graphs

which we call amplifier of fixation, where the probability to fix a mutant is higher than that of the complete graph, regardless of the mutant fitness value. The star graph under temperature initialised dB updating dB<sup>p</sup>, i.e. when the parent individual moves to the neighboring node, is a piecewise *AoF* for finite  $N$  and only in the limit  $N \rightarrow \infty$ , it is a universal *AoF*, see Fig. 3.2 B. Intuitively, in a very large population, under dB<sup>p</sup> updating the initial mutant will most likely appear at the central node. Assuming the mutant does appear at the central node, in the next step an individual is selected with uniform probability to die. Most likely it is a leaf node. With this the case, the mutant at the central node replaces the dead individual. This way, the initial mutant can survive in the population with higher probability, regardless of its fitness. Taking the infinite  $N$  limit of the fixation probability profile, we find,

$$\lim_{N \rightarrow \infty} \Phi_{\text{dB}, \star}^{\mathcal{T}}(f', f) = \lim_{N \rightarrow \infty} \phi_{\text{dB}, \star}^{\bullet}(f', f) = \frac{f'}{f + f'}, \quad \text{for } f' > 0. \quad (3.8)$$

In this fixation probability profile, the probability to fix deleterious mutant ( $f' < f$ ) is non-zero even in the limit of  $N \rightarrow \infty$ . – which contradicts the intuition that the fixation probability for deleterious mutants should be zero for large populations.

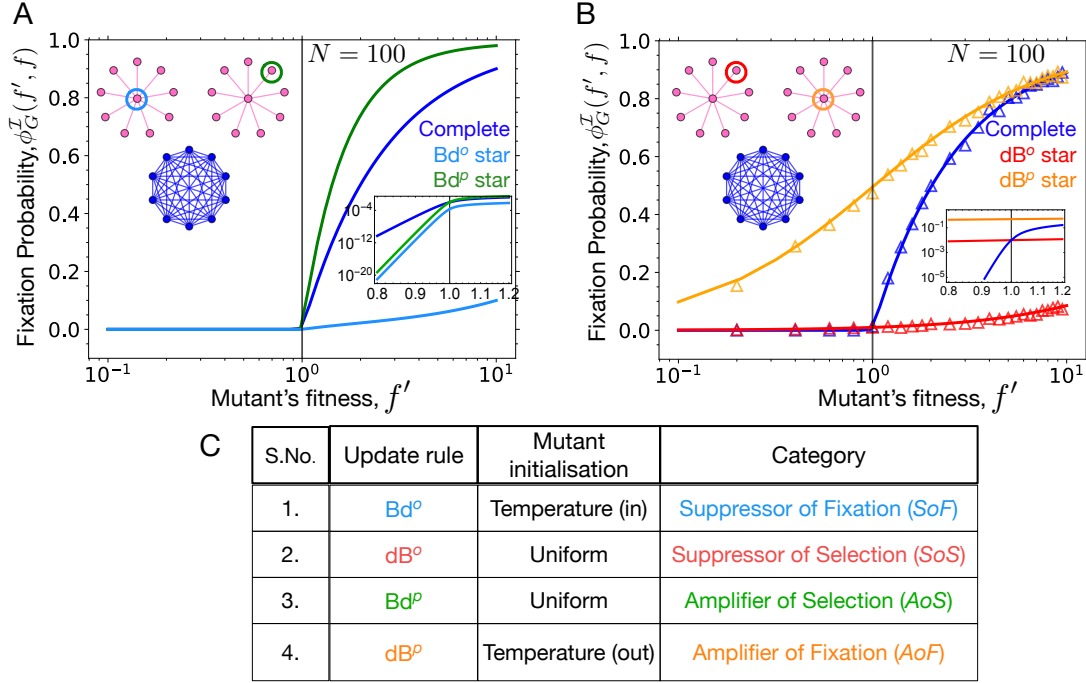


**Figure 3.2: Star graph and update rules.** A) Under temperature initialised Bd updating (Bd°), star graph is a suppressor of fixation whereas under uniform initialised Bd updating (BdP) star is an amplifier of selection. B) The uniform initialised star graph under dB updating (dB°) is a suppressor of selection. A new category of graphs namely, amplifiers of fixation, is also introduced here. An amplifier of fixation has higher fixation probability for a mutant regardless its fitness than the complete graph. Under temperature initialised dB updating (dBP) the star graph is an amplifier of fixation. C) A brief summary of how the choice of update rule affects the fixation dynamics for one of the most studied spatial structure, the star graph, is shown in the table. An update rule specifies the order of birth and death event, event(s) where selection operates and the choice of individual type moving to vacant sites.

Based on the assumption of a vanishing fixation probability of deleterious mutant for large populations, a concept called “implied scale of fitness” has been introduced in ref. [28, 40]. The implied scale of fitness of a graph,  $h_G^I$ ,

is defined as

$$\lim_{N \rightarrow \infty} \Phi_G^{\mathcal{I}}(f', f) = 1 - \frac{1}{h_G^{\mathcal{I}}(f', f)}. \quad (3.9)$$

For the complete graph,  $h_C(f', f) = \frac{f'}{f}$ . A graph  $G$  is called an *AoS*, if  $h_G^{\mathcal{I}}(f', f) > h_C(f', f)$ . Otherwise, it is a *SoS*. A caveat in the definition of the implied scale of fitness is that it is implicitly assumed that the probability to fix deleterious mutants goes to zero in the limit of large  $N$ , and ignores the deleterious mutant regime while categorising graph. The concept of implied scale of fitness thus fails to distinguish between graphs like *AoS* and *AoF*: In the limit of  $N \rightarrow \infty$  an *AoS* has zero probability to fix deleterious mutants, whereas an *AoF* can have a finite non-zero probability and therefore, it can be wrongly classified as an *AoS*. For example, the star graph under  $\text{dB}^p$  updating can be wrongly classified as an *AoS*. Therefore, the definition of implied scale of fitness should also include the deleterious mutant regime to avoid errors.

### 3.3.2 Random graphs

In the previous section we have analysed the star graph under 4 different updating scheme,  $\text{Bd}^p$ ,  $\text{Bd}^o$ ,  $\text{dB}^p$  and  $\text{dB}^o$ . Here we will study the fixation probability profiles for random graphs of size 8 for these different updating schemes to see to what extent the observations made for the star graph in Sec. 3.5.1 extend to random graphs. To check that, we first randomly generate many Erdős Rényi graphs [69] for different probabilities of link connection,  $p$ . Setting  $p = 0$  generates fully disconnected graphs whereas,  $p = 1$  generates the complete graph. As fixation probability is defined only for connected graphs, we focus on these graphs [70, 10]. Assuming the wild-type fitness to be 1, for every generated connected graph, we numerically compute the fixation probability for mutant with fitness values 0.5, 0.75, 1, 1.25, 1.5, 1.75, 2, 2.25 and 2.5, see App. 3.5.2 for more details. We classify a given connected graph  $G$  as

- *AoS*, if  $\Phi_G^{\mathcal{I}}(f', f) < \Phi_C(f', f)$  for  $f' = 0.5, 0.75$  and  $\Phi_G^{\mathcal{I}}(f', f) > \Phi_C(f', f)$  for  $f' \geq 1.25$ .
- *SoS*, if  $\Phi_G^{\mathcal{I}}(f', f) > \Phi_C(f', f)$  for  $f' = 0.5, 0.75$  and  $\Phi_G^{\mathcal{I}}(f', f) < \Phi_C(f', f)$  for  $f' \geq 1.25$ .

- *SoF*, if  $\Phi_G^{\mathcal{I}}(f', f) < \Phi_C(f', f)$  for all  $f'$ .
- *AoF*, if  $\Phi_G^{\mathcal{I}}(f', f) > \Phi_C(f', f)$  for all  $f'$ .
- *Piecewise AoF*, if  $\Phi_G^{\mathcal{I}}(f', f) > \Phi_C(f', f)$  for  $f' \leq f^*$  and  $\Phi_G^{\mathcal{I}}(f', f) < \Phi_C(f', f)$  for  $f' > f^*$ , where  $f^* \geq 1$ .
- *Isothermal* graph if every node has the same degree. In that case, the graph has the same fixation probability as the complete graph. However, this definition specifically applies to the Bd updating.

Note that these definitions assume that at neutrality all the graphs have the fixation probability  $1/N$ , as the complete graph which is chosen as the basis for comparison. However, this is true only under uniform mutant initialisation. Under temperature mutant initialisation, the fixation probabilities for graphs at neutrality need not be  $1/N$  [71].

From Fig. 3.3 A, we find that just as the star graph most random graphs are *SoF* under the temperature initialised Bd process (equivalent to  $\text{Bd}^o$ ).

Similarly, most of the random graphs under temperature initialised dB (equivalent to  $\text{dB}^p$ ) are (piecewise) *AoF*, see Fig. 3.3 B. Therefore, *AoF*s and *SoF*s are ubiquitous.

Under uniform initialised Bd process (equivalent to  $\text{Bd}^p$ ) and dB process (equivalent to  $\text{dB}^o$ ) most of the random graphs are *AoS* and *SoS* respectively, see Figs. 3.3 C,D. The ubiquity of these categories has been shown earlier in ref. [37].



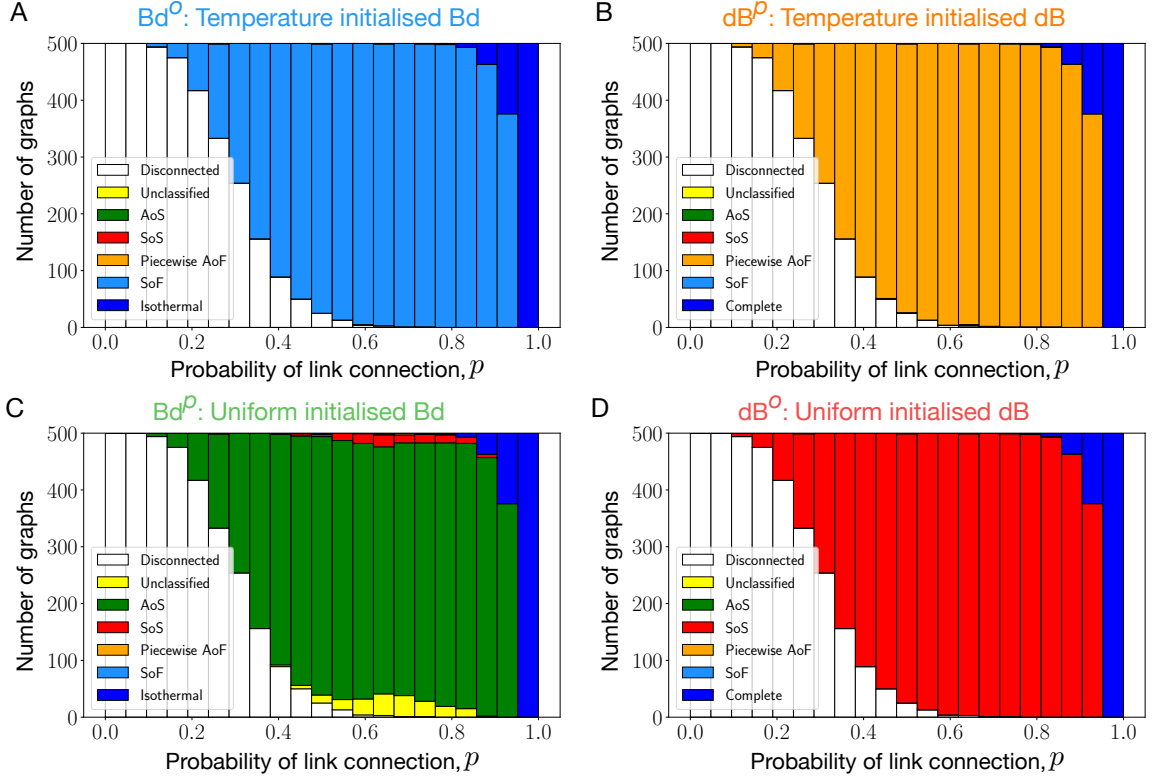


**Figure 3.3: Suppressors and amplifiers of fixation are ubiquitous.** We generate Erdős Rényi graphs of size  $N = 8$  for several values of probability of link connection,  $p$ . Fixation probability profiles for connected graphs are numerically obtained for temperature/uniform initialised Bd and dB updating. A) Most of the graphs are suppressors of fixation under temperature initialised Bd updating, i.e., most of the graphs have lower fixation probability for a mutant regardless of its fitness than the complete graph, whereas, B) most of the connected random graphs are amplifiers of fixation under temperature initialised dB updating. To be precise, most graphs are piecewise amplifiers of fixation i.e. the graphs have higher fixation probability for a mutant with fitness below a certain value,  $f^*$ , and lower fixation probability beyond  $f^* \geq 1$ . Here  $f^* = 1$ . Similarly, C) most of the connected graphs are amplifiers of selection under uniform initialised Bd updating [37], whereas, D) most of the connected random graphs are suppressors of fixation under uniform initialised dB updating [37].

### 3.4 Long time scales: Mutation-selection balance

After studying spatial structures for short-term fixation dynamics, we now move our focus to long-term mutation-selection dynamics. We assume that the state space is a one dimensional fitness line where the fitness  $f$  is bounded by  $f_{\min}$  and  $f_{\max}$  from below and above respectively. During a birth event, with probability  $1 - \mu$  the offspring resembles its parent and have the same fitness, otherwise it mutates to a new fitness sampled from a mutational fitness distribution  $\rho(f', f)$  [72].  $\rho(f', f)$  is the probability that the mutant offspring has fitness  $f'$  given that its parent's fitness is  $f$  and is also known by the name of neighbour fitness distribution [73].

We work in the regime of low mutation rates,  $\mu \ll 1$  where the population is monomorphic and all the individuals have the same fitness value. Specifically, the average time between two successive mutations is large enough so that the initial mutant reaches fixation or goes extinct before the next mutation appears. Any change in the state of the population requires the fixation of a new mutation. Thus, in the low mutation rate regime, the fixation probability and the mutant initialisation (depending on the details of the update rule)  $\phi_G^{\mathcal{I}}$  drive the long-term mutation-selection dynamics. These dynamics are known by multiple names, e.g., sequential dynamics, or origin-fixation dynamics [74]. The Moran origin-fixation dynamics on a population structure  $G$  are random walks in the fitness state space and satisfies the master equation,

$$\begin{aligned} \frac{\partial P_G(f, t)}{\partial t} = & \int df' \underbrace{\Phi_G^{\mathcal{I}}(f, f') \rho(f, f') \mu}_{T_{f \leftarrow f'}} P_G(f', t) \\ & - \int df' \underbrace{\Phi_G^{\mathcal{I}}(f', f) \rho(f', f) \mu}_{T_{f' \leftarrow f}} P_G(f, t), \end{aligned} \quad (3.10)$$

where  $P_G(f, t)$  is the probability density function for the structure  $G$  to be in between fitness state  $f$  and  $f + df$  at time  $t$ .

At long times a steady-state for the fitness distribution is attained. At stationarity we have,

$$\int df' T_{f \leftarrow f'} P_G^*(f') = \int df T_{f' \leftarrow f} P_G^*(f). \quad (3.11)$$

The steady-state solution to the master equation is obtained by assuming detailed balance AKA reversibility [75, 76],

$$T_{f \leftarrow f'} P_G^*(f') = T_{f' \leftarrow f} P_G^*(f), \quad \text{for all } f', f. \quad (3.12)$$

Normalising  $P_G^*(f')$ , the steady-state solution then takes the form,

$$P_G^*(f) = \frac{1}{\int df' \frac{T_{f' \leftarrow f}}{T_{f \leftarrow f'}}} = \frac{1}{\int df' \frac{\Phi_G^{\mathcal{I}}(f', f)}{\Phi_G^{\mathcal{I}}(f, f')} \cdot \frac{\rho(f', f)}{\rho(f, f')}} = \frac{1}{\int df' \Psi_G^{\mathcal{I}}(f', f) \cdot \frac{\rho(f', f)}{\rho(f, f')}}. \quad (3.13)$$

The assumption for the dynamics being reversible (hence, satisfying detailed balance) is justified subsequently for various graphs. Here, we have introduced the ratio of fixation probabilities  $\Psi_G^{\mathcal{I}}(f', f)$ .

For the complete graph, under dB updating  $\Psi_G^{\mathcal{I}}(f', f)$  takes the form

$$\Psi_C^{\mathcal{I}}(f', f) = \Psi_C(f', f) = \frac{\Phi_C(f', f)}{\Phi_C(f, f')} = \left( \frac{f'}{f} \right)^{N-2}. \quad (3.14)$$

In Ref. [77], it has been shown that the Moran origin-fixation dynamics is reversible if and only if  $\Psi_G^{\mathcal{I}}(f', f)$  is a power-law, i.e.,

$$\Psi_G^{\mathcal{I}}(f', f) = \left( \frac{f'}{f} \right)^{\nu}, \quad (3.15)$$

where  $\nu$  is constant, see App. 3.5.4 for more details. Thus, the Moran dB origin-fixation dynamics is fully reversible for the complete graph with  $\nu = N - 2$ . We can therefore use the steady-state probability fitness density function of the complete graph obtained by assuming detailed balance,

$$P_C^*(f) = \frac{N-1}{f_{\max}^{N-1} - f_{\min}^{N-1}} f^{N-2} = \frac{N-1}{f_{\max}^{N-1} - f_{\min}^{N-1}} \exp[(N-2) \log f]. \quad (3.16)$$

Here, we assume that the mutant's fitness is sampled from a uniform distribution, i.e.,  $\rho(f', f) = \frac{1}{f_{\max} - f_{\min}}$ . This adaptation scheme on a fitness line is similar to the House of Cards model [78]. From now onwards we use the notation  $P_G$  for  $P_G^*$ .

Similarly, for the Moran Bd origin-fixation dynamics, in Refs. [77, 79] reversibility is shown to hold for the complete graph with  $\nu = N - 1$ . The

steady-state fitness density function in Eq. 3.16 takes the form of exponential Boltzmann-like distribution. This form of the density function drawing an analogy between statistical mechanics models and evolutionary theory models has been obtained in numerous former studies [80, 81, 79, 82, 83]. Under this analogy, a physical system's thermal energy is equivalent to the logarithm of fitness, and the inverse physical temperature is equivalent to the effective population size. Just like high physical temperatures results in strong thermal fluctuations, low effective population sizes leads to highly stochastic population dynamics. The effective population size of a graph is equal to  $\nu$ . This particular definition for the effective population size holds if the long-term Moran origin fixation dynamics is reversible. There are several different definitions of effective population sizes [11, 84, 85]. Here, we use the definition arising from Moran origin-fixation dynamics. The higher the effective population size, the weaker the strength of genetic drift. For the complete graph, the effective population size is  $N - 2$  for dB updating and  $N - 1$  for Bd updating. Later we will extend this analogy to spatial graphs where different graphs have different effective population sizes leading to fluctuations of varied strengths in the evolutionary dynamics.

The steady-state average fitness for the Moran dB origin-fixation dynamics on the complete graph is

$$\langle f \rangle_C = \int df f P_C(f) = \frac{N-1}{N} \frac{f_{\max}^N - f_{\min}^N}{f_{\max}^{N-1} - f_{\min}^{N-1}}. \quad (3.17)$$

In the limit  $N \rightarrow \infty$ ,

$$\lim_{N \rightarrow \infty} \Phi_C(f', f) = \begin{cases} 1 - \frac{f}{f'}, & \text{if } f' > f, \\ 0 & \text{otherwise.} \end{cases} \quad (3.18)$$

Thus, under the Moran dB origin-fixation dynamics, an infinitely sized well-mixed population can only move forward on the fitness space with long-term fitness converging to  $f_{\max}$ . This can also be seen by performing the  $N \rightarrow \infty$  on the average steady-state fitness in Eq. 3.17. The same result holds for the Moran origin-fixation Bd dynamics.

We also study the long-term dB mutation-selection dynamics for other regular graphs: Cycle graph, a *SoF* under dB updating [37, 86], has a lower probability of fixing mutants regardless of the fitness of the mutant compared to the well-mixed population. The cycle graph is worse at fixing beneficial mutations but is better at preventing the fixation of deleterious mutants.

The ratio of the fixation probabilities  $\Psi_{\circ}$  is exactly the same as that for the complete graph, i.e.,

$$\Psi_{\circ}(f', f) = \Psi_C(f', f) = \left(\frac{f'}{f}\right)^{N-2}. \quad (3.19)$$

That is in the long run, the lower probability of fixing beneficial mutants for the cycle graph get compensated by higher probability of rejecting deleterious mutants. As a result, under Moran dB origin-fixation dynamics, the steady-state statistics for the cycle graph is the same as the complete graph. Similarly, the two-dimensional grid with periodic boundary conditions, although having a different fixation probability profile [65], attains the same steady-state statistics for the long-term mutation-selection dynamics as the complete graph, see App. 3.5.3 for more details. For Moran Bd updating, the complete graph, the cycle graph and the two-dimensional lattice (with periodic boundary conditions) have the same fixation probabilities [18], therefore they all have the same steady-state statistics for the Moran Bd origin-fixation dynamics.

### 3.4.1 The star graph

We now study long-term mutation-selection dynamics on the star graph under Moran Bd<sup>p</sup>, Bd<sup>o</sup>, dB<sup>p</sup> and dB<sup>o</sup>. In the long-term Moran dB<sup>o</sup> origin-fixation dynamics, the complete graph leads to a higher average fitness than the star graph, see Fig. 3.4 B. This is expected, as the star graph under dB<sup>o</sup> updating is a *SoS*.

For the Moran dB<sup>p</sup> origin-fixation dynamics, the star has a higher probability to fix mutants than the complete graph. However, in the long-term dynamics the complete graph leads to a higher average fitness than the star graph. Moreover, the star graph with dB<sup>o</sup> updating attains higher fitness balance than the star graph subjected to dB<sup>p</sup> updating. This happens because the star graph under dB<sup>p</sup> updating has a higher probability to fix deleterious mutants. As the population gets closer to the fitness peak (here  $f_{\max}$ ), the probability for the mutations to have deleterious fitness effects also increases. Consequently, the fate of deleterious mutants has a strong influence on the steady-state fitness of the population.

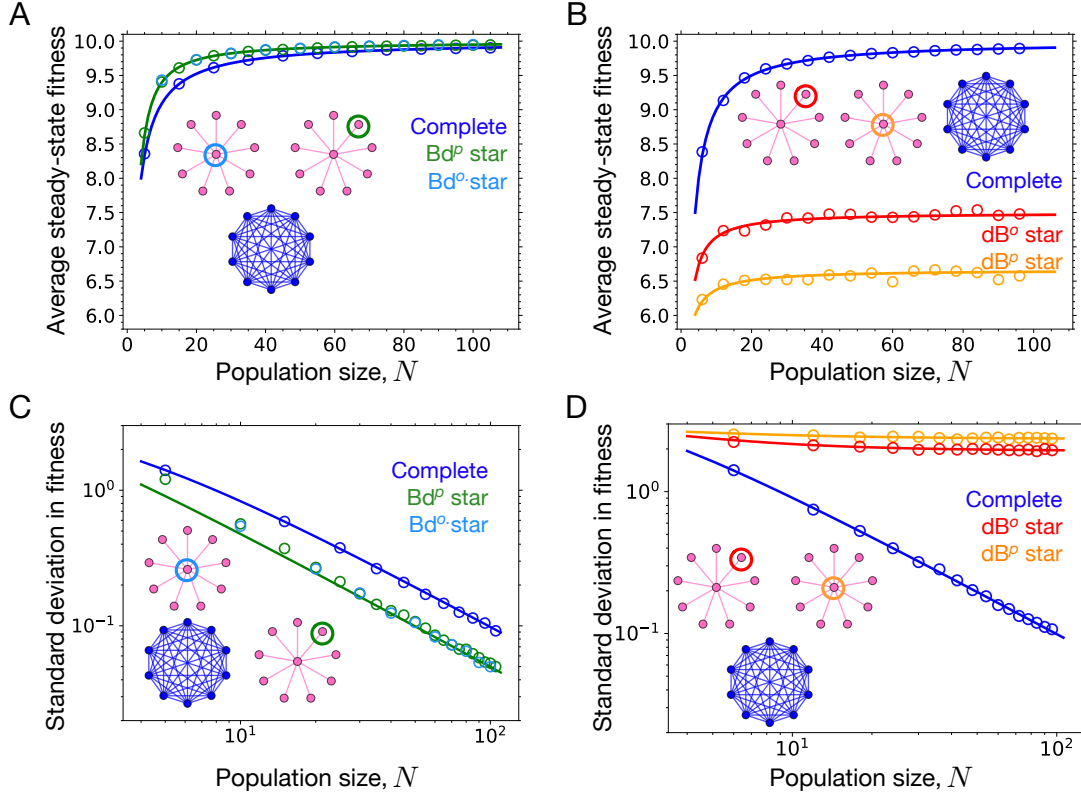


**Figure 3.4: Moran origin-fixation dynamics on star: average fitness and fluctuations.** A) For Moran  $Bd^o$  origin-fixation dynamics, the star graph despite being a suppressor of fixation, attain not only higher average fitness than the complete graph but identical fitness as the star graph under  $Bd^p$  dynamics where it is an amplifier of selection. This happens because  $Bd^o$  star compensates for its inability to fix beneficial mutants by rejecting deleterious mutants efficiently. B) For Moran  $dB^p$  origin-fixation dynamics, the star graph being an amplifier of fixation not only attains lower steady-state average fitness than the well-mixed population but also the star graph subjected to  $dB^o$  where it is a suppressor of selection. This happens because  $dB^p$  star is worse in rejecting deleterious mutations than the  $dB^o$  star. Therefore, being good at fixing beneficial mutants is not sufficient to attain higher fitness in the long-term evolution. C) The star graph under  $Bd$  long-term dynamics not only attain higher average fitness but also lower fluctuations in the steady-state than the well-mixed population. This can again be understood by the higher effective population size of star graph. D) Compared to the order of the average fitnesses under  $dB$  dynamics in panel B, the order for the standard deviation in fitness for the 3 graphs is reversed: temp-star, uni-star and the complete graph. Moreover, the standard deviation for the star graphs under  $dB$  long-term dynamics saturates to finite value for large  $N$  as their effective population sizes are independent of  $N$ .

To understand this further, we study the large  $N$  behaviour of the steady-state for the various Moran origin-fixation dynamics on the star graph. In the limit of large  $N$  for Moran  $\text{dB}^p$  updating,

$$\Psi_{\text{dB}^p, \star}(f', f) \approx \frac{f'}{f}, \quad (3.20)$$

and thus the steady-state fitness density function in the large  $N$  limit is

$$P_{\text{dB}^p, \star}(f) = \frac{2f}{f_{\max}^2 - f_{\min}^2} = \frac{2}{f_{\max}^2 - f_{\min}^2} \exp(\log f). \quad (3.21)$$

From the above equation, we find that the effective population size in the large  $N$  limit for the star graph under long-term  $\text{dB}^p$  updating is 1. Consequently, the steady-state average fitness is,

$$\begin{aligned} \langle f \rangle_{\text{dB}^p, \star} &= \int df f P_{\text{dB}^p, \star}(f) = \frac{2}{3} \frac{f_{\max}^3 - f_{\min}^3}{f_{\max}^2 - f_{\min}^2}, \\ &\approx \frac{2}{3} f_{\max}, \text{ for } f_{\max} \gg f_{\min}. \end{aligned} \quad (3.22)$$

Similarly, the large  $N$  limit for the star graph under  $\text{dB}^o$  updating gives,

$$\begin{aligned} \Psi_{\text{dB}^o, \star}(f', f) &\approx \left( \frac{f'}{f} \right)^2, \\ P_{\text{dB}^o, \star}(f) &= \frac{3f^2}{f_{\max}^3 - f_{\min}^3} = \frac{3}{f_{\max}^3 - f_{\min}^3} \exp(2 \log f). \end{aligned} \quad (3.23)$$

In the limit of large  $N$ , the effective population of the star graph subjected to long-term  $\text{dB}^o$  dynamics is twice when subjected to the long-term  $\text{dB}^p$  dynamics. Therefore, the star graph under long-term  $\text{dB}^o$  obtains higher average fitness in the steady-state with,

$$\begin{aligned} \langle f \rangle_{\text{dB}^o, \star} &= \int df f P_{\text{dB}^o, \star}(f) = \frac{3}{4} \frac{f_{\max}^4 - f_{\min}^4}{f_{\max}^3 - f_{\min}^3}, \\ &\approx \frac{3}{4} f_{\max} \text{ for } f_{\max} \gg f_{\min}. \end{aligned} \quad (3.24)$$

From Eqs. 3.22 and 3.24, we find that although  $\lim_{N \rightarrow \infty} \Phi_{\text{dB}^o, \star}(f', f) = 0$  and  $\lim_{N \rightarrow \infty} \Phi_{\text{dB}^p, \star}(f', f) \neq 0$ , we have  $\langle f \rangle_{\text{dB}^o, \star} > \langle f \rangle_{\text{dB}^p, \star}$ . The star graph

under long-term  $\text{dB}^\circ$  dynamics experiences stronger force of selection than the star graph subjected to long-term  $\text{dB}^p$  dynamics.

Performing a similar analysis for the Birth-death updating, we find that the star graph under  $\text{Bd}^p$  and  $\text{Bd}^\circ$  satisfies,

$$\Psi_{\text{Bd}^p, \star}(f', f) \approx \left(\frac{f'}{f}\right)^{2N-2} \approx \Psi_{\text{Bd}^\circ, \star}(f', f). \quad (3.25)$$

The first approximation follows from Ref. [49] and the second approximation follows from Ref. [53]. What this means is that although under Moran  $\text{Bd}^p$  and  $\text{Bd}^\circ$  updating the star have quite different fixation probability profiles, see Fig. 3.2 A, in the long term to a good approximation they have identical steady-state statistics because in both of the cases the star graph has the same effective population size of  $2N$ . This also means that the star graph under long-term Moran  $\text{Bd}$  dynamics attains higher average fitness in the steady-state than the well-mixed population.

The corresponding steady-state fitness density function is

$$\begin{aligned} P_{\text{Bd}^p, \star}(f) &= P_{\text{Bd}^\circ, \star}(f) = \frac{2N-1}{f_{\max}^{2N-1} - f_{\min}^{2N-1}} f^{2N-2} \\ &= \frac{2N-1}{f_{\max}^{2N-1} - f_{\min}^{2N-1}} \exp[(2N-2) \log f]. \end{aligned} \quad (3.26)$$

The average steady-state fitness is,

$$\langle f \rangle_{\text{Bd}^p, \star} = \langle f \rangle_{\text{Bd}^\circ, \star} = \frac{2N-1}{2N} \frac{f_{\max}^{2N} - f_{\min}^{2N}}{f_{\max}^{2N-1} - f_{\min}^{2N-1}} \quad (3.27)$$

with

$$\langle f \rangle_{\text{Bd}, \star} - \langle f \rangle_C \approx \frac{f_{\max}}{2N}. \quad (3.28)$$

That is the star graph under  $\text{Bd}^p$  updating, an *AoS* (Fig. 3.2 A), expectedly attains higher fitness than the well-mixed population because it is better in fixing beneficial mutations and preventing the fixation of deleterious mutations. However, the star graph under  $\text{Bd}^\circ$  updating, a *SoF*, also attains an even higher steady-state average fitness because it is much better at rejecting deleterious mutants which compensates for its lower probability to fix beneficial mutations [53].



The effective population size also tells us about the fluctuations in the steady-state. Because the effective population size of the star graph under dB updating is independent of  $N$ , the standard deviation in fitness does not change at large  $N$ . *AoF* star experiences higher fluctuations than the *SoF* star because of its lower effective population size, see Fig. 3.4 D. Under Bd updating, the effective population size of the star graph is twice the effective population size of the complete graph. Therefore, the star experiences lower fluctuations than the complete graph and the standard deviation decreases with increasing  $N$ , see Fig. 3.4 C. For more details, see App. 3.5.5.

### 3.4.2 Random graphs

For long-term evolution on the star graph, the deleterious mutant regime can substantially affect the fate of the dynamics. Does this effect extend to other graphs? Can we expect *SoF* that we found in Fig. 3.3 A to have higher long-term fitness than the well-mixed population? The answer is not obvious. Similarly, what can we say about the long-term fitness fate of the *AoF* found in Fig. 3.3 B? Do all of them attain lower steady-state average fitness in the steady-state than the complete graph just like the star graph under dB<sup>p</sup> updating?

We explore these questions next. We move forward by discretising the fitness space and study the Moran Bd<sup>p</sup>, Bd<sup>o</sup>, dB<sup>p</sup> and dB<sup>o</sup> origin-fixation dynamics on it for several random graphs. Steady-state statistics of these graphs is obtained by solving the respective Markov chains numerically, see App. 3.5.6 for details.

Computing the steady-state average fitness for all connected random graphs, we find that for long-term Bd<sup>o</sup> dynamics, almost all *SoF* attain higher steady-state average fitness than the complete graph, whereas for long-term dB<sup>p</sup> dynamics, all the piecewise *AoF* attain lower steady-state average fitness than the complete graph. Interestingly, for the case of Bd<sup>p</sup> dynamics where most of the connected graphs are *AoS*, the graphs attain exactly the same average fitness as they do when subjected to the Bd<sup>o</sup> dynamics. In Fig. 3.4 A, we have seen that the star graph attains same fitness for the two kinds of Bd long-term dynamics. Now we confirm this for all other graphs. Expectedly, for the long-term dB<sup>o</sup> dynamics where most of the random connected graphs are *SoS*, the majority of random graphs attain lower average fitness.

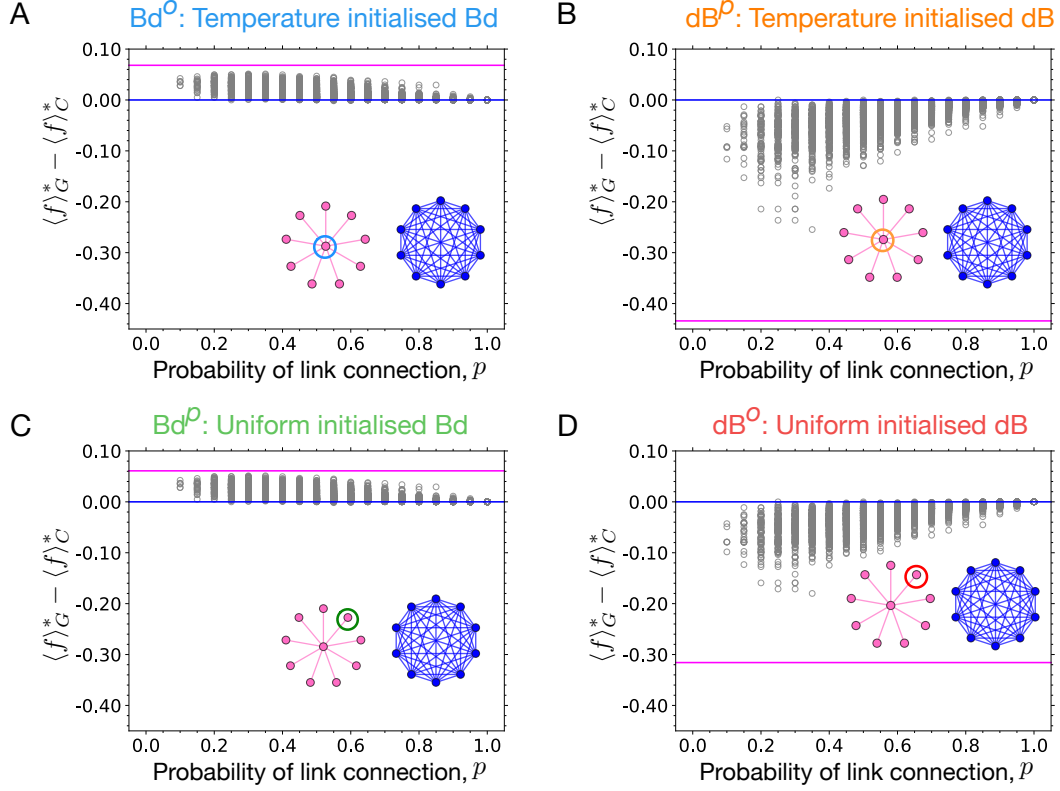


Figure 3.5: **Suppressors of fixation attain higher fitness whereas amplifiers of fixation attain lower fitness.** Numerical solutions of the Markov chain on the fitness space for several random graphs of size 8 are shown here via grey symbols. The magenta horizontal lines represent the steady-state fitness obtained by the star graph relative to the well-mixed population under different dynamics. A) Most of the random graphs are suppressors of fixation under  $\text{dB}^0$  updating, yet they attain higher fitness than the well-mixed population. B) Similarly, most of the random graphs are (piecewise) amplifiers of fixation under  $\text{dB}^p$  updating, yet they attain lower steady-state average fitness. C), D) Expectedly, amplifiers of selection attain higher fitness for  $\text{Bd}^0$  dynamics and suppressors of selection attain lower fitness for  $\text{dB}^p$  dynamics. Thus, the deleterious mutant regime is important for a generic spatial structure when subjected to long-term dynamics.

In App. 3.5.7, we derive a sufficient condition for a graph to have higher average fitness in the steady-state of a long term evolution.

### 3.5 Discussion

Most of the initial research in evolutionary graph theory has focused on the Moran Birth-death (Bd) update with uniform initialisation [18, 49, 39]. The uniform initialisation is typically justified by considering spontaneous mutations during an individual’s lifetime [87], thus obviating the need for reproduction for variation. However, when mutations occur during reproduction instead [28], justifying the use of uniform initialised Bd updating becomes more challenging. In that scenario, temperature initialisation is a more natural choice. Our findings demonstrate that the uniform initialisation in the Bd update naturally arises when parent-type offspring move to vacant nodes ( $\text{Bd}^p$ ) rather than offspring individuals ( $\text{Bd}^o$ ). Furthermore, by necessitating parent-type individuals to move instead of offspring individuals, we have uncovered the existence of temperature-initialised dB updating ( $\text{dB}^p$ ), an update scheme previously considered non-existent. In conclusion, we emphasise that a mutant initialisation scheme is an outcome of an update rule and need not be specified on top of it. An update rule should be sufficient to generate the fixation dynamics on a graph.

Moran  $\text{dB}^p$  updating introduces a new category of graphs known as *AoF* (amplifiers of fixation), where the fixation probability is higher regardless of the fitness values compared to the complete graph. The star graph under  $\text{dB}^p$  updating is an *AoF* with non-zero probability to fix deleterious mutants, even in the limit of infinite population size. For all other previously known graphs, such as *AoS*, *SoS*, *SoF*, the complete graph, the probability of fixing any deleterious mutant goes to zero for large population sizes. Consequently, the deleterious mutant regime has not been extensively explored in the fixation dynamics literature. The discovery of *AoF* underscores the need to consider the deleterious mutant regime in graph classification, and its importance in the computation of fixation probabilities and time.

The results derived from the analysis of the star graph for different update rules also extends to Erdős-Rényi random graphs. Specifically, we observe that the majority of small random graphs are *SoF* under  $\text{Bd}^o$  updating, and piecewise *AoF*s under  $\text{dB}^p$  updating. This finding closely resembles the result of Ref. [37], where most random graphs were identified as *AoS* under  $\text{Bd}^p$  updating and *SoS* under  $\text{dB}^o$  updating. Consequently, it is not only the order of birth and death events, but also the choice of the individual moving to vacant sites significantly impacts the results at the short-term fixation time scale.

The choice of moving individuals also affects the long-term Moran origin-fixation dynamics. The star graph, a *SoF* under  $\text{Bd}^o$  updating, despite having lower probability to fix advantageous mutants attains higher fitness in the long-term dynamics than the well-mixed population. Similarly under  $\text{dB}^p$  updating, the star graph despite being an *AoF* with higher probability of fixing beneficial mutants attains lower fitness. In the former case, the star graph is better in rejecting deleterious mutants compensating for its lower probabilities to fix beneficial mutations. In the later scenario, the star graph is not good is preventing the fixation of disadvantageous mutants despite being better at fixing beneficial mutations.

More concretely, the effective population sizes of the star graph for different updating explain the corresponding steady-states and the contribution coming from the deleterious mutant regime. The *SoF* star graph has a higher effective population size than the *AoF* star graph. Additionally, the results obtained for the long-term evolution on the star graph also extends to random graphs. Under  $\text{Bd}^o$  updating, most of the random graphs despite being *SoF* attain higher fitness than the isothermal graphs. Whereas, under  $\text{dB}^p$  updating, most of the random graphs despite being piecewise *AoF* attain lower fitness than the isothermal graphs. To summarise, extra care should be taken before making speculations about the fate of long-term evolution on spatial structures based on the short-term fixation dynamics. For a population adapting on a fitness landscape, the outcome depends on two factors. First, how effective the population is in stepping forward. And, the second how good it is in not falling backward. The effect of deleterious mutant regime can also be seen in the transient phase of an evolutionary dynamics [72]. The likelihood for the average fitness trajectory to non-monotonic increases with the probability to accept deleterious mutations, see App. 3.5.8 for more details. Overall, the deleterious mutant regime is important when it comes to long-term evolution on spatial structures, something that is often ignored in adaptive evolution theories with well-mixed populations.

Experimental evolution has started to align closely with the research of evolutionary graph theory [88]. It is only a matter of time before more of such studies are conducted. Consequently, an extension of evolutionary graph theory to the structured metapopulation level is necessary to meet the demands of these experimental challenges [89, 64]. While our work focuses on the theory of one-node-one-individual, it is expected that the results obtained here should be transferable to metapopulation studies. The analysis in this paper can be adapted for the study of metapopulations, and we have identi-

fied the amplifiers and suppressors of fixation among the metastar structures presented in Ref.[90]. Please refer to App.3.5.9 for more details. Examining the role of the deleterious mutant regime for structured metapopulations is clearly an important future direction.

## Appendix

### 3.5.1 Exact formula for the fixation probability of a mutant on the star graph under dB and Bd updating

The state of the population can be described by  $(\bullet/\circ, i)$  where the first index indicates if the central node is occupied by a mutant ( $\bullet$ ) or not ( $\circ$ ) and the second index gives the number of mutants in the leaf nodes. Let us denote  $\phi_i^\bullet$  as the fixation probability of the mutant type when started with  $i$  mutant individuals in the leaf nodes and a mutant at the central node. Similarly,  $\phi_i^\circ$  is the fixation probability of the mutant type when started with  $i$  mutant individuals in the leaf nodes with the central node occupied by a wild-type individual. With  $n$  number of leaves,  $\phi_i^\bullet$  and  $\phi_i^\circ$  satisfy the following recursion relations [49],

$$\begin{aligned}\phi_i^\bullet &= T_{i,i+1}^{\bullet\bullet} \phi_{i+1}^\bullet + T_{i,i}^{\bullet\circ} \phi_i^\circ + (1 - T_{i,i+1}^{\bullet\bullet} - T_{i,i}^{\bullet\circ}) \phi_i^\bullet, & 0 \leq i \leq n-1, \\ \phi_i^\circ &= T_{i,i-1}^{\circ\circ} \phi_{i-1}^\circ + T_{i,i}^{\circ\bullet} \phi_i^\bullet + (1 - T_{i,i-1}^{\circ\circ} - T_{i,i}^{\circ\bullet}) \phi_i^\circ, & 1 \leq i \leq n,\end{aligned}\tag{3.29}$$

where

- $T_{i,i+1}^{\bullet\bullet}$  is the probability to transition from the state  $(\bullet, i)$  to the state  $(\bullet, i+1)$ .
- $T_{i,i}^{\bullet\circ}$  is the probability to transition from the state  $(\bullet, i)$  to the state  $(\circ, i)$ .
- $T_{i,i-1}^{\circ\circ}$  is the probability to transition from the state  $(\circ, i)$  to the state  $(\circ, i-1)$ .
- $T_{i,i}^{\circ\bullet}$  is the probability to transition from the state  $(\circ, i)$  to the state  $(\bullet, i)$ .

On rearranging the recursion relations we get,

$$\begin{aligned}\phi_i^\bullet &= \pi_{i,i+1}^{\bullet\bullet} \phi_{i+1}^\bullet + \pi_{i,i}^{\bullet\circ} \phi_i^\circ, & 0 \leq i \leq n, \\ \phi_i^\circ &= \pi_{i,i-1}^{\circ\circ} \phi_{i-1}^\circ + \pi_{i,i}^{\circ\bullet} \phi_i^\bullet, & 1 \leq i \leq n,\end{aligned}\tag{3.30}$$

where,

- $\pi_{i,i+1}^{\bullet\bullet}$  is the conditional probability to transition from the state  $(\bullet, i)$  to the state  $(\bullet, i+1)$  given that the number of mutant changes.
- $\pi_{i,i}^{\bullet\circ}$  is the conditional probability to transition from the state  $(\bullet, i)$  to the state  $(\circ, i)$  given that the number of mutant changes.
- $\pi_{i,i-1}^{\circ\circ}$  is the conditional probability to transition from the state  $(\circ, i)$  to the state  $(\circ, i-1)$  given that the number of mutant changes.
- $\pi_{i,i}^{\circ\bullet}$  is the conditional probability to transition from the state  $(\circ, i)$  to the state  $(\bullet, i)$  given that the number of mutant changes.

The conditional probabilities are given by,

$$\begin{aligned}\pi_{i,i+1}^{\bullet\bullet} &= \frac{T_{i,i+1}^{\bullet\bullet}}{T_{i,i+1}^{\bullet\bullet} + T_{i,i}^{\bullet\circ}} = 1 - \pi_{i,i}^{\bullet\circ}, \\ \pi_{i,i-1}^{\circ\circ} &= \frac{T_{i,i-1}^{\circ\circ}}{T_{i,i-1}^{\circ\circ} + T_{i,i}^{\circ\bullet}} = 1 - \pi_{i,i}^{\circ\bullet},\end{aligned}\tag{3.31}$$

For the Moran dB updating the transition probabilities are,

$$T_{i,i+1}^{\bullet\bullet} = \frac{n-i}{n+1} \quad \text{and} \quad T_{i,i}^{\bullet\circ} = \frac{1}{n+1} \frac{n-i}{ir+n-i}.\tag{3.32}$$

$$T_{i,i-1}^{\circ\circ} = \frac{i}{n+1} \quad \text{and} \quad T_{i,i}^{\circ\bullet} = \frac{1}{n+1} \frac{ir}{ir+n-i}.\tag{3.33}$$

Consequently the conditional probabilities are,

$$\pi_{i,i+1}^{\bullet\bullet} = \frac{n-i+ir}{n-i+ir+1} \quad \text{and} \quad \pi_{i,i-1}^{\circ\circ} = \frac{ir+n-i}{ir+n-i+r}.\tag{3.34}$$

From the ref. [50], we know that the probability of fixation of a mutant appearing at the center node is

$$\phi_{\text{dB},\star}^\bullet(f', f) = \frac{\pi_{0,1}^{\bullet\bullet}}{A(1, n)}\tag{3.35}$$

where,

$$A(l, m) = 1 + \sum_{j=l}^{m-1} \pi_{j,j}^{\bullet\circ} \prod_{k=l}^j \frac{\pi_{k,k-1}^{\circ\circ}}{\pi_{k,k+1}^{\bullet\bullet}}. \quad (3.36)$$

After substituting for the conditional probabilities, we get

$$\phi_{\text{dB},\star}^{\bullet}(f', f) = \frac{N-1}{N} \frac{1}{1 + \frac{N-2}{1+(N-1)\frac{f'}{f}}}. \quad (3.37)$$

Similarly, we find

$$\phi_{\text{dB},\star}^{\circ}(f', f) = \frac{\pi_{1,1}^{\circ\bullet}}{A(1, n)} = \frac{\frac{f'}{f}}{\left(N - 2 + 2\frac{f'}{f}\right) \left(1 + \frac{N}{1+(N-1)\frac{f'}{f}}\right)}. \quad (3.38)$$

$\phi_{\text{dB},\star}^{\bullet}$  and  $\phi_{\text{dB},\star}^{\circ}$  are used to compute uniform and temperature initialised dB fixation probabilities for the star graph.

The uniform (when offspring move to vacant node) and temperature (when parent move to vacant node) initialised fixation probability under Moran dB updating are,

$$\begin{aligned} \Phi_{\text{dB},\star}^{\mathcal{U}}(f', f) &= \Phi_{\text{dB}^o,\star}(f', f) = \frac{\phi_{\text{dB},\star}^{\bullet}(f', f) + (N-1)\phi_{\text{dB},\star}^{\circ}(f', f)}{N}, \\ \Phi_{\text{dB},\star}^{\mathcal{T}}(f', f) &= \Phi_{\text{dB}^p,\star}(f', f) = \frac{(N-1)\phi_{\text{dB},\star}^{\bullet}(f', f) + \phi_{\text{dB},\star}^{\circ}(f', f)}{N}, \end{aligned} \quad (3.39)$$

From Fig. 3.2B, the uniform initialised star graph is a suppressor of selection [54, 86] whereas the temperature initialised star graph is an amplifier of fixation.

Similarly, for Bd updating,

$$\phi_{\text{Bd},\star}^{\bullet}(f', f) = \frac{\left(\left(\frac{f'}{f}\right)^2 - 1\right) \left(N - 1 + \frac{f'}{f}\right)}{\frac{f'}{f} \left( \frac{f'}{f} \left(N - 1 + \frac{f'}{f}\right) - \left((N-1)\frac{f'}{f} + 1\right) \left( \frac{N-1+\frac{f'}{f}}{(N-1)\left(\frac{f'}{f}\right)^2 + \frac{f'}{f}} \right)^{N-1} \right)}, \quad (3.40)$$

and the fixation probability for a mutant initially placed on a leaf node is,

$$\phi_{\text{Bd},\star}^{\circ}(f', f) = \frac{(N-1) \left( \left( \frac{f'}{f} \right)^2 - 1 \right) \left( N-1 + \frac{f'}{f} \right)}{\left( (N-1) \frac{f'}{f} + 1 \right) \left( \frac{f'}{f} \left( N-1 + \frac{f'}{f} \right) + \left( (N-1) \frac{f'}{f} + 1 \right) \left( \frac{N-1 + \frac{f'}{f}}{(N-1) \left( \frac{f'}{f} \right)^2 + \frac{f'}{f}} \right)^{N-1} \right)}.$$

(3.41)

Eqs. 3.40, 3.41 are used to compute uniform and temperature initialised fixation probabilities for the star graph under Bd updating.

### 3.5.2 Matrix approach to compute fixation probability on a random graph

The matrix method solves the Markov chain for the fixation dynamics on a graph. This method is generally used to compute the fixation probability for an arbitrary connected graph [91]. The primary reference for this section is [92]. With states being the configurations of mutant and wild-type, the transition matrix  $\mathbf{M}_{s \times s}$  is defined as

$$\mathbf{M}_{s \times s} = \begin{pmatrix} \mathbf{Q}_{t \times t} & \mathbf{R}_{t \times a} \\ \mathbf{0}_{a \times t} & \mathbf{I}_{a \times a} \end{pmatrix}, \quad (3.42)$$

where  $s$  denotes the total number of states and is equal to  $t + a$ , with  $t$  being the number of transient states and  $a$  being the number of absorbing states.  $\mathbf{Q}$  is the transition probability matrix corresponding to the transitions among the transient states, while  $\mathbf{R}$  represents transitions from the transient to the absorbing states. Since by definition there is no jump possible from an absorbing to the transient sector, the lower left matrix is a zero matrix. By similar reasoning, the lower right matrix is an identity matrix.

We denote the fundamental matrix as  $\mathbf{F}$ . It is equal to  $\sum_{n=0}^{\infty} \mathbf{Q}^n = (\mathbf{I} - \mathbf{Q})^{-1}$ . The fixation probability to the absorbing state  $j$  when started in a transient state  $i$  is given by the relation,

$$\phi_{i,j} = (\mathbf{F} \cdot \mathbf{R})_{i,j}. \quad (3.43)$$



Notice that the indices  $i, j$  etc., do not represent the number of mutants but the configurations themselves. The second index of the subscript can represent two absorbing states, every individual being the wild-type or the mutant type. It represents the position of the node where the initial mutant appears.

The fixation probability of a mutant to state  $j$  on a graph  $G$  with mutant initialisation  $\mathcal{I}$  is equal to,

$$\Phi_{j,G}^{\mathcal{I}} = \sum_{i=0}^{N-1} p_i \phi_{i,j}. \quad (3.44)$$

The index  $i$  in the equation above corresponds to the states where the initial mutant appears at different positions on the graph.

### Transition matrix for the Bd process

For a network of size  $N$ , we have the transition matrices of dimensions  $2^N \times 2^N$ . One can decrease the size of these matrices by considering the symmetries of the graph. This has been done in [93] where all the undirected connected networks of size four were considered. After considering the symmetries, the size of the transition matrices for the complete, diamond, and ring graph were reduced from 16 ( $2^4$ ) to 5, 9, and 5, respectively. It is not straightforward to account for these symmetries for larger networks; thus, we work with maximum-size transition matrices. We compute the transition matrix for the Moran Bd dynamics with a focus on undirected graphs and unweighted having symmetric adjacency matrices,  $\mathbf{A}$ . We work only with connected graphs as the fundamental matrix  $\mathbf{F}$  becomes singular for the disconnected graphs.

The matrix element  $\mathbf{M}_{ij}$  with  $i \neq j$ , the probability of going from state  $i$  to state  $j$  with  $i \neq j$  is given as,

$$\mathbf{M}_{ij} = \begin{cases} \frac{1}{rn^i + N - n^i} \sum_k \tilde{a}_{km} \left[ rn_k^i n_m^j + (1 - n_k^i)(1 - n_m^j) \right], & \text{if } \sum_s |n_s^i - n_s^j| = 1 \\ & \text{and } n_m^i \neq n_m^j, \\ 0, & \text{otherwise.} \end{cases} \quad (3.45)$$

where every node of the configuration  $i$  can either take a value 0 (for wild-type) or 1 (for mutant). The number of mutants in state  $i$  is given by  $n^i = \sum_{k=0}^{N-1} n_k^i$ . Here, we have also introduced  $\tilde{a}_{km} = \frac{a_{km}}{\sum_l a_{kl}}$ . The diagonal elements  $\mathbf{M}_{ii}$  are equal to  $1 - \sum_{j \neq i} \mathbf{M}_{ij}$ .

### Transition matrix for dB process

Like the Bd process, here we write down the transition matrix for the dB process. The matrix element  $\mathbf{M}_{ij}$  with  $i \neq j$  is given as :

$$\mathbf{M}_{ij} = \begin{cases} \frac{1}{N} \sum_k \frac{a_{km} \left[ r n_k^i n_m^j + (1 - n_k^i)(1 - n_m^j) \right]}{r \sum_l a_{lm} n_l^i + \sum_l a_{lm} (1 - n_l^i)}, & \text{if } \sum_s |n_s^i - n_s^j| = 1 \text{ and } n_m^i \neq n_m^j, \\ 0, & \text{otherwise.} \end{cases} \quad (3.46)$$

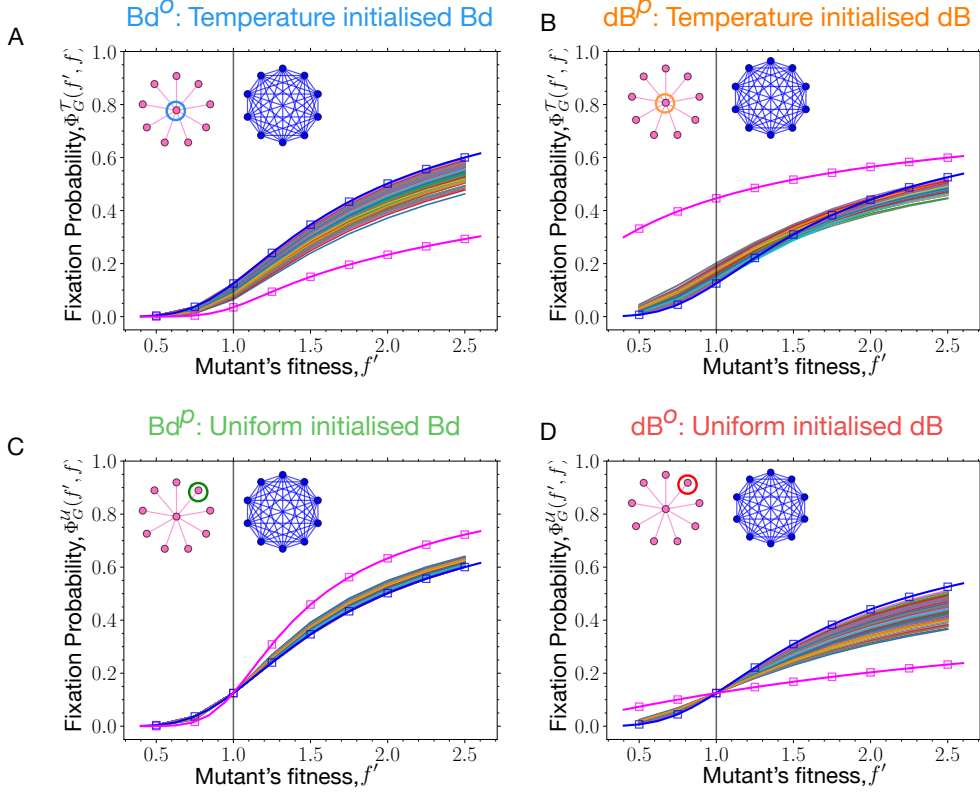


Figure 3.6: **Fixation probability profiles of random graphs.** The relative fitness values of the mutant are chosen to be, 0.5, 0.75, 1, 1.25, 1.5, 1.75, 2, 2.25 and 2.5 with wild-type fitness being 1. The fixation probability profiles under different update rules for connected random graphs with the probability of link connection,  $p = 0.5$  are shown. The fixation profiles for the complete graph (in blue) and the star graph (in magenta) in both numerical (square markers) and analytical (solid lines) form are also shown. A) Most of the random graphs are suppressors of fixation under temperature initialised  $Bd$  updating. B) Most graphs are piecewise amplifiers of fixation under  $dB^O$  updating i.e. the graphs have higher fixation probability for a mutant with fitness below a certain value,  $f^*$ , and lower fixation probability beyond  $f^*$ . We observe that beyond  $f' \approx 1.5$ , the fixation probabilities become lower than the fixation probability on the well-mixed population. C) Most of the graphs are amplifiers of selection under  $(Bd^O)$  uniform initialised  $Bd$  updating, and D) suppressors of selection under  $(dB^O)$  uniform initialised  $dB$  updating.

### 3.5.3 Long-term evolution on regular graphs

Under the Moran dB updating, regular graphs have different fixation probability profiles compared to the complete graph [65]. It is in contrast to the Moran Birth-death (Bd) rule, where according to the isothermal theorem [18, 19] all the regular graphs have the same fixation probability profiles as the well-mixed population. For example, under Moran dB updating, the cycle graph has the fixation probability [37],

$$\Phi_{\circ}(f', f) = \frac{2 \left(1 - \frac{f}{f'}\right)}{3 - \frac{f}{f'} + \left(1 - 3\frac{f}{f'}\right) \left(\frac{f}{f'}\right)^{N-2}}. \quad (3.47)$$

Under the Moran dB updating, the cycle graph is a suppressor of fixation [37], because  $\Phi_{\circ}(f', f) < \Phi_C(f', f)$  for all pairs of  $f'$  and  $f$  (ignoring the neutral point  $f' = f$ , where  $\Phi_{\circ}(f', f) = \Phi_C(f', f) = \frac{1}{N}$ ), see Fig. 3.7 B. The ratio of fixation probabilities entering the steady-state detailed balance solution however is the same as complete graph,

$$\begin{aligned} \Psi_{\circ}(f', f) &= \frac{\Phi_{\circ}(f', f)}{\Phi_{\circ}(f, f')}, \\ &= \frac{2 \left(1 - \frac{f}{f'}\right)}{3 - \frac{f}{f'} + \left(1 - 3\frac{f}{f'}\right) \left(\frac{f}{f'}\right)^{N-2}} \cdot \frac{3 - \frac{f'}{f} + \left(1 - 3\frac{f'}{f}\right) \left(\frac{f'}{f}\right)^{N-2}}{2 \left(1 - \frac{f'}{f}\right)}, \\ &= \frac{f' - 3f + (3f' - f) \left(\frac{f'}{f}\right)^{N-2}}{3f' - f + (f' - 3f) \left(\frac{f'}{f}\right)^{N-2}}, \\ &= \left(\frac{f'}{f}\right)^{N-2}. \end{aligned} \quad (3.48)$$

Because  $\Psi_{\circ}(f', f)$  is a power law, the Moran dB origin-fixation dynamics on the cycle graph is reversible. Moreover,

$$P_{\circ}^*(f) = P_C^*(f). \quad (3.49)$$

Consequently,  $\langle f \rangle_{\circ}^* = \langle f \rangle_C^*$ .

What did we just learn? We learnt that the cycle graph despite being a suppressor of fixation, attains the same average fitness in the mutation-selection balance as the complete graph, see Fig. 3.7 D. In the limit of  $N \rightarrow \infty$ ,

$$\lim_{N \rightarrow \infty} \Phi_o(f', f) = \begin{cases} \frac{2\left(\frac{f'}{f}-1\right)}{3\frac{f'}{f}-1}, & \text{if } f' > f, \\ 0 & \text{otherwise.} \end{cases} \quad (3.50)$$

Now,  $\frac{2\left(\frac{f'}{f}-1\right)}{3\frac{f'}{f}-1} < 1 - \frac{f}{f'}$  for all  $f' > f$ , therefore, in the limit of very large population sizes, the cycle graph is less likely to fix beneficial mutants than the complete graph, see Fig. 3.7 A. Yet the cycle and the complete graph attain the same steady-state average fitness for all population sizes. It happens because the cycle graph is better at rejecting deleterious mutants than the complete graph. The ability of the cycle graph to prevent the fixation of disadvantageous mutants compensates for its lower probability to fix beneficial mutants in a way that  $\Psi_o(f', f)$  becomes equal to  $\Psi_C(f', f)$ .

We also explore the steady-state statistics of the long-term dB mutation-selection dynamics on the two dimensional lattice with periodic boundary conditions. With each node having  $k$  neighbors, the fixation probability of a mutant to fix on the 2d lattice is [65],

$$\Phi_{2d}(f', f) \approx \frac{k \left(1 - \frac{f}{f'}\right)}{k \left(1 - \frac{f}{f'}\right) + \left(1 - \left(\frac{f}{f'}\right)^{N-2}\right) \left(1 + (k-1) \frac{f}{f'}\right)}. \quad (3.51)$$

We focus on the case of  $k = 4$ . The ratio of fixation probabilities takes the form,

$$\Psi_{2d}(f', f) = \frac{\Phi_{2d}(f', f)}{\Phi_{2d}(f, f')} \approx \left(\frac{f'}{f}\right)^{N-2} \frac{5 - \frac{f'}{f} - \left(\frac{f'}{f}\right)^{N-2} \left(3\frac{f'}{f} + 1\right)}{3 + \frac{f'}{f} + \left(\frac{f'}{f}\right)^{N-2} \left(1 - 5\frac{f'}{f}\right)}. \quad (3.52)$$

From Fig. 3.7 A and C, it is clear that the fixation probability profile of the 2d lattice is different from the well-mixed population, but the graph category to which the 2d lattice belongs is not clear. This could be due to the approximation made in Ref. [65] to compute Eq. 3.51. As a result, for small

$N$ , the 2d lattice attains different (lower) steady-state average fitness in the mutation-selection balance than the complete and cycle graph. However, with an increase in population size, the steady-state average fitness attained by the 2d lattice asymptotes to the one attained by the well-mixed population, see Fig. 3.7 D. This can be understood by performing the large  $N$  expansion on  $\Psi_{2d}(f', f)$  yielding,

$$\Psi_{2d}(f', f) \approx \begin{cases} \left(\frac{f'}{f}\right)^{N-2} \frac{3\frac{f'}{f}+1}{5\frac{f'}{f}-1} + \mathcal{O}\left(\left(\frac{f'}{f}\right)^{N-3}\right), & \text{if } f' > f, \\ \left(\frac{f'}{f}\right)^{N-2} \frac{5-\frac{f'}{f}}{3+\frac{f'}{f}} + \mathcal{O}\left(\left(\frac{f'}{f}\right)^{N-3}\right), & \text{otherwise.} \end{cases} \quad (3.53)$$

For large population sizes,  $\Psi_{2d} \sim \left(\frac{f'}{f}\right)^{N-2}$ ,  $P_{2d}^*(f)$  and therefore,  $\langle f \rangle_{2d}^*$  take the same limit as the complete graph. In the argument made, we have assumed reversibility to hold. In the subsequent section, we justify the assumption.

From the above two case studies, we have learnt that although the complete graph, the cycle graph, and the 2d lattice behave differently at fixation time scales under dB updating [65], their steady-state statistics for the long-term Moran dB origin-fixation dynamics are identical.

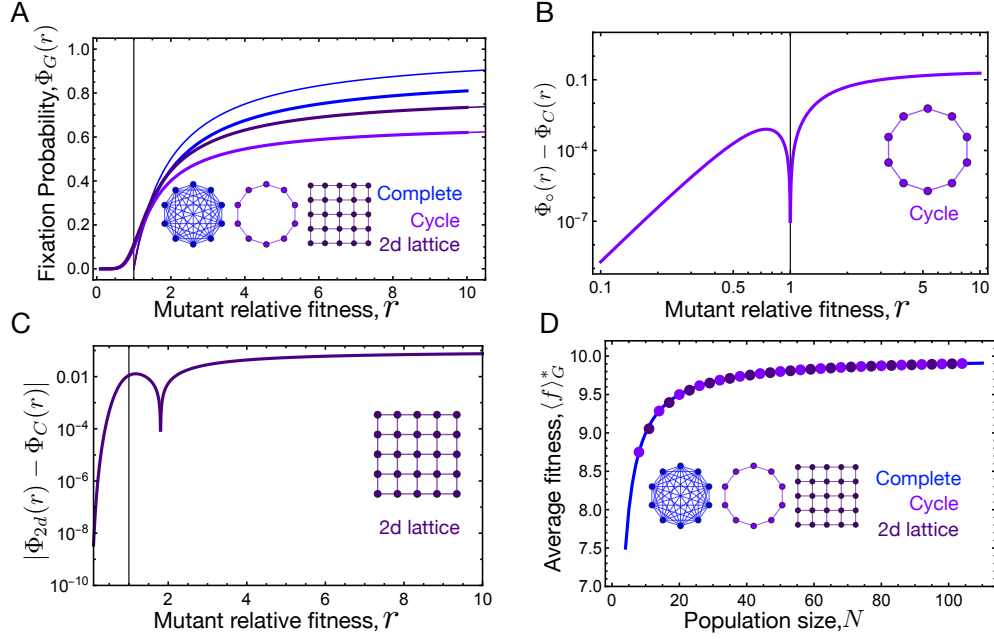


Figure 3.7: **Regular graph: dB fixation probability and long-term evolution.** A) Fixation probability for regular graphs, the cycle graph, the 2d lattice with periodic boundaries and the complete graph, under dB updating are shown. Thick lines correspond to population size  $N = 10$ . Thin lines represents  $\lim_{N \rightarrow \infty} \phi_G(f', f)$ . At fixation time scales, regular graphs behave differently. B) The cycle graph is a suppressor of fixation under dB updating. C) For small  $N$  ( $N=10$  here), the 2d lattice behaves like a suppressor of selection. D) The cycle graph being a suppressor of fixation, attains the same steady-state average fitness in the mutation selection balance as the complete graph. For large  $N$ , 2d lattice attains the same fitness as the other graphs. At longer time scales, regular graphs have identical steady-state statistics contrary to their differences at shorter fixation time scales. Parameters: mutant fitness distribution,  $\rho(f', f) = \frac{1}{f_{\max} - f_{\min}}$  with  $f_{\min} = 0.1$  and  $f_{\max} = 10$ .

### 3.5.4 Reversibility

The primary reference for this section is [77]. Using the Kolmogorov criterion [94], the neutral Moran origin-fixation dynamics turns out to be reversible. With this, the origin-fixation dynamics under selection is reversible if  $\Psi_G^T(r)$

is a power law,

$$\Psi_G^{\mathcal{I}}(r) = r^\nu, \quad (3.54)$$

where  $r$  is used as a shorthand for  $\frac{f'}{f}$ , and  $\nu$  is given by the relation,

$$\nu = 2 \frac{\frac{d\phi_G^{\mathcal{I}}}{dr}}{\phi_G^{\mathcal{I}}(r)} \Big|_{r=1}. \quad (3.55)$$

In general,  $\Psi_G^{\mathcal{I}}(r)$  need not be a power law. Therefore, to check the scope for reversibility a logarithmic expansion is performed on  $\Psi_G^{\mathcal{I}}(r)$ ,

$$\begin{aligned} \log \Psi_G^{\mathcal{I}}(r) &= \sum_{j=0}^{\infty} \frac{c_{2j+1}}{(2j+1)!} (\log r)^{2j+1}, \\ &= c_1 \log r \left[ 1 + \frac{1}{c_1} \sum_{j=1}^{\infty} \frac{c_{2j+1}}{(2j+1)!} (\log r)^{2j} \right], \\ &= \nu \log r \left[ 1 + \frac{1}{\nu} \sum_{j=1}^{\infty} \frac{c_{2j+1}}{(2j+1)!} (\log r)^{2j} \right], \end{aligned} \quad (3.56)$$

where,

$$c_i = \frac{d^i \log \Psi_G^{\mathcal{I}}}{d(\log r)^i} \Big|_{r=1}. \quad (3.57)$$

The second term of the series gives us the conservative estimate of the range of fitness values for which the origin-fixation dynamics is reversible,  $(r_0^{-1}, r_0)$  and  $r_0$  is found by setting a tolerance  $\varepsilon$ ,

$$\frac{|c_3|}{6\nu} (\log r_0)^2 = \varepsilon. \quad (3.58)$$

For the complete and the cycle graph,  $\Psi_G$  is a strict power-law with  $c_3 = 0$ , which is why  $r_0 \rightarrow \infty$  for these structures. However, for the 2d lattice,  $\frac{|c_3|}{6\nu}$  saturates to a finite value at larger  $N$ , see Fig. 3.8, as both  $c_3$  and  $\nu$  scales as  $N$  at large population sizes.

$$\begin{aligned} c_3 &= \frac{(N-2)^2(4N^2-9N+6)}{16(N-1)^3} \approx \frac{N}{4} + \mathcal{O}\left(\frac{1}{N^2}\right), \\ \nu &= N - \frac{5}{2} + \frac{1}{2(N-1)}. \end{aligned} \quad (3.59)$$



This makes  $r_0$  finite with a value approximately equal to 3 and the range of fitness values where the Moran dB origin-fixation dynamics is reversible is  $r \in (0.33, 3)$ . Similarly,  $\frac{|c_3|}{6\nu} \sim \frac{1}{N}$  for the temperature initialised star graph under dB (dB<sup>p</sup>) dynamics. As a result  $r_0 \rightarrow \infty$  in the limit  $N \rightarrow \infty$ . The same result holds for the star graph under dB<sup>o</sup> dynamics.

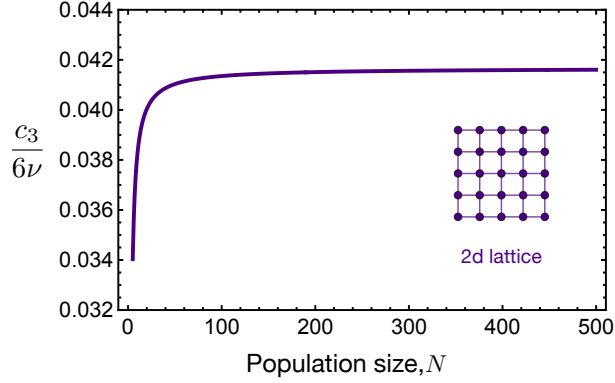


Figure 3.8: **Reversible Moran dB origin-fixation dynamics on the 2d lattice.** Coefficient  $\frac{|c_3|}{6\nu}$  of the second term of Eq. 3.56 saturates to finite value for large  $N$ , which results in the range of fitness values where the origin-fixation dynamics is reversible to be  $r \in (0.33, 3)$ .

### 3.5.5 Standard deviation in the steady-state fitness distribution

In this section, we derive the expressions for the standard deviation in fitness in the steady-state. For the complete graph we know that,

$$P_C(f) = \frac{N-1}{f_{\max}^{N-1} - f_{\min}^{N-1}} f^{N-2} \quad \text{and} \quad \langle f \rangle_C = \frac{N-1}{N} \frac{f_{\max}^N - f_{\min}^N}{f_{\max}^{N-1} - f_{\min}^{N-1}}, \quad (3.60)$$

and

$$\langle f^2 \rangle_C = \frac{N-1}{N+1} \frac{f_{\max}^{N+1} - f_{\min}^{N+1}}{f_{\max}^{N-1} - f_{\min}^{N-1}}. \quad (3.61)$$

Therefore, the variance turns out to be

$$\begin{aligned}
\text{Var}_C &= \langle f^2 \rangle_C - (\langle f \rangle_C)^2, \\
&= f_{\min}^2 \left[ \frac{N-1}{N+1} \frac{\left(\frac{f_{\max}}{f_{\min}}\right)^{N+1} - 1}{\left(\frac{f_{\max}}{f_{\min}}\right)^{N-1} - 1} - \left(\frac{N-1}{N}\right)^2 \left( \frac{\left(\frac{f_{\max}}{f_{\min}}\right)^N - 1}{\left(\frac{f_{\max}}{f_{\min}}\right)^{N-1} - 1} \right)^2 \right], \\
&\approx f_{\max}^2 \left( \frac{N-1}{N+1} - \left(\frac{N-1}{N}\right)^2 \right), \\
&= \frac{f_{\max}^2}{N^2} + \mathcal{O}\left(\frac{1}{N^3}\right).
\end{aligned} \tag{3.62}$$

Therefore, the standard deviation in fitness for the complete scales as  $\sim 1/N$ . For the star graph under  $\text{dB}^o$  dynamics, in the limit of large  $N$

$$P_{\text{dB}^o, \star}(f) = \frac{3f^2}{f_{\max}^3 - f_{\min}^3} \quad \text{and} \quad \langle f \rangle_{\text{dB}^o, \star} = \frac{3}{4} \frac{f_{\max}^4 - f_{\min}^4}{f_{\max}^3 - f_{\min}^3}, \tag{3.63}$$

and

$$\langle f^2 \rangle_{\text{dB}^o, \star} = \frac{3}{5} \frac{f_{\max}^5 - f_{\min}^5}{f_{\max}^3 - f_{\min}^3}. \tag{3.64}$$

Therefore the variance,

$$\begin{aligned}
\text{Var}_{\text{dB}^o, \star} &= \langle f^2 \rangle_{\text{dB}^o, \star} - (\langle f \rangle_{\text{dB}^o, \star})^2, \\
&\approx \frac{3}{80} f_{\max}^2.
\end{aligned} \tag{3.65}$$

The standard deviation for the  $\text{dB}^o$  star graph is independent of  $N$  and asymptotes to a finite value. Similarly, for the  $\text{dB}^p$  star graph, for  $N \gg 1$  we have

$$\begin{aligned}
\text{Var}_{\text{dB}^p, \star} &= \langle f^2 \rangle_{\text{dB}^p, \star} - (\langle f \rangle_{\text{dB}^p, \star})^2, \\
&\approx \frac{1}{18} f_{\max}^2,
\end{aligned} \tag{3.66}$$

which is again independent of  $N$ . Note that for large  $N$ ,  $\text{Var}_{\text{dB}^p, \star} > \text{Var}_{\text{dB}^o, \star} > \text{Var}_C$ . The order of fluctuations can be understood from the large  $N$  limit

effective population size of the three structures—  $N$  for the complete graph, 2 for the dB<sup>o</sup> star graph and 1 for the dB<sup>p</sup> star graph.

Under Bd updating, we have seen that  $\Psi_\star$  is same for both the Bd<sup>o</sup> (Bd temperature initialisation) and Bd<sup>p</sup> (Bd uniform initialisation) star graph. Consequently, the Bd<sup>o</sup> and Bd<sup>p</sup> have the same steady-state statistics and thus, variance in the steady-state,

$$\begin{aligned}
\text{Var}_{\text{Bd}^o, \star} &= \text{Var}_{\text{Bd}^p, \star}, \\
&= \langle f^2 \rangle_{\text{Bd}^p, \star} - (\langle f \rangle_{\text{Bd}^p, \star})^2, \\
&= \left[ \frac{2N-1}{2N+1} \frac{f_{\max}^{2N+1} - f_{\min}^{2N+1}}{f_{\max}^{2N-1} - f_{\min}^{2N-1}} - \left( \frac{2N-1}{2N} \frac{f_{\max}^{2N} - f_{\min}^{2N}}{f_{\max}^{2N-1} - f_{\min}^{2N-1}} \right)^2 \right], \\
&\approx f_{\max}^2 \left[ \frac{2N-1}{2N+1} - \left( \frac{2N-1}{2N} \right)^2 \right], \\
&= \frac{f_{\max}^2}{4N^2} + \mathcal{O}\left(\frac{1}{N^3}\right).
\end{aligned} \tag{3.67}$$

Therefore, the standard deviation for the star graph under Moran origin-fixation Bd updating scales as  $\sim \frac{1}{2N}$ .

### 3.5.6 Long-term evolution on discrete fitness space

To study Bd and dB long-term dynamics on random graphs we define a Markov chain. To proceed we first discretise the fitness space. The states are labelled with integer values from  $0, 1, \dots, z$ . For  $1 \leq i \leq z-1$ , the fitness of state  $i$  is equal to  $f_i = f_{\min} + i \cdot \delta$ . The boundaries fitness are  $f_0 = f_{\min}$  and  $f_z = f_{\max}$ . The long-term dynamics on a graph  $G$  is a Markov chain obeying the equation,

$$\mathbf{P}_G(t+1) = \mathbf{P}_G(t) \cdot \mathbf{T}_G, \tag{3.68}$$

where  $\mathbf{P}_G(t) = (P_{G,0}(t), P_{G,1}(t), \dots, P_{G,z}(t))$  with  $P_{G,i}(t)$  being the probability for the population to be in fitness state  $f_i$  at time step  $t$ . The transition

matrix  $\mathbf{T}_G$  on the fitness space is given as,

$$T_{G,ij} = \begin{cases} \frac{1}{2}\Phi_G^{\mathcal{I}}(f_{j+1}, f_j), & \text{if } i = j + 1 \text{ and } 0 \leq j < z, \\ \frac{1}{2}\Phi_G^{\mathcal{I}}(f_{j-1}, f_j), & \text{if } i = j - 1 \text{ and } 0 < j \leq z, \\ 1 - \sum_{k \neq i} T_{G,ki}, & \text{if } i = j. \end{cases} \quad (3.69)$$

Matrix  $\mathbf{T}_G$  is a positive and an irreducible matrix, therefore we can find the steady-state distribution  $\mathbf{P}_G^*$  using the Perron-Frobenius theorem [95].  $\mathbf{P}_G^*$  is the left eigenvector of the matrix  $\mathbf{T}_G$  corresponding to eigenvalue 1,

$$\mathbf{P}_G^* \cdot \mathbf{T}_G = 1 \cdot \mathbf{P}_G^*. \quad (3.70)$$

The steady-state average fitness is then,

$$\langle f \rangle_G^* = \mathbf{f} \cdot \mathbf{P}_G^*, \quad (3.71)$$

where  $\mathbf{f} = (f_{\min}, f_1, f_2, \dots, f_{\max})$  is the fitness vector.

### 3.5.7 Criterion for a graph to have higher steady-state fitness than the complete graph

Just by looking at the  $\Phi_G^{\mathcal{I}}(f', f)$  it is not easy to predict if the graph  $G$  will outcompete the complete graph in the mutation-selection balance of the Moran origin-fixation dynamics. The useful quantity for that purpose is the ratio of fixation probabilities,  $\Psi_G^{\mathcal{I}}(f', f)$  as defined in Eq. 3.13. A sufficient condition for  $\langle f \rangle_G^* > \langle f \rangle_C^*$  is

$$\Psi_G^{\mathcal{I}}(f', f_{\max}) < \Psi_C(f', f_{\max}), \text{ for all } f'. \quad (3.72)$$

Let us show this.

Let us consider two graphs,  $G_1$  and  $G_2$  and denote the respective steady-state probability density functions for the Moran origin-fixation dynamics on these structures by,  $P_{G_1}^*(f)$  and  $P_{G_2}^*(f)$ . Without loss of generality, let us assume that  $\langle f \rangle_{G_1}^* > \langle f \rangle_{G_2}^*$ . This means,

$$\int df f \cdot P_{G_1}^*(f) > \int df f \cdot P_{G_2}^*(f) \quad (3.73)$$

Given that  $\int df P_{G_{1/2}}^*(f)$  is equal to 1, for the above inequality to hold, the functions  $P_{G_1}^*(f)$  and  $P_{G_2}^*(f)$  must intersect at some point, say  $\hat{f}$  so that

$$P_{G_1}^*(f_{\max}) > P_{G_2}^*(f_{\max}). \quad (3.74)$$

We assume that the intersection takes place at one fitness point,  $\hat{f}$ . With this assumption, below we show that Eq. 3.73 follows from the Eq. 3.74. Now

$$P_{G_1}^*(f) = \begin{cases} P_{G_2}^*(f) + \varepsilon^<(f), & \text{if } f \leq \hat{f} \quad \text{with } \varepsilon^<(f) < 0 \\ P_{G_2}^*(f) + \varepsilon^>(f), & \text{otherwise} \quad \text{with } \varepsilon^>(f) > 0. \end{cases}$$

Because

$$\int df P_{G_1}^*(f) = \int df P_{G_2}^*(f) + \int_{f_{\min}}^{\hat{f}} df \varepsilon^< + \int_{\hat{f}}^{f_{\max}} df \varepsilon^> = 1, \quad (3.75)$$

therefore,

$$\left| \int_{f_{\min}}^{\hat{f}} df \varepsilon^< \right| = \left| \int_{\hat{f}}^{f_{\max}} df \varepsilon^> \right|. \quad (3.76)$$

$$\langle f \rangle_{G_1}^* = \langle f \rangle_{G_2}^* + \int_{f_{\min}}^{\hat{f}} df f \varepsilon^< + \int_{\hat{f}}^{f_{\max}} df f \varepsilon^>. \quad (3.77)$$

Now,

$$\left| \int_{\hat{f}}^{f_{\max}} df f \varepsilon^> \right| > \hat{f} \left| \int_{\hat{f}}^{f_{\max}} df \varepsilon^> \right| = \hat{f} \left| \int_{f_{\min}}^{\hat{f}} df \varepsilon^< \right| > \left| \int_{f_{\min}}^{\hat{f}} df f \varepsilon^< \right|. \quad (3.78)$$

This implies,

$$\begin{aligned} \int_{f_{\min}}^{\hat{f}} df f \varepsilon^< + \int_{\hat{f}}^{f_{\max}} df f \varepsilon^> &= - \left| \int_{f_{\min}}^{\hat{f}} df f \varepsilon^< \right| + \left| \int_{\hat{f}}^{f_{\max}} df f \varepsilon^> \right| \\ &> 0. \end{aligned} \quad (3.79)$$

Therefore,  $\langle f \rangle_{G_1}^* > \langle f \rangle_{G_2}^*$ . Now what does it mean for  $P_{G_1}^*(f_{\max}) > P_{G_2}^*(f_{\max})$ ? One possibility for the inequality to hold is,

$$\Psi_{G_1}^{\mathcal{I}}(f', f_{\max}) < \Psi_{G_2}^{\mathcal{I}}(f', f_{\max}), \text{ for all } f'. \quad (3.80)$$

The criterion  $\Psi_G^{\mathcal{I}}(f', f_{\max}) < \Psi_C(f', f_{\max})$  for all  $f'$ , is easily satisfied by amplifiers of selection. It follows directly from the definition of amplifiers of selection. Amplifiers of selection are better in preventing the fixation of deleterious mutations and fixing advantageous mutants. Therefore, for an amplifier of selection,

$$\underbrace{\frac{\Phi_{AoS}^{\mathcal{I}}(f', f_{\max})}{\Phi_{AoS}^{\mathcal{I}}(f_{\max}, f')}}_{\Psi_{AoS}^{\mathcal{I}}(f', f_{\max})} < \underbrace{\frac{\Phi_C(f', f_{\max})}{\Phi_C(f_{\max}, f')}}_{\Psi_C(f', f_{\max})} \text{ for all } f'. \quad (3.81)$$

Subscript  $AoS$  denotes an amplifier of selection. Similarly for a suppressor of selection,

$$\underbrace{\frac{\Phi_{SoS}^{\mathcal{I}}(f', f_{\max})}{\Phi_{SoS}^{\mathcal{I}}(f_{\max}, f')}}_{\Psi_{SoS}^{\mathcal{I}}(f', f_{\max})} > \underbrace{\frac{\Phi_C(f', f_{\max})}{\Phi_C(f_{\max}, f')}}_{\Psi_C(f', f_{\max})} \text{ for all } f'. \quad (3.82)$$

Subscript  $SoS$  denotes a suppressor of selection.

For suppressors of fixation, it is not obvious if they satisfy the criterion to attain higher average steady-state fitness in the mutation-selection balance. Suppressors of fixation have lower probability to fix beneficial mutations, as a result,  $[\Phi_{SoF}^{\mathcal{I}}(f_{\max}, f')]^{-1} > [\Phi_C(f_{\max}, f')]^{-1}$  (here  $SoF$  denotes a suppressor of fixation). However, they are also good in preventing the fixation of deleterious mutants,  $\Phi_{SoF}^{\mathcal{I}}(f', f_{\max}) < \Phi_C(f', f_{\max})$ . This means that a suppressor of fixation can satisfy the criterion 3.72 by compensating for its lower probability of fixation of beneficial mutants by rejecting deleterious mutants more efficiently. An example is presented in ref. [53]. Note that the criterion 3.72 holds for any update rule.

Let us apply derived the sufficient condition to the complete graph,  $\text{dB}^o$  and  $\text{dB}^p$  star graph. From Fig. 3.9, we see that the steady-state probability density functions for any two graphs intersect at only point, and thus we can use our criteria here. From Eqs. 3.14, 3.20, 3.23, we have

$$\Psi_C^{\mathcal{I}}(f', f_{\max}) < \Psi_{\text{dB}^o, \star}(f', f_{\max}) < \Psi_{\text{dB}^p, \star}(f', f_{\max}), \quad (3.83)$$

therefore,  $\langle f \rangle_C^* > \langle f \rangle_{dB^o, \star}^* > \langle f \rangle_{dB^p, \star}^*$ .

As a side remark the steady-state density functions are monotonic w.r.t fitness. Their monotonicity follows from the monotonicity in the corresponding fixation profiles.

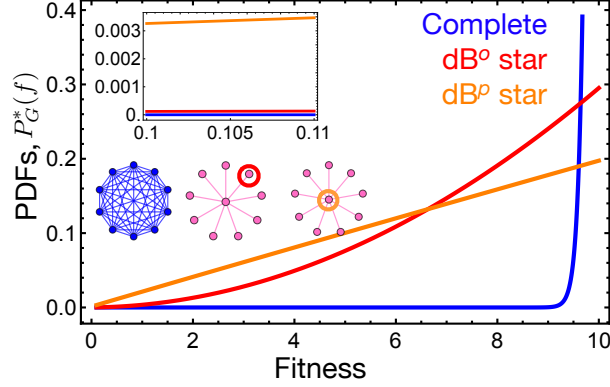


**Figure 3.9: A pair of probability density functions intersect at one fitness point.** The steady-state probability density functions (PDFs) for the complete graph, the  $dB^o$  and the  $dB^p$  star graph are shown. Firstly, the PDFs are monotonically increasing w.r.t fitness. Secondly, any pair of PDFs intersects at one point. Thus the sufficient condition 3.72 gives the ordering of average fitnesses. Parameters:  $N = 100$ ,  $f_{\min} = 0.1$ ,  $f_{\max} = 10$ ,  $\rho(f', f) = \frac{1}{f_{\max} - f_{\min}}$ .

To proceed, we recall that the steady-state fitness probability density function for a graph  $G$  is

$$P_G^*(f) = \frac{1}{\int df' \frac{\Phi_G^{\mathcal{I}}(f', f)}{\Phi_G^{\mathcal{I}}(f, f')} \cdot \frac{\rho(f', f)}{\rho(f, f')}}. \quad (3.84)$$

Assuming uniform mutational fitness distribution, we have

$$P_G^*(f) = \frac{1}{\int df' \frac{\Phi_G^{\mathcal{I}}(f', f)}{\Phi_G^{\mathcal{I}}(f, f')}}. \quad (3.85)$$

Taking derivative w.r.t  $f$ ,

$$\begin{aligned} \frac{dP_G^*(f)}{df} = & - \frac{1}{\left( \int df' \frac{\Phi_G^{\mathcal{I}}(f', f)}{\Phi_G^{\mathcal{I}}(f, f')} \right)^2} \left[ \int df' \left( \frac{1}{\Phi_G^{\mathcal{I}}(f, f')} \frac{d}{df} \Phi_G^{\mathcal{I}}(f', f) \right. \right. \\ & \left. \left. - \frac{\Phi_G^{\mathcal{I}}(f', f)}{\Phi_G^{\mathcal{I}2}(f, f')} \frac{d}{df} \Phi_G^{\mathcal{I}}(f, f') \right) \right] \end{aligned} \quad (3.86)$$

If we assume monotonicity in the fixation probability profiles, that is,

$$\frac{d}{df} \Phi_G^{\mathcal{I}}(f', f) < 0, \quad \text{and} \quad \frac{d}{df} \Phi_G^{\mathcal{I}}(f, f') > 0, \quad (3.87)$$

We obtain,

$$\frac{dP_G^*(f)}{df} > 0 \quad \text{for all } f. \quad (3.88)$$

Hence, the steady-state probability density functions are monotonic in fitness.

### 3.5.8 Effects of deleterious mutants on the initial phase of the long-term dynamics

So far we have studied the effect of preventing/fixing deleterious mutants on the steady-state fitness statistics of graph. In this section, we explore the role of deleterious mutant regime on the initial phase of the mutation-selection dynamics, particularly the average selection coefficient of the first substitution given that the initial fitness is  $f$ ,

$$\frac{\Delta_G f}{f} = \int df' \frac{f' - f}{f} \Phi_G^{\mathcal{I}}(f', f) \rho(f', f). \quad (3.89)$$

This quantity is also equal to the instantaneous rate of evolution [39], [62]. From Fig. 3.10 A, we see that the mean selection coefficient decreases as the population is started with initial population fitness closer to the average steady-state fitness. The mean selection coefficient is anticipated to be positive if the initial fitness is below the average steady-state fitness and negative if started with higher fitness values. However, in Ref. [72], for the complete



graph it has been shown that the mean selection coefficient of the first substitution is negative even if the population is initialised with fitness below the average steady-state fitness. We observe this effect to be more pronounced for the case of  $\text{dB}^p$  star graph. We investigate further by working out the large  $N$  case.

In the limit of  $N \rightarrow \infty$ , for the  $\text{dB}^p$  star graph under Moran  $\text{dB}^o$  updating and uniform mutational fitness distribution, we have

$$\begin{aligned} \frac{\Delta_{\text{dB}^p, \star} f}{f} &= \frac{1}{f_{\max} - f_{\min}} \int df' \frac{f' - f}{f} \frac{f'}{f + f'} \\ &= \frac{f_{\max} + f_{\min} - 4f}{2f} - \frac{1}{f_{\max} - f_{\min}} 2f \log \left( \frac{f_{\max} + f}{f_{\min} + f} \right). \end{aligned} \quad (3.90)$$

The value of  $f$  for which the mean selection coefficient (right hand side of the above equation) goes to zero is obtained numerically. The difference of the obtained fitness value and the average steady-state fitness for the  $\text{dB}^p$  graph,  $\delta f$  is shown in Fig. 3.10 B. For the parameters we use throughout the manuscript, the  $\delta f$  for the  $\text{dB}^p$  star graph is finite, even in the limit of  $N \rightarrow \infty$ . This means that if the long-term mutation-selection dynamics is initiated with fitness value in between  $\langle f \rangle_{\text{dB}^p, \star}^* - \delta f$  and  $\langle f \rangle_{\text{dB}^p, \star}^*$ , the first mutation to fix on average is deleterious. Therefore, the corresponding average fitness trajectories does not have monotonically increasing fitnesses. For the complete graph, in the limit of  $N \rightarrow \infty$ ,

$$\begin{aligned} \frac{\Delta_C f}{f} &= \frac{1}{f_{\max} - f_{\min}} \int df' \frac{f' - f}{f} \frac{f' - f}{f'} \\ &= \frac{1}{f_{\max} - f_{\min}} \left( -2f_{\max} + \frac{f_{\max}^2}{2f} + \frac{3f}{2} + f \log \frac{f_{\max}}{f} \right). \end{aligned} \quad (3.91)$$

The r.h.s in the above equation goes to 0 for  $f = f_{\max}$ . Therefore, while  $\delta f$  is non-zero for finite population sizes, in the limit of  $N \rightarrow \infty$ ,  $\delta f = 0$  for the complete graph.

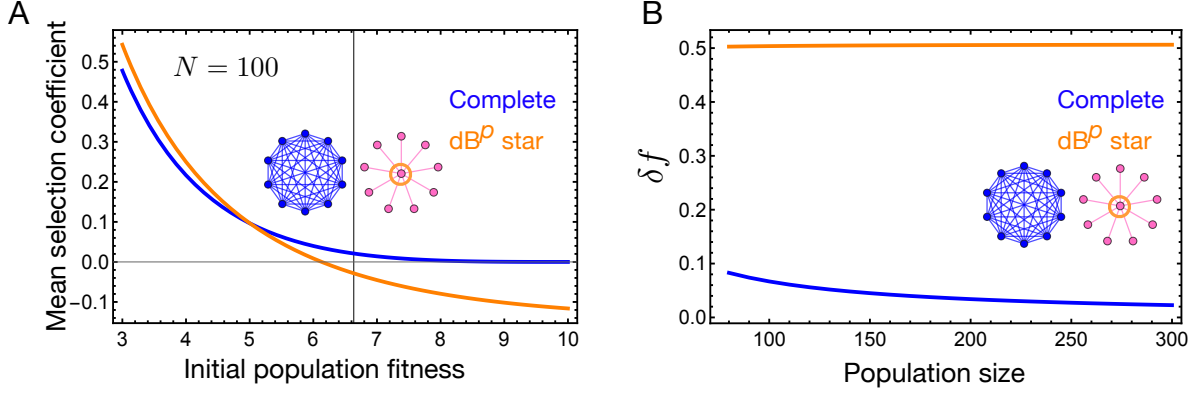


Figure 3.10: **Mean selection coefficient of the first substitution.** The black grid line in A) corresponds to the average steady-state fitness of the dB<sup>p</sup> star graph. The mean selection coefficient is negative even if the population's initial fitness is below the steady-state average fitness, thus leading to non-monotonic average fitness trajectories. B) Denoting  $\delta f$  as the region of fitness values below the steady-state average fitness for which the mean selection coefficient is negative, in the limit of large  $N$   $\delta f$  asymptotes to 0.5 for the dB<sup>p</sup> star graph, whereas the gap decays to 0 for the complete graph. Parameters:  $N = 100$ ,  $f_{\min} = 0.1$ ,  $f_{\max} = 10$ ,  $\rho(f', f) = \frac{1}{f_{\max} - f_{\min}}$ .

### 3.5.9 Amplifier of fixation and suppressor of fixation in a metapopulation model

The amplifiers and suppressors of fixation are not solely restricted to one node one individual models, but can also be found in the network structured metapopulations [90]. The model in ref. [90] assumes time scale separation. The model has been analysed in the low migration rate regime where each node/deme is mainly in a monomorphic state. That is, when an individual migrates to a neighboring patch with a different type, either the migrating individual fixes or goes extinct before the next migration event occurs. The wild-type and the mutant type are assumed to have non-zero death rates, as a consequence of which the population sizes of fully mutant and wild-type demes are different. Here we assume that for both the individual types, the death rate is incorporated with the birth rate to give an effective growth rate. In this way, the population size for the mutant and wild-type deme is the same. The number of leaf demes is denoted by  $d$ . The probability

that an individual from a given leaf deme migrates to the center deme is  $m_I$ , whereas the probability that an individual from the central deme migrates to leaf deme is  $m_O$ . The parameter  $\alpha = m_I/m_O$  quantifies the migration asymmetry. The probability that the mutant type with relative fitness  $r$  takes over the entire star network-structured metapopulation given that the population is initialised with central deme being the mutant deme and leaf demes being the wild-type demes is given by,

$$\Phi_{\star}^{\bullet} = \frac{1 - \gamma^2}{1 + \alpha\gamma - \gamma(\alpha + \gamma) \left( \frac{\gamma(1+\alpha\gamma)}{\alpha+\gamma} \right)^d}, \quad (3.92)$$

where

$$\alpha = \frac{m_I}{m_O} \quad \text{and} \quad \gamma = \frac{\Phi_{C_W}}{\Phi_{C,M}} \quad (3.93)$$

with

$$\Phi_{C,M} = \frac{1 - \frac{1}{r}}{1 - \frac{1}{r^N}} \quad \text{and} \quad \Phi_{C,W} = \frac{1 - r}{1 - r^N}. \quad (3.94)$$

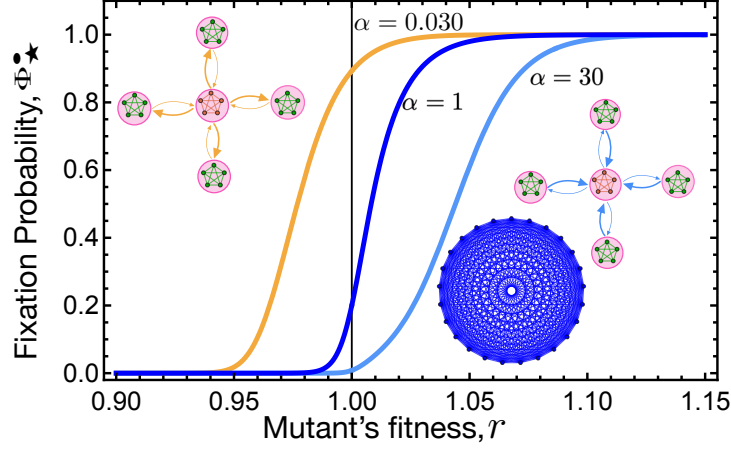


Figure 3.11: **Amplifier and suppressor of fixation in meta-star.** The probability that a mutant fixates in a star-structured metapopulation is shown given that the population is initialised with the central deme being the mutant deme. The probability that an individual from the central migrates to a leaf deme is  $m_O$ , and the probability of migration for an individual migrating from a leaf node to the central node is  $m_I$ . Parameter  $\alpha = m_I/m_O$  quantifies the migration asymmetry. According to the generalized circulation theorem in ref. [90], for  $\alpha = 1$ , the mega-star's fixation probability is the same as in the well-mixed population when started with  $N$  mutant individuals. Changing  $\alpha$  from 1 gives two different fixation probability profiles: the amplifier of fixation (for lower  $\alpha$ ) and the suppressor of fixation (for higher  $\alpha$ ). We have encountered these profiles in the main text for one node one individual star under  $\text{Bd}^o$  and  $\text{dB}^p$ . Parameters: size of a each deme,  $N = 80$  and the total number of demes  $D = d + 1 = 5$ .

# Chapter 4

## Self-loops: friends or foes?

Chapters 2 and 3 focus on the long-term dynamics with low mutation rates. The mutation rates are sufficiently low so that the next mutation occurs only when the previous mutation has either fixed or become extinct. Thus, the low mutation long-term dynamics is essentially a fixation-like dynamics. While it is expected that amplifiers of selection achieve higher fitness than the well-mixed population for low mutation rates, it is not clear what happens for higher mutation rates. This is the aspect we explore in this chapter.

This chapter underwent peer-review and is published with open access in PLoS Computational Biology as: Sharma, Yagoobi, and Traulsen 2023, [96]—Self-loops in evolutionary graph theory: Friends or foes? The authors contributions are detailed at the end of the thesis.

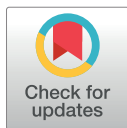
RESEARCH ARTICLE

# Self-loops in evolutionary graph theory: Friends or foes?

Nikhil Sharma, Sedigheh Yagoobi, Arne Traulsen \*

Department of Theoretical Biology, Max Planck Institute for Evolutionary Biology, Plön, Germany

\* [traulsen@evolbio.mpg.de](mailto:traulsen@evolbio.mpg.de)



## Abstract

Evolutionary dynamics in spatially structured populations has been studied for a long time. More recently, the focus has been to construct structures that amplify selection by fixing beneficial mutations with higher probability than the well-mixed population and lower probability of fixation for deleterious mutations. It has been shown that for a structure to substantially amplify selection, self-loops are necessary when mutants appear predominately in nodes that change often. As a result, for low mutation rates, self-looped amplifiers attain higher steady-state average fitness in the mutation-selection balance than well-mixed populations. But what happens when the mutation rate increases such that fixation probabilities alone no longer describe the dynamics? We show that self-loops effects are detrimental outside the low mutation rate regime. In the intermediate and high mutation rate regime, amplifiers of selection attain lower steady-state average fitness than the complete graph and suppressors of selection. We also provide an estimate of the mutation rate beyond which the mutation-selection dynamics on a graph deviates from the weak mutation rate approximation. It involves computing average fixation time scaling with respect to the population sizes for several graphs.

## OPEN ACCESS

**Citation:** Sharma N, Yagoobi S, Traulsen A (2023) Self-loops in evolutionary graph theory: Friends or foes? PLoS Comput Biol 19(9): e1011387. <https://doi.org/10.1371/journal.pcbi.1011387>

**Editor:** Yamir Moreno, University of Zaragoza: Universidad de Zaragoza, SPAIN

**Received:** March 27, 2023

**Accepted:** July 25, 2023

**Published:** September 1, 2023

**Peer Review History:** PLOS recognizes the benefits of transparency in the peer review process; therefore, we enable the publication of all of the content of peer review and author responses alongside final, published articles. The editorial history of this article is available here: <https://doi.org/10.1371/journal.pcbi.1011387>

**Copyright:** © 2023 Sharma et al. This is an open access article distributed under the terms of the [Creative Commons Attribution License](https://creativecommons.org/licenses/by/4.0/), which permits unrestricted use, distribution, and reproduction in any medium, provided the original author and source are credited.

**Data Availability Statement:** All relevant data are within the manuscript. Our code and data is available at [https://gitlab.gwdg.de/nsharma/self\\_loops\\_egt](https://gitlab.gwdg.de/nsharma/self_loops_egt).

**Funding:** This work was funded by the Max Planck Society. The funders had no role in study design,

## Author summary

Evolutionary and ecological dynamics is strongly affected by the underlying population structure. Evolutionary graph theory considers networks in which individuals are placed on the nodes and replace each other via the links. Amplifiers and suppressors of selection are particularly intriguing structures that can effectively change the selective advantage of a mutant compared to unstructured populations. For very low mutation rates, strong amplification requires that mutants can replace their parents via self-loops. We show that this beneficial role of self-loops is reversed when the mutation rate is increased: In this case, self looped-graphs have a lower average fitness in mutation-selection balance. More generally, we show that suppressors of fixation—structures that reduce the fixation of mutants regardless of their relative fitness—can increase the fitness in mutation selection balance both for weak mutation and for strong mutation. This calls for a closer investigation of structures other than the amplifiers of selection.

data collection and analysis, decision to publish, or preparation of the manuscript.

**Competing interests:** The authors have declared that no competing interests exist.

## 1 Introduction

Evolutionary graph theory (EGT) studies the role of spatial structure in evolutionary dynamics [1]. In this framework, a spatially structured population is modelled as a graph with nodes representing asexually reproducing individuals, while the links dictate the interactions among these nodes. In general, the links of a graph can be weighted and directed. So far, the main focus of the EGT has been to study quantities like fixation probability and fixation times for different graphs. The fixation probability is the probability that a mutant individual takes over the population of wild-types, and the time it takes to do so, is called the fixation time. The fixation probability is a central object in evolutionary biology [2–6]. For low mutation rates, it determines the rate of evolution [7, 8]. Based on the fixation probability, most graphs can be categorised into two categories: Amplifiers of selection and suppressors of selection [9]. An amplifier of selection is a structure that—compared to the complete graph (the well-mixed population)—has higher probability to fix beneficial mutants, and lower probability to fix deleterious mutants [10]. On the other hand, a suppressor of selection has higher probability to fix deleterious mutants, and lower probability to fix beneficial mutants than the complete graph.

In a complete graph, every node is alike; therefore, the fixation probability for a mutant starting from any of the nodes is equal. However, this is not true in general. For an arbitrary structure, the fixation probability depends crucially on the node where the initial mutant appears [11, 12]. Hence, the mutant initialisation scheme needs to be specified while stating the fixation probability for a graph. Two commonly used mutant initialisation schemes are uniform mutant initialisation and temperature mutant initialisation. Under the uniform mutant initialisation scheme, the initial mutant is equally likely to appear in every node. Under the temperature mutant initialisation scheme, the initial mutant appears in a node with probability proportional to its temperature, where the temperature of a node is the sum of the weights of the links directed towards the focal node [10]. In general, a graph can have very different fixation probability profiles under different mutant initialisation schemes. For example, the star graph is an amplifier of selection under the uniform mutant initialisation scheme, whereas, it is a suppressor of selection (in the limit of infinite population size) under the temperature mutant initialisation scheme [13].

Recently, evolutionary dynamics on graphs has been studied beyond the fixation time scales by allowing mutations to appear continuously [14–16]. The main quantities of interest in those long-term mutation-selection dynamics are the mutation-selection balance [17] and the mixing time, the time it takes for the dynamics to reach the steady-state [18, 19]. For very low mutation rates, amplifiers of selection attain higher average steady-state fitness in the mutation-selection balance than the well-mixed population, and, suppressors of selection attain lower average steady-state fitness in the mutation-selection balance than the well-mixed population [16]. A suppressor of selection attains lower average steady-state fitness in the mutation-selection balance because it is worse in fixing beneficial mutants and better in fixing deleterious mutants than the complete graph. An amplifier of selection attains higher average steady-state fitness in the mutation-selection balance, because it is better in fixing beneficial mutants and in preventing the fixation of deleterious mutants. In Ref. [20], it has been proven that self-loops are necessary to generate substantial amplification. While we know that in the low mutation rate regime, the self-looped star—an amplifier of selection—adapts better than the complete graph, it is not clear what happens to these self-looped amplifiers when the mutation rate is increased beyond the low mutation rate regime. This is what we investigate here. We find that self-loops can have a detrimental effect on average fitness when the mutation rate increases.

## 2 Methods

### 2.1 Moran Birth-death dynamics with mutation

To study evolutionary dynamics on graphs, we use the Moran Birth-death (Bd) updating. The letter B of the shorthand Bd stands for birth, whereas d stands for death. In Bd updating selection operates during the birth event, and it is represented by the capital letter B. Death occurs randomly with uniform probability, and it is represented by the small letter d. The first letter of a shorthand represents a global event where every individual of the population participates. The second letter of the shorthand represents a local event where only individuals neighbouring the selected individual from the first event participate. More details on the types of evolutionary update rules in spatially structured populations can be found in [21].

To study mutation-selection dynamics on graphs, we use a modified version of Moran Bd updating where mutations occur with probability  $\mu$  when an offspring is produced, see Fig 1. One Moran Bd with mutation update step can be described as follows:

1. Birth: First, an individual at node  $i$  is selected with probability proportional to its fitness,  $\frac{f_i}{\sum_j f_j}$  to reproduce.
2. Mutation: The offspring is identical to the parent individual with probability  $1 - \mu$  or a mutant with probability  $\mu$ . If the offspring is a mutant, its fitness  $f'$  is sampled from the mutant fitness distribution  $\zeta(f', f_i)$  with  $f_i$  being the parent's fitness.
3. Death: A random neighbour of node  $i$ , say node  $k$ , is chosen for replacement with probability  $\frac{w_{ik}}{\sum_j w_{ij}}$ . With probability,  $\frac{w_{ii}}{\sum_j w_{ij}}$ , the same parent individual can be chosen for replacement via a self-loop. The offspring finally replaces the chosen individual.

An individual's fitness  $f$  belongs to a continuous interval bounded by  $f_{\min}$  and  $f_{\max}$  and remains constant throughout the dynamics as long as it survives. The fitness of an individual is also independent of the frequencies of other types of individuals. In this work, we primarily consider uniform mutant fitness distribution, i.e.,  $\zeta(f', f) = \frac{1}{f_{\max} - f_{\min}}$ . In Sec. 3.5, we investigate evolutionary dynamics with Gaussian mutant fitness distribution.

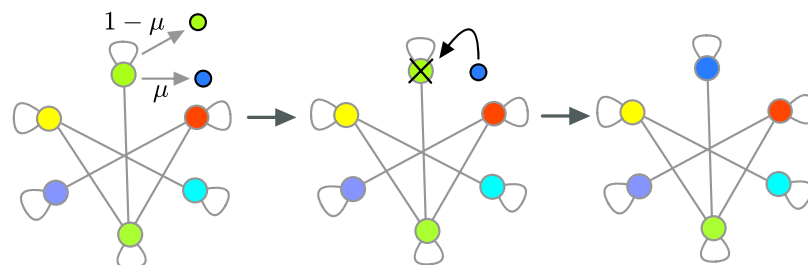


**Fig 1. Birth-death (Bd) updating with mutation.** Here we show an example of the single time step of the Moran Bd updating rule with mutation. First an individual is selected with probability proportional to its fitness to give birth to an offspring. The offspring resembles the parent with probability  $1 - \mu$ , or mutates with probability  $\mu$ . If the mutation occurs, the offspring fitness  $f'$  is then sampled from the distribution  $\zeta(f', f)$  with  $f$  being the parent's fitness. In the figure, we have shown the case when mutation takes place. The mutant offspring will then replace one of the individuals neighboring the parent individual, or the parent individual itself via the self-loop. The choice is made at random with probability proportional to the outgoing weight from the parent node. Here, we have shown the case when the parent individual is replaced by the offspring via the self-loop. The stronger the self-loop, more likely it is for the parent to be replaced by its offspring.

<https://doi.org/10.1371/journal.pcbi.1011387.g001>



At the level of graphs where each node is occupied by an individual, self-loops were introduced as mathematical objects [13]. However, they make clear sense when each node of a graph is occupied by a population. In that case, a graph is a population of populations [22] where the dynamics in the regime of low migration rate can be interpreted as the dynamics on a graph with strong self-looping [21, 23–27]. However, this work focuses on graphs with one individual per node.

### 3 Results

#### 3.1 Amplification in the low mutation rate regime

In this section we briefly summarise the results of Ref. [16] where the Moran Bd mutation-selection dynamics was studied in the low mutation rate regime. In this regime, a newly appeared mutant either reaches fixation or goes extinct before the next mutant appears in the population [28, 29]. For low mutation rates, the population is effectively monomorphic throughout the mutation-selection dynamics and thus, the dynamics can be modelled as a random walk problem on a bounded fitness space where a steady-state is attained in the long run. When a new mutation appears in the population, its fitness  $f'$  is sampled from the  $\zeta(f', f)$  distribution with  $f$  being parent's fitness. Only when the mutation also fixes (which happens with probability  $\phi_G^T(f', f)$ ), the fitness of population  $G$  transitions from  $f$  to  $f'$ . Thus, the combined transition rate from point  $f$  to  $f'$  equal to  $\phi_G^T(f', f) \zeta(f', f) \mu$ . The steady-state for a graph  $G$  subjected to a low mutation rate can be computed by assuming detailed-balance [30] as

$$P_G^*(f) = \frac{1}{\int df' \frac{\phi_G^T(f', f)}{\phi_G^T(f, f')} \cdot \frac{\zeta(f', f)}{\zeta(f, f')}}. \quad (1)$$

The fixation probabilities entering the steady-state expression 1 are temperature initialised ( $T$ ), because when a new mutant appears in a homogeneous population, according to the Moran Bd updating stated in Sec. 2.1, it is more likely to appear on the high temperature nodes.

The fixation probability of a mutant with fitness  $f'$  on the complete graph with background fitness  $f$  is given by [10]

$$\phi_c^T(f', f) = \phi_c(f', f) = \frac{1 - \frac{f}{f'}}{1 - \left(\frac{f}{f'}\right)^N}. \quad (2)$$

Using the above expression for the fixation probability and the Eq 1, we obtain the average steady-state fitness for the complete graph with uniform mutant fitness distribution,

$$\langle f \rangle_c^* = \int df f P_c^*(f) = \frac{N}{N+1} \frac{f_{\max}^{N+1} - f_{\min}^{N+1}}{f_{\max}^N - f_{\min}^N}. \quad (3)$$

Amplifiers of selection attain a higher steady-state average fitness than the well-mixed population. On the other hand, suppressors of selection attain lower steady-state fitness than the well-mixed population, see Ref. [16] for a formal proof. However, a suppressor of fixation, a structure that has lower fixation probabilities than the complete graph regardless of the mutant fitness values, can attain higher average fitness in the mutation-selection balance than the complete graph. This happens because of its ability to reject mutants more efficiently than the complete graph, compensating for its poor ability to fix beneficial mutants. These structures can also attain higher fitness than amplifiers of selection in the steady-state. Therefore, amplifiers

of selection are not the only structures that adapt better than well-mixed populations in the long-term evolutionary dynamics.

### 3.2 Beyond the low mutation rate regime

It has been suggested that the thresholds for mutation rates, beyond which amplifiers of selection deviate from the low mutation approximation are lower compared to the threshold at which the complete graph deviates from the same approximation [8, 31]. This happens because amplification of selection in graphs comes at the cost of higher fixation times of mutants [32, 33]. Thus, amplifiers are more likely to violate the low mutation rate criterion where a mutant appearing in the population should either reach fixation or go extinct before the next mutation appears [8]. However with high fixation times, a new mutant can appear while the previous mutation is still under way towards fixation or extinction, and thus leading to effects like clonal interference [34, 35].

Inside the low mutation rate regime, the steady-state average fitness of the population is independent of the mutation rate. However, the average steady-state fitnesses of various structures are expected to decrease as the mutation rate is increased beyond the low mutation rate regime. Outside the weak mutation rate regime, it is not clear how amplifiers of selection, suppressors of selection, suppressors of fixation, and the well-mixed population are ordered in terms of their average steady-state fitness. To analyse this, we simulate the Moran Birth-death update with mutation for the self-looped star graph (weighted), the complete graph, the cycle graph, the star graph, and the directed line with self-loops. These graphs are shown in Fig 2A. Notice that without self-loops, nodes of the directed graphs that have no incoming links are frozen during the mutation-selection dynamics and their states remain the same throughout the dynamics. To avoid this situation we focus instead on a structure where self-loops are added to all the nodes of the directed line to facilitate their participation in the evolutionary dynamics. The weight matrix of the self-looped star graph is given in Eq 23 with  $\lambda$  being the weight of the links directed from leaves to the center and  $\delta/(N-1)$  is the weight of the link directed from the center to leaves.

The self-looped star graph is a piecewise amplifier of selection (higher fixation probability for mutations up to a finite fitness advantage) [13] for finite population size. Only in the limit  $N \rightarrow \infty$ , it is a true amplifier of selection. The complete graph, and the cycle graph are isothermal graphs [1]. Under temperature initialisation, for finite  $N$ , the star graph is suppressor of fixation [13, 16]. The directed line with self-loops is a suppressor of selection [10]. From Fig 2B, we find that in the low mutation rate regime, the steady-state average fitness is highest for the self-looped star graph and the star graph, slightly lower for the complete and the cycle graph, and much lower for the self-looped directed line.

In Ref. [31], it has been shown that the temperature initialised star graph has a lower effective rate of evolution compared to the complete graph. However from Fig 2B, we see that the star graph attains higher steady-state average fitness than the complete graph. Therefore, a structure that speeds up evolution does not necessarily lead to higher fitness in the long-term evolutionary dynamics. Similarly, a structure that slows down evolution does not necessarily lead to lower fitness in the long-term evolutionary dynamics. Although at low mutation rates, the self-looped star graph outperforms all other graphs by attaining the highest steady state fitness, outside the low mutation rate regime, it performs poorly. On increasing the mutation rates, the star with self-loops not only attains lower steady-state fitness than the complete graph, but also lower than the directed line with self-loops, a suppressor of selection. The main reason for this poor adaptation of the self-looped star graph outside the low mutation rate regime are self-loops. We explore this in detail in the following section.

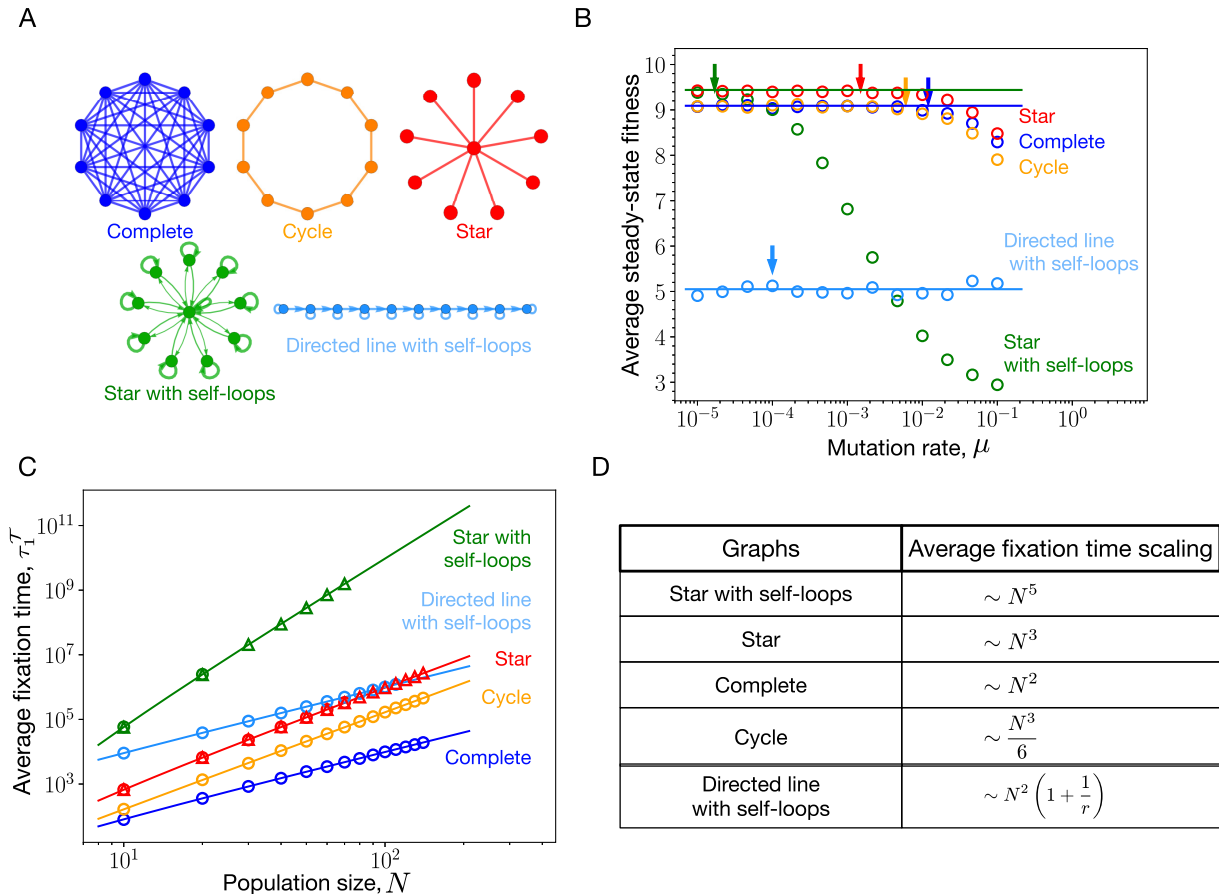


**Fig 2. Mutation rate threshold,  $\mu_{th}$ .** (A) We mostly work with these five graphs throughout the manuscript. (B) The steady-state average fitnesses obtained using the Moran Birth-death mutation-selection dynamics simulations for the self-looped (weighted) star graph, an amplifier of selection, the star graph, a suppressor of fixation, the self-looped directed line, a suppressor of selection, the cycle graph, an isothermal graph, and the complete graph are shown via circles as a function of mutation rates. Solid horizontal lines represent steady-state average fitnesses for different graphs obtained under the low mutation rate approximation, Eq 1. The arrows mark the mutation rates beyond which the low mutation rate approximation is violated for respective graphs. The graphs with higher average fixation time is expected to deviate earlier, see Eq 4. (C) The average fixation time scaling with  $N$  at neutrality is shown for different graphs. Solid lines are the analytical results whereas circles represent Moran Bd simulations. For larger  $N$ , it gets computationally expensive to work with microscopic Moran Bd simulations, in such cases we use a Gillespie algorithm, shown via triangles. For details on the Gillespie algorithm, refer to App. 5.3.3. (D) The scaling of the average fixation time with population size  $N$  for the different graphs. (Parameters: (B) population size,  $N = 10$ , uniform mutant fitness distribution, i.e.,  $\zeta(f', f) = \frac{1}{f_{max} - f_{min}}$ , (B,C) with 2000 total number of independent realisations used for averaging,  $f_{min} = 0.1$  and  $f_{max} = 10$ ).

<https://doi.org/10.1371/journal.pcbi.1011387.g002>

We conclude this section by providing an estimate for the threshold mutation rate  $\mu_{th}$  beyond which the dynamics is considered to be outside the low mutation rate regime. It is given by

$$\frac{1}{\mu_{th}} \approx \max_r \left\{ \tau_1^T(r), \bar{\tau}_1^T(r) \right\}, \quad (4)$$

where  $\tau_1^T(r)$  is the average fixation time and  $\bar{\tau}_1^T(r)$  is the average extinction time of a mutant with fitness  $r$  relative to the wild-type. Mutants appear according to the temperature

initialisation. Eq 4 follows from the criterion for the dynamics to be in the low mutation rate regime. Recall that the criterion for an evolutionary dynamics to be in the low mutation rate regime is that the time between any two successive mutations should be larger than the time to fixation or extinction (whichever is higher for a given pair of mutant and wild-type fitness) of a mutant. The fixation time and the extinction time of a mutant take random values from specific distributions [36–39]. To arrive at Eq 4, we make an approximation to the criterion by working at the level of average fixation and extinction times. By studying the average fixation and extinction time of the five graphs shown in Fig 2A, except the self-looped directed line, we found the average fixation time of a mutant to be consistently higher than the average extinction time of the mutant, see App. 5.3 for more details. Moreover, it is the average fixation time near neutrality that determines the mutation rate threshold for these graphs. For the complete graph, the phenomenon where the average fixation time peaks near neutrality was discussed in Ref. [40]. For the case of self-looped directed line, we found that the average fixation time decreases as the mutant relative fitness is increased, whereas, the average extinction time increases with increasing mutant fitness, see App. 5.3.5 for more details. However, for a given fitness domain, it is the average fixation time corresponding to the lowest possible mutant's relative fitness that determines the  $\mu_{th}$  for the self-looped directed line graph. The star with self-loops has the lowest mutation threshold, since it has the longest average fixation time. At neutrality, for large  $N$  the average fixation time for the self-looped star graph scales as  $N^5$ , whereas for the star graph it scales as  $N^3$ . The average fixation time scaling for the complete graph is  $N^2$ , and the average fixation time scaling for the cycle graph is  $N^3/6$ . For the self-looped directed line graph, the average fixation time scaling which determines  $\mu_{th}$  is,  $N^2(1 + 1/r)$ . The scalings for  $\mu_{th}$  for the above-mentioned structures are simply the inverse of the average fixation time scalings mentioned in Tab. D of the Fig 2. The scaling relations are derived in App. 5.3.

### 3.3 Self-loops and high mutation rate regime

Under the Moran Bd update scheme, an offspring always replaces one of the parent's neighbours—unless the parent node is self-looped. For an individual occupying a self-looped node, the offspring can replace the individual with a finite probability. Thus, self-loops effectively decrease the fitness of the parent individual, as the parent cannot spread its offspring freely into the population. The extent of this effect on the parent's fitness depends on the weight of the self-loops. This suggests that the fitness of a highly advantageous strain can be decreased by placing it on a self-looped node with negligible outward flowing weight to the neighbouring nodes [20]. Under Bd updating, the fixation probability of a mutant on a structured population with the weight matrix,  $w$ , decreases as the diagonal weights of the matrix are increased [41].

For update schemes like bD and dB, and a given structure with the weight matrix  $w$ , it is necessary to have self-loops ( $w_{ii} > 0$ ) for all  $i$ , in order for the fixation probability of mutants on that structure to be equivalent to the fixation probability of mutants under a birth death process (of any type) on the self-looped complete graph [41]. Self-loops also fix some issues for the bD and dB dynamics that seem to make them unattractive from a modelling perspective [42]: One problem with the bD updating is that a mutant with fitness tending to zero can have a finite fixation probability. On the other hand, for the dB updating, an infinitely fit mutant can have a fixation probability smaller than one. Self-loops fix these issues.

In order for a structure to be a strong amplifier (a spatial structure where the fixation of a beneficial mutant is guaranteed), self-loops have been proven to be necessary [20], both under the uniform and the temperature initialisation. Though the concept of strong amplifiers is defined for infinite  $N$ , the self-loops also play a quintessential role in generating amplifiers of

finite  $N$  [20]. Intuitively, for a structure to be an amplifier of selection, it should have a sufficient number of cold temperature nodes so that the mutants are less likely to get replaced by wild-type individuals [33] and thus, a mutant type can persist in the population for longer time and spread its offspring into the population. This is where self-loops come into play, they help in creating more of these cold nodes, thereby amplifying selection. Consequently, self-loops contribute substantially in attaining higher fitness in the mutation-selection balance [16].

However as seen in Fig 2B, the steady-state average fitness of the self-looped star, an amplifier of selection, decreases fitness as the mutation rate is increased beyond the mutation threshold. Outside the low mutation rate regime, clonal interference starts to play an important role in the evolutionary dynamics. Therefore, to systematically investigate the effects of self-loops on evolutionary dynamics, we need to analyze the dynamics on structured populations for higher mutation rates. While this can be studied by simulations, it is challenging to obtain analytical insights for arbitrary mutation rates  $\mu$ . Thus, in addition to simulations we study another—biologically not relevant—extreme of the high mutation rate limit, i.e.,  $\mu \rightarrow 1$ . While this seems to be an irrelevant limit, its analysis reveals some crucial properties of evolutionary dynamics that are already relevant for much lower mutation rates.

### 3.4 Sampling fitness from the uniform distribution

In the limit  $\mu \rightarrow 1$ , every time a parent reproduces, the offspring is a mutant. We start with a uniform mutant fitness distribution,  $\zeta(f', f) = \frac{1}{f_{\max} - f_{\min}}$  for  $f_{\min} \leq f, f' \leq f_{\max}$ .

**3.4.1 Reference graph- complete graph with self-loops.** When studying evolutionary dynamics on structured populations, the results are always compared with the dynamics on a reference graph. The standard choice in Evolutionary graph theory for the reference graph is the complete graph (without self-loops). For example, for the case of fixation probabilities and for the mutation-selection dynamics under mutation rates, the complete graph serves as the reference graph. However, for high mutation rates, instead of the complete graph, we choose the self-looped complete graph as a reference. This is because every node of the self-looped complete graph has an equal chance of being replaced by a mutant offspring during every birth event. This also implies that after a sufficiently long time, the states of the nodes would be completely uncorrelated in space and time. The coarse-grained evolutionary dynamics satisfies a master equation where each offspring's fitness  $f'$  is chosen randomly from the mutational jump distribution  $\zeta(f', f) = \frac{1}{f_{\max} - f_{\min}}$  with  $f$  being the parent's fitness. The probability density function corresponding to population's state,  $P_{SC}(f, t)$  changes as

$$\frac{dP_{SC}(f, t)}{dt} = \int df' \underbrace{\left( \prod_{i=0}^{N-1} \zeta(f_i, f'_i) \right)}_{T_{f' \leftarrow f}} P_{SC}(f', t) - \int df' \underbrace{\left( \prod_{i=0}^{N-1} \zeta(f'_i, f_i) \right)}_{T_{f \leftarrow f'}} P_{SC}(f, t), \quad (5)$$

where the subscript SC stands for the self-looped complete graph, and,  $f = (f_0, f_2, \dots, f_{N-1})$  is the fitness state of the population of size  $N$ . By assuming detailed balance [30], i.e.

$$P_{SC}^*(f') = \frac{T_{f' \leftarrow f}}{T_{f \leftarrow f'}} P_{SC}^*(f), \quad (6)$$

and the normalisation condition  $\int df' P_{SC}^*(f') = 1$ , we find the steady-state for the high

mutation rate dynamics on the self-looped complete graph

$$P_{sc}^*(f) = \frac{1}{\prod_{i=0}^{N-1} \int df'_i \frac{\zeta(f'_i, f_i)}{\zeta(f_i, f'_i)}} = p^*(f_0) \cdot p^*(f_2) \cdots p^*(f_{N-1}). \quad (7)$$

Here,  $p^*(f_i) = \left( \int df'_i \frac{\zeta(f'_i, f_i)}{\zeta(f_i, f'_i)} \right)^{-1}$  is the marginal probability density function for the node  $i$  to have fitness  $f_i$ . The marginal probability density function also satisfies the normalisation condition  $\int df p^*(f) = 1$ . The average steady-state fitness of the self-looped complete graph in terms of the individual node's average steady-state fitness satisfies  $\langle f \rangle_{sc}^* = \langle f \rangle^*$ , i.e. the average fitness of the population is the same as the average fitness of a node. This follows from the symmetry of the graph. Using the explicit form of the uniform mutational jump density function in Eq 7, we obtain  $p^*(f) = \frac{1}{f_{\max} - f_{\min}}$ , which is independent of  $f$ . At very high mutation rates, the self-looped complete graph is totally blind to the fitness advantage/disadvantage of a mutant. Therefore, for the self-looped complete graph the average steady-state fitness with  $\mu = 1$ , and the uniform mutational distribution is  $\langle f \rangle_{sc}^* = \frac{f_{\max} + f_{\min}}{2}$  which is independent of the population size. Also, the standard deviation of the steady-state fitness is  $\frac{f_{\max} - f_{\min}}{\sqrt{12N}}$ , see Fig 3. For derivation, see App. 5.2. With this, we are now ready to discuss the evolutionary dynamics on various self-looped graphs.

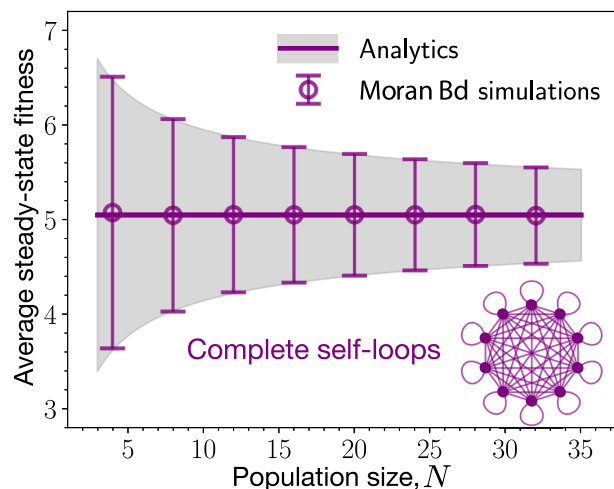


**Fig 3. Reference graph: Complete graph with self-loops.** Here, the mutation-selection dynamics is studied for the self-looped complete graph with  $\mu \rightarrow 1$ . We find a very good agreement for the steady-state statistics between the analytics and the simulations. The thick line represents the analytical average fitness, while the shaded grey area represents the standard deviation around the average. Symbols and error bars show simulations. In the steady-state, on average the self-looped complete graph attains the midpoint of the fitness domain, as the fitness dynamics for each individual node of the population becomes uncorrelated in the fitness space and time. The steady-state average fitness is also independent of the population size. The fluctuations in the steady-state however depends on the population size and decreases with the increase in population size as  $1/\sqrt{N}$  (Parameters:  $f_{\min} = 0.1$ ,  $f_{\max} = 10$ , number of independent realisations is equal to 2000, mutant fitness distribution,  $\zeta(f', f) = 1/(f_{\max} - f_{\min})$ ).

<https://doi.org/10.1371/journal.pcbi.1011387.g003>

**3.4.2 Self-looped directed line beats the self-looped star.** In this section, we study the high mutation rate dynamics,  $\mu \rightarrow 1$ , on the self-looped directed line and the weighted self-looped star graph. To recall, the self-looped directed line is a suppressor of selection [10, 16], whereas, the (weighted) self-looped star graph is an amplifier of selection. In the low mutation rate dynamics, the self-looped weighted star attains higher steady-state fitness than the self-looped directed line. However, it is unclear what happens in the high mutation rate regime, which is far from a fixation-like dynamics. Simulating the Moran Bd dynamics with  $\mu = 1$  for these two graphs, we find that the weighted self-looped star attains lower steady-state fitness not only than the self-looped complete graph, but also in comparison with the self-looped directed line, see Fig 4.

For the case of (weighted) self-looped star graph, from the Fig 4A, all the leaf nodes attain the same steady-state fitness. This is expected due to symmetry reasons. The central node, node 0, stands out, and has the highest fitness. This is because the fitness decreasing effect of the self-loop is minimised by the vast number of outgoing (incoming) links from (to) the central node.

A self-loop affects the node's steady-state fitness depending on the node's connections to other nodes. As an example, the root node 0 of the directed line attains the lowest steady-state fitness among all other nodes, Fig 4B. This is because the only incoming link to node 0 is the self-loop. In a mutation-selection dynamics, a self-loop leads to the decrease in the long-term fitness of a node. This can be understood by the following argument: If a given node is currently occupied by a highly fit individual, it is more likely that during the next Moran Bd update this particular node is selected to reproduce. If this node is self-looped, assuming small outgoing weight to other nodes for now, with high probability the mutated offspring replaces

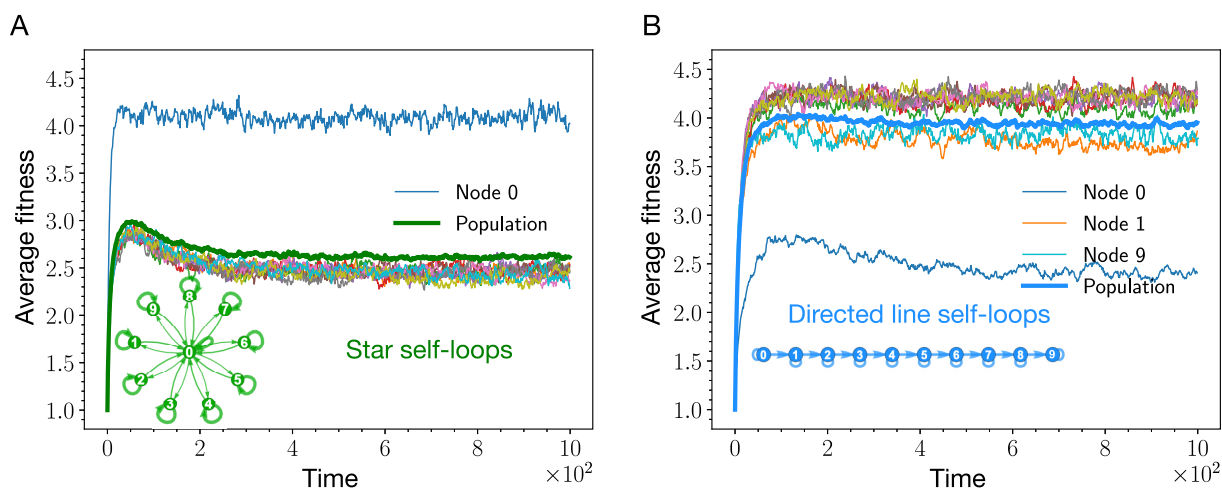


**Fig 4. Nodewise analysis of the star graph with self-loops and the directed line with self-loops.** Here, the average fitness trajectories for each node of the self-looped star graph (shown in panel A) and the self-looped directed line (shown in panel B) are shown. Thick lines represent average fitness trajectories at the population level, whereas, thin lines represent average fitness trajectories for the nodes. The effect of self-loops on a node's fitness depends on the incoming and outgoing weight flowing out of that node. In panel A, self-loops have the least effect on the central node because of relatively higher incoming and outgoing weight. As a result, the central node attains higher average steady-state fitness than the leaf nodes. In panel B, the root node of the directed line has the lowest steady-state average fitness because of the absence of an incoming link to the root node. (Parameters:  $N = 10$ ,  $\mu = 1$ ,  $f_{\min} = 0.1$ ,  $f_{\max} = 10$ , number of independent realisations is equal to 2000, mutant fitness distribution,  $\zeta(f', f) = \frac{1}{f_{\max} - f_{\min}}$ . For the directed line with self-loops, every outgoing link from a node (including the self-loop) has the same weight. For the self-looped star graphs, the weights of the links follows Eq (23), such that  $\lambda = 1/(N - 1)$  and  $\delta = 1/(N - 1)^2$ ).

<https://doi.org/10.1371/journal.pcbi.1011387.g004>

its parent via the self-loop. If the mutated offspring is again very fit, this offspring will again be more likely to be selected to reproduce, and thus, repeating the cycle. This process will repeat until the node's fitness decreases. Therefore, self-loops make it harder for highly fit individuals to persist in the population.

On the other hand, incoming and outgoing links decrease the stated negative effect of self-loops. When a highly fit individual occupying a self-looped node is selected to give birth, its mutated offspring can be placed on a neighbouring node if the parent node has a substantial outgoing weight to other nodes. This decreases the participation of the self-loops in the update process and leads to diminished effects of the self-loops. The role of incoming links is more subtle. Incoming links make a node's fitness state more randomised in accordance with the mutational jump distribution. In the long run, for the case of uniform distribution, the mean of the fitness states attained by an individual node solely via the incoming links is the mid-point of fitness domain. Thus, depending on the mutational fitness jump distribution, incoming links can have beneficial or detrimental effects on a node's fitness. For the case of uniform distribution, compared to self-loops, incoming links have beneficial effect on the population's fitness as adding self-loops decreases the population's fitness below the mid-point of the fitness domain. These arguments explain, why the end node of the directed line has higher steady-state fitness than the root node, but lower fitness than the bulk nodes (node 9 in Fig 4B). The incoming link to the end node decreases the self-loops effect by making the node's fitness more randomised. However, the absence of an outgoing link from the end node makes the negative impact of self-loop still substantial. The steady-state fitness for the node 1 is an interesting case. As a bulk node, its steady-state fitness is lower than other bulk nodes fitnesses. This is because the incoming link to node 1 does not reach its full potential in randomising the fitness. This limitation occurs because the incoming link is activated solely when the root node 0 is selected for reproduction. However since the root node has the lowest fitness, it is less likely to be selected during the update steps.

### 3.5 Sampling fitness from the Gaussian distribution

Until now, in the Moran Bd with mutation update scheme, the mutant's fitness has been sampled from a uniform distribution. However, a lack of correlation between offspring's fitness and parent's fitness is an extreme assumption. Therefore, to examine the robustness of the negative effects of the self-loops observed previously, we study the evolutionary dynamics with the fitness of a mutant offspring sampled from a truncated Gaussian distribution on the fitness domain  $[f_{\min}, f_{\max}]$ . At a given point of the dynamics, the Gaussian distribution is centered around the parent's fitness with a standard deviation of  $\sigma$ .

From Fig 5A, we see that adding self-loops decreases the steady-state fitnesses for all the graphs. The effect of adding self-loops is the smallest for the complete graph. This is what we have also observed for the case of uniform mutation fitness distribution. To compare fitnesses, in Fig 5 every self-looped graph has a non self-looped counterpart. For the self-looped directed line, we have the molded directed line which is directed line with an additional link directed from node 1 to the root node (node 0). On increasing the  $\sigma$  from 0.1 to 1, compared to other graphs, the self-looped star undergoes a considerable decrease in the steady-state average fitness, Fig 5B. For  $\sigma = 1$ , the self-looped star graph, an amplifier of selection, attains lower steady-state fitness than the self-looped directed line, a suppressor of selection. For very large  $\sigma$ , we recover the uniform distribution limit, as expected, see Fig 5C, where all the non-self looped graphs attain the same mutation-selection balance. The average fitness in this case is higher than that of the self-looped complete graph. All self-looped graphs have lower average



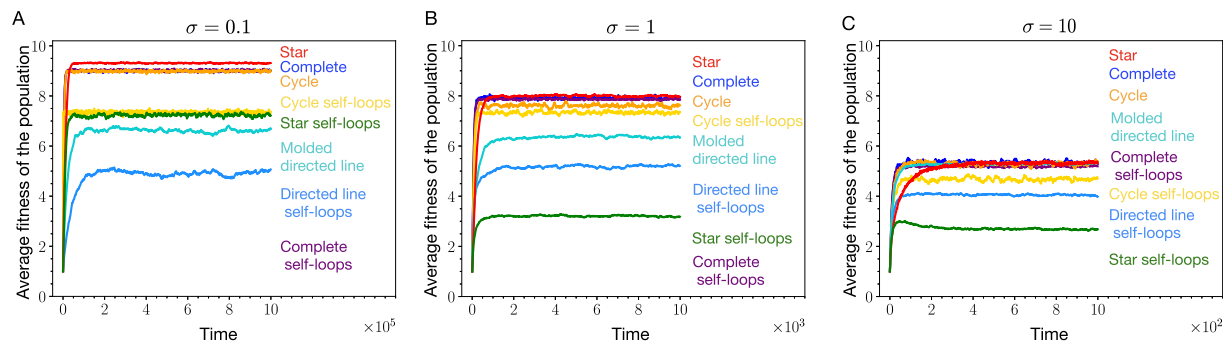


**Fig 5. Sampling mutant's fitness from the Gaussian.** (A) When mutant fitness is sampled from the (truncated) Gaussian distribution with  $\sigma = 0.1$ , we find that adding self-loops decreases the population fitness in all the graphs. (B) Increasing the  $\sigma$  from 0.1 to 1, the average fitness in the steady-state goes down for many graphs. The effect of increasing the  $\sigma$  is largest in the heterogeneous star graphs and smallest in the more homogeneous structure like the complete graph. (C) We recover the uniform mutant fitness distribution case for very large  $\sigma$ , here  $\sigma = 10$ . In this case, all the non-self looped graphs attain the same steady-state. All self-looped graphs have lower average steady-state fitness than a non-self looped graph and the self-looped complete graph (Parameters:  $N = 10$ ,  $\mu = 1$ ,  $f_{\min} = 0.1$ ,  $f_{\max} = 10$ , 2000 independent realisations).

<https://doi.org/10.1371/journal.pcbi.1011387.g005>

fitness compared to the self-looped complete graph. Refer to App. 5.4 for more details on the high mutation rate dynamics for the non self-looped graphs.

Overall, the average steady-state fitness for different graphs increases as  $\sigma$  is decreased. This trend agrees with the intuition that low  $\sigma$  values provide directionality to the evolutionary dynamics towards higher fitness values. However, not all the self-looped graphs are affected by this directionality equally. The steady-state average fitness for the heterogeneous self-looped graph like, the self-looped star, decreases substantially with increasing  $\sigma$ , compare Fig 5A and 5B. In contrast, regular self-looped structures like the self-looped complete graph and the self-looped cycle graph, do not experience such a sharp fitness decrease, see again Fig 5A and 5B.

In nutshell, from Fig 5, we conclude that the negative effect of self-loops on the fitness is not limited solely to the uniform mutant fitness distribution.

## 4 Discussion

Amplifiers of selection [1, 10] are fascinating spatial structures. For low mutation rates, these structures can speed up evolution [8] by enhancing the fixation of beneficial mutants. A randomly generated connected spatial structure, under Moran Bd updating with uniform initialisation, is very likely to be an amplifier of selection [9]. Due to their ability to amplify selection and ubiquity, amplifiers of selection have been in the focus of research recently [13, 20, 33, 43–47].

Not only at the fixation time scales but also for the long-term weak mutation rate mutation-selection dynamics, amplifiers of selection perform better than the well-mixed population by attaining higher average fitness [16]. Since mutations occur during reproduction, the fixation probabilities entering the steady-state distribution (mutation-selection balance) for spatial structures are temperature initialised. It has been shown that for structures to amplify selection substantially under temperature initialisation, self-loops are important [20]. However, non self-looped amplifiers of selection with temperature mutant initialisation do exist [48].

In the low mutation rate regime, self-loops help structures perform better but outside the low mutation rate regime, self-looped graphs do not attain higher average fitness than the well-mixed population. In fact, outside the weak mutation rate regime, amplifiers of selection

can even perform worse than suppressors of selection in terms of maximizing fitness. An example is shown in the Fig 2, where the self-looped star graph, an amplifier of selection, attains lower fitness in the mutation-selection balance than the complete and self-looped directed line, a suppressor of selection. To further investigate the effect of self-loops, we have worked in the extreme mutation probability regime,  $\mu \rightarrow 1$ . The idea was to remove other effects from the evolutionary dynamics, and focus solely on the effect of self-loops on the adaptation of a spatially structured population. The insights we obtain working in the high mutation regime can be useful for the intermediate mutation rate regime as well. While we worked with extremely high mutation rates, high mutation rate studies are not uncommon. One of the celebrated theories dealing with high mutation rate mutation-selection dynamics is quasispecies theory [49, 50]. Quasispecies theory is a deterministic theory used to study mutation-selection dynamics in infinite well-mixed population. Its variants have also been used to study finite well-mixed populations [51, 52]. However, the effect of spatial structure remains to be analysed in the quasispecies theory.

While studying mutation-selection dynamics with high mutation rates, the self-looped complete graph naturally serves as the reference graph instead of the complete graph. The fitness dynamics for the self-looped complete graph is random in fitness space and time, i.e., at a given time, the fitness state of a node is independent of its fitness states in the past and the current fitness state of its neighbours. We found that self-loops have a strong fitness-decreasing effect on a node having lower outgoing and incoming weight. In the limit  $\mu \rightarrow 1$ , we found that the non-self-looped graphs attain higher steady-state fitness than their self-looped counterparts. Maybe more surprisingly, all the non-self-looped graphs attain the same average fitness in the mutation-selection balance. All self-looped graphs attain lower steady-state fitness than the complete graph. We also observed the fitness-decreasing effects of the self-loops for the case where the mutant's fitness is sampled from a Gaussian distribution. Thus, the fitness-decreasing effects of the self-loops are not an artefact of a uniform mutant fitness distribution.

We also provide a heuristic measure of the low mutation rate thresholds,  $\mu_{th}$ , the mutation rate beyond which the evolutionary dynamics is outside the low mutation rate regime. The mutation rate threshold  $\mu_{th}$  for a graph depends on the average fixation times and the extinction times of mutants on that graph [8]. As expected, structures with higher fixation times have lower mutation rate thresholds. Therefore, compared to the complete graph and suppressors of selection, amplifiers of selection show deviation from the low mutation rate approximation at lower mutation rates. For a majority of the spatial structures, these thresholds are estimated using the structures' near-neutrality average fixation time scaling with population size. For the directed line with self-loops, the average fixation time grows monotonically with the decrease in mutant's fitness and therefore,  $\mu_{th}$  is computed from the average fixation time of a mutant with least possible relative fitness for a fitness domain. In this work, we have derived the large  $N$  average fixation time scalings for the star graph, the self-looped star graph and the cycle graph, which in return give the  $\mu_{th}$  scalings. Knowing these thresholds one can avoid running heavy simulations deep in the low mutation regime. Since in the low mutation rate regime, the steady-state statistics is independent of the mutation rate, it is sufficient to access the steady-state via simulations by going slightly below the computed mutation rate thresholds but not deep into the low mutation rate regime. Due to higher sojourn times (see Appendix), it is expected for a self-looped graph to have a higher average fixation time for a mutant than its non self-looped counterpart. This however needs a further detailed investigation.

Amplifiers of selection have been in the focus of EGT. However, their promising aspects to optimise fixation of fit mutants are somewhat limited to short-term time scales, where they come with the caveat that they tend to have long fixation times [8, 43]. In the long-term

mutation-selection dynamics, it has been shown in Ref. [16] that suppressors of fixation have the potential to perform better than the amplifiers of selection. This is because of the ability of the suppressor of fixation to reject deleterious mutations more efficiently compensating for its poor probability of fixation for beneficial mutations. Moreover, outside the low mutation rate regime, we see that the temperature initialised star graph, a suppressor of fixation, takes over the self-looped star graph, an amplifier of selection, and maintains higher average fitness in the steady-state throughout the mutation rate regime. However, the reason for the star graph to take over the self-looped star outside the weak mutation rate regime is not clear and requires further investigation. In conclusion, we suggest to broaden the scope of evolutionary graph theory to other structures and to gently move its focus away from amplifiers of selection.

## 5 Appendix

### 5.1 Kolmogorov's Criterion

In the section 3.4.1, we have used the detailed balance condition. Here, we justify the use of detailed balance by proving that the stochastic process at hand is indeed reversible. To do so we make use of Kolmogorov's criterion [53]. According to this criterion, a Markov chain on a fitness space spanned by  $\mathbf{f}$  is reversible if and only if:

$$T(\mathbf{f}_1, \mathbf{f}_n) \cdots T(\mathbf{f}_3, \mathbf{f}_2) T(\mathbf{f}_2, \mathbf{f}_1) = T(\mathbf{f}_1, \mathbf{f}_2) T(\mathbf{f}_2, \mathbf{f}_3) \cdots T(\mathbf{f}_n, \mathbf{f}_1), \quad (8)$$

for any finite set of ordered fitness states  $\mathbf{f}_1, \mathbf{f}_2, \dots, \mathbf{f}_n$ .

The basic idea behind the Kolmogorov's criterion relies on the fact that a reversible Markov chain has zero probability current in the steady-state. In our case,

$$T(\mathbf{f}, \mathbf{f}') = \prod_{i=0}^{N-1} \zeta(\mathbf{f}_i, \mathbf{f}'_i). \quad (9)$$

Since,  $\zeta(\mathbf{f}_i, \mathbf{f}'_i) = \frac{1}{f_{\max} - f_{\min}}$ , the transition probabilities are independent of fitness. Thus, Kolmogorov's criterion in Eq 8 is satisfied and the Markov chain for the self-looped complete graph presented in the Sec. 3.4.1 is reversible.

### 5.2 Complete graph with self-loops: Fluctuations in the fitness

The standard deviation in the steady-state population fitness for self-looped complete graph is given by  $\sqrt{\text{Var}(f)^*}$  where,

$$\text{Var}(f)^* = \langle f^2 \rangle_{SC}^* - (\langle f \rangle_{SC}^*)^2. \quad (10)$$

Here we derive the expression of the second moment for the steady-state of the high mutation rate dynamics of the self-looped complete graph.

$$\begin{aligned} \langle f^2 \rangle_{SC}^* &= \frac{1}{N^2} \left\langle \sum_{i=0}^{N-1} \sum_{j=0}^{N-1} f_i f_j \right\rangle^*, \\ &= \frac{1}{N^2} \left( \sum_{i=0}^{N-1} \sum_{j \neq i}^{N-1} \langle f \rangle^* \langle f \rangle^* + \sum_{i=0}^{N-1} \langle f^2 \rangle^* \right), \\ &= \frac{1}{N^2} \left( N(N-1) \langle f \rangle^{*2} + N \langle f^2 \rangle^* \right), \\ &= \left( 1 - \frac{1}{N} \right) \langle f \rangle^{*2} + \frac{1}{N} \langle f^2 \rangle^*, \end{aligned} \quad (11)$$

where  $\langle f \rangle^*$  is the average fitness, and  $\langle f^2 \rangle^*$  is the second moment of fitness for a node in the steady-state. In the second equality above, we have used that fitness states on a coarse-grained time scale on different nodes of a self-looped complete graph are independently and identically distributed. Therefore the variance in fitness for the population reduces to,

$$\begin{aligned}\text{Var}(f)^* &= \frac{1}{N} \left( \langle f^2 \rangle^* - \langle f \rangle^{*2} \right) \\ &= \frac{1}{N} \text{var}(f)^*,\end{aligned}\quad (12)$$

where  $\text{var}(f)^*$  is the variance in fitness for a node. Using the probability density for fitness of a node,  $p^*(f) = \frac{1}{f_{\max} - f_{\min}}$ , we get the standard deviation of the steady-state fitness to be  $\frac{f_{\max} - f_{\min}}{\sqrt{12N}}$ .

### 5.3 Mutation rates threshold and fixation times

Here we derive the expressions for the average fixation times of a mutant,  $\tau_1$  on various network topologies like the self-looped star, star, complete, cycle and the self-looped directed line.

**5.3.1 Star graphs.** To compute the fixation time for the star graph and self-looped weighted star graph, we use the method of solving recursions inspired from Ref. [54]. To proceed, we write down the recursion satisfied by  $\tau_i^*$ , the average fixation time starting with  $i$  mutants in the leaves and a mutant in the center node. We denote this state by  $(\bullet, i)$ . Similarly,  $\tau_i^\circ$  is the average fixation time starting with the state  $(\circ, i)$ , i.e.,  $i$  mutants in the leaves and a wild-type individual in the central node.

$$\begin{aligned}\phi_i^{\bullet\bullet} &= T_{i,i+1}^{\bullet\bullet} \phi_{i+1}^{\bullet\bullet} \tau_{i+1}^{\bullet\bullet} + T_{i,i}^{\bullet\circ} \phi_i^{\circ\circ} \tau_i^{\circ\circ} + (1 - T_{i,i+1}^{\bullet\bullet} - T_{i,i}^{\bullet\circ}) \phi_i^{\bullet\bullet} \tau_i^{\bullet\bullet} + \phi_i^{\bullet\bullet}, & 0 \leq i \leq n-1, \\ \phi_i^{\circ\circ} &= T_{i,i}^{\circ\bullet} \phi_i^{\bullet\bullet} \tau_i^{\bullet\bullet} + T_{i,i-1}^{\circ\circ} \phi_{i-1}^{\circ\circ} \tau_{i-1}^{\circ\circ} + (1 - T_{i,i}^{\circ\bullet} - T_{i,i-1}^{\circ\circ}) \phi_i^{\circ\circ} \tau_i^{\circ\circ} + \phi_i^{\circ\circ}, & 1 \leq i \leq n,\end{aligned}\quad (13)$$

where,

- (i).  $\phi_i^{\bullet\bullet}$  is the fixation probability with the initial state being  $(\bullet, i)$ ,
- (ii).  $\phi_i^{\circ\circ}$  is the fixation probability with the initial state  $(\circ, i)$ .
- (iii).  $T_{i,i\pm 1}^{\bullet\bullet}$  is the transition probability from the state  $(\bullet, i)$  to the state  $(\bullet, i \pm 1)$ ,
- (iv).  $T_{i,i\pm 1}^{\circ\circ}$  is the transition probability from the state  $(\circ, i)$  to the state  $(\circ, i \pm 1)$ ,
- (v).  $T_{i,i}^{\bullet\circ}$  is the transition probability from the state  $(\bullet, i)$  to the state  $(\circ, i)$ .
- (vi).  $T_{i,i}^{\circ\bullet}$  is the transition probability from the state  $(\circ, i)$  to the state  $(\bullet, i)$ .

The recursions in Eq 13 satisfy the boundary conditions:  $\phi_0^{\circ\circ} = 0$  and  $\tau_n^{\bullet\bullet} = 0$ . These recursions can be simplified further by dividing the recursion one by  $T_{i,i+1}^{\bullet\bullet} + T_{i,i}^{\circ\bullet}$ , and recursion two by  $T_{i,i}^{\circ\bullet} + T_{i,i-1}^{\circ\circ}$ ,

$$\begin{aligned}\phi_i^{\bullet\bullet} \tau_i^{\bullet\bullet} &= \frac{T_{i,i+1}^{\bullet\bullet}}{T_{i,i+1}^{\bullet\bullet} + T_{i,i}^{\circ\bullet}} \phi_{i+1}^{\bullet\bullet} \tau_{i+1}^{\bullet\bullet} + \frac{T_{i,i}^{\bullet\circ}}{T_{i,i+1}^{\bullet\bullet} + T_{i,i}^{\circ\bullet}} \phi_i^{\circ\circ} \tau_i^{\circ\circ} + \frac{\phi_i^{\bullet\bullet}}{T_{i,i+1}^{\bullet\bullet} + T_{i,i}^{\circ\bullet}}, & 0 \leq i \leq n-1, \\ \phi_i^{\circ\circ} \tau_i^{\circ\circ} &= \frac{T_{i,i}^{\circ\bullet}}{T_{i,i}^{\circ\bullet} + T_{i,i-1}^{\circ\circ}} \phi_i^{\bullet\bullet} \tau_i^{\bullet\bullet} + \frac{T_{i,i-1}^{\circ\circ}}{T_{i,i}^{\circ\bullet} + T_{i,i-1}^{\circ\circ}} \phi_{i-1}^{\circ\circ} \tau_{i-1}^{\circ\circ} + \frac{\phi_i^{\circ\circ}}{T_{i,i}^{\circ\bullet} + T_{i,i-1}^{\circ\circ}}, & 1 \leq i \leq n.\end{aligned}\quad (14)$$

Introducing

$$\pi_{i,i+1}^{\bullet\bullet} = 1 - \pi_{i,i}^{\bullet\circ} = 1 - \frac{T_{i,i}^{\bullet\circ}}{T_{i,i+1}^{\bullet\bullet} + T_{i,i}^{\bullet\circ}}, \quad 0 \leq i \leq n-1 \quad (15)$$

and

$$\pi_{i,i}^{\circ\bullet} = 1 - \pi_{i,i-1}^{\circ\circ} = 1 - \frac{T_{i,i-1}^{\circ\circ}}{T_{i,i}^{\circ\bullet} + T_{i,i-1}^{\circ\circ}}, \quad 1 \leq i \leq n, \quad (16)$$

we finally have,

$$\begin{aligned} \phi_i^{\bullet\bullet} \tau_i^{\bullet} &= \pi_{i,i+1}^{\bullet\bullet} \phi_{i+1}^{\bullet} \tau_{i+1}^{\bullet} + \pi_{i,i}^{\bullet\circ} \phi_i^{\circ} \tau_i^{\circ} + \frac{\phi_i^{\bullet}}{T_{i,i+1}^{\bullet\bullet} + T_{i,i}^{\bullet\circ}}, \quad 0 \leq i \leq n-1, \\ \phi_i^{\circ\circ} \tau_i^{\circ} &= \pi_{i,i}^{\circ\bullet} \phi_i^{\bullet} \tau_i^{\bullet} + \pi_{i,i-1}^{\circ\circ} \phi_{i-1}^{\circ} \tau_{i-1}^{\circ} + \frac{\phi_i^{\circ}}{T_{i,i}^{\circ\bullet} + T_{i,i-1}^{\circ\circ}}, \quad 1 \leq i \leq n. \end{aligned} \quad (17)$$

Here,

- (i).  $\pi_{i,i+1}^{\bullet\bullet}$  is the conditional transition probability from the state  $(\bullet, i)$  to the state  $(\bullet, i+1)$ , with the condition that the number of mutants changes.
- (ii).  $\pi_{i,i}^{\bullet\circ}$  is the conditional transition probability from the state  $(\circ, i)$  to the state  $(\bullet, i)$ , given that the number of mutants changes.
- (iii).  $\pi_{i,i}^{\circ\bullet}$  is the conditional transition probability from the state  $(\circ, i)$  to the state  $(\bullet, i)$ , with the condition that the number of mutants changes.
- (iv).  $\pi_{i,i-1}^{\circ\circ}$  is the conditional transition probability from the state  $(\circ, i)$  to the state  $(\circ, i-1)$ , given that the number of mutants changes.

Solving the recursions 17 using boundary conditions  $\phi_0^{\circ} = 0$  and  $\tau_n^{\bullet} = 0$  we get

$$\tau_0^{\bullet} = \tau_1^{\bullet} + 1 = \sum_{l=2}^n A(l, n) C(l) + 1, \quad (18)$$

where,

$$A(l, m) = 1 + \sum_{j=l}^{m-1} \pi_{j,j}^{\bullet\circ} \prod_{k=l}^j \frac{\pi_{k,k-1}^{\circ\circ}}{\pi_{k,k+1}^{\bullet\bullet}} \quad (19)$$

and

$$C(l) = \frac{\pi_{l-1,l-1}^{\circ\circ}}{\pi_{l-1,l}^{\bullet\bullet}} \sum_{j=1}^{l-1} \left( \frac{\phi_j^{\circ}}{T_{j,j-1}^{\circ\circ} + T_{j,j}^{\circ\bullet}} \prod_{k=j+1}^{l-1} \pi_{k,k-1}^{\circ\circ} \right) + \frac{\phi_{l-1}^{\bullet}}{T_{l-1,l}^{\bullet\bullet}}. \quad (20)$$

The expressions for  $\phi_i^{\circ}$  and  $\phi_i^{\bullet}$  are derived in Ref. [54],

$$\begin{aligned} \phi_i^{\bullet} &= \frac{A(1, i)}{A(1, n)}, \\ \phi_i^{\circ} &= \sum_{j=1}^i \pi_{j,j}^{\bullet\circ} \phi_j^{\bullet} \prod_{k=j+1}^i \pi_{k,k-1}^{\circ\circ}. \end{aligned} \quad (21)$$

Now,

$$\begin{aligned}\tau_1^\circ &= \tau_1^\bullet + \frac{1}{T_{1,0}^\circ + T_{1,1}^\bullet}, \\ &= \sum_{l=2}^n A(l, n) C(l) + \frac{1}{T_{1,0}^\circ + T_{1,1}^\bullet}.\end{aligned}\quad (22)$$

The self-looped (weighted) star graph is defined by the weighted adjacency matrix

$$\mathbf{w} = \begin{pmatrix} 1 - \delta & \frac{\delta}{n} & \frac{\delta}{n} & \cdots & \frac{\delta}{n} \\ \lambda & 1 - \lambda & 0 & \cdots & 0 \\ \vdots & \vdots & \ddots & \ddots & \vdots \\ \lambda & 0 & \cdots & 1 - \lambda & 0 \\ \lambda & 0 & \cdots & 0 & 1 - \lambda \end{pmatrix} \quad (23)$$

with  $0 < \lambda \leq 1$  and  $0 < \delta \leq 1$ . Here,  $w_{ij}$  is the weight of the link directed from node  $i$  to node  $j$  with the center being node number 0. With this, the transition probabilities for a weighted self-looped star graph for the transitions from state  $(\bullet, i)$  are

$$T_{i,i+1}^{\bullet\bullet} = \frac{r}{r + ir + n - i} \cdot \frac{\delta}{n} (n - i), \quad \text{and} \quad T_{i,i}^{\bullet\circ} = \frac{n - i}{r + ir + n - i} \cdot \lambda. \quad (24)$$

The related conditional transition probabilities are

$$\pi_{i,i+1}^{\bullet\bullet} = \frac{r\delta}{n\lambda + r\delta} \quad \text{and} \quad \pi_{i,i}^{\bullet\circ} = \frac{n\lambda}{n\lambda + r\delta}. \quad (25)$$

Similarly, the transition probabilities for the transitions from state  $(\circ, i)$  are

$$T_{i,i}^{\circ\bullet} = \frac{ir}{1 + ir + n - i} \cdot \lambda \quad \text{and} \quad T_{i,i-1}^{\circ\circ} = \frac{1}{1 + ir + n - i} \cdot \frac{\delta}{n} i. \quad (26)$$

The corresponding conditional transition probabilities are

$$\pi_{i,i}^{\circ\bullet} = \frac{n\lambda r}{n\lambda r + \delta} \quad \text{and} \quad \pi_{i,i-1}^{\circ\circ} = \frac{\delta}{n\lambda r + \delta}. \quad (27)$$

We can use these probabilities along with Eq 22 to obtain the temperature initialised fixation probability and the average fixation time for the self-looped star graph,  $\tau^\tau$ . In the following, we define the temperature for the center and leaf nodes. The central node temperature is

$$\mathcal{T}_0 = \sum_{i=0}^N w_{i0} = 1 - \delta + n\lambda \quad (28)$$

and the leaf node temperature is

$$\mathcal{T}_{j \neq 0} = \sum_{i=0}^N w_{ij} = \frac{\delta}{n} + 1 - \lambda. \quad (29)$$

The temperature initialised fixation probability for the self-looped star graph is

$$\phi^\tau(\delta, \lambda) = \frac{1 - \delta + n\lambda}{n + 1} \phi_0^\bullet + \frac{n(\frac{\delta}{n} + 1 - \lambda)}{n + 1} \phi_1^\circ. \quad (30)$$

The temperature initialised average fixation time for the self-looped star graph is

$$\tau^T(\delta, \lambda) = \frac{1 - \delta + n\lambda}{n + 1} \tau_0^\bullet + \frac{n(\frac{\delta}{n} + 1 - \lambda)}{n + 1} \tau_1^\circ. \quad (31)$$

Substituting  $\lambda = \frac{1}{n}$  and  $\delta = \frac{1}{n^2}$  in the above equation, we get the temperature initialised average fixation time for the self-looped weighted star graph. Setting  $\lambda = \delta = 1$  yields the temperature initialised average fixation time for the standard star graph.

To compute the average extinction time, we use symmetry arguments in Eqs 18, 19, 20, 21 and, 22. With this, we replace

$$\begin{aligned} T_{i,i+1}^{\bullet\bullet} &\text{ by } T_{n-i,n-i-1}^{\circ\circ}, \\ T_{i,i}^{\bullet\circ} &\text{ by } T_{n-i,n-i}^{\circ\bullet}, \\ T_{i,i-1}^{\circ\circ} &\text{ by } T_{n-i,n-i+1}^{\bullet\bullet}, \\ T_{i,i}^{\circ\bullet} &\text{ by } T_{n-i,n-i}^{\bullet\circ}, \\ \phi_i^\bullet &\text{ by } \tilde{\phi}_{n-i}^\circ, \text{ and,} \\ \phi_i^\circ &\text{ by } \tilde{\phi}_{n-i}^\bullet. \end{aligned} \quad (32)$$

Doing so, we obtain

$$\tilde{\phi}_{n-i}^\circ = \frac{\tilde{A}(1, i)}{\tilde{A}(1, n)}, \quad (33)$$

where

$$\tilde{A}(l, m) = 1 + \sum_{j=l}^{m-1} \pi_{n-j,n-j}^{\circ\bullet} \prod_{k=l}^j \frac{\pi_{n-k,n-k+1}^{\bullet\bullet}}{\pi_{n-k,n-k-1}^{\circ\circ}}. \quad (34)$$

$\tilde{\phi}_i^\circ$  is the extinction probability of mutants starting with the state  $(\circ, i)$  node, and is equal to  $1 - \phi_i^\circ$ . Similarly, the average extinction time starting with the state  $(\circ, n - i)$  obeys

$$\tilde{\tau}_{n-i}^\circ = \sum_{l=2}^n \tilde{A}(l, n) \tilde{C}(l) - \frac{1}{\tilde{\phi}_{n-i}^\circ} \sum_{l=2}^i \tilde{A}(l, i) \tilde{C}(l), \quad (35)$$

where

$$\tilde{C}(l) = \frac{\tilde{\phi}_{n-l+1}^\circ}{T_{n-l+1,n-l}^{\circ\circ}} + \frac{\pi_{n-l+1,n-l+1}^{\bullet\circ}}{\pi_{n-l+1,n-l}^{\circ\circ}} \sum_{j=1}^{l-1} \left( \frac{\tilde{\phi}_{n-j}^\bullet}{T_{n-j,n-j+1}^{\bullet\bullet} + T_{n-j,n-j}^{\circ\bullet}} \prod_{k=j+1}^{l-1} \pi_{n-k,n-k+1}^{\bullet\bullet} \right), \quad (36)$$

with  $\tilde{\phi}_i^\bullet$  being the extinction probability of mutants starting in state  $(\bullet, i)$ . It is given by

$$\tilde{\phi}_{n-i}^\bullet = \sum_{j=1}^i \pi_{n-j,n-j}^{\bullet\circ} \tilde{\phi}_{n-j}^\circ \prod_{k=j+1}^i \pi_{n-k,n-k+1}^{\bullet\bullet}. \quad (37)$$

The average extinction time starting in state  $(\bullet, n - i)$  is

$$\tilde{\tau}_{n-i}^\bullet = \frac{1}{\tilde{\phi}_{n-i}^\bullet} \sum_{j=1}^i \pi_{n-j,n-j}^{\bullet\circ} \left( \tilde{\phi}_{n-j}^\circ \tilde{\tau}_{n-j}^\circ + \frac{\tilde{\phi}_{n-j}^\bullet}{T_{n-j,n-j}^{\circ\bullet}} \right) \prod_{k=j+1}^i \pi_{n-k,n-k+1}^{\bullet\bullet}. \quad (38)$$

Finally, using Eqs 38 and 35, the temperature initialised average extinction time of a mutant

on the looping star graph is

$$\bar{\tau}^T(\delta, \lambda) = \frac{1 - \delta + n\lambda}{n + 1} \bar{\tau}_0^\bullet + \frac{n(\frac{\delta}{n} + 1 - \lambda)}{n + 1} \bar{\tau}_1^\circ. \quad (39)$$

From Fig 6, we see that the average fixation time of a mutant is higher than the average extinction time of the mutant regardless of its relative fitness. Moreover, the fixation time peaks near neutrality. Therefore, according to the Eq 4, the  $\mu_{th}$  for the stars graphs is the inverse of the average fixation times at neutrality. In the next section, we derive the scaling of  $\tau_1^T$  at neutrality with respect to the population size  $N$  for the star graphs.

**5.3.2 Scaling of the average fixation time with population size for the star graphs at neutrality.** While the approach used above to compute the fixation and the extinction time on star graph has many merits like extension to the frequency dependent selection case, it is not straightforward to use this approach to derive the exact formula even at neutrality. Therefore, to compute the scaling relation for the fixation time on star graphs, we use a method inspired from Ref. [55]. To start, we recast the recursion Eq 14 into the form

$$\phi_i^\bullet \tau_i^\bullet = \pi_{\leftarrow} \phi_{i+1}^\bullet \tau_{i+1}^\bullet + \pi_{\downarrow} \phi_i^\circ \tau_i^\circ + \phi_i^\bullet t_i^\bullet, \quad 0 \leq i \leq n-1, \quad (40)$$

$$\phi_i^\circ \tau_i^\circ = \pi_{\uparrow} \phi_i^\bullet \tau_i^\bullet + \pi_{\leftarrow} \phi_{i-1}^\circ \tau_{i-1}^\circ + \phi_i^\circ t_i^\circ, \quad 1 \leq i \leq n, \quad (41)$$

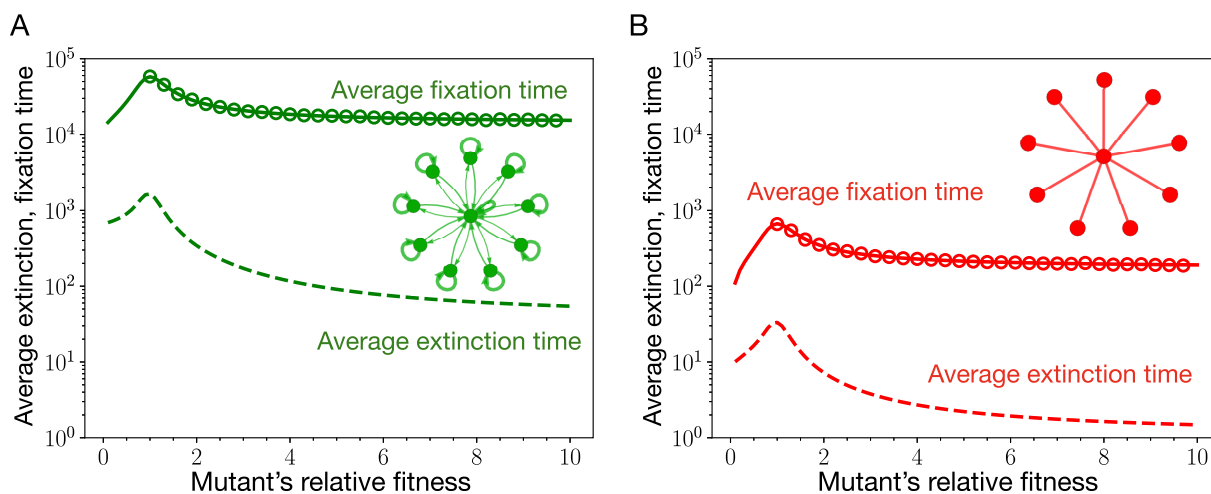


**Fig 6. Average extinction and fixation time for the self-looped star graph and the standard star graph.** Here, we plot the average extinction and fixation time of a mutant for the self-looped (weighted) star graph (panel A) and the star graph (panel B) as a function of mutant's relative fitness. Solid lines corresponds to the analytic results, Eqs 31 and 39. The circles represent Moran Bd simulations. Firstly, we observe that for both the graphs, the average fixation time of a mutant is higher than its extinction time, regardless of the mutant's relative fitness. Secondly, the average fixation time peaks near neutrality for both of the graphs. Therefore, according to Eq 4,  $\mu_{th}$  for the star graphs scales as the inverse average fixation time at neutrality. Because the fixation of a mutant takes longer on the self-looped star graph, the weak mutation rate approximation is more restrictive for the self-looped star graph than the star graph. (Parameters:  $N = 10$ , wild-type fitness,  $f = 1$ , and the number of independent realisations conditioned on mutant's fixation or extinction are 2000).

<https://doi.org/10.1371/journal.pcbi.1011387.g006>



Here, we have replaced,

$$\begin{aligned}\pi_{i,i+1}^{\bullet\bullet} &\text{ by } \pi_{\rightarrow}, \\ \pi_{i,i}^{\bullet\circ} &\text{ by } \pi_{\downarrow}, \\ \pi_{i,i}^{\circ\bullet} &\text{ by } \pi_{\uparrow}, \\ \pi_{i,i-1}^{\circ\circ} &\text{ by } \pi_{\leftarrow},\end{aligned}\quad (42)$$

because the conditional transition probabilities are independent of the number of mutants, see Eq 25. The horizontal arrows in the subscript of  $\pi$  represent change in the number of mutants in the leaf nodes, right arrow for the increase, and left arrow for the decrease in the number of mutants. The vertical arrows in the subscript of  $\pi$  represent change in individual type at the central node, upward arrow for the change from the wild-type to mutant type, and downward arrow for the change from the mutant type to the wild-type. We also use the shorthand notations

$$\begin{aligned}t_i^{\bullet} &= \frac{1}{T_{i,i+1}^{\bullet\bullet} + T_{i,i}^{\bullet\circ}}, \\ t_i^{\circ} &= \frac{1}{T_{i,i}^{\circ\bullet} + T_{i,i-1}^{\circ\circ}}.\end{aligned}\quad (43)$$

Here,  $t_i^{\bullet}$  is the average time spent in the state  $(\bullet, i)$  (the sojourn time of state  $(\bullet, i)$ ) and  $t_i^{\circ}$  is the sojourn time of state  $(\circ, i)$ . Shifting the index  $i$  to  $i-1$  in recursion Eq 40, and solving for  $\phi_i^{\bullet}\tau_i^{\bullet}$  gives,

$$\phi_i^{\bullet}\tau_i^{\bullet} = \frac{1}{\pi_{\rightarrow}} \phi_{i-1}^{\bullet}\tau_{i-1}^{\bullet} - \frac{\pi_{\downarrow}}{\pi_{\rightarrow}} \phi_{i-1}^{\circ}\tau_{i-1}^{\circ} - \frac{1}{\pi_{\rightarrow}} \phi_{i-1}^{\bullet}t_{i-1}^{\bullet}. \quad (44)$$

Now we substitute this relation for  $\phi_i^{\bullet}\tau_i^{\bullet}$  in the recursion Eq 41, and obtain,

$$\phi_i^{\circ}\tau_i^{\circ} = \frac{\pi_{\uparrow}}{\pi_{\leftarrow}} \phi_{i-1}^{\bullet}\tau_{i-1}^{\bullet} + \left(\pi_{\leftarrow} - \frac{\pi_{\uparrow}\pi_{\downarrow}}{\pi_{\rightarrow}}\right) \phi_{i-1}^{\circ}\tau_{i-1}^{\circ} + \phi_i^{\circ}t_i^{\circ} - \frac{\pi_{\uparrow}}{\pi_{\leftarrow}} \phi_{i-1}^{\bullet}t_{i-1}^{\bullet}. \quad (45)$$

Recursion Eqs 44 and 45, can be written in a matrix representation as,

$$\underbrace{\begin{bmatrix} \phi_i^{\bullet}\tau_i^{\bullet} \\ \phi_i^{\circ}\tau_i^{\circ} \end{bmatrix}}_{\mathbf{V}_i} = \underbrace{\begin{bmatrix} \frac{1}{\pi_{\rightarrow}} & -\frac{\pi_{\downarrow}}{\pi_{\rightarrow}} \\ \frac{\pi_{\uparrow}}{\pi_{\leftarrow}} & \pi_{\leftarrow} - \frac{\pi_{\uparrow}\pi_{\downarrow}}{\pi_{\rightarrow}} \end{bmatrix}}_{\mathbf{A}} \underbrace{\begin{bmatrix} \phi_{i-1}^{\bullet}\tau_{i-1}^{\bullet} \\ \phi_{i-1}^{\circ}\tau_{i-1}^{\circ} \end{bmatrix}}_{\mathbf{V}_{i-1}} + \underbrace{\begin{bmatrix} -\frac{1}{\pi_{\rightarrow}} \phi_{i-1}^{\bullet}t_{i-1}^{\bullet} \\ \phi_i^{\circ}t_i^{\circ} - \frac{\pi_{\uparrow}}{\pi_{\leftarrow}} \phi_{i-1}^{\bullet}t_{i-1}^{\bullet} \end{bmatrix}}_{\mathbf{U}_{i-1}}. \quad (46)$$

The matrix equation can be further simplified,

$$\begin{aligned}\mathbf{V}_i &= \mathbf{A}\mathbf{V}_{i-1} + \mathbf{U}_{i-1} \\ &= \mathbf{A}^i\mathbf{V}_0 + \sum_{j=0}^{i-1} \mathbf{A}^{i-j-1}\mathbf{U}_j.\end{aligned}\quad (47)$$

Remember that we want to compute the scaling for  $\tau^T$ , and for that we need to solve the above matrix equation for  $\tau_0^{\bullet}$  and  $\tau_1^{\circ}$ . The first thing that we need to calculate for Eq 47 is  $\mathbf{A}^i$ . Using

Eq 25 we substitute for the conditional probabilities in the definition of matrix  $\mathbf{A}$ ,

$$\mathbf{A} = \begin{bmatrix} \frac{n\lambda}{\delta} + 1 & -\frac{n\lambda}{\delta} \\ \frac{n\lambda}{\delta} & 1 - \frac{n\lambda}{\delta} \end{bmatrix} = \frac{n\lambda}{\delta} \begin{bmatrix} 1 & -1 \\ 1 & -1 \end{bmatrix} + \begin{bmatrix} 1 & 0 \\ 0 & 1 \end{bmatrix} \quad (48)$$

In this way we find,

$$\mathbf{A}^i = i \frac{n\lambda}{\delta} \begin{bmatrix} 1 & -1 \\ 1 & -1 \end{bmatrix} + \begin{bmatrix} 1 & 0 \\ 0 & 1 \end{bmatrix} \quad (49)$$

To evaluate  $\tau_0^*$ , we take the first row of the matrix Eq 47, and set  $i = n$ ,

$$\phi_n^* \tau_n^* = \left( \frac{n^2\lambda}{\delta} + 1 \right) \phi_0^* \tau_0^* + \sum_{j=0}^{n-1} [\mathbf{A}^{n-j-1} \mathbf{U}_j]_0, \quad (50)$$

where  $\begin{bmatrix} \cdot \\ \cdot \\ \cdot \end{bmatrix}_0$  is the 0<sup>th</sup> element of the column vector  $\begin{bmatrix} \cdot \\ \cdot \\ \cdot \end{bmatrix}$ . Using the boundary condition,  $\tau_n^* = 0$  in Eq 50 we find

$$\tau_0^* = - \frac{\sum_{j=0}^{n-1} [\mathbf{A}^{n-j-1} \mathbf{U}_j]_0}{\left( \frac{n^2\lambda}{\delta} + 1 \right) \phi_0^*}. \quad (51)$$

From Refs. [54, 56] we know that at neutrality

$$\phi_i^* = \frac{\delta + in\lambda}{\delta + n^2\lambda}, \quad \text{and} \quad \phi_i^\circ = \frac{in\lambda}{\delta + n^2\lambda}. \quad (52)$$

These relations for the fixation probability also follow by substituting for the transition probabilities in Eq 21. Using  $\phi_0^*$  in Eq 51, we find

$$\tau_0^* = - \sum_{j=0}^{n-1} [\mathbf{A}^{n-j-1} \mathbf{U}_j]_0. \quad (53)$$

In order to simplify the r.h.s of the above equation, we need expressions for the waiting times in the state  $i$ , namely,  $t_i^*$ , and  $t_i^\circ$ . We compute these expressions using Eqs 24, 26 and 43,

$$t_i^* = \frac{n(n+1)}{(n-i)(\delta + n\lambda)} \quad \text{and} \quad t_i^\circ = \frac{n(n+1)}{i(\delta + n\lambda)}. \quad (54)$$

With all these expressions, we can now simplify the r.h.s of the Eq 53,

$$\sum_{j=0}^{n-1} [\mathbf{A}^{n-j-1} \mathbf{U}_j]_0 = \sum_{j=0}^{n-1} \left[ \left( (n-j-1) \frac{n\lambda}{\delta} + 1 \right) \left( - \left( \frac{n\lambda + \delta}{\delta} \right) \phi_j^\bullet t_j^\bullet \right) \right. \quad (55)$$

$$\left. - (n-j-1) \frac{n\lambda}{\delta} \left( \phi_{j+1}^\circ t_{j+1}^\circ - \frac{n\lambda}{\delta} \phi_j^\bullet t_j^\bullet \right) \right], \quad (56)$$

$$= \frac{n(n+1)}{(\delta + n\lambda)(\delta + n^2\lambda)} \sum_{j=0}^{n-1} \left[ \frac{\delta + n^2\lambda}{j-n} - (n-1) \frac{n^2\lambda^2}{\delta} \right], \quad (57)$$

$$= - \frac{n(n+1)}{(\delta + n\lambda)(\delta + n^2\lambda)} \left[ (\delta + n^2\lambda) H_n + (n-1) \frac{n^3\lambda^2}{\delta} \right], \quad (58)$$

where  $H_n = \sum_{k=1}^n \frac{1}{k}$  is the harmonic number. This gives us an expression for the conditional average fixation time at neutrality on the self-looped weighted star graph starting with the state  $(\bullet, 0)$ ,

$$\tau_0^\bullet = \frac{n^4(n^2-1)}{\delta(\delta + n\lambda)(\delta + n^2\lambda)} + \frac{n(n+1)}{\delta + n\lambda} H_n. \quad (59)$$

Next, we show that  $\tau_1^\circ$  is related to  $\tau_0^\bullet$ . To see this, let us take the second row of the matrix Eq 47, and set  $i = 1$ ,

$$\phi_1^\circ \tau_1^\circ = \frac{\pi_{\uparrow}}{\pi_{\leftarrow}} \phi_0^\bullet \tau_0^\bullet + \left( \pi_{\leftarrow} - \frac{\pi_{\uparrow} \pi_{\downarrow}}{\pi_{\leftarrow}} \right) \underbrace{\phi_0^\circ \tau_0^\circ}_{=0} + \phi_1^\circ t_1^\circ - \frac{\pi_{\uparrow}}{\pi_{\leftarrow}} \phi_0^\bullet t_0^\bullet \quad (60)$$

Upon substituting for various quantities, we find,

$$\tau_1^\circ = \tau_0^\bullet + \frac{n^2-1}{\delta + n\lambda}. \quad (61)$$

Using the temperature initialised definition of the average fixation time for the star graph, see Eq 31, we can evaluate the expressions for the temperature initialised fixation time  $\tau^T$  for the self-looped star graph and the star graph without self-loops. For the self-looped star graph, setting,  $\lambda = 1/n$  and  $\delta = 1/n^2$ , we have

$$\tau_{\substack{\lambda = 1/n \\ \delta = 1/n^2}}^T = \frac{(n-1)((n(n^4+n-2)+2)n^3-n+1)+(n^6+n^3)H_n}{((n-1)n+1)(n^2+1)} \quad (62)$$

$$\stackrel{N \gg 1}{\approx} n^5 - \mathcal{O}(n^3). \quad (63)$$

For the star graph (without self-loops), setting,  $\lambda = \delta = 1$ , we have

$$\tau_{\lambda=1, \delta=1}^T = \frac{(n-1)(n^5 + n^4 + n^2 + 1)}{(n+1)(n^2 + 1)} + nH_n, \quad (64)$$

$$\stackrel{N \gg 1}{\approx} n^3 - \mathcal{O}(n^2). \quad (65)$$

**5.3.3 Gillespie algorithm.** In the Moran process, the fixation/extinction dynamics goes through many inactive steps where the configuration of the population does not change. This happens when one type is replaced by an offspring of its own type. This causes the individual-based simulation to be time-consuming, especially for large population sizes [57]. To tackle this problem, we use the Gillespie algorithm [58, 59] for the Moran fixation dynamics. We apply the Gillespie algorithm to calculate the fixation time in the star with and without self-loops for large population sizes. Simulation steps are as follows:

1. Calculate the transition probability for each possible transition which changes the configuration of the population. The possible transitions and their corresponding transition probabilities for the star graphs are discussed in the Sec. 5.3.1.
2. Calculate the total transition probability, which is the sum of all the transition probabilities. For example if the current state is  $(\bullet, i)$ , then the total transition probability is  $T_{i,i+1}^{\bullet\bullet} + T_{ii}^{\bullet\circ}$ .
3. Generate two random numbers, one to determine the time of the next event and another to determine which event occurs. The first random number determining the time to the next event is drawn from an exponential distribution with the mean equal to the total propensity. The second random number is drawn from a uniform distribution.
4. Update the system state according to the event chosen in the previous step.
5. Repeat steps 1-4 until the system reaches fixation.

**5.3.4 Complete and cycle graph.** Compared to the star graph family, the fixation time for the complete graph (i.e. the well-mixed population) can be computed easily. From the Refs. [60–62], we know that the time to fixation for a single mutant in a population of size  $N$  is given by

$$\tau_1 = \sum_{k=1}^{N-1} \sum_{l=1}^k \frac{\phi_l}{T_{l+}} \prod_{m=l+1}^k \gamma_m, \quad (66)$$

where  $\gamma_m = \frac{T_{m-}}{T_{m+}}$ , and  $\phi_i$  is the fixation probability for mutant type to fix when started with  $i$  individuals and  $T_{i\pm}$  is the probability to transition from the state with  $i$  mutants to the state with  $i \pm 1$  mutants. The fixation probability  $\phi_i$  is given by

$$\phi_i = \frac{1 + \sum_{k=1}^{i-1} \prod_{l=1}^k \gamma_l}{1 + \sum_{k=1}^{N-1} \prod_{l=1}^k \gamma_l}. \quad (67)$$

The average fixation time on the complete when started with  $i$  individuals is,

$$\tau_i = -\tau_1 \frac{\phi_1}{\phi_i} \sum_{k=i}^{N-1} \prod_{m=1}^k \gamma_m + \sum_{k=i}^{N-1} \sum_{l=1}^k \frac{\phi_l}{\phi_i} \frac{1}{T_{l+}} \prod_{m=l+1}^k \gamma_m. \quad (68)$$

Using symmetry arguments, similar to the ones used for the case of star graph in the previous subsection, the formula for the extinction time of  $i$  mutants has been computed in Ref. [62],

$$\tilde{\tau}_i = -\tilde{\tau}_{N-1} \frac{\tilde{\phi}_{N-1}}{\tilde{\phi}_i} \sum_{k=N-i}^{N-1} \prod_{m=1}^k \frac{1}{\gamma_{N-m}} + \sum_{k=N-i}^{N-1} \sum_{l=1}^k \frac{\tilde{\phi}_{N-l}}{\tilde{\phi}_i} \frac{1}{T_{(N-l)-}} \prod_{m=l+1}^k \frac{1}{\gamma_{N-m}}, \quad (69)$$

where the extinction probability of  $i$  mutants is  $\tilde{\phi}_i = 1 - \phi_i$  and

$$\tilde{\tau}_{N-1} = \sum_{k=1}^{N-1} \sum_{l=1}^k \frac{\tilde{\phi}_{N-l}}{T_{(N-l)-}} \prod_{m=l+1}^k \frac{1}{\gamma_{N-m}}. \quad (70)$$

For the complete graph, the transition probabilities are,

$$T_{i-} = \frac{N-i}{ir+N-i} \cdot \frac{i}{N-1} \quad \text{and} \quad T_{i+} = \frac{ir}{ir+N-i} \cdot \frac{N-i}{N-1}. \quad (71)$$

These transition probabilities are plugged into Eqs 66 and 69 to obtain  $\tau_1$  and  $\tilde{\tau}_1$ , respectively. From Fig 7A, we find that the fixation time of a mutant is higher than its extinction time regardless of its relative fitness. Moreover, the fixation time of a mutant peaks near neutrality, therefore according to Eq 4, it is the fixation time at neutrality that decides the mutation rate threshold  $\mu_{th}$  for the complete graph. We now compute how the fixation time scales with  $N$  for

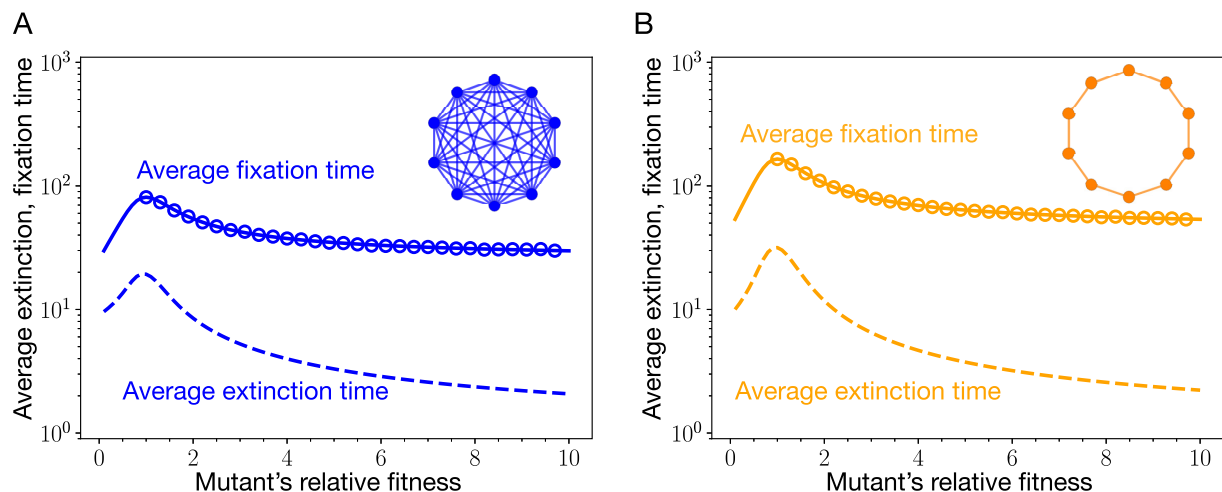


**Fig 7. Average extinction and fixation time for the isothermal graphs.** The average fixation (via solid lines) and average extinction (via dashed lines) times for the two isothermal graphs, namely, the complete graph and the cycle graph. To plot the analytical results, we have used Eqs 66 and 69. Open circles represent microscopic Moran Bd simulations. Although, the probability for a mutant to fix on any of these structures is the same due to isothermal theorem, the times it takes to reach fixation are different. Fixation on the cycle graph is slower than on the complete graph. As a result, the cycle graph is more restrictive to the weak mutation approximation. The parameters are same as in Fig 6.

<https://doi.org/10.1371/journal.pcbi.1011387.g007>

the complete graph. At neutrality,  $r = 1$ ,

$$T_{i-} = \frac{N-i}{N} \cdot \frac{i}{N-1}, \text{ and } T_{i+} = \frac{i}{N} \cdot \frac{N-i}{N-1}. \quad (72)$$

Therefore,  $\gamma_i = 1$ , for all  $i$ . The fixation probability simplifies as to

$$\phi_i = \frac{1 + \sum_{k=1}^{i-1} \prod_{l=1}^k 1}{1 + \sum_{k=1}^{N-1} \prod_{l=1}^k 1} = \frac{i}{N}, \quad (73)$$

which is expected as every neutral mutant is equally likely to fix as any other individual of the population. Using the Eq 66, the average fixation time for a neutral mutant on the complete graph is,

$$\tau_1 = \sum_{k=1}^{N-1} \sum_{l=1}^k \frac{N-1}{N-l} = (N-1)^2, \quad (74)$$

which scales as  $N^2$  for  $N \gg 1$  [60, 63].

We now move to the cycle graph. To compute  $\tau_1$  and  $\tilde{\tau}_1$  for the cycle graph, the following transition probabilities are used in the Eqs 66 and 69,

$$T_{i-} = \frac{2}{ir + N - i} \cdot \frac{1}{2} \quad \text{and} \quad T_{i+} = \frac{2r}{ir + N - i} \cdot \frac{1}{2}. \quad (75)$$

Similar to the case of complete graph, from the Fig 7B, we find that the fixation time of a mutant is higher than the extinction time regardless of its relative fitness. Also, the fixation time of a mutant peaks near neutrality, the fixation time at neutrality decides the mutation rate threshold  $\mu_{th}$  for the cycle graph.

Since  $\gamma_m$  for the cycle graph is identical to the complete graph [10], we find the same fixation probabilities for any fitness value and initial state. In particular, at neutrality, we have  $\phi_i = \frac{i}{N}$  for the cycle graph. For the cycle graph, the average fixation time for a neutral mutant is,

$$\tau_1 = \sum_{k=1}^{N-1} \sum_{l=1}^k l = \frac{N(N^2 - 1)}{6}, \quad (76)$$

which scales as  $N^3/6$  for large  $N$ .

**5.3.5 Directed line with self-loops.** Here we compute the average fixation and extinction time for the self-looped directed line. Let us first study the case of fixation time. A mutant can fix on the self-looped directed line if and only if it appears at the root node. Assuming this to be the case, we have

$$T_{i-}^* = 0 \quad \text{and} \quad T_{i+}^* = \frac{r}{ir + N - i} \cdot \frac{1}{2}, \quad (77)$$

where  $T_{i-}^*$  is the probability to transition from the state with  $i$  mutants to the state with  $i + 1$  mutants given that the initial mutant appears at the root node. Similarly,  $T_{i+}^*$  is the probability to transition from the state with  $i + 1$  mutants to the state with  $i$  mutants given that the initial mutant appears at the root node. If the first mutant appears at the root node, the number of mutants at any time in the population can only increase. Taking this into account, we have the

average fixation time for a mutant on the directed self-looped line,

$$\tau_1 = \sum_{k=1}^{N-1} \frac{1}{T_{k+}^*}, \quad (78)$$

where  $1/T_{i+}^*$  is average waiting time in the state with  $i$  mutants, assuming that the initial mutant appeared on the root node. This expression for the  $\tau_1$  can also be derived from the Eq 66. On substituting the transition probabilities  $T_{i+}^*$  in the r.h.s of the Eq 78, we find

$$\tau_1 = \sum_{k=1}^{N-1} \frac{2}{r} (kr + N - k) = N(N-1) \left(1 + \frac{1}{r}\right), \quad (79)$$

which scales as  $N^2(1 + 1/r)$  for large  $N$ . Unlike other graphs, the fixation time for the self-looped directed line does not peak near neutrality, see Fig 8. Time to fixation of a mutant increases as its relative fitness decreases. Moreover, for the directed line we have  $\tau_1^T = \tau_1$ . In fact for any mutant initialisation scheme, the fixation time is given by the formula 79. This independency of the fixation time from the initialisation scheme holds for all the single rooted graphs.

Now, we proceed to compute the extinction time of a mutant on the self-looped directed line. However, computing the average extinction time is not as straightforward as the fixation time. Extinction takes place when an initial mutant appears on any of the non-root node. Contrary to the case of fixation where the number of mutants can only increase, here the number of mutants can increase as well as decrease. What makes things slightly complicated is that the

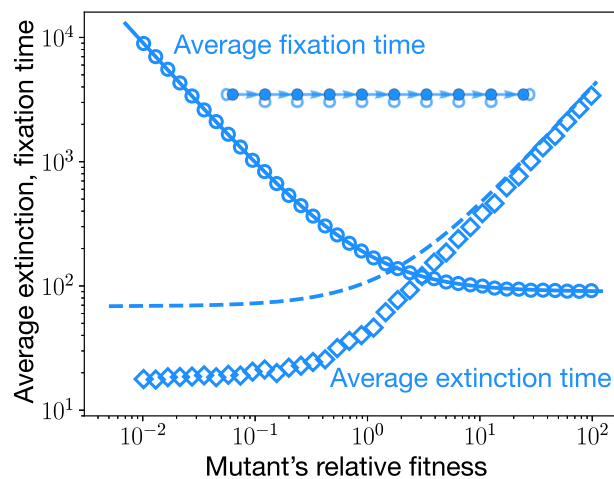


**Fig 8. Average extinction and fixation time for the self-looped directed line.** The average extinction time (dashed line) and the average fixation time (solid line) are shown for the self-looped directed line. Circles represent the total average time of the trajectories that lead to the fixation of mutants, whereas diamonds represent the average time spanned by the trajectories where mutants get extinct. We see a good agreement between analytical results and the corresponding simulations. The approximated formula for the average extinction time, Eq 82, works well in the regime of high relative fitness, as the dashed line starts coinciding with the simulations. Note that the average extinction time for a mutant can exceed the average fixation time. This is different from what we have observed in Figs 6 and 7. Also, for a given fitness domain, the average extinction and fixation time peaks away from the neutrality. Therefore, to decide the validity of the weak mutation rate approximation, fitness regions different from neutrality must be considered.

<https://doi.org/10.1371/journal.pcbi.1011387.g008>

number of mutants stops to increase once the terminal node is occupied with a mutant individual. In that scenario, the transition probabilities are given as,

$$T_{i-}^{\circ} = \frac{1}{ir + N - i} \cdot \frac{1}{2} \quad \text{and} \quad T_{i+}^{\circ} = 0, \quad (80)$$

where  $T_{i\pm}^{\circ}$  is the transition probability from the state with  $i$  mutants to the state with  $i \pm 1$  mutants, given that the initial mutant appears at a non-root node and the terminal node (node  $N - 1$ ) of the directed line is occupied by a mutant type. We approximate the average extinction time by considering the trajectory where the number of mutants keep on increasing until the terminal node get occupied by the mutant type, and then followed by the decrease in mutants leading to extinction. An example case is shown in the Fig 9 (category third). This approximation works well in the limit of  $f'/f \gg 1$ . With this approximation, we have the extinction time of a mutant when appeared on a non-root node  $\alpha$ ,

$$\tilde{\tau}_{\alpha} = N - 1 - \alpha + \sum_{k=N-\alpha}^{N-1} \frac{1}{T_{(N-k)-}^{\circ}}. \quad (81)$$

Here,  $1/T_{(N-i)-}^{\circ}$  is the average waiting time in the state with  $N - i$  mutants, given that the initial mutant appeared on a non-root node (node 0) and the terminal node is occupied by the mutant type. The above equation can also be derived from the Eq 69. The temperature initialised average extinction time of a mutant on the self-looped directed line is,

$$\tilde{\tau}_1^T = \sum_{\alpha=1}^{N-1} \frac{T_{\alpha}}{\sum_{\beta=1}^{N-1} T_{\beta}} \tilde{\tau}_{\alpha}, \quad (82)$$

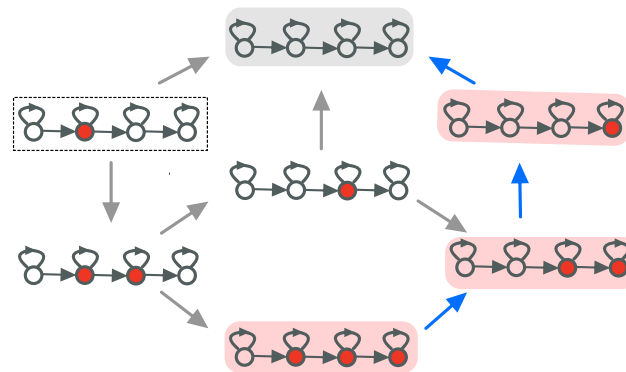


**Fig 9. Paths to extinction.** Here, the possible mutant extinction routes are shown for the self-looped directed line when the initial mutant appears on a non-root node. For purpose of illustrations, we have chosen  $N = 4$ . Broadly speaking, there are three categories of extinction trajectories. (i) The case where the initial mutant goes extinct without spreading in the population. This would be a one time step extinction process, shown by arrow leading from the boxed initial state to the wild-type state, highlighted in grey. (ii) The second category corresponds to the case, where the initial mutant spreads, but the mutant goes extinct before the terminal node is ever occupied by a mutant. This would contain all the paths that go from the boxed state via two mutants to the grey highlighted state without going through the states highlighted in red. (iii) The third category refers to the case, where the initial mutant spreads and reach the state highlighted in red. After the terminal node is occupied by the mutant type, the number of mutants then starts to decrease from the left (shown via the trajectory marked with blue arrows). This third category is especially relevant when the mutant's relative fitness is very high. We make use of this argument to approximate the extinction time for the self-looped directed line by computing the time covered by the blue arrowed trajectory.

<https://doi.org/10.1371/journal.pcbi.1011387.g009>



where  $T_\alpha$  is the temperature of node  $\alpha$ .  $T_\alpha / \sum_{\beta=1}^{N-1} T_\beta$  is the probability that the initial mutant appears at the node  $\alpha$ , given that the mutant ultimately goes extinct, i.e., given that it appears at a non-root node. From the Fig 8, we see that the average extinction time of a mutant increases with relative fitness. However, for a given fitness domain, we find that the contribution to the mutation threshold  $\mu_{th}$  comes from the average fixation time computed for the lowest possible mutant's relative fitness.

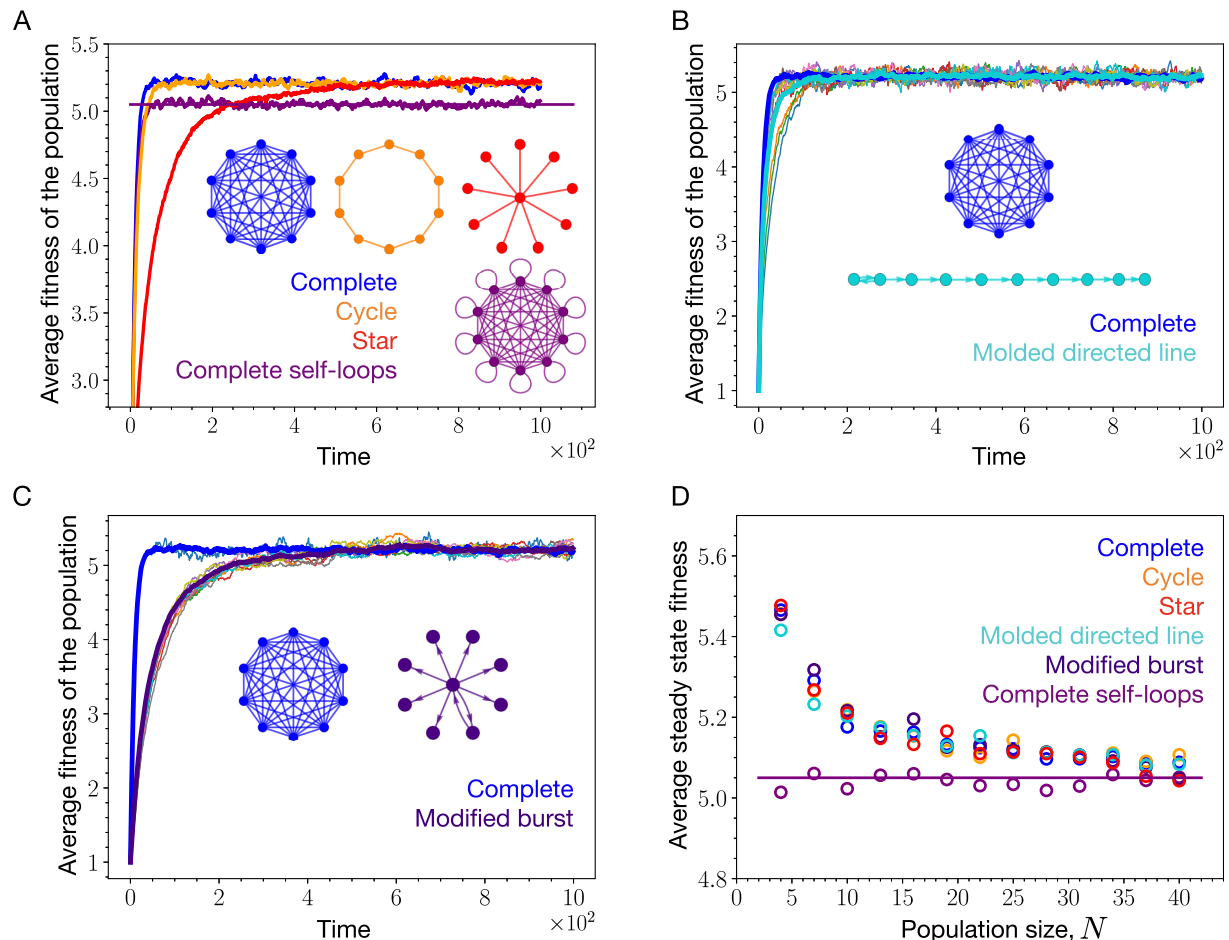


**Fig 10. Universal steady-state fitness among non self-looped graphs.** (A) In the steady-state, the complete graph, the cycle graph, and the star graph, attain the same average fitness in the mutation-selection balance. The steady-state average fitness obtained by these graphs is higher than that of the self-looped complete graph, indicating that the dynamics on these graphs—unlike the self-looped complete graph—is not entirely uncorrelated in the fitness space and time. One common thing in these three graphs is that every node has at least one incoming link. (B) The molded directed line is constructed by adding a link directed from node 1 to node 0, the root node, so that every node has non-zero incoming links. In the steady-state, not only the molded directed line attains the same average fitness as the complete graph (non self-looped), but every single node becomes indistinguishable. (C) The same observation is made for the modified burst graph. (D) These observations remain valid for different population sizes. The difference between the steady-state average fitness of the non self-looped and the self-looped complete graph decreases with increasing  $N$ , indicating that the evolutionary dynamics becomes more random with increasing  $N$  (Parameters: same as Fig 3).

<https://doi.org/10.1371/journal.pcbi.1011387.g010>

### 5.4 Non self-looped graphs and universality at equilibrium

Here, we study the evolutionary dynamics, considering both directed as well as undirected graphs, but without self-loops.

In the absence of self-loops, the average steady-state fitness for all the graphs, whether directed or not, is the same, see Fig 10A. We hypothesise that all the graphs where every node has a finite temperature attain the same steady-state fitness in the mutation-selection balance. All the nodes for these graphs become indistinguishable in their fitness in the steady-state. The steady-state fitness attained by these graphs in the mutation-selection balance is higher than the self-looped complete graph. For these graphs, the fitnesses of nodes in the steady-state are not completely uncorrelated in time as opposed to nodes of the self-looped complete graph where the fitness states of nodes are entirely uncorrelated in time. To test our hypothesis, we analysed a few variants of the directed line and burst graph in Fig 10B and 10C, where each node has a finite temperature. To achieve this, we add a link from node 1 to the root node of the directed line yielding a molded directed line. Similarly, the modified burst is constructed by adding a link from the leaf node to the center in a burst graph. In both the cases, we find that the steady-state fitness attained by these two variant graphs in the mutation-selection balance is the same as that of the complete graph and hence, the other non-self looped graphs considered in Fig 10A. We further check the validity of our hypothesis by varying the population size. In Fig 10D, we see that all the non self-looped graph attain the same steady-state fitness for all population sizes.

Another interesting observation is that the steady-state fitness balance of the non self-looped graphs decreases with increasing  $N$ . This is interesting, because with increasing  $N$  one typically expects that the associated increase in the selection strength leads to an increase in the fitness. However, the opposite is seen here. A possible explanation for this is that in the Moran Birth-death update scheme, high fitness nodes are more likely to be selected for reproduction, but since there are no self-loops, highly fit individuals can persist in the population for longer times than the low fitness nodes which eventually leads to an the increase in population fitness. However, with the increase in the population size, the high fitness nodes tend to get replaced relatively more often as they get less selected for birth. On increasing  $N$ , the steady-state average fitness of the non self-looped graphs get closer to that of the average steady-state fitness of the self-looped complete graph. In Sec. 3.4.1, we saw that at long times the fitness of nodes for the self-looped complete graph becomes uncorrelated in time and hence the dynamics becomes completely random. With the increase in  $N$ , the strength of randomness increases over selection of high fitness valued individuals.

### Acknowledgments

We are thankful to Julien Dutheil, Christian Hilbe and Javier Lopez Garrido for helpful discussions.

### Author Contributions

**Conceptualization:** Nikhil Sharma, Arne Traulsen.

**Formal analysis:** Nikhil Sharma, Sedigheh Yagoobi.

**Investigation:** Nikhil Sharma.

**Methodology:** Nikhil Sharma.

**Software:** Nikhil Sharma.

**Validation:** Nikhil Sharma, Sedigheh Yagoobi, Arne Traulsen.

**Visualization:** Nikhil Sharma, Arne Traulsen.

**Writing – original draft:** Nikhil Sharma.

**Writing – review & editing:** Nikhil Sharma, Sedigheh Yagoobi, Arne Traulsen.

## References

1. Lieberman E, Hauert C, Nowak MA. Evolutionary dynamics on graphs. *Nature*. 2005; 433:312–316. <https://doi.org/10.1038/nature03204> PMID: 15662424
2. McCandlish DM, Epstein CL, Plotkin JB. Formal properties of the probability of fixation: identities, inequalities and approximations. *Theoretical population biology*. 2015; 99:98–113. <https://doi.org/10.1016/j.tpb.2014.11.004> PMID: 25450112
3. Ewens WJ. *Mathematical Population Genetics. I. Theoretical Introduction*. New York: Springer; 2004.
4. Kimura M. Evolutionary rate at the molecular level. *Nature*. 1968; 217:624–626. <https://doi.org/10.1038/217624a0> PMID: 5637732
5. Patwa Z, Wahl LM. The fixation probability of beneficial mutations. *Journal of The Royal Society Interface*. 2008; 5:1279–1289. <https://doi.org/10.1098/rsif.2008.0248> PMID: 18664425
6. Kuo YP, Nombela-Arrieta C, Carja O. A theory of evolutionary dynamics on any complex spatial structure. *bioRxiv*. 2021;.
7. Park SC, Simon D, Krug J. The speed of evolution in large asexual populations. *Journal of Statistical Physics*. 2010; 138(1):381–410. <https://doi.org/10.1007/s10955-009-9915-x>
8. Frean M, Rainey P, Traulsen A. The effect of population structure on the rate of evolution. *Proceedings of the Royal Society B*. 2013; 280:20130211. <https://doi.org/10.1098/rspb.2013.0211> PMID: 23677339
9. Hindersin L, Traulsen A. Most undirected random graphs are amplifiers of selection for Birth-death dynamics, but suppressors of selection for death-Birth dynamics. *PLoS Computational Biology*. 2015; 11:e1004437. <https://doi.org/10.1371/journal.pcbi.1004437> PMID: 26544962
10. Nowak MA. *Evolutionary dynamics: Exploring the equations of life*. Harvard University Press; 2006.
11. Antal T, Redner S, Sood V. Evolutionary dynamics on degree-heterogeneous graphs. *Physical Review Letters*. 2006; 96(18):188104. <https://doi.org/10.1103/PhysRevLett.96.188104> PMID: 16712402
12. Broom M, Rychtář J, Stadler BT. Evolutionary dynamics on graphs—the effect of graph structure and initial placement on mutant spread. *Journal of Statistical Theory and Practice*. 2011; 5(3):369–381. <https://doi.org/10.1080/15598608.2011.10412035>
13. Adlam B, Chatterjee K, Nowak MA. Amplifiers of selection. *Proceedings of the Royal Society A*. 2015; 471(2181):20150114. <https://doi.org/10.1098/rspa.2015.0114>
14. Yagoobi S, Yousefi H, Samani KA. Mutation-selection stationary distribution in structured populations. *Physical Review E*. 2018; 98(4):042301. <https://doi.org/10.1103/PhysRevE.98.042301>
15. McAvoy A, Adlam B, Allen B, Nowak MA. Stationary frequencies and mixing times for neutral drift processes with spatial structure. *Proceedings of the Royal Society A: Mathematical, Physical and Engineering Sciences*. 2018; 474(2218):20180238. <https://doi.org/10.1098/rspa.2018.0238>
16. Sharma N, Traulsen A. Suppressors of fixation can increase average fitness beyond amplifiers of selection. *Proceedings of the National Academy of Sciences*. 2022; 119(37):e2205424119. <https://doi.org/10.1073/pnas.2205424119> PMID: 36067304
17. Bürger R. *The Mathematical Theory of Selection, Recombination, and Mutation*. John Wiley and Sons; 2000.
18. Black AJ, Traulsen A, Galla T. Mixing times in evolutionary games. *Physical Review Letters*. 2012; 109:028101. <https://doi.org/10.1103/PhysRevLett.109.028101> PMID: 23030206
19. Levin DA, Peres Y, L Wilmer E. *Markov chains and mixing times*. American Mathematical Society; 2009.
20. Pavlogiannis A, Tkadlec J, Chatterjee K, Nowak MA. Construction of arbitrarily strong amplifiers of natural selection using evolutionary graph theory. *Communications Biology*. 2018; 1(78). <https://doi.org/10.1038/s42003-018-0078-7> PMID: 30271952
21. Yagoobi S, Sharma N, Traulsen A. Categorizing update mechanisms for graph-structured metapopulations. *Journal of the Royal Society Interface*. 2023; 20(200):20220769. <https://doi.org/10.1098/rsif.2022.0769> PMID: 36919418
22. Levins R. Some Demographic and Genetic Consequences of Environmental Heterogeneity for Biological Control. *Bulletin of the Entomological Society of America*. 1969; 15:237–240. <https://doi.org/10.1093/besa/15.3.237>

23. Marrec L, Lamberti I, Bitbol AF. Toward a universal model for spatially structured populations. *Physical Review Letters*. 2021; 127(21):218102. <https://doi.org/10.1103/PhysRevLett.127.218102> PMID: [34860074](#)
24. Yagoobi S, Traulsen A. Fixation probabilities in network structured meta-populations. *Scientific Reports*. 2021; 11(1):1–9. <https://doi.org/10.1038/s41598-021-97187-6> PMID: [34504152](#)
25. Houchmandzadeh B, Vallade M. The fixation probability of a beneficial mutation in a geographically structured population. *New Journal of Physics*. 2011; 13(7):073020. <https://doi.org/10.1088/1367-2630/13/7/073020>
26. Pattni K, Ali W, Broom M, Sharkey KJ. Eco-evolutionary dynamics in finite network-structured populations with migration. *arXiv preprint arXiv:230401903*. 2023;.
27. Abbara A, Bitbol AF. Frequent asymmetric migrations suppress natural selection in spatially structured populations. *bioRxiv*. 2023; p. 2023–06.
28. McCandlish DM, Stoltzfus A. Modeling evolution using the probability of fixation: history and implications. *The Quarterly review of biology*. 2014; 89(3):225–252. <https://doi.org/10.1086/677571> PMID: [25195318](#)
29. Wu B, Gokhale CS, Wang L, Traulsen A. How small are small mutation rates? *Journal of Mathematical Biology*. 2012; 64:803–827. <https://doi.org/10.1007/s00285-011-0430-8> PMID: [21626364](#)
30. van Kampen NG. *Stochastic Processes in Physics and Chemistry*. 2nd ed. Amsterdam: Elsevier; 1997.
31. Tkadlec J, Pavlogiannis A, Chatterjee K, Nowak MA. Population structure determines the tradeoff between fixation probability and fixation time. *Communications biology*. 2019; 2(1):1–8. <https://doi.org/10.1038/s42003-019-0373-y> PMID: [31044163](#)
32. Möller M, Hindersin L, Traulsen A. Exploring and mapping the universe of evolutionary graphs identifies structural properties affecting fixation probability and time. *Communications Biology*. 2019; 2(137). <https://doi.org/10.1038/s42003-019-0374-x> PMID: [31044162](#)
33. Tkadlec J, Pavlogiannis A, Chatterjee K, Nowak MA. Fast and strong amplifiers of natural selection. *Nature Communications*. 2021; 12:4009. <https://doi.org/10.1038/s41467-021-24271-w> PMID: [34188036](#)
34. Gerrish PJ, Lenski RE. The fate of competing beneficial mutations in an asexual population. *Genetica*. 1998; 102–103:127–144. <https://doi.org/10.1023/A:1017067816551> PMID: [9720276](#)
35. Park SC, Krug J. Clonal interference in large populations. *Proceedings of the National Academy of Sciences USA*. 2007; 104(46):18135–18140. <https://doi.org/10.1073/pnas.0705778104> PMID: [17984061](#)
36. Ashcroft P, Traulsen A, Galla T. When the mean is not enough: Calculating fixation time distributions in birth-death processes. *Physical Review E*. 2015; 92:042154. <https://doi.org/10.1103/PhysRevE.92.042154>
37. Hathcock D, Strogatz SH. Fitness dependence of the fixation-time distribution for evolutionary dynamics on graphs. *Physical Review E*. 2019; 100(1):012408. <https://doi.org/10.1103/PhysRevE.100.012408> PMID: [31499887](#)
38. Hathcock D, Strogatz SH. Asymptotic absorption-time distributions in extinction-prone Markov processes. *Physical Review Letters*. 2022; 128(21):218301. <https://doi.org/10.1103/PhysRevLett.128.218301> PMID: [35687454](#)
39. Teimouri H, Khavas DS, Spaulding C, Li C, Kolomeisky A. Theoretical understanding of evolutionary dynamics on inhomogeneous networks. *bioRxiv*. 2023; p. 2023–02. PMID: [37023763](#)
40. Altrock PM, Gokhale CS, Traulsen A. Stochastic slowdown in evolutionary processes. *Physical Review E*. 2010; 82:011925. <https://doi.org/10.1103/PhysRevE.82.011925> PMID: [20866666](#)
41. Pattni K, Broom M, Rychtář J, Silvers LJ. Evolutionary graph theory revisited: when is an evolutionary process equivalent to the Moran process? *Proceedings of the Royal Society A: Mathematical, Physical and Engineering Sciences*. 2015; 471(2182):20150334. <https://doi.org/10.1098/rspa.2015.0334>
42. Broom M, Rychtář J. *Game-Theoretical Models in Biology*. Chapman and Hall/CRC; 2013.
43. Jamieson-Lane A, Hauert C. Fixation probabilities on superstars, revisited and revised. *Journal of Theoretical Biology*. 2015; 382:44–56. <https://doi.org/10.1016/j.jtbi.2015.06.029> PMID: [26122591](#)
44. Giakkoupis G. Amplifiers and suppressors of selection for the moran process on undirected graphs. *arXiv preprint arXiv:161101585*. 2016;.
45. Pavlogiannis A, Tkadlec J, Chatterjee K, Nowak MA. Amplification on Undirected Population Structures: Comets Beat Stars. *Scientific Reports*. 2017; 7(82). <https://doi.org/10.1038/s41598-017-00107-w> PMID: [28250441](#)

46. Goldberg LA, Lapinskas J, Lengler J, Meier F, Panagiotou K, Pfister P. Asymptotically optimal amplifiers for the Moran process. *Theoretical Computer Science*. 2019; 758:73–93. <https://doi.org/10.1016/j.tcs.2018.08.005>
47. Tkadlec J, Pavlogiannis A, Chatterjee K, Nowak MA. Limits on amplifiers of natural selection under death-Birth updating. *PLoS computational biology*. 2020; 16(1):e1007494. <https://doi.org/10.1371/journal.pcbi.1007494> PMID: 31951609
48. Allen B, Sample C, Steinhagen P, Shapiro J, King M, Hedspeth T, et al. Fixation probabilities in graph-structured populations under weak selection. *PLoS computational biology*. 2021; 17(2):e1008695. <https://doi.org/10.1371/journal.pcbi.1008695> PMID: 33529219
49. Eigen M, McCaskill J, Schuster P. The molecular quasi-species. *Advances in Chemical Physics*. 1989; 75:149–263.
50. Wilke CO. Quasispecies theory in the context of population genetics. *BMC Evolutionary Biology*. 2005; 5:44. <https://doi.org/10.1186/1471-2148-5-44> PMID: 16107214
51. Van Nimwegen E, Crutchfield JP, Huynen M. Neutral evolution of mutational robustness. *Proceedings of the National Academy of Sciences*. 1999; 96(17):9716–9720. <https://doi.org/10.1073/pnas.96.17.9716> PMID: 10449760
52. Nowak M, Schuster P. Error thresholds of replication in finite populations mutation frequencies and the onset of Muller's ratchet. *Journal of theoretical Biology*. 1989; 137(4):375–395. [https://doi.org/10.1016/S0022-5193\(89\)80036-0](https://doi.org/10.1016/S0022-5193(89)80036-0) PMID: 2626057
53. Kelly FP. *Reversibility and stochastic networks*. Cambridge University Press; 2011.
54. Hadjichrysanthou C, Broom M, Rychtář J. Evolutionary Games on Star Graphs Under Various Updating Rules. *Dynamic Games and Applications*. 2011; 1(3):386–407. <https://doi.org/10.1007/s13235-011-0022-7>
55. Askari M, Samani KA. Analytical calculation of average fixation time in evolutionary graphs. *Physical Review E*. 2015; 92(4):042707. <https://doi.org/10.1103/PhysRevE.92.042707> PMID: 26565272
56. Broom M, Rychtář J. An analysis of the fixation probability of a mutant on special classes of non-directed graphs. *Proceedings of the Royal Society A*. 2008; 464:2609–2627. <https://doi.org/10.1098/rspa.2008.0058>
57. Hindersin L, Wu B, Traulsen A, Garcia J. Computation and Simulation of Evolutionary Game Dynamics in Finite Populations. *Scientific Reports*. 2019; 9 (6946). <https://doi.org/10.1038/s41598-019-43102-z> PMID: 31061385
58. Gillespie D. A general method for numerically simulating the stochastic time evolution of coupled chemical reactions. *Journal of Computational Physics*. 1976; 22:403–434. [https://doi.org/10.1016/0021-9991\(76\)90041-3](https://doi.org/10.1016/0021-9991(76)90041-3)
59. Gillespie DT. Exact Stochastic Simulation of coupled chemical reactions. *The Journal of Physical Chemistry*. 1977; 81(25):2340–2361. <https://doi.org/10.1021/j100540a008>
60. Goel NS, Richter-Dyn N. *Stochastic Models in Biology*. Academic Press, New York; 1974.
61. Antal T, Scheuring I. Fixation of strategies for an evolutionary game in finite populations. *Bulletin of Mathematical Biology*. 2006; 68:1923–1944. <https://doi.org/10.1007/s11538-006-9061-4> PMID: 17086490
62. Traulsen A, Hauert C. Stochastic evolutionary game dynamics. In: Schuster HG, editor. *Reviews of Nonlinear Dynamics and Complexity*. vol. II. Weinheim: Wiley-VCH; 2009. p. 25–61.
63. Altrock PM, Traulsen A. Fixation times in evolutionary games under weak selection. *New Journal of Physics*. 2009; 11:013012. <https://doi.org/10.1088/1367-2630/11/1/013012>

## Chapter 5

# Categorising update rules for network structured metapopulations

In our view, any new theory in evolutionary biology should either aim to introduce novel conceptual insights or explain empirical observations. The framework of evolutionary graph theory not only generates fresh insights on paper but also holds potential for experimental testing in the lab. Consequently, we hope to validate the role of spatial structures and the deleterious mutant regime using experimental evolution techniques. To initiate experiments, the transition from one-node-one-individual models, used in chapters 2, 3, and 4, to metapopulation models is required. However, it is known that the results from the one-node-one-individual theory cannot be directly applied to metapopulation theories [89]. This calls for parallel research in network-structured metapopulations. While the list of possible update rules for one-node-one individual setup is known [21, 22], the list for the metapopulation case has not been discussed yet. To further facilitate the research in metapopulation theories, in this chapter, we provide categories of update rules for metapopulations.

This chapter underwent peer-review and is published with open access in Journal of the Royal Society Interface as: Yagoobi, Sharma, and Traulsen 2023, [64]—Categorizing update mechanisms for graph-structured metapopulations. The authors contributions are detailed at the end of the thesis.



**Cite this article:** Yagoobi S, Sharma N, Traulsen A. 2023 Categorizing update mechanisms for graph-structured metapopulations. *J. R. Soc. Interface* **20**: 20220769.  
<https://doi.org/10.1098/rsif.2022.0769>

Received: 20 October 2022  
Accepted: 21 February 2023

**Subject Category:**  
Life Sciences—Mathematics interface

**Subject Areas:**  
evolution, computational biology

**Keywords:**  
evolutionary graph theory, graph-structured metapopulation, network-structured metapopulation, update mechanism,

**Author for correspondence:**  
Sedigheh Yagoobi  
e-mail: [yagoobi@evolbio.mpg.de](mailto:yagoobi@evolbio.mpg.de)

## Categorizing update mechanisms for graph-structured metapopulations

Sedigheh Yagoobi, Nikhil Sharma and Arne Traulsen

Department of Evolutionary Theory, Max Planck Institute for Evolutionary Biology, August-Thienemann Strasse 2, Plön 24306, Germany

SY, 0000-0003-2203-663X; NS, 0000-0003-0598-016X; AT, 0000-0002-0669-5267

The structure of a population strongly influences its evolutionary dynamics. In various settings ranging from biology to social systems, individuals tend to interact more often with those present in their proximity and rarely with those far away. A common approach to model the structure of a population is evolutionary graph theory. In this framework, each graph node is occupied by a reproducing individual. The links connect these individuals to their neighbours. The offspring can be placed on neighbouring nodes, replacing the neighbours—or the progeny of its neighbours can replace a node during the course of ongoing evolutionary dynamics. Extending this theory by replacing single individuals with subpopulations at nodes yields a graph-structured metapopulation. The dynamics between the different local subpopulations is set by an update mechanism. There are many such update mechanisms. Here, we classify update mechanisms for structured metapopulations, which allows to find commonalities between past work and illustrate directions for further research and current gaps of investigation.

### 1. Introduction

The spatial structure of a population has a considerable impact on the evolutionary dynamics of a population. One of the most popular theories for studying the effect of underlying structure on the evolution of a population is evolutionary graph theory [1], where the nodes of a graph represent individuals, and links indicate individual's neighbours. A link determines where an individual can place their offspring. An update mechanism describes which individuals produce offspring and how this offspring is placed. Here, we focus on fixed structures, but the framework can be extended to the case where a spatial structure itself varies over time [2–4].

An extension of evolutionary graph theory is given by graph-structured metapopulations in which the nodes indicate subpopulations, and the links indicate the migration between subpopulations [5–8]. Evolutionary dynamics in subdivided populations has been studied by researchers for a long time [9]. Models investigating the evolution of frequencies of different individuals in a subdivided population are also known as ‘island models’ [10]. A simplified version of these models considers individuals migrating from every island (subpopulation) to all the other islands with the assumption of a constant migration rate. In the language of evolutionary graph theory this is equivalent to the migration dynamics on a complete graph of subpopulations. To make this model more realistic, the stepping stone model was introduced where the migration rate depends on the distance between islands [11]. For a long time, the studies were mainly focused on the fully connected metapopulation. Patwa & Wahl [12] gives a good overview of the earlier work done on fixation probabilities for metapopulations. More recently, structures other than the complete graph are also being investigated. As an example, the star graph-structured metapopulation, where nodes are connected to each other via a central node, is studied in Constable & McKane [5], Yagoobi & Traulsen [6] and Marrec *et al.* [7]. Depending on the



system, different update mechanisms have been applied to describe the dynamics. In general, evolutionary dynamics are not robust to the choice of update mechanisms [13–16]. An important factor that changes the system's dynamics is how selection acts.

Depending on the update mechanism, selection can be global or local. This can affect the evolutionary dynamics dramatically. The two most important events that govern the dynamics of the population are birth and death. The order in which birth and death occur, which often determines if selection is local or global, has a high impact on the fate of the population [17]. We categorize different update mechanisms for the evolution of structured metapopulations to facilitate future work. First, we recall the update mechanisms on graphs of individuals, and then we generalize them to graphs of subpopulations.

## 2. Update mechanisms for graphs of individuals

In graphs of individuals, three main events influence the evolution of a population: birth, mutation and death. In the long run, a mutation–selection balance is reached [8,18–21]. Typically, the focus is on the low mutation regime in which the system reaches fixation or extinction of the mutant before the next mutation occurs. In that case, the population is typically homogeneous, and mutations reach fixation one after another. In the low mutation regime, the two quantities of most interest are the fixation probability and the average time to fixation.

If the fixation probability for advantageous mutants on a graph is higher than the fixation probability of the complete graph (and vice versa for disadvantageous mutations), the graph is called an amplifier of selection. On the other hand, if the fixation probability for advantageous mutants on a graph is less than the fixation probability on the complete graph (and vice versa for disadvantageous mutations), this graph is called a suppressor of selection. These notions have been first introduced in [1].

The order of birth and death events and how selection acts upon them can substantially influence the population's fate. We use the following scheme to differentiate between the update mechanisms. For birth, we use **b** if birth is random, i.e. a birth-giving individual is chosen uniformly at random, and **B** if the birth-giving individual is chosen with probability proportional to its selection parameter for birth. Similarly, we represent the death event by **d** if the individual dies uniformly at random and by **D** if the individual is selected for death with a probability proportional to its selection parameter for death.

Accordingly, the eight possible update mechanisms are **BD**, **Bd**, **bD**, **bd**, **DB**, **Db**, **dB** and **db**, where the order shows which event is first (see table 1). In all these update mechanisms, the first event is global, meaning that the individual is selected from the whole population. By contrast, the second event is local because the individual is selected only from the neighbourhood of the first individual, which is a subset of the population.

As an example, applying the update mechanism **Bd** in a well-mixed population of size  $N$  consisting of two types of individuals,  $N - n$  wild-types and  $n$  mutants, with mutants having a relative selection parameter for birth  $r$  with respect to wild-types. Let us consider that the number of mutants in the population is increased by one: one mutant is selected for

**Table 1.** Update mechanisms in graphs of individuals. In these update mechanisms, birth and death change the state of the population. The first event is global and the second event is local.

update mechanism	comment	references
<b>BD</b>	—	[17,22,23]
<b>Bd</b>	—	[1,17,22,24–40]
<b>bD</b>	—	[17,22,27,28,36]
<b>bd</b>	equivalent to a completely neutral model	[17,36,39–41]
<b>DB</b>	—	[17,22]
<b>Db</b>	biased voter model	[17,22,26–28,32,36,42–44]
<b>dB</b>	biased voter model	[16,17,22,27–31,36,45–47]
<b>db</b>	equivalent to a completely neutral model	[17,41]

reproduction (global event). Then, from the neighbours of the mutant, one wild-type is selected for death (local event). The offspring fills the empty spot of the dead individual. The probability of increasing the number of mutants by one is then

$$T_{\text{Bd}}^{n+} = \frac{rn}{rn + N - n} \frac{N - n}{N - 1} \quad (2.1)$$

birth of mutant death of wild-type

Similarly, the probability of decreasing the number of mutants by one is

$$T_{\text{Bd}}^{n-} = \frac{N - n}{rn + N - n} \frac{n}{N - 1} \quad (2.2)$$

birth of wild-type death of mutant

Note that  $T_{\text{Bd}}^{n-}/T_{\text{Bd}}^{n+} = 1/r$ . Using the recursive relation for the fixation probability [24,48], the fixation probability starting from  $n$  mutants is

$$\phi^{(n)} = \frac{1 + \sum_{i=1}^{n-1} \prod_{j=1}^i \frac{T_{\text{Bd}}^{j+}}{T_{\text{Bd}}^{j-}}}{1 + \sum_{i=1}^{N-1} \prod_{j=1}^i \frac{T_{\text{Bd}}^{j+}}{T_{\text{Bd}}^{j-}}} = \frac{1 - \frac{1}{r^n}}{1 - \frac{1}{r^N}} \quad (2.3)$$

The update rule **Bd** has been vastly explored in both structured and well-mixed populations [1,22,25,42,45,49,50]. For small populations, under the update mechanism **Bd**, most undirected unweighted structures are amplifiers of selection, and only a small fraction of random structures suppress selection [15]. In general, the fixation probabilities for mutants are computed using numerical approaches [51,52]. Only for highly symmetric graphs like the star graph or the complete bipartite graph, can the fixation probability be computed analytically [25,53]. Under the **Bd** updating scheme, the star graph is an amplifier of selection for all population sizes [1]. In [54], a few small-sized undirected, unweighted suppressors of selection have been studied. In larger



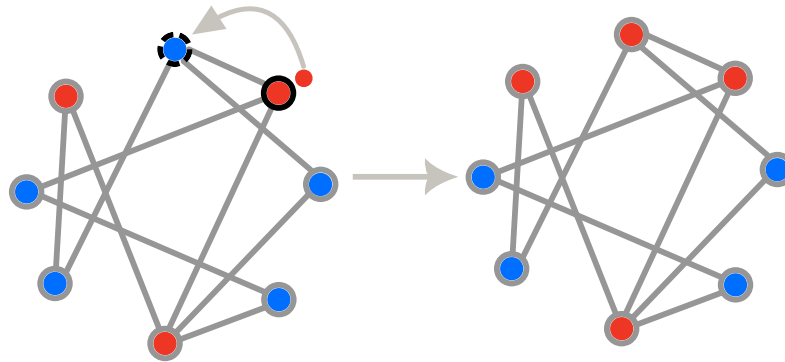


**Figure 1.** Different update schemes for graph of individuals. We consider an arbitrary population structure of size eight with five wild-type individuals (blue) and three mutant individuals (red). Neighbours are connected via links. Individual marked with solid black circle represents the birth giving parent, whereas, the individual marked with black dashed circle is the one chosen for death. The population size remains constant throughout the dynamics with offspring replacing dead individuals. Assuming that the selection parameter for birth of a mutant individual is  $r = 2$  (1 for the wild-type) and that the selection parameter for death of the mutant is  $t = 1/2$  (1 for the wild-type), the probabilities that the transition shown in the figure takes place are different for the different update mechanisms shown in table 1. For example, in the case of **BD**, the probability to choose this particular mutant individual for birth is  $\frac{2}{3 \cdot 2 + 5 \cdot 1} = \frac{2}{11}$ . The probability to choose this particular wild-type neighbour for death is  $\frac{1}{1 \cdot 1/2 + 2 \cdot 1} = \frac{2}{5}$ , which leads to a probability  $\frac{4}{55} \approx 0.072$  for the event shown. Similarly, we find: **Bd**:  $\frac{2}{3 \cdot 2 + 5 \cdot 1} \cdot \frac{1}{3} \approx 0.061$ . **bD**:  $\frac{1}{8} \cdot \frac{1}{1 \cdot 1/2 + 2 \cdot 1} = 0.05$ . **bd**:  $\frac{1}{8} \cdot \frac{1}{3} \approx 0.042$ . **DB**:  $\frac{1}{3 \cdot 1/2 + 5 \cdot 1} \cdot \frac{2}{1 \cdot 1/2 + 2 \cdot 1} \approx 0.077$ . **Db**:  $\frac{1}{3 \cdot 1/2 + 5 \cdot 1} \cdot \frac{1}{3} \approx 0.51$ . **dB**:  $\frac{1}{8} \cdot \frac{2}{1 \cdot 1/2 + 2 \cdot 1} \approx 0.062$ . **db**:  $\frac{1}{8} \cdot \frac{1}{3} \approx 0.042$ .

populations, in the weak selection regime, a lot of graphs have been shown to suppress selection [55,56]. Furthermore, under **Bd** updating, regular structures have the same fixation probability as the complete graph regardless of the mutant's fitness. To be specific, a graph where the total incoming weight to all the nodes are equal, then according to the 'isothermal theorem' [1,24] the graph has the same fixation probability as the complete graph.

Many studies are also dedicated to **dB** updating [15–17,22,45–47,49,57,58]. Contrary to **Bd**, under **dB** updating only a small fraction of undirected random graphs amplify selection while the majority of graphs suppresses selection [15]. The star graph is a suppressor of selection under the **dB** update mechanism [13,15]. Another popular update mechanism is **Db** which is equivalent to the voter model in statistical physics [26,42,50,59], but which is also used in biology [43]. In [22], it is shown that the evolutionary dynamics on a lattice under update mechanisms **Bd** and **Db** are equivalent when the selection parameter for death in the update mechanism **Db** equals the inverse of selection parameter for birth in the update mechanism **Bd**. However, it is illustrated that the dynamics on this lattice under update mechanisms **dB** and **bD** are fundamentally different.

Among the eight update mechanisms for graphs of individuals, **bd** and **db** are identical, describing a system where natural selection has no role in the evolution of the population [17,41]. For the update mechanisms **DB** and **BD**, selection acts both on death and birth [17,22,23], but they are not equivalent in general. Intuitively, one may expect that the fixation probability of an advantageous mutant is higher in the presence of update mechanisms **DB** and **BD** than in the other update mechanisms—but this is not always the case. The general transition probabilities for these eight update mechanisms are given in appendix A. In figure 1, the transition probabilities for a specific example are given for the eight update mechanisms.

In addition to the above update mechanisms, there are other update mechanisms in which, instead of two

individuals (one for birth, one for death), one edge is selected [27,42,44]. Then an individual dies at one end, the other gives birth, and the offspring fills the neighbouring empty spot. In this update mechanism, selection can act on death and/or birth events. Here, we will not consider this kind of update mechanism.

For more information about the comparison of different update mechanisms on various graphs with different features, we refer to the following references: in [44], the authors ask when the fixation probability in an evolutionary graph equals the fixation probability in a Moran process. A Moran process [60] is equivalent to the update mechanism **Bd** in a complete graph. In [28], the authors investigate the evolutionary game dynamics on the star graph in the presence of different update mechanisms. They show that the evolutionary dynamics of heterogeneous graphs is not robust under the choice of update mechanism. In [27], the effect of the directionality of a graph on its evolutionary dynamics for different update mechanisms is investigated. It has been shown that regardless of the update mechanism, the directionality always suppresses selection. In this manuscript, we extend the above update mechanisms to graphs of subpopulations where each node comprises a well-mixed subpopulation. The links indicate the migration between the patches (see figure 2).

### 3. Categorizing update mechanisms for graphs of subpopulations

In most of the potential applications of evolutionary graph theory, both in biology and in social dynamics, each node represents a population rather than an individual: individuals tend to interact locally in subpopulations, with some rare interactions with other groups of individuals. This is because the populations are segregated for various reasons, and they are geographically distant. Individuals in the same geographical area compete over resources or provide

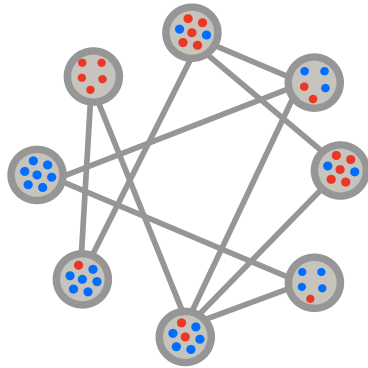


**Figure 2.** Graph of subpopulations. Each node in the graph includes a well-mixed subpopulation and each link indicates migration between two subpopulations.

common goods. However, there is an occasional migration to and from other geographical areas. In [6], it has been shown that for the **Bd** update mechanism, some results of evolutionary graph theory do not carry over into graphs of subpopulations. For example, a star-structured metapopulation does not always amplify selection—in some migration regimes, it suppresses selection. It will be interesting to see if this is the case for other update mechanisms.

In a model with fixed local population sizes, birth and death either happen in the same subpopulation, or the first event can be followed by an individual's migration to or from another subpopulation. Having this in mind, we can categorize update mechanisms into two groups:

- a set of update rules where there is always the possibility that the first event (birth or death) is accompanied by migration (figure 3*a,b*); and
- a set of updates where birth and death events are always in the same subpopulation and migration happens independently from birth and death, (see figure 3*a,c*).

We refer to the former category as update mechanisms with coupled migration and the latter as update mechanisms with uncoupled migration. The order of events (birth and death) in each of these classes and how selection acts upon them might affect the dynamics considerably. In both categories of update mechanisms, selection for the first event can act on both patch and individual levels, i.e. one first selects a patch and then an individual from the chosen patch. Selection on the second event can act both on the patch and individual levels in the update mechanisms with coupled migration. However, in the update mechanisms with uncoupled migration, selection in the second event always acts on the individual level since the second event must happen in the same patch as the first event.

We code the update mechanisms as follows: the first letter stands for migration to show if it is coupled (**M**) or uncoupled (**m**). The order of letters, except for the letter for migration, indicates the order of events. In addition, if selection is associated with selection parameters, we assign a capital letter and, otherwise, a lower-case letter. For uncoupled migration we need only three letters (the patch of the second event is fixed), for coupled migration we

need four letters (we can select the patch and the individual for the first and for the second event).

4

royalsocietypublishing.org/journal/rsif J. R. Soc. Interface 20: 20220769

### 3.1. Update mechanisms with coupled migration

In this class of update mechanisms, the first event is directly coupled with migration. The first event can be birth or death. If the birth occurs first, one of the patches is selected randomly proportional to the size of the patch (**b**) or randomly proportional to the sum of selection parameters of that patch for birth (**B**). Next, an individual from the patch is selected uniformly at random (**b**) or randomly proportional to its selection parameter for birth (**B**) to produce an identical offspring. The offspring can either stay and substitute one of the individuals in its patch (figure 3*a*) or migrate to one of the neighbouring patches and replace one of the individuals there (figure 3*b*).

If the offspring stays in its own patch, one of the individuals is chosen for death uniformly at random (**d**) or proportional to its selection parameter for death (**D**) (a common choice is the inverse of the selection parameter for birth). If the offspring migrates to a neighbouring patch, an individual in an adjacent patch is selected in two stages. First, among the neighbouring patches, one patch is selected randomly proportional to the size of the patch (**d**) or randomly proportional to the collective selection parameter for death of the patch (**D**). Finally, one of its individuals is selected for death uniformly at random (**d**) or randomly proportional to its selection parameter for death (**D**).

As an example, consider the update mechanism **MbBdd**. In this update mechanism,

- (i) First, a patch is selected uniformly at random.
- (ii) Then, from the random patch, one individual is selected with probability proportional to its selection parameter for birth to produce an offspring.
- (iii) Next, with a certain probability, the offspring will migrate to one of the adjacent patches or remain in its innate patch. In the former case, one of the neighbouring patches is selected uniformly at random as a function of its collective selection parameter for death.
- (iv) Finally, in the selected patch, which can be either an adjacent patch or the innate patch, one individual dies uniformly at random, and the offspring fills its empty spot.

In general, selection can be uniformly at random or proportional to a selection parameter in each step.

Based on such procedures, there are 16 different update mechanisms, with birth being the first event (see table 2). Similarly, if the first event is death, there are 16 different update mechanisms (see table 3). So far, only a few of these mechanisms have been studied in detail. For example, **MBBdd** is adopted in [5,6,61]. Not all of the observations made in graphs of individuals with the **Bd** update rule carry over to a graph of subpopulations when the update rule is **MBBdd** [6,61]. In fact, in the graph of subpopulations, the dynamics and, in particular, the fate of advantageous mutants are highly dependent on the pattern of migration, local population size and the graph structure itself. Also, applying **MddBB** in the graph of subpopulations reduces the chance of advantageous mutants compared with the equivalent well-mixed population with the update

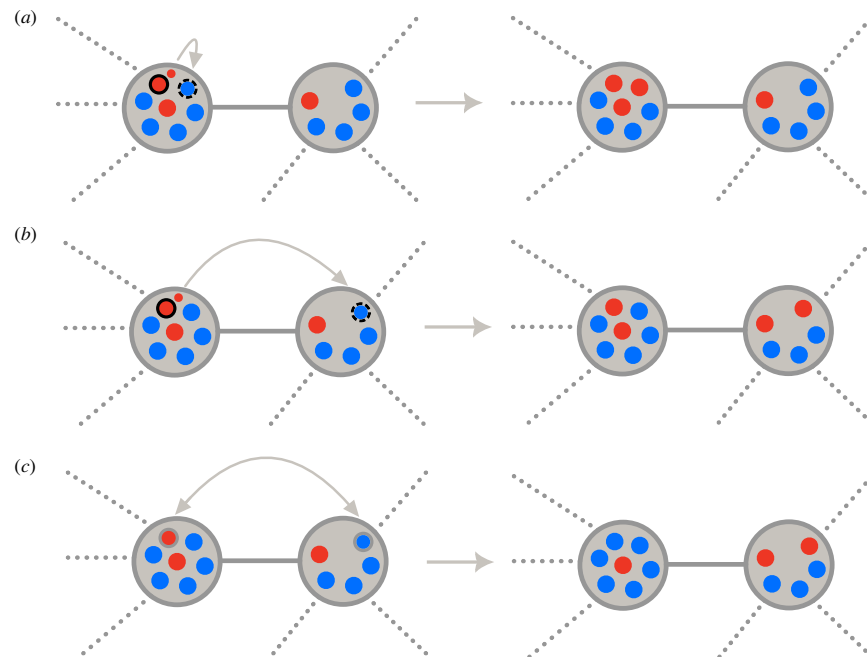


**Figure 3.** Update mechanisms in a graph-structured metapopulation. The population consists of two types of individuals, wild-types (blue) and mutants (red). The individual marked with the solid black circle gives birth and the individual marked with black dashed circle is selected for death. (a) Birth–death or death–birth in one patch without migration: this includes birth–death or death–birth in a coupled update mechanism without migration as well as an uncoupled update mechanism in which both death and birth happen in the same subpopulation. (b) A coupled update mechanism with migration: if birth is coupled with migration after each birth the newborn migrates to an adjacent patch and replaces one of its individual. If death is coupled to migration, a death in one patch is followed by birth of an individual in one of the adjacent patches where newborn occupies the place of dead individual. (c) Migration in an uncoupled update mechanism: migration happens independently from birth or death and it only exchanges the position of two individuals from different patches. This process is completely random.

mechanism **dB** [61]. Furthermore, employing **MddBB** in the star of islands in which many subpopulations are connected only via a central subpopulation, it is shown that it is the relative size of the local population in the leaves and the centre that determines whether the star of islands is an amplifier, reducer or transient amplifier of selection [16]. In general, in this class of update mechanisms, intuition suggests that the more selection is associated with the selection parameters, the more likely a beneficial mutant will spread through the population. However, in appendix D.1, we see that this is not true for the metastar in the low migration rate regime when birth is the first event.

### 3.2. Equivalence to weighted graphs of individuals

In the mechanisms with coupled migration, some update mechanisms reduce to simpler ones in a weighted graph of individuals, where the weights of the links that connect individuals in the same subpopulation are different from the weights of the links that connect individuals in different subpopulations (see figure 4). For instance, for the update rule **MDDBB**, first a patch is selected randomly proportional to its collective selection parameter for death. Afterwards, within the patch, an individual is chosen for death randomly proportional to its selection parameter for death. This is equivalent to selecting one individual from the whole population with a probability proportional to its selection parameter for death. Similarly, selection at birth both at the

patch and individual levels is equivalent to selecting an individual for birth proportional to its selection parameter for birth from the whole population (for more details see appendix C).

Hence, **MDDBB** on a graph-structured metapopulation can be treated as a **DB** on the equivalent graph of individuals with weighted links between individuals such that the weights of links that connect the individuals belonging to one patch differ from the ones that connect individuals from different patches. In fact, in the coupled update mechanisms, whenever selection on each of the birth and death events both on the patch level and individual level is either uniformly random or randomly proportional to selection parameters (**BB** or **bb** and **DD** or **dd**), the update mechanism reduces to an update mechanism in an equivalent graph of individuals, as mentioned in tables 2 and 3.

### 3.3. Update mechanisms with uncoupled migration

Migration is said to be uncoupled if birth and death events take place within a single patch (figure 3a), and individuals migrate independently such that the population size in each patch remains constant, independent of birth and death (figure 3c). In this scenario, we can model migration as follows: with a certain probability, two random individuals from two random connected patches exchange their positions. In this way, the local population size will remain constant.

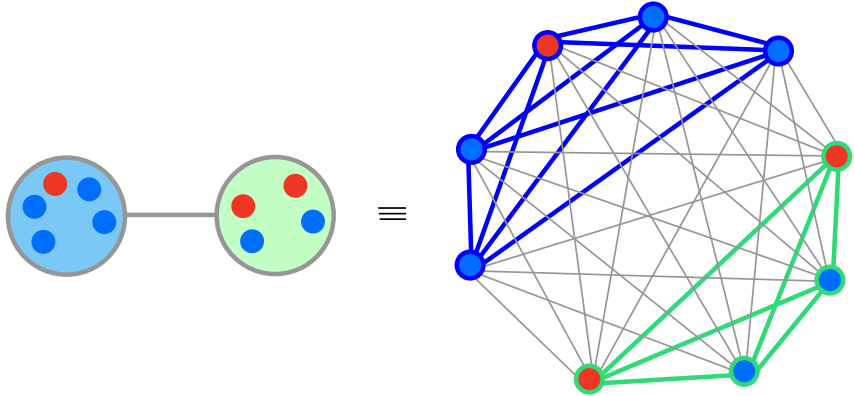


**Figure 4.** Equivalence of an update mechanism in a graph of subpopulation to an update mechanism in a graph of individuals. In a coupled update mechanism whenever selection on each of the birth and death events both on the patch and individual levels is either uniformly random or randomly proportional to selection parameters, the update mechanism is equivalent to an update mechanism in an associated weighted graph of individuals. In this weighted graph, the weights of the links that connect local individuals are different from the weights of the links that connect individuals in neighbouring subpopulations and depend on the migration probability as well as local population sizes.

**Table 2.** Birth–death processes with migration coupled to reproduction. In all these update mechanisms in graph-structured metapopulations, the individual producing offspring is identified first and the individual to be removed afterwards. In both steps, we can select for the patch and for the individual separately, leading to 16 such update mechanisms. As an example, the evolutionary dynamics on the metastar under this category of update mechanisms is investigated in appendix D.

update mechanism	comments	references
MBBDD	equivalent to <b>BD</b> in a graph of individuals	—
MBBDd	—	—
MBBdD	—	—
MBBdd	equivalent to <b>Bd</b> in a graph of individuals	[5,6,61]
MbBDD	—	—
MbBDd	—	—
MbBdD	—	—
MbBdd	—	[5]
MbBDD	—	—
MbBDd	—	—
MbBdD	—	—
MbBdd	—	—
MbbDD	equivalent to <b>bd</b> in a graph of individuals	—
MbbDd	—	—
MbbdD	—	—
Mbbdd	equivalent to a completely neutral model	—

The first event can be birth or death. If birth happens first, one of the patches is selected uniformly at random (**b**) or randomly proportional to its selection parameter for birth (**B**).

**Table 3.** Death–birth processes with migration coupled to death. In all these update mechanisms in graph-structured metapopulations, the individual being removed is identified first and the individual producing offspring afterwards. Again, there are 16 such update mechanisms. As an example, the evolutionary dynamics on the metastar under this category of update mechanisms is investigated in appendix D.

update mechanism	comments	references
MDDBB	equivalent to <b>DB</b> in a graph of individuals	—
MDDBb	—	—
MDDbB	—	—
MDDbb	equivalent to <b>Db</b> in a graph of individuals	—
MdDBB	—	—
MdDBb	—	—
MdBbB	—	—
MdDbb	—	—
MdDBB	—	—
MdDBb	—	—
MdBbB	—	—
MdDbb	—	—
MddBB	equivalent to <b>dB</b> in a graph of individuals	[16,61]
MddBb	—	—
MddbB	—	—
Mddbb	equivalent to a completely neutral model	—

From the chosen patch, one individual is selected for birth uniformly at random (**b**) or randomly proportional to its selection parameter for birth (**B**) and produces an identical offspring.

Once an individual is selected for birth, one individual is selected for death uniformly at random (**d**) or randomly proportional to its selection parameter for death (**D**) from the same patch. The new offspring replaces the empty spot of the dead individual. Since there is no patch selection for the second event, the second event is indicated by a single letter.

In this category, there are eight different update mechanisms. As an example, let us consider **mbbD**. At each time step, with the migration probability,  $\lambda$ , a migration happens, and with the probability,  $1 - \lambda$ , the population gets updated through the birth–death process. The birth–death process is as follows,

- (i) First, a patch is selected uniformly at random (**b**).
- (ii) From this patch, an individual is selected with probability proportional to its selection parameter for birth to reproduce (**B**).
- (iii) After that, one of the individuals from the same patch is chosen randomly with probability proportional to its selection parameter for death to die (**D**) and the offspring will fill the empty spot.

Similarly, when death happens first, there are eight other update mechanisms. In the update mechanisms **mbbd** and **mddb**, where selection is not active in either of the events, the update mechanism is identical to the neutral model, i.e. **bd**.

In many popular models of the population genetics literature, migration is assumed to be independent from birth and death [7,9,11,62–65]. However, most of these studies use the Wright–Fisher model as the local update mechanism and thus are not captured by our metapopulation framework of evolutionary graph theory.

## 4. Discussion

Evolutionary graph theory is a mathematical framework that has been used to think of the role of population structure in evolutionary dynamics. More recently, empirical scientists have become interested in this framework, but in most of the systems in their focus, the nodes are subpopulations and not individuals. Here, we have classified different classes of update mechanisms on such graph-structured metapopulations. We focus on update mechanisms that are natural extensions of the update mechanisms typically used in evolutionary graph theory for graphs of individuals.

Our classification is based on three factors:

- (i) first, if migration is coupled to reproduction or not;
- (ii) second, the order of birth and death events; and
- (iii) third, how selection acts on the growth and survival of the population.

Each of these update mechanisms can result in different dynamics—using different update mechanisms can affect not only the fixation probability and fixation time of newly arising mutations but also other features of the dynamics.

The fixation probability in graphs of individuals under **Bd** (where selection for birth is proportional to a selection parameter) and **Db** (where selection for death is proportional to the inverse of the selection parameter for birth) are equivalent in undirected regular graphs [42] and they both follow the isothermal theorem [1]. For more details, see appendix A.2. In addition, in a fully connected graph of individuals,

where all individuals are equivalent, and every node in the graph includes a self-loop, meaning that the individual selected for birth can die or the individual selected for death can give birth, **Bd** is equivalent to **dB**, **bD** is equivalent to **Db** and **BD** is equivalent to **DB**. It is worth mentioning that in an update mechanism where death is followed by birth, having self-loops in the graphs makes only limited sense if we think of the actual physical death of individuals. However, it is sensible if we think of it in the social setting where death and birth are interpreted as imitating one's idea or sticking to your own [15]. Furthermore, in a fully connected graph including self-loops, if the selection parameter for death equals the inverse of the selection parameter for birth, then the fixation probabilities in the update mechanisms **Bd**, **dB**, **bD** and **Db** and are the same as the fixation probability of the well-mixed population under the update mechanism **Bd** [44]. However, in this condition, the fixation probability of a beneficial mutant in an arbitrary graph under **BD** and **DB** is higher than the respective fixation probability in the corresponding well-mixed population under **Bd**.

In a system where individuals with a higher selection parameter for birth have a lower selection parameter for death, the more the birth and death are associated with these selection parameters, the higher the probability for advantageous individuals to take over the population. This implies that the fixation probability of a beneficial mutant under **BD** is higher than the corresponding fixation probability under **Bd** and **bD**. Also the fixation probability of a beneficial mutant under **DB** is higher than the corresponding fixation probability under **Db** and **dB**. In addition, the fixation probability of a beneficial mutant in an arbitrary graph under an update mechanism in which selection is global is more than or equal to its fixation probability under an update mechanism in which selection is local [17]. Equality holds for a well-mixed population which includes self-loops meaning that every individual can also replace itself.

In a graph of subpopulations with update mechanisms where migration is coupled with death or birth, the fixation probability of an advantageous mutant in an arbitrary graph is higher under some update mechanisms compared with others. In appendix B, we consider two update mechanisms that are exactly the same except that the individual selection for birth or death in one is uniformly random and in the other is random proportional to selection parameters. The fixation probability of an advantageous mutant for selection proportional to selection parameters is higher than the fixation probability where selection is uniformly at random. For example, the update mechanism **MBBDD** has a higher fixation probability for advantageous mutants than **MBbDD**. In addition, one intuitively expects that if selection on the patch level is associated with a collective selection parameter, the beneficial mutant has a higher chance of being fixed. Nevertheless, it is not straightforward to prove this. In appendix B, we show this in more detail.

Similarly, as it is shown in appendix B, for the update mechanisms with uncoupled migration, if we have two update mechanisms that are only different in individual selection on birth or death, the fixation probability of an advantageous mutant under the update mechanism in which individual selection is uniformly random is smaller than the corresponding fixation probability under the update mechanism in which individual selection is associated

with selection parameters. For instance, the fixation probability of an advantageous mutant under **mBBD** is higher than the corresponding fixation probability under **mBBd** in an arbitrary graph.

In addition, it is interesting to see under which of the coupled or uncoupled update mechanisms the beneficial mutant has a higher chance of taking over the whole population. Intuitively, under the coupled update mechanism, migration helps to spread beneficial mutants, whereas under uncoupled migration, exchanges of the individual between the patches occur uniformly at random and independent of the selection parameters.

In appendix D, we investigate the fixation probability for the star-structured metapopulation (metastar) under update mechanisms with coupled migration. The analysis is done in the low migration rate regime where every node (subpopulation) is in a homogeneous state at the time of migration. In the low migration rate regime, selection on the individual level plays an important role, whereas selection on the patch level changes the fixation probability only slightly. This leads to grouping of the update mechanisms into three classes based on the fixation probability of an advantageous mutant: update mechanisms in which both birth and death on the individual level are associated with the selection parameters, update mechanisms in which either birth or death on the individual level is associated with the selection parameter, and update mechanisms in which neither birth and nor death on the individual level are associated with the selection parameters.

Various update mechanisms have been applied to study biological, ecological and social systems. It has been argued that death–birth processes can be applied to study the evolutionary dynamics of trees in a tropical forest: a new seed grows into an adult tree when one of the trees in the forest dies [66]. Here, death happens first. Similarly, birth–death processes have been employed in cancer evolution [67,68]. Cancer cells grow excessively, and since they exhaust the nutrients and resources, the healthy cells die due to the lack of resources and leave empty spaces for the cancer cells to grow further. The evolutionary dynamics of the cancer cells arising in the crypts of the inner lining of the intestine can be modelled by a birth–death process in a line structure [69,70]. In this case, birth triggers death.

In a graph of subpopulations, coupled migration could denote the natural tendency of the species to look for a better place to live. Uncoupled migration can describe dispersal caused by humans or abiotic factors such as wind or water streams. The selection pressure on the patch level makes sense when patches share common and limited resources but still are partly isolated.

We hope that this paper paves the way for future work on the evolutionary dynamics of graph-structured metapopulations. Here, we only classify possible update mechanisms on metapopulations and only partly analyse some of them. However, the update mechanism is a crucial ingredient of evolutionary graph theory, and a better understanding of how it affects evolutionary dynamics in structured metapopulations will be necessary to move the field forward.

**Data accessibility.** This article has no additional data.

**Authors' contributions.** S.Y.: conceptualization, formal analysis, investigation, validation, visualization, writing—original draft; N.S.: validation, visualization, writing—review and editing; A.T.: conceptualization, funding acquisition, supervision, validation, writing—review and editing.

All authors gave final approval for publication and agreed to be held accountable for the work performed therein.

**Conflict of interest declaration.** We declare we have no competing interests.

**Funding.** No funding has been received for this article.

## Appendix A. Evolutionary dynamics on graphs of individuals

Assume a connected graph of individuals where  $w_{ij}$  is the weight of the link connecting node  $i$  to  $j$ . The population consists of two types, wild-type A and mutant B. The variable  $s_i$  indicates the status of node  $i$ ,  $s_i = 0$  if it is occupied by a wild-type, and  $s_i = 1$  if it is occupied by a mutant. The selection parameter for the birth of the mutant with respect to the wild-type is  $r$ , and the selection parameter for the death of the mutant with respect to the wild-type is  $t$ . In the following section, we explain the transition probabilities for both birth–death and death–birth processes on graphs of individuals.

### A.1. Transition probabilities

In an update mechanism where birth is global and death is local, one individual is selected for birth, and then one of its neighbours is chosen for death. The offspring will replace the empty spot. Based on this model, there are two possible transitions: increasing and decreasing the number of mutants by one. The probability  $T_{\text{birth-death}}^{n+}$  of increasing the number of mutants,  $n = \sum_i s_i$ , by one is

$$T_{\text{birth-death}}^{n+} = \sum_i \underbrace{\frac{rs_i}{r \sum_k s_k + \sum_k (1 - s_k)}}_{\text{birth}} \underbrace{\frac{\sum_j w_{ij}(1 - s_j)}{t \sum_l w_{il}s_l + \sum_l w_{il}(1 - s_l)}}_{\text{death}}. \quad (\text{A.1})$$

This equation is the summation over all the possibilities that the number of mutants increases. The probability  $T_{\text{birth-death}}^{n-}$  of decreasing the number of mutants  $n$  by one is

$$T_{\text{birth-death}}^{n-} = \sum_i \underbrace{\frac{1 - s_i}{r \sum_k s_k + \sum_k (1 - s_k)}}_{\text{birth}} \underbrace{\frac{t \sum_j w_{ij}s_j}{t \sum_l w_{il}s_l + \sum_l w_{il}(1 - s_l)}}_{\text{death}}. \quad (\text{A.2})$$

When death is global and birth is local, an individual is selected for death, and then from its neighbour, one individual is selected for birth. In this case the transition probabilities are

$$T_{\text{death-birth}}^{n+} = \sum_i \underbrace{\frac{1 - s_i}{t \sum_k s_k + \sum_k (1 - s_k)}}_{\text{death}} \underbrace{\frac{r \sum_j w_{ij}s_j}{r \sum_l w_{il}s_l + \sum_l w_{il}(1 - s_l)}}_{\text{birth}} \quad (\text{A.3})$$

and

$$T_{\text{death-birth}}^{n-} = \sum_i \underbrace{\frac{ts_i}{t \sum_k s_k + \sum_k (1 - s_k)}}_{\text{death}} \underbrace{\frac{\sum_j w_{ij}(1 - s_j)}{r \sum_l w_{il}s_l + \sum_l w_{il}(1 - s_l)}}_{\text{birth}}. \quad (\text{A.4})$$

Based on the values of  $r$  and  $t$ , the update mechanisms can be categorized as follows:



- (i) In the above equations if  $r \neq 1$  and  $t \neq 1$  there are selection pressures both on the birth and the death. This corresponds to the update mechanism **Bd** in which birth is global and death is local, and the update mechanism **Db** in which death is global and death is local.
- (ii) If  $r \neq 1$  and  $t = 1$  birth–death corresponds to update mechanism **Bd** and death–birth corresponds to **dB**.
- (iii) If  $r = 1$  and  $t \neq 1$ , birth–death correspond to **bD** and death–birth correspond to **Db**.
- (iv) If  $r = 1$  and  $t = 1$  birth–death corresponds to **bd** and death–birth corresponds to **db**.

## A.2. Equivalence of **Bd** and **Db** in undirected regular graphs

Generalizing the transition probabilities from appendix A.1, to an arbitrary weighted graph with weights  $w_{ij}$  under the update mechanisms **Bd** leads to

$$T_{\text{Bd}}^{n+} = \sum_i \frac{r s_i}{r \sum_k s_k + \sum_k (1 - s_k)} \frac{\sum_j w_{ij} (1 - s_j)}{\sum_l w_{il}} \quad (\text{A.5})$$

and

$$T_{\text{Bd}}^{n-} = \sum_i \frac{1 - s_i}{r \sum_k s_k + \sum_k (1 - s_k)} \frac{\sum_j w_{ij} s_j}{\sum_l w_{il}}. \quad (\text{A.6})$$

The transition probabilities of an arbitrary graph under the update mechanisms **Db** are

$$T_{\text{Db}}^{n+} = \sum_i \frac{1 - s_i}{t \sum_k s_k + \sum_k (1 - s_k)} \frac{\sum_j w_{ij} s_j}{\sum_l w_{il}} \quad (\text{A.7})$$

and

$$T_{\text{Db}}^{n-} = \sum_i \frac{t s_i}{t \sum_k s_k + \sum_k (1 - s_k)} \frac{\sum_j w_{ij} (1 - s_j)}{\sum_l w_{il}}. \quad (\text{A.8})$$

In a regular graph,  $\sum_l w_{il}$  is identical for all the nodes. Thus we can set it as  $\sum_l w_{il} = \alpha$ . As a result, the transition probabilities for update mechanism **Bd** are simplified to

$$T_{\text{Bd}}^{n+} = \frac{r}{\alpha(rn + N - n)} \sum_{i,j} w_{ij} s_i (1 - s_j) \quad (\text{A.9})$$

and

$$T_{\text{Bd}}^{n-} = \frac{1}{\alpha(rn + N - n)} \sum_{i,j} w_{ij} (1 - s_i) s_j. \quad (\text{A.10})$$

Since in the regular graphs  $w_{ij} = w_{ji}$ , therefore,  $\sum_{i,j} w_{ij} (1 - s_i) s_j = \sum_{i,j} w_{ij} (1 - s_j) s_i$  and consequently  $T_{\text{Bd}}^{n-}/T_{\text{Bd}}^{n+} = 1/r$  is independent of the  $s_i$ . As a result the fixation probability is  $\phi^{(n)} = \frac{1 - 1/r^n}{1 - 1/r^N}$ .

Similarly, the transition probabilities for the update mechanism **Db** simplify to

$$T_{\text{Db}}^{n+} = \frac{1}{\alpha(rn + N - n)} \sum_{i,j} w_{ij} (1 - s_i) s_j \quad (\text{A.11})$$

**Table 4.** Parameters for a graph of subpopulations.

parameter	description
$N_i$	population size in patch $i$
$n_i$	number of mutants in patch $i$
$n$	total number of mutants, $\sum_i n_i$
$N$	total population size, $\sum_i N_i$
$r$	selection parameter for birth of the mutant
$t$	selection parameter for death of the mutant
$\lambda$	migration probability
$w_{ij}$	weight of the link from patch $i$ to patch $j$

and

$$T_{\text{Db}}^{n-} = \frac{t}{\alpha(rn + N - n)} \sum_{i,j} w_{ij} s_i (1 - s_j). \quad (\text{A.12})$$

Since  $T_{\text{Db}}^{n-}/T_{\text{Db}}^{n+} = t$ , the fixation probability is  $\phi^{(n)} = \frac{1 - t^n}{1 - t^N}$ ; cf. equation (2.3). If we set  $t = 1/r$  the fixation probability is the same as the fixation probability of the equivalent well-mixed population under the update mechanism **Bd**.

## Appendix B. Evolutionary dynamics on graphs of subpopulations

This appendix discusses why some update mechanisms fix beneficial mutants with higher probability. Assume that we have two types of individuals, mutants and wild-types. The transition probabilities of increasing and decreasing the total number of mutants  $n$  are given by  $T^{n+}$  and  $T^{n-}$ , respectively. We use a mean-field approximation and assume that the transition probabilities are the summation of the transition probabilities for all the possible configurations for a specific number of mutants  $n$ . The other parameters are described in table 4.

If we start with a single randomly placed mutant in a wild-type population, the fixation probability of the mutant is given by [24]

$$\phi^{(1)} = \frac{1}{1 + \sum_{i=1}^{N-1} \prod_{j=1}^i (T^j - / T^{j+})}. \quad (\text{B.1})$$

Therefore, in order to investigate how the fixation probabilities in different update rules vary, it is sufficient to compare the transition probabilities.

### B.1. Comparison of update mechanism with or without individual-level selection

By comparing the transition probabilities, we can see that for both coupled and uncoupled update mechanisms, if two update mechanisms only differ in individual-level selection for either birth or death, the fixation probability of the beneficial mutant under the update mechanism in which individual selection is associated with selection parameter is higher than the one in which individual selection is uniformly random. Here, we compare the transition probabilities of update mechanisms **MBDD**, **MBbDD**, **MBDD**. The transition probabilities of increasing and decreasing the total

number of mutants,  $n = \sum_i n_i$  update mechanism **MBDD** are

$$T_{\text{MBDD}}^{n+} = \sum_i \underbrace{\frac{rn_i + N_i - n_i}{rn + N - n}}_{\text{birth patch}} \underbrace{\frac{rn_i}{rn_i + N_i - n_i}}_{\text{birth of individual}} \times \left( \lambda \sum_j w_{ij} \underbrace{\frac{tn_j + N_j - n_j}{\sum_k w_{ik}(tn_k + N_k - n_k)}}_{\text{choosing a patch to migrate to}} \underbrace{\frac{N_j - n_j}{tn_j + N_j - n_j}}_{\text{death of individual}} + (1 - \lambda) \underbrace{\frac{N_i - n_i}{tn_i + N_i - n_i}}_{\text{death of individual in parental patch}} \right) \quad (\text{B.2})$$

and

$$T_{\text{MBDD}}^{n-} = \sum_i \underbrace{\frac{rn_i + N_i - n_i}{rn + N - n}}_{\text{selection patch birth}} \underbrace{\frac{N_i - n_i}{rn_i + N_i - n_i}}_{\text{birth of individual}} \times \left( \lambda \sum_j w_{ij} \underbrace{\frac{tn_j + N_j - n_j}{\sum_k w_{ik}(tn_k + N_k - n_k)}}_{\text{choosing a patch to migrate to}} \underbrace{\frac{tn_j}{tn_j + N_j - n_j}}_{\text{death of individual}} + (1 - \lambda) \underbrace{\frac{tn_i}{tn_i + N_i - n_i}}_{\text{death of individual in parental patch}} \right). \quad (\text{B.3})$$

The transition probabilities for the update mechanism **MBbDD** are

$$T_{\text{MBbDD}}^{n+} = \sum_i \frac{rn_i + N_i - n_i}{rn + N - n} \frac{n_i}{N_i} \times \left( \lambda \sum_j w_{ij} \frac{tn_j + N_j - n_j}{\sum_k w_{ik}(tn_k + N_k - n_k)} \frac{N_j - n_j}{tn_j + N_j - n_j} + (1 - \lambda) \frac{N_i - n_i}{tn_i + N_i - n_i} \right) \quad (\text{B.4})$$

and

$$T_{\text{MBbDD}}^{n-} = \sum_i \frac{rn_i + N_i - n_i}{rn + N - n} \frac{N_i - n_i}{N_i} \times \left( \lambda \sum_j w_{ij} \frac{tn_j + N_j - n_j}{\sum_k w_{ik}(tn_k + N_k - n_k)} \frac{tn_j}{tn_j + N_j - n_j} + (1 - \lambda) \frac{tn_i}{tn_i + N_i - n_i} \right). \quad (\text{B.5})$$

The transition probabilities for the update mechanism **MBBDd** are

$$T_{\text{MBBDd}}^{n+} = \sum_i \frac{rn_i + N_i - n_i}{rn + N - n} \frac{rn_i}{rn_i + N_i - n_i} \times \left( \lambda \sum_j w_{ij} \frac{tn_j + N_j - n_j}{\sum_k w_{ik}(tn_k + N_k - n_k)} \frac{N_j - n_j}{N_j} + (1 - \lambda) \frac{N_i - n_i}{N_i} \right) \quad (\text{B.6})$$

and

$$T_{\text{MBBDd}}^{n-} = \sum_i \frac{rn_i + N_i - n_i}{rn + N - n} \frac{N_i - n_i}{rn_i + N_i - n_i} \times \left( \lambda \sum_j w_{ij} \frac{tn_j + N_j - n_j}{\sum_k w_{ik}(tn_k + N_k - n_k)} \frac{n_j}{N_j} + (1 - \lambda) \frac{n_i}{N_i} \right). \quad (\text{B.7})$$

Comparing equations (B.2) and (B.4), all the terms are the same except the second term which is the probability of choosing a mutant in patch  $i$  for birth. Since

$$\frac{rn_i}{rn_i + N_i - n_i} > \frac{n_i}{N_i}, \quad (\text{B.8})$$

for beneficial mutants,  $r > 1$  (except for  $n_i = N_i$  and  $n_i = 0$ , where the transition probabilities are zero) that implies

$$T_{\text{MBDD}}^{n+} > T_{\text{MBbDD}}^{n+}. \quad (\text{B.9})$$

Also if we compare equations (B.3) and (B.5) since

$$\frac{N_i - n_i}{rn_i + N_i - n_i} < \frac{N_i - n_i}{N_i}, \quad (\text{B.10})$$

for beneficial mutants,  $r > 1$  (except for  $n_i = N_i$  and  $n_i = 0$ , where the transition probabilities are zero). Thus, we find

$$T_{\text{MBDD}}^{n-} < T_{\text{MBbDD}}^{n-}. \quad (\text{B.11})$$

As a result,

$$\frac{T_{\text{MBDD}}^{n-}}{T_{\text{MBDD}}^{n+}} < \frac{T_{\text{MBbDD}}^{n-}}{T_{\text{MBbDD}}^{n+}} \quad \text{for all } 1 < n < N - 1. \quad (\text{B.12})$$

The ratio  $T^{n-}/T^{n+}$  appears in the denominator of equation (B.1). This implies that the fixation probability of an advantageous mutant under **MBDD** is higher than the corresponding fixation probability under **MBbDD** for an arbitrary graph,  $\phi_{\text{MBDD}} > \phi_{\text{MBbDD}}$ . Similarly, we can show that the fixation probability of a deleterious mutant under **MBDD** is lower than the corresponding fixation probability under **MBbDD** for an arbitrary graph,  $\phi_{\text{MBDD}} < \phi_{\text{MBbDD}}$ .

In addition, comparing equations (B.2) and (B.6), since

$$\frac{N_j - n_j}{tn_j + N_j - n_j} > \frac{N_j - n_j}{N_j}, \quad (\text{B.13})$$

for beneficial mutants,  $t < 1$ , we have

$$T_{\text{MBDD}}^{n+} > T_{\text{MBBDd}}^{n+}. \quad (\text{B.14})$$

Also by comparing equations (B.3) and (B.7), we have

$$T_{\text{MBDD}}^{n-} < T_{\text{MBBDd}}^{n-} \quad (\text{B.15})$$

because

$$\frac{dn_j}{dn_j + N_j - n_j} < \frac{n_j}{N_j}, \quad (\text{B.16})$$

for all  $1 < n_j < N_j - 1$  and for  $n_j = N_j$  both sides are equal. In conclusion, the fixation probability of an advantageous mutant in an arbitrary graph under **MBBDd** is smaller than the corresponding fixation probability under **MBDD**. On the other hand, for deleterious mutants,  $\phi_{\text{MBBDd}} > \phi_{\text{MBDD}}$ .

We can show in a similar way as above that for beneficial mutants that the fixation probability,  $\phi$  of an arbitrary graph under update mechanism **MBDD**, **MBbDD** and **MBbDd** have the following relationship with each other:

$$\phi_{\text{MBDD}} > \phi_{\text{MBbDD}} > \phi_{\text{MBbDd}}, \quad (\text{B.17})$$

and similarly the relation between the fixation probability of a deleterious mutant for an arbitrary graph under update mechanisms **MBDD**, **MBBDd** and **MBbDd** is

$$\phi_{\text{MBbDD}} > \phi_{\text{MBBDd}} > \phi_{\text{MBbDd}}. \quad (\text{B.18})$$

In the above expressions, one cannot simply state which of



the  $\phi_{\text{MBbDd}}$  and  $\phi_{\text{MBbDD}}$  is higher. The relation between these two values might be dependent on the graph structure.

On the other hand, the relation between the fixation probabilities,  $\phi$ , of a deleterious mutant in an arbitrary graph under the update mechanisms, **MBBDD**, **MBbDD** and **MBbDd** is

$$\phi_{\text{MBBDD}} < \phi_{\text{MBbDD}} < \phi_{\text{MBbDd}}, \quad (\text{B.19})$$

and similarly, we can simply show that the fixation probabilities of a deleterious mutant in an arbitrary graph under the update mechanisms **MBBDD**, **MBbDd** and **MBbDD** has the following relationship:

$$\phi_{\text{MBBDD}} < \phi_{\text{MBbDd}} < \phi_{\text{MBbDD}}. \quad (\text{B.20})$$

As we see from these equations, for an arbitrary graph, if an update mechanism is more associated with selection parameters, the fixation probability of advantageous mutants increases and the fixation probability of deleterious mutants decreases.

## B.2. Comparison of update mechanism with or without patch level selection

Comparing the transition probabilities of a beneficial mutant under two update mechanisms that only differ in patch level selection for either birth or death is not as straightforward. Intuitively we expect that the update mechanism in which patch level selection is associated with the collective selection parameter of the patch has a higher fixation probability. In the following, we show why one cannot easily infer from the transition probabilities which one is higher. Let us compare the transition probabilities for increasing the mutant population size by one under the update mechanisms **MBBDD** and **MbBDD**.

$$T_{\text{MbBDD}}^{n+} = \sum_i \underbrace{\frac{N_i}{N}}_{\text{birth patch}} \underbrace{\frac{r_{m_i}}{r_{m_i} + N_i - n_i}}_{\text{birth of individual}} \times \left( \underbrace{\lambda \sum_j w_{ij} \frac{tn_j + N_j - n_i}{\sum_k w_{ik}(tn_k + N_k - n_k)}}_{\text{choosing a patch to migrate to}} \underbrace{\frac{N_j - n_i}{tn_j + N_j - n_i}}_{\text{death of individual}} + (1 - \lambda) \underbrace{\frac{N_i - n_i}{tn_i + N_i - n_i}}_{\text{death of individual in parental patch}} \right) \quad (\text{B.21})$$

Comparing the equations (B.2) and (B.21), the only difference is the term for the birth patch.  $T_{\text{MBBDD}}^{n+} > T_{\text{MbBDD}}^{n+}$  if for all  $i$  values

$$\frac{r_{m_i} + N_i - n_i}{r_{m_i} + N - n} \geq \frac{N_i}{N}. \quad (\text{B.22})$$

The above relation holds if and only if

$$\frac{n_i}{N_i} \geq \frac{n}{N}. \quad (\text{B.23})$$

However, the above relation does not always hold, and it depends on the configuration of the population. Hence, it is not easy to compare equations (B.2) and (B.21).

## B.3. Comparison of update mechanism with uncoupled migration

Similarly, by comparing the transition probabilities for uncoupled update mechanisms, we can see that the fixation probability of an advantageous mutant under update mechanisms in which individual selection is associated

with selection parameters is higher than the corresponding fixation probability under update mechanisms in which individual selection is independent of selection parameters. The transition probabilities of this update mechanism only include the non-migrative terms because the migrative term does not change the number of mutants in the whole population. The transition probabilities for the update mechanism **mBBD** are

$$T_{\text{mBBD}}^{n+} = (1 - \lambda) \times \sum_i \frac{r_{m_i} + N_i - n_i}{r_{m_i} + N - n} \frac{r_{m_i}}{r_{m_i} + N_i - n_i} \frac{N_i - n_i}{tn_i + N_i - n_i} \quad (\text{B.24})$$

and

$$T_{\text{mBBD}}^{n-} = (1 - \lambda) \times \sum_i \frac{r_{m_i} + N_i - n_i}{r_{m_i} + N - n} \frac{N_i - n_i}{r_{m_i} + N_i - n_i} \frac{tn_i}{tn_i + N_i - n_i}, \quad (\text{B.25})$$

and the transition probabilities for the update mechanism **mBBd** are

$$T_{\text{mBBd}}^{n+} = (1 - \lambda) \times \sum_i \frac{r_{m_i} + N_i - n_i}{r_{m_i} + N - n} \frac{r_{m_i}}{r_{m_i} + N_i - n_i} \frac{N_i - n_i}{N_i} \quad (\text{B.26})$$

and

$$T_{\text{mBBd}}^{n-} = (1 - \lambda) \sum_i \frac{r_{m_i} + N_i - n_i}{r_{m_i} + N - n} \frac{N_i - n_i}{r_{m_i} + N_i - n_i} \frac{n_i}{N_i}. \quad (\text{B.27})$$

From equations (B.24) and (B.26), we can see that for beneficial mutants,  $t < 1$ ,

$$T_{\text{mBBD}}^{n+} > T_{\text{mBBd}}^{n+}, \quad (\text{B.28})$$

because for  $1 < n_i < N_i$  we have

$$\frac{N_i - n_i}{dn_i + N_i - n_i} > \frac{N_i - n_i}{N_i}. \quad (\text{B.29})$$

Analogously, for the beneficial mutants we have

$$T_{\text{mBBD}}^{n-} < T_{\text{mBBd}}^{n-}. \quad (\text{B.30})$$

Thus, the fixation probability of an advantageous mutant under **mBBD** is higher than the corresponding fixation probability under **mBBd**,  $\phi_{\text{mBBD}} > \phi_{\text{mBBd}}$ . Similarly we can see that for a beneficial mutant

$$\phi_{\text{mBbd}} < \phi_{\text{mBbd}} < \phi_{\text{mBBD}}. \quad (\text{B.31})$$

On the other hand, for the deleterious mutants we have an opposite relation between the fixation probabilities:

$$\phi_{\text{mBbd}} > \phi_{\text{mBbd}} > \phi_{\text{mBBD}}. \quad (\text{B.32})$$

## Appendix C. Equivalence of evolutionary dynamics on graphs of subpopulations and graphs of individuals

In the mechanisms with coupled migration, some update mechanisms reduce to simpler ones in a weighted graph of individuals, where the weights of the links that connect

individuals locally are different from the weights of the links that connect individuals in adjacent subpopulations (see figure 4).

In order for an update mechanism to reduce to a simpler update mechanism, selection for birth and death should be either associated with selection parameter or not for both patch and individual levels. As an example **MBBdd** reduces to **Bd**. This can be easily shown by transition probabilities; in order to increase the number of mutants by one through selecting one mutant from the patch  $i$  consists of two parts; first selecting a mutant from patch  $i$  with probability

$$\frac{m_i + N_i - n_i}{m + N - n} \frac{r}{m_i + N_i - n_i}. \quad (\text{C.1})$$

This probability is simplified to  $r/(rn + N - n)$ , which is equivalent to the probability of selecting one mutant from the whole population regardless of the collective selection parameter of the patches. The second part is choosing one of the wild-type neighbours of the selected mutant for death. The neighbour could be either selected from the parental patch with probability

$$(1 - \lambda) \frac{N_i - n_i}{N_i}, \quad (\text{C.2})$$

or from the neighbouring patches with probability

$$\lambda \sum_j w_{ij} \frac{N_j - n_j}{\sum_k w_{ik} N_k}. \quad (\text{C.3})$$

The above two equations for the death probability of a wild-type imply that a graph of patches can be reduced to a graph of individuals. In the equivalent graph of individuals the weight of the link between each two individuals within the patch  $i$  is  $(1 - \lambda)/N_i$  if we take into account self-loops, and the weight of the link from an individual from patch  $i$  to an individual from patch  $j$  is  $\lambda w_{ij}/\sum_k w_{ik} N_k$ . Therefore, the update mechanism **MBBdd** on a graph of subpopulations is equivalent to the update mechanism **Bd** on a graph of individuals in which the weight of the links that connect local individuals differ from the weight of links that connect individuals in different patches. The weight of the links depends on the migration probability as well as the local population sizes.

## Appendix D. Evolutionary dynamics on the metastar

In this appendix, we calculate the fixation probability for the metastar in the low migration rate regime. A metastar is a star graph where every node is occupied by a subpopulation. The internal structure of each subpopulation is well mixed. These subpopulations are connected to each other through the central node. We denote the total population size by  $N$  and assume it is distributed evenly into  $M$  patches, so that the size of each patch is  $N_1 = N/M$ .

When the migration probability is sufficiently low, and the population sizes of the patches are comparable, the individual migrating to a neighbouring patch either reaches fixation or goes extinct in that respective patch before the next migration event occurs. Therefore, the subpopulations are in a homogeneous configuration at the time of a migration event. By homogeneous configuration, we mean that each

patch is either occupied by the mutant type or the wild-type individuals. In the low migration rate regime, to calculate the fixation probability, instead of considering the transition probabilities between  $2^N$  states, the state space is reduced to  $2^M$ . The transition probabilities between these  $2^M$  states are sufficient to compute fixation probabilities. As a result, we can look at the problem as if we have a graph of individuals. However, the probability of replacing a node with the offspring of a neighbouring node needs to be modified. In a graph of individuals, the probability that the offspring of a chosen node  $i$  replaces the individual of node  $k$  is equal to the weight of the link directed from node  $i$  to node  $k$ ,  $w_{ik}$ . In a graph of subpopulations, assuming the low migration rate regime, this probability is modified to  $w_{ik} \phi_{wm}^{N_k}$ , where  $\phi_{wm}^{N_k}$  is the fixation probability of the migrating offspring to take over the patch  $k$  of size  $N_k$ , and  $w_m$  stands for well-mixed. With the individual-selection parameters  $r$  and  $t$ , we obtain from equation (B.1)

$$\phi_{wm}^{N_k} = \frac{1 - (t/r)}{1 - (t/r)^{N_k}}. \quad (\text{D.1})$$

Here, we focus on the update mechanisms with coupled migration described in §3.1.

### D.1. Update mechanisms with birth first

We start with writing the transition probabilities for all the 16 update mechanisms in table 2 in a compact way. To do so, in addition to the selection parameters  $r$  and  $t$  introduced in table 4, we introduce two more parameters  $r'$  and  $t'$ . Parameters  $r$  and  $t$  represent selection at the individual level for birth and death, respectively, whereas, parameters  $r'$  and  $t'$  represent selection at the patch level for birth and death, respectively. If the selection for birth at the individual level is uniformly at random, then  $r = 1$ , otherwise  $r \neq 1$ . Similarly, if the selection for death at the individual level is uniformly at random, then  $t = 1$ , otherwise  $t \neq 1$ . The same holds for the parameters defined at the patch level. As an example, for the update mechanism **MbBDD**, since the birth selection at the patch level is uniformly random,  $r' = 1$ . But the parameters  $r$ ,  $t$  and  $t'$  are not equal to 1. The parameters  $r'$  and  $t'$  describe the contribution of an individual to the collective selection parameters of a patch. When a patch is occupied by mutants, its collective selection parameters for the birth and the death events equal  $r'N_1$  and  $t'N_1$ , respectively. When a patch is occupied by wild-types, its collective selection parameters for the birth and the death events equal  $N_1$ . With this in mind, we generalize the transition probabilities for update mechanisms with coupled migration, with birth being the first event.

A state of the metastar is denoted by  $(\bullet / \circ, j)$ , where the first index represents the state of the central patch:  $\bullet$  if the central node is occupied by mutant individuals,  $\circ$  if it is occupied by wild-type individuals. The second index denotes the number of mutant occupied leaf patches. The transition from the state  $(\bullet, j)$  to the state  $(\bullet, j + 1)$  occurs with probability

$$T_{\bullet \rightarrow \bullet}^{j+1} = \frac{r'N_1}{(j+1)r'N_1 + (M-1-j)N_1} \frac{(M-1-j)N_1}{(M-1-j)N_1 + jt'N_1} \lambda \phi_{wm}^{N_1}(r, t). \quad (\text{D.2})$$

The transition from the state  $(\circ, j)$  to the state  $(\bullet, j)$  occurs

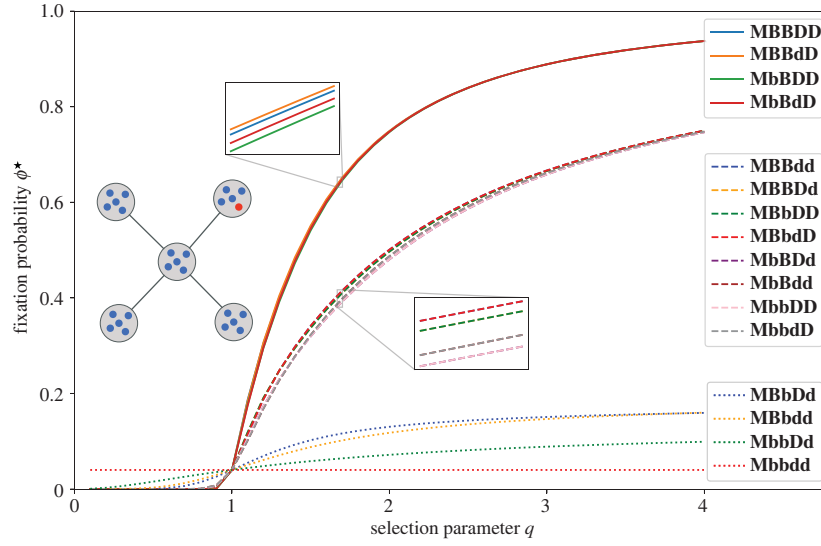


**Figure 5.** The fixation probability of the metatar in the low migration rate regime under the coupled update mechanisms with birth being first, starting from a single mutant. In terms of the value of fixation probability, one can put the update mechanisms into three classes: (H) a class of four update mechanisms with high fixation probability in which selection on the individual level both in both birth and death is associated with the selection parameter (solid lines), (I) a class of eight update mechanisms with medium fixation probability in which selection on the individual level is associated with the selection parameter either for birth or death (dashed lines), and (L) a class of four update mechanisms with low fixation probability in which selection on the individual level is uniformly random for both birth and death (dotted lines). Parameters: number of patches,  $M = 5$ , patch size,  $N_1 = 5$ .

with probability

$$T_{o \rightarrow \bullet}^j = \frac{j r' N_1}{j r' N_1 + (M-j) N_1} \lambda \phi_{\text{wm}}^{N_1}(r, t). \quad (\text{D.3})$$

The transition from the state  $(o, j)$  to the state  $(o, j-1)$  occurs with probability

$$T_{o \rightarrow o}^{j-} = \frac{N_1}{j r' N_1 + (M-j) N_1} \frac{j t' N_1}{(M-1-j) N_1 + j t' N_1} \lambda \phi_{\text{wm}}^{N_1} \left( \frac{1}{r'}, \frac{1}{t} \right). \quad (\text{D.4})$$

The transition from the state  $(\bullet, j)$  to the state  $(o, j)$  occurs with probability

$$T_{\bullet \rightarrow o}^j = \frac{(M-1-j) N_1}{(j+1) r' N_1 + (M-1-j) N_1} \lambda \phi_{\text{wm}}^{N_1} \left( \frac{1}{r'}, \frac{1}{t} \right). \quad (\text{D.5})$$

The fixation probability of a mutant taking over the entire metatar depends on the patch where the initial mutant appears. It can be a leaf patch or the central patch. Let us denote the fixation probability of a mutant starting from the central patch by  $\phi_{\bullet}^0$ . Using [6,25], we find

$$\phi_{\bullet}^0 = \frac{\pi_{\bullet}^{0+}}{1 + (1 - \pi_{\bullet}^{0+}) \sum_{j=1}^{M-2} \left( \frac{\pi_{\bullet}^{j+}}{\pi_{\bullet}^{j+}} \right)^j} \quad (\text{D.6})$$

Here,  $\pi_{o \rightarrow \bullet}^{j-}$  is the conditional probability of the transition from the state  $(o, j)$  to the state  $(o, j-1)$  given that the

population starts from state  $(o, j)$ ,

$$\pi_{o \rightarrow \bullet}^{j-} = \frac{T_{o \rightarrow \bullet}^{j-}}{T_{o \rightarrow \bullet}^j + T_{o \rightarrow o}^{j-}} = \frac{\frac{t'}{r'} \phi_{\text{wm}}^{N_1}(1/r, 1/t)}{\frac{t'}{r'} \phi_{\text{wm}}^{N_1}(1/r, 1/t) + (M-1-j+j t') \phi_{\text{wm}}^{N_1}(r, t)}. \quad (\text{D.7})$$

Similarly,  $\pi_{\bullet}^{j+}$  is the conditional probability of the transition from the state  $(\bullet, j)$  to the state  $(\bullet, j+1)$  given that the population starts from state  $(\bullet, j)$ ,

$$\pi_{\bullet}^{j+} = \frac{T_{\bullet \rightarrow \bullet}^{j+}}{T_{\bullet \rightarrow \bullet}^{j+} + T_{\bullet \rightarrow o}^j} = \frac{r' \phi_{\text{wm}}^{N_1}(r, t)}{r' \phi_{\text{wm}}^{N_1}(r, t) + (M-1-j+j t') \phi_{\text{wm}}^{N_1}(1/r, 1/t)}. \quad (\text{D.8})$$

The fixation probability of a mutant starting from a leaf patch,  $\phi_{\circ}^1$ , can be obtained by using the relation

$$\phi_{\circ}^1 = \frac{1 - \pi_{\circ}^{1-}}{\pi_{\bullet}^{1+}} \phi_{\bullet}^0. \quad (\text{D.9})$$

Thus, the average fixation probability of a metatar starting from a single fully occupied mutant patch is,

$$\phi^{\star} = \frac{M-1}{M} \phi_{\circ}^1 + \frac{1}{M} \phi_{\bullet}^0. \quad (\text{D.10})$$

Consequently, the average fixation probability of a metatar starting from an individual mutant is

$$\phi^{\star} = \phi^{\star} \cdot \phi_{\text{wm}}^{N_1}(r, t). \quad (\text{D.11})$$

Using equations (D.6), (D.9) and (D.11), we find

$$\begin{aligned}\phi^* &= \left( \frac{M-1}{M} \phi_o^1 + \frac{1}{M} \phi_o^0 \right) \phi_{\text{wm}}^{N_1}(r, t), \\ &= \left( \frac{M-11-\pi_o^{1-}}{M} + \frac{1}{M} \right) \frac{\pi_o^{0+}}{1 + (1-\pi_o^{0+}) \sum_{j=1}^{M-2} \left( \frac{\pi_o^{1-}}{\pi_o^{0+}} \right)^j} \phi_{\text{wm}}^{N_1}(r, t).\end{aligned}\quad (\text{D.12})$$

To illustrate the fixation probability  $\phi^*$  using equation (D.12), we assume that all selection parameters are controlled by the same variable,  $q$ . If any of the selection parameters for birth is not equal to 1, then it is set to  $q$ . That is, if  $r \neq 1$ , then  $r = q$  and if  $r' \neq 1$ , then  $r' = q$ . Similarly, if  $t \neq 1$ , then  $t = 1/q$  and if  $t' \neq 1$ , then  $t' = 1/q$ . Figure 5 shows the fixation probability of the metastar under different update schemes with migration coupled to the birth event. Based on the fixation probabilities for  $q > 1$ , the birth first update mechanisms with coupled migration can be broadly categorized into three classes with high, intermediate and low fixation probabilities:

- The class with high fixation probability consists of the update rules where selection acts at the individual level, both in the birth and the death event. That is in the high fixation probability class,  $r \neq 1$  and  $t \neq 1$ .
- The class with intermediate fixation probability consists of the update mechanisms where selection acts at the individual level but only in one event, either birth ( $r \neq 1$ ) or death ( $t \neq 1$ ).
- The low fixation probability class consists of the update mechanisms where selection does not operate at the individual level. For this class,  $r = t = 1$ .

The ordering of the fixation probabilities corresponding to the update mechanisms of these three classes is consistent with the inequalities (B.17) and (B.18) obtained in appendix B.1. For example in inequality (B.17), it is shown that

$$\underbrace{\phi_{\text{MBBDD}}}_{\text{high fixation probability class}} > \underbrace{\phi_{\text{MBBDd}}}_{\text{intermediate fixation probability class}} > \underbrace{\phi_{\text{MBbDd}}}_{\text{low fixation probability class}} \quad (\text{D.13})$$

In the class with high fixation probability, for a given value of  $q$ , the fixation probabilities for the update rules of the class are nearly the same. Let us understand the reason behind this small difference in the fixation probabilities. Recall for the update rules of high fixation probability class both  $r$  and  $t$  are not equal to 1, i.e. selection operates at the individual level for the high fixation probability class update rules. We have

$$\frac{\phi_{\text{wm}}^{N_1}(r, t)}{\phi_{\text{wm}}^{N_1}(1/r, 1/t)} = \left( \frac{r}{t} \right)^{N_1-1}. \quad (\text{D.14})$$

We first focus on the regime  $q > 1$ , with  $r = q$ ,  $t = \frac{1}{q}$ ,

$$\frac{\phi_{\text{wm}}^{N_1}(r, t)}{\phi_{\text{wm}}^{N_1}(1/r, 1/t)} = q^{2(N_1-1)} \gg 1. \quad (\text{D.15})$$

As a result, the fraction

$$\frac{\pi_o^{j-}}{\pi_o^{j+}} = \frac{1 + \frac{M-1-j+t'j}{r'} \frac{\phi_{\text{wm}}^{N_1}(1/r, 1/t)}{\phi_{\text{wm}}^{N_1}(r, t)}}{1 + \frac{r'}{t'} (M-1-j+t'j) \frac{\phi_{\text{wm}}^{N_1}(r, t)}{\phi_{\text{wm}}^{N_1}(1/r, 1/t)}} \ll 1, \quad (\text{D.16})$$

and consequently, equation (D.2) reduces to

$$\phi^* \approx \left( \frac{M-11-\pi_o^{1-}}{M} + \frac{1}{M} \right) \pi_o^{0+} \phi_{\text{wm}}^{N_1}(r, t). \quad (\text{D.17})$$

In the above equation,  $\frac{1-\pi_o^{1-}}{\pi_o^{1+}}$  can be simplified when  $M$  is

sufficiently small such that  $(M-2+t') \frac{\phi_{\text{wm}}^{N_1}(\frac{1}{r}, \frac{1}{t})}{\phi_{\text{wm}}^{N_1}(r, t)} \ll 1$ . In this case,

$$\frac{1-\pi_o^{1-}}{\pi_o^{1+}} \approx 1 \quad (\text{D.18})$$

and

$$\pi_o^{0+} \approx 1. \quad (\text{D.19})$$

Hence,

$$\phi^* \approx \phi_{\text{wm}}^{N_1}(r, t), \quad (\text{D.20})$$

which is independent of the selection parameters  $r'$  and  $t'$ . This implies that the fixation probability of a mutant on the metastar for an update rule of high class fixation probability (update rule where  $r \neq 1$  and  $t \neq 1$ ) is the same regardless of the nature of selection at the patch level. This in turn explains why the fixation probability profiles in the high fixation probability class are so similar.

We use similar arguments to study the differences in the fixation probability profiles of the intermediate fixation probability class where either  $r \neq 1$  or  $t \neq 1$ . From figure 5, we observe that for a given  $q$  value, the differences among the fixation probability for different update rules of the class is higher. For the update rules with  $r \neq 1$  and  $t = 1$ , we have

$$\frac{\phi_{\text{wm}}^{N_1}(r, t)}{\phi_{\text{wm}}^{N_1}(1/r, 1/t)} = r^{N_1-1}. \quad (\text{D.21})$$

Similarly, for the update rules with  $r = 1$  and  $t \neq 1$ , we have

$$\frac{\phi_{\text{wm}}^{N_1}(r, t)}{\phi_{\text{wm}}^{N_1}(1/r, 1/t)} = \left( \frac{1}{t} \right)^{N_1-1}. \quad (\text{D.22})$$

Substituting  $r = q$  and  $t = \frac{1}{q}$ , we get,

$$\frac{\phi_{\text{wm}}^{N_1}(r, t)}{\phi_{\text{wm}}^{N_1}(1/r, 1/t)} = q^{N_1-1}. \quad (\text{D.23})$$

which for  $q > 1$  is less than what we have in the class with the high fixation probability (see equation (D.15)). As a result, we expect that in the class with the intermediate fixation probability, the patch level selection is more important.

In the class of low fixation probability with  $r = t = 1$ , since

$$\frac{\phi_{\text{wm}}^{N_1}(r, t)}{\phi_{\text{wm}}^{N_1}(1/r, 1/t)} = 1, \quad (\text{D.24})$$

the effect of patch selection on the fixation probability is more notable compared with the two other classes. As a result, the

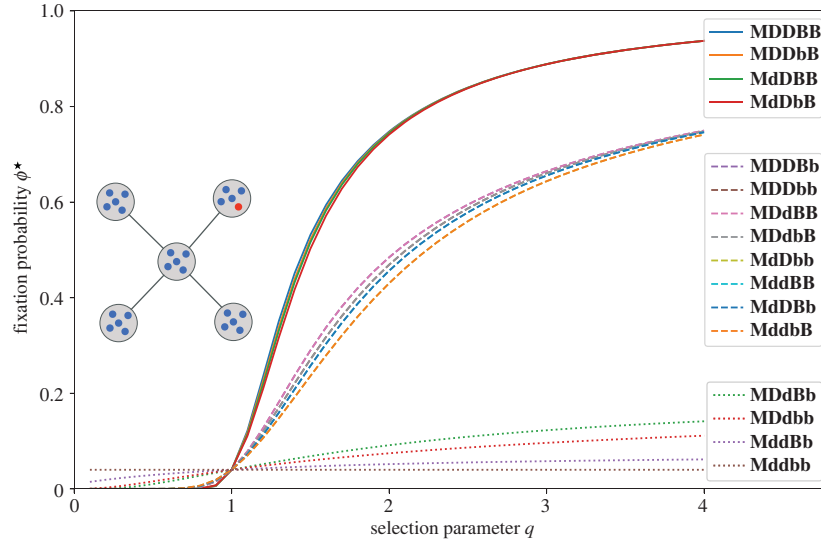


**Figure 6.** The fixation probability of the metastar in the low migration rate regime under coupled update mechanisms with death being first, starting from a single mutant. In terms of the value of fixation probability, one can again put the update mechanisms into three classes: (H) the class with high fixation probability in which selection on the individual level both in both birth and death is associated with the selection parameter, (I) the class with medium fixation probability in which selection on the individual level is associated with the selection parameter either for birth or death, and (L) the class with the low fixation probability in which selection on the individual level is uniformly random for both birth and death. Parameters: number of patches,  $M = 5$ , patch size,  $N_1 = 5$ .

differences in the fixation probabilities for the update rules of this class is larger than what we found in the previous two classes. Also, the conditional transition probabilities in equations (D.7) and (D.8) become identical to the transition probabilities of star graph with one individual per node. Therefore, for the case of low fixation probability class update rules, the fixation probability on the metastar starting from a single mutant patch is equivalent to the fixation probability on the star graph starting from a single mutant, is then the fixation probability of the mutant on the star graph of size  $M$  times the probability  $\phi_{wm}^{N_1}$ .

Let us now focus on the case of  $q < 1$ . In the class with high fixation probability, for  $q < 1$  and  $N_1 \gg 1$ ,

$$\frac{\phi_{wm}^{N_1}(r, t)}{\phi_{wm}^{N_1}(1/r, 1/t)} = q^{2(N_1-1)} \ll 1, \quad (D.25)$$

and hence,

$$\frac{\pi_{\sigma}^{-}}{\pi_{\sigma}^{+}} = \frac{1 + \frac{M-1-j+t'j}{r'} \frac{\phi_{wm}^{N_1}(1/r, 1/t)}{\phi_{wm}^{N_1}(r, t)}}{1 + \frac{r'}{t'} \frac{\phi_{wm}^{N_1}(r, t)}{\phi_{wm}^{N_1}(1/r, 1/t)}} \gg 1. \quad (D.26)$$

As a consequence, from equation (D.12), we find

$$\phi^* \ll 1. \quad (D.27)$$

Therefore, the effect of patch level selection in the class with high fixation probability is negligible. Similarly, we find that for the class with intermediate fixation probability,  $\phi^* \ll 1$ .

Although the variation in fixation probabilities is very small for the high fixation probability class, from figure 5, we find seemingly unintuitive fixation probabilities ordering for the different update mechanisms. Intuitively, an update

mechanism with higher selection associated events is expected to yield higher fixation probabilities of beneficial mutants. In our numerical investigation, we observe that this holds only for a finite range of  $q$ . In fact, for a certain value of  $q$ , we have

$$\phi_{MBbD}^* > \phi_{MBbDD}^* > \phi_{MbBd}^* > \phi_{MbBDD}^*, \quad (D.28)$$

which is counterintuitive. Similarly, based on the numerical calculations, in the class with the intermediate fixation probability, for a range of  $q$ ,

$$\phi_{MBbD}^* > \phi_{MBbDD}^* > \phi_{MbBd}^* > \phi_{MbBDD}^*, \quad (D.29)$$

which again is counterintuitive.

In the fixation probability for metastar  $\phi^*$ , the selection at the individual level always enters the formula via  $\phi_{wm}^{N_1}(r, t)$ . Since  $\phi_{wm}^{N_1}(\frac{r}{t}) = \phi_{wm}^{N_1}(rt)$ , we have  $\phi_{wm}^{N_1}(r=1, t=1/q) = \phi_{wm}^{N_1}(r=q, t=1)$ . Therefore, in the intermediate fixation probability class, two update mechanisms that are similar at the patch level selection, but different at the individual level selection, have the same fixation probabilities. For example, **MBbDd** and **MBbDD**, have the same fixation probabilities. This is the reason that instead of eight, we have four distinct curves for the fixation probabilities of intermediate fixation probability class (see inset of figure 5).

## D.2. Update mechanisms with death first

A similar analysis using the metastar can be performed for the case of 16 update mechanisms where migration is coupled to death, introduced in table 3. We recover a similar grouping of update mechanisms into three fixation probability classes as encountered for the birth first coupled migration update mechanisms (see figure 6).

1. Lieberman E, Hauert C, Nowak MA. 2005 Evolutionary dynamics on graphs. *Nature* **433**, 312–316. (doi:10.1038/nature03204)
2. Tkadlec J, Kaveh K, Chatterjee K, Nowak MA. 2021 Natural selection of mutants that modify population structure. *arXiv Preprint*. (<https://arxiv.org/abs/2111.10890>)
3. Gross T, Blasius B. 2008 Adaptive coevolutionary networks—a review. *J. R. Soc. Interface* **5**, 259–271. (doi:10.1098/rsif.2007.1229)
4. Perc M, Szolnoki A. 2010 Coevolutionary games—a mini review. *BioSystems* **99**, 109–125. (doi:10.1016/j.biosystems.2009.10.003)
5. Constable GW, McKane AJ. 2014 Population genetics on islands connected by an arbitrary network: an analytic approach. *J. Theor. Biol.* **358**, 149–165. (doi:10.1016/j.jtbi.2014.05.033)
6. Yagoobi S, Traulsen A. 2021 Fixation probabilities in network structured meta-populations. *Sci. Rep.* **11**, 1–9. (doi:10.1038/s41598-021-97187-6)
7. Marrec L, Lamberti I, Bitbol A-F. 2021 Toward a universal model for spatially structured populations. *Phys. Rev. Lett.* **127**, 218102. (doi:10.1103/PhysRevLett.127.218102)
8. Kreger J, Brown D, Komarova NL, Wodarz D, Pritchard J. 2022 The role of migration in mutant dynamics in fragmented populations. *J. Evol. Biol.* **36**, 444–460. (doi:10.1111/jeb.14131)
9. Wright S. 1931 Evolution in Mendelian populations. *Genetics* **16**, 97–159. (doi:10.1093/genetics/16.2.97)
10. Maruyama T. 1970 On the fixation probability of mutant genes in a subdivided population. *Genet. Res.* **15**, 221–225. (doi:10.1017/S0016672300001543)
11. Kimura M, Weiss G. 1964 The stepping stone model of population structure and the decrease of genetic correlation with distance. *Genetics* **49**, 561–575. (doi:10.1093/genetics/49.4.561)
12. Patwa Z, Wahl LM. 2008 The fixation probability of beneficial mutations. *J. R. Soc. Interface* **5**, 1279–1289. (doi:10.1098/rsif.2008.0248)
13. Baxter G, Frean M. 2008 Death–birth ordering and suppression of fitness in networks. Working Paper. See <https://homepages.ecs.vuw.ac.nz/~marcus/manuscripts/FreanBaxterJB.pdf>.
14. Zukewich J, Kurella V, Doebeli M, Hauert C. 2013 Consolidating birth–death and death–birth processes in structured populations. *PLoS ONE* **8**, e54639. (doi:10.1371/journal.pone.0054639)
15. Hindersin L, Traulsen A. 2015 Most undirected random graphs are amplifiers of selection for birth–death dynamics, but suppressors of selection for death–birth dynamics. *PLoS Comput. Biol.* **11**, e1004437. (doi:10.1371/journal.pcbi.1004437)
16. Allen B *et al.* 2020 Transient amplifiers of selection and reducers of fixation for death–birth updating on graphs. *PLoS Comput. Biol.* **16**, e1007529. (doi:10.1371/journal.pcbi.1007529)
17. Kaveh K, Komarova NL, Kohandel M. 2015 The duality of spatial death–birth and birth–death processes and limitations of the isothermal theorem. *R. Soc. Open Sci.* **2**, 140465. (doi:10.1098/rsos.140465)
18. Bürger R. 1998 Mathematical properties of mutation–selection models. *Genetica* **102**, 279–298.
19. Johnson T. 1999 The approach to mutation–selection balance in an infinite asexual population, and the evolution of mutation rates. *Proc. R. Soc. Lond. B* **266**, 2389–2397. (doi:10.1098/rspb.1999.0936)
20. Yagoobi S, Yousefi H, Samani KA. 2018 Mutation–selection stationary distribution in structured populations. *Phys. Rev. E* **98**, 042301. (doi:10.1103/PhysRevE.98.042301)
21. Sharma N, Traulsen A. 2022 Suppressors of fixation can increase average fitness beyond amplifiers of selection. *Proc. Natl Acad. Sci. USA* **119**, e2205424119. (doi:10.1073/pnas.2205424119)
22. Foo J, Gunnarsson EB, Leder K, Sivakoff D. 2022 Dynamics of advantageous mutant spread in spatial death–birth and birth–death Moran models. *arXiv Preprint*. (<https://arxiv.org/abs/2209.11852>)
23. Altrock PM, Traulsen A. 2009 Deterministic evolutionary game dynamics in finite populations. *Phys. Rev. E* **80**, 011909. (doi:10.1103/PhysRevE.80.011909)
24. Nowak MA. 2006 *Evolutionary dynamics: exploring the equations of life*. Cambridge, MA: Harvard University Press.
25. Broom M, Rychtář J. 2008 An analysis of the fixation probability of a mutant on special classes of non-directed graphs. *Proc. R. Soc. A* **464**, 2609–2627. (doi:10.1098/rspa.2008.0058)
26. Masuda N, Ohtsuki H. 2009 Evolutionary dynamics and fixation probabilities in directed networks. *New J. Phys.* **11**, 033012. (doi:10.1088/1367-2630/11/3/033012)
27. Masuda N. 2009 Directionality of contact networks suppresses selection pressure in evolutionary dynamics. *J. Theor. Biol.* **258**, 323–334. (doi:10.1016/j.jtbi.2009.01.025)
28. Hadjichrysanthou C, Broom M, Rychtář J. 2011 Evolutionary games on star graphs under various updating rules. *Dyn. Games Appl.* **1**, 386–407. (doi:10.1007/s13235-011-0022-7)
29. McAvoy A, Allen B. 2021 Fixation probabilities in evolutionary dynamics under weak selection. *J. Math. Biol.* **82**, 1–41. (doi:10.1007/s00285-021-01568-4)
30. Allen B, McAvoy A. 2019 A mathematical formalism for natural selection with arbitrary spatial and genetic structure. *J. Math. Biol.* **78**, 1147–1210. (doi:10.1007/s00285-018-1305-z)
31. Allen B, Tarnita CE. 2012 Measures of success in a class of evolutionary models with fixed population size and structure. *J. Math. Biol.* **68**, 109–143. (doi:10.1007/s00285-012-0622-x)
32. Ottino-Löffler B, Scott JG, Strogatz SH. 2017 Evolutionary dynamics of incubation periods. *ELife* **6**, e30212. (doi:10.7554/eLife.30212)
33. Broom M, Rychtář J, Stadler BT. 2011 Evolutionary dynamics on graphs—the effect of graph structure and initial placement on mutant spread. *J. Stat. Theory Pract.* **5**, 369–381. (doi:10.1080/15598608.2011.10412035)
34. Broom M, Hadjichrysanthou C, Rychtář J. 2010 Evolutionary games on graphs and the speed of the evolutionary process. *Proc. R. Soc. A* **466**, 1327–1346. (doi:10.1098/rspa.2009.0487)
35. Monk T. 2018 Martingales and the fixation probability of high-dimensional evolutionary graphs. *J. Theor. Biol.* **451**, 10–18. (doi:10.1016/j.jtbi.2018.04.039)
36. Broom M, Rychtář J. 2013 *Game-theoretical models in biology*. Boca Raton, FL: Chapman and Hall/CRC.
37. Askari M, Samani KA. 2015 Analytical calculation of average fixation time in evolutionary graphs. *Phys. Rev. E* **92**, 042707. (doi:10.1103/PhysRevE.92.042707)
38. Hajhashemi M, Samani KA. 2019 Fixation time in evolutionary graphs: a mean-field approach. *Phys. Rev. E* **99**, 042304. (doi:10.1103/PhysRevE.99.042304)
39. Hathcock D, Strogatz SH. 2019 Fitness dependence of the fixation-time distribution for evolutionary dynamics on graphs. *Phys. Rev. E* **100**, 012408. (doi:10.1103/PhysRevE.100.012408)
40. Hathcock D, Strogatz SH. 2022 Asymptotic absorption-time distributions in extinction-prone Markov processes. *Phys. Rev. Lett.* **128**, 218301. (doi:10.1103/PhysRevLett.128.218301)
41. Gaiimo S, Arranz J, Traulsen A. 2018 Invasion and effective size of graph-structured populations. *PLoS Comput. Biol.* **14**, e1006559. (doi:10.1371/journal.pcbi.1006559)
42. Antal T, Redner S, Sood V. 2006 Evolutionary dynamics on degree-heterogeneous graphs. *Phys. Rev. Lett.* **96**, 188104. (doi:10.1103/PhysRevLett.96.188104)
43. Nakamaru M, Matsuda H, Iwasa Y. 1997 The evolution of cooperation in a lattice-structured population. *J. Theor. Biol.* **184**, 65–81. (doi:10.1006/jtbi.1996.0243)
44. Pattni K, Broom M, Rychtář J, Silvers LJ. 2015 Evolutionary graph theory revisited: when is an evolutionary process equivalent to the Moran process? *Proc. R. Soc. A* **471**, 20150334. (doi:10.1098/rspa.2015.0334)
45. Ohtsuki H, Hauert C, Lieberman E, Nowak MA. 2006 A simple rule for the evolution of cooperation on graphs. *Nature* **441**, 502–505. (doi:10.1038/nature04605)
46. Allen B, Lippner G, Chen YT, Fotouhi B, Momeni N, Yau ST, Nowak MA. 2017 Evolutionary dynamics on any population structure. *Nature* **544**, 227–230. (doi:10.1038/nature21723)



47. Tkadlec J, Pavlogiannis A, Chatterjee K, Nowak MA. 2020 Limits on amplifiers of natural selection under death–birth updating. *PLoS Comput. Biol.* **16**, e1007494. (doi:10.1371/journal.pcbi.1007494)
48. Ewens WJ. 2004 *Mathematical population genetics. I. Theoretical introduction*. New York, NY: Springer.
49. Ohtsuki H, Nowak MA. 2006 The replicator equation on graphs. *J. Theor. Biol.* **243**, 86–97. (doi:10.1016/j.jtbi.2006.06.004)
50. Sood V, Antal T, Redner S. 2008 Voter models on heterogeneous networks. *Phys. Rev. E* **77**, 13.
51. Hindersin L, Traulsen A. 2014 Counterintuitive properties of the fixation time in network-structured populations. *J. R. Soc. Interface* **11**, 20140606. (doi:10.1098/rsif.2014.0606)
52. Hindersin L, Wu B, Traulsen A, Garcia J. 2019 Computation and simulation of evolutionary game dynamics in finite populations. *Sci. Rep.* **9**, 6946. (doi:10.1038/s41598-019-43102-z)
53. Monk T, Green P, Paulin M. 2014 Martingales and fixation probabilities of evolutionary graphs. *Proc. R. Soc. A* **470**, 20130730. (doi:10.1098/rspa.2013.0730)
54. Alcalde Cuesta F, González Sequeiros P, Lozano Rojo Á. 2017 Suppressors of selection. *PLoS ONE* **12**, e0180549. (doi:10.1371/journal.pone.0180549)
55. Kuo YP, Nombela-Arrieta C, Carja O. 2021 A theory of evolutionary dynamics on any complex spatial structure. *BioRxiv*. (doi:10.1101/2021.02.07.430151)
56. Liu R, Masuda N. 2023 Fixation dynamics on hypergraphs. *arXiv Preprint*. (https://arxiv.org/abs/2301.05343)
57. Nakamaru M, Nogami H, Iwasa Y. 1998 Score-dependent fertility model for the evolution of cooperation in a lattice. *J. Theor. Biol.* **194**, 101–124. (doi:10.1006/jtbi.1998.0750)
58. Nowak MA, May RM. 1992 Evolutionary games and spatial chaos. *Nature* **359**, 826–829. (doi:10.1038/359826a0)
59. Holley RA, Liggett TM. 1975 Ergodic theorems for weakly interacting infinite systems and the voter model. *Ann. Probab.* **3**, 643–663. (doi:10.1214/aop/1176996306)
60. Moran PAP. 1958 Random processes in genetics. *Proc. Camb. Philos. Soc.* **54**, 60–71. (doi:10.1017/S0305004100033193)
61. Houchmandzadeh B, Vallade M. 2011 The fixation probability of a beneficial mutation in a geographically structured population. *New J. Phys.* **13**, 073020. (doi:10.1088/1367-2630/13/7/073020)
62. Slatkin M. 1981 Fixation probabilities and fixation times in a subdivided population. *Evolution* **35**, 477–488. (doi:10.2307/2408196)
63. Barton NH. 1993 The probability of fixation of a favoured allele in a subdivided population. *Genet. Res.* **62**, 149–157. (doi:10.1017/S0016672300031748)
64. Whitlock MC. 2003 Fixation probability and time in subdivided populations. *Genetics* **164**, 767–779. (doi:10.1093/genetics/164.2.767)
65. Wodarz D, Komarova NL. 2020 Mutant evolution in spatially structured and fragmented expanding populations. *Genetics* **216**, 191–203. (doi:10.1534/genetics.120.303422)
66. Hubbell SP. 2001 *The unified neutral theory of biodiversity and biogeography*. Monographs in Population Biology. Princeton, NJ: Princeton University Press.
67. Komarova NL, Sengupta A, Nowak MA. 2003 Mutation–selection networks of cancer initiation: tumor suppressor genes and chromosomal instability. *J. Theor. Biol.* **223**, 433–450. (doi:10.1016/S0022-5193(03)00120-6)
68. Komarova NL. 2007 Viral reproductive strategies: how can lytic viruses be evolutionarily competitive? *J. Theor. Biol.* **249**, 766–784. (doi:10.1016/j.jtbi.2007.09.013)
69. Nowak MA, Michor F, Iwasa Y. 2003 The linear process of somatic evolution. *Proc. Natl Acad. Sci. USA* **100**, 14 966–14 969. (doi:10.1073/pnas.2535419100)
70. Vermeulen L, Snippert HJ. 2014 Stem cell dynamics in homeostasis and cancer of the intestine. *Nat. Rev. Cancer* **14**, 468–480. (doi:10.1038/nrc3744)

# Chapter 6

## Discussion

Studying evolutionary dynamics in well-mixed populations has provided insights into the operation of natural selection alongside genetic drift. However, the well-mixed population, also known as the complete graph, represents a special case where each individual interacts with every other individual with equal propensity. This way, the well-mixed populations are ideal populations. In contrast, natural populations often exhibit spatial structures. Evolutionary graph theory (EGT) serves as a platform for comprehending how various evolutionary forces interact within these spatial structures. EGT not only aids in understanding the interplay of these forces but also provides a framework for engineering populations, with a prospect to tune the strengths of these forces.

Within the EGT community, it is widely recognised that the choice of update rules, such as Birth-death (Bd) or death-Birth (dB), considerably impacts evolutionary outcomes [65, 37]. In this thesis, we introduced an additional factor into this decision-making process: the choice of individuals moving to vacant sites, either the parent ( $p$ ) or the (mutant) offspring ( $o$ ). This added choice gives rise to more complex update rules, denoted as  $Bd^o$ ,  $Bd^p$ ,  $dB^o$ , and  $dB^p$ . With these complex update rules, the need for a specific mutant initialisation scheme becomes unnecessary as it naturally follows from the choice of the birth-death scheme and the moving individual. For example,  $Bd^o$  corresponds to the temperature-initialised Bd updating [28], while  $Bd^p$  is equivalent to the widely recognised uniform-initialised Bd updating. So far, uniform-initialised Bd updating has been supported by the occurrence of spontaneous mutations [87]. We have shown that it can also be recovered with mutants appearing during reproduction, if parents move to vacant sites.



Additionally, allowing parents to move within the dB scheme, equivalent to  $\text{dB}^p$ , also opens up possibilities for new update rules such as the temperature-initialised dB updating.

Working with  $\text{dB}^p$  updating, we have discovered a completely new category of graphs: amplifiers of fixation (*AoF*)—structures with a higher probability of fixing mutants regardless of their fitness values. Notably, for  $\text{dB}^p$  updating, the star graph is an amplifier of fixation. Even in the limit  $N \rightarrow \infty$ , the probability of fixing deleterious mutants for the star graph under  $\text{dB}^p$  updating remains non-zero. This is the first example where disadvantageous mutants can achieve fixation, even within an infinitely large population size. Consequently, the relevance of the deleterious mutant regime begins to manifest, even at short-term fixation time scales. While we have found that majority of the small random graphs are piecewise amplifiers of fixation under  $\text{dB}^p$  updating, it remains to be seen what happens for large random graphs.

Research in EGT has primarily focused on studying the fixation probability of mutants on graphs [18, 49, 39, 51, 97, 28, 98, 66, 99, 100, 101, 89, 90]. This thesis advances EGT research by investigating long-term evolution on single-peaked fitness landscapes, where mutations continuously appear in evolving populations. In chapters 2 and 3, we worked within the low mutation rate regime, where the long-term mutation-selection dynamics is sequential.

Our findings revealed that suppressors of fixation (*SoF*), which are spatial structures with a lower probability of fixing mutants regardless of their fitness values, achieve higher fitness, while *AoF* attain lower fitness than the complete graph. These results suggest that the long-term fate of adaptive evolution in spatially structured populations cannot be predicted solely by considering the fixation of advantageous mutants. Rejecting deleterious mutations is equally crucial. A structure better at rejecting deleterious mutants can achieve higher fitness than the well-mixed population despite being less effective at fixing beneficial mutants. Similarly, a structure better at fixing advantageous mutants can attain lower fitness than the well-mixed population if it is poor at rejecting disadvantageous mutants. Therefore, the fate of deleterious mutants substantially influences the long-term evolution on spatial structures. This thesis emphasises the importance of the deleterious mutant regime, even for very large population sizes, something that has been so far overlooked in the literature. Fig. 6.1 shows how the choice of moving the parent individual to vacant sites and studying long-term evolutionary dynamics lead to our main finding about the role of deleterious mutant regime.

The new category of graphs, *AoF*, holds the potential to advance the current understanding in the following two areas: Crossing fitness valleys and the evolution of cooperation.

Like well-mixed populations, a single-peaked fitness landscape can serve as a good starting point for mathematical analysis. However, mutations typically interact with their fitness effects, leading to ruggedness in the landscape [102, 103, 104], see Fig. 6.2. Investigating evolutionary dynamics on spatial structures subjected to rugged fitness landscapes is therefore a natural future direction. An important quantity in this context is the time taken by the population to cross fitness valleys [105, 106, 107, 108]. Valley crossing can occur via one of two processes: sequential fixation and simultaneous fixation [109].

In sequential fixation, a deleterious valley-genotype mutant first appears on the local-peak genotype background and then fixates. This is followed by the appearance and fixation of a beneficial escape-genotype mutant on the valley-genotype background. This way, the population moves from a local fitness peak to higher peaks via a series of fixation steps through fitness valleys. Sequential fixation is a common mode for valley crossing for low mutation rates and small population sizes. With no back mutations, *AoF* can substantially reduce the valley crossing times compared to the well-mixed population. This is because *AoF* have a higher probability of fixing both deleterious and beneficial mutants. Thus, for low mutation rates, *AoF* have higher navigability through rugged fitness landscapes. For higher mutation rates, simultaneous fixation becomes more frequent. In this process, a quasi mutation-selection equilibrium is established between the local-peak genotype and the valley genotypes. Subsequently, a valley genotype mutates to an escape genotype, which eventually fixes in the population. This mechanism allows the population to ascend to a higher fitness peak without requiring fixation in the valley, which is why simultaneous fixation is also known as stochastic tunneling. For the case of the complete graph, the valley genotypes are found at a very low frequency in the mutation-selection equilibrium [110, 111]. However, the mutation-selection balance for *AoF* at higher mutation rates is not known and thus needs to be determined before investigating simultaneous fixation. Overall, *AoF* can result in a considerably larger span of genotype space covered during the course of evolution and thus, making higher fitness peaks more accessible.

The fitness landscape can also vary over time as a population evolves. One such scenario occurs when selection is frequency-dependent. The rele-

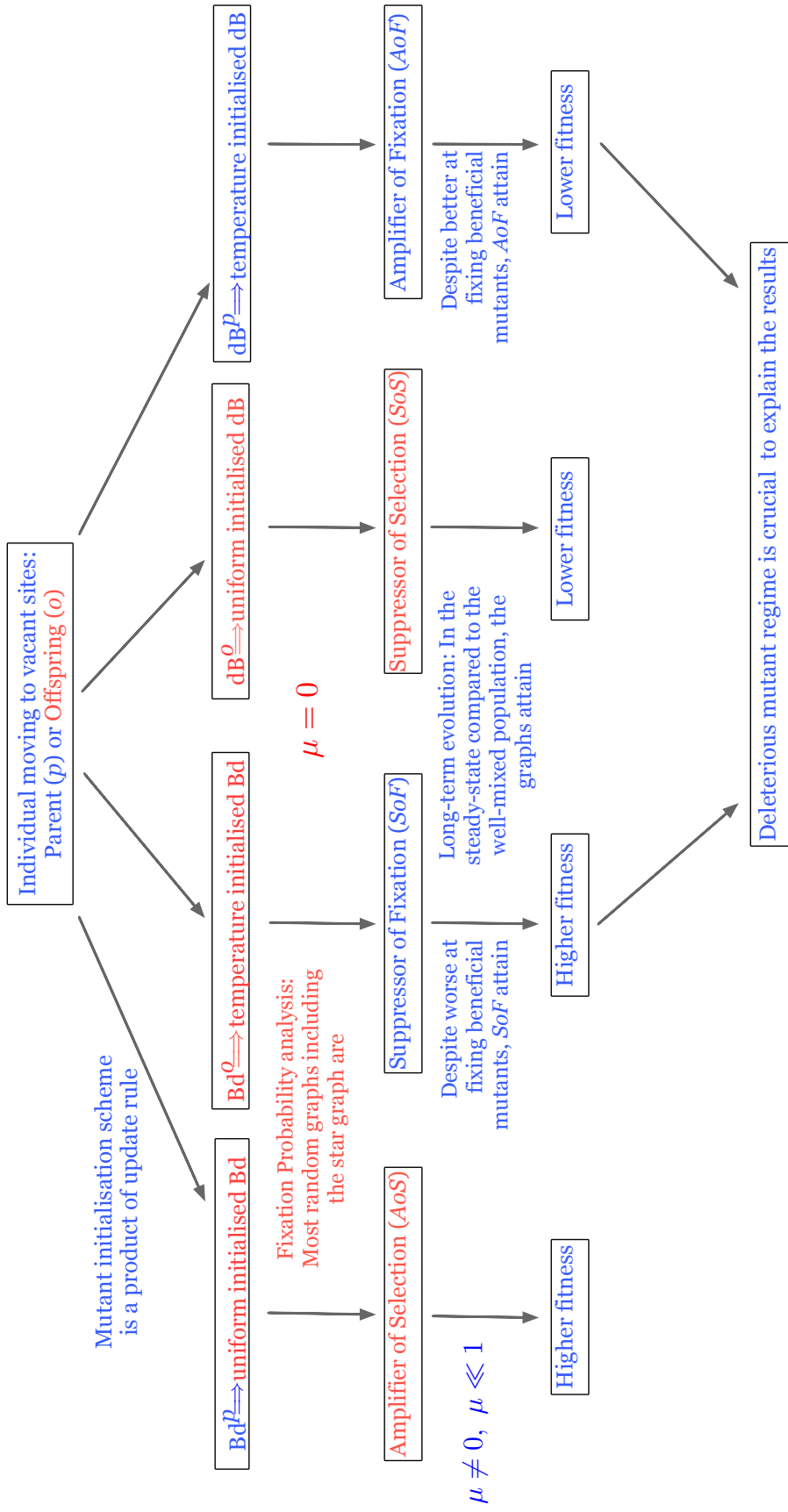


Figure 6.1: **A tree summarising some of our key findings.** The tree demonstrates how allowing parent individuals to replace dead individuals led to one of our main findings: the importance of the deleterious mutant regime for long-term evolution. Text coloured in red represents previously known information, while text coloured in blue indicates our contributions.

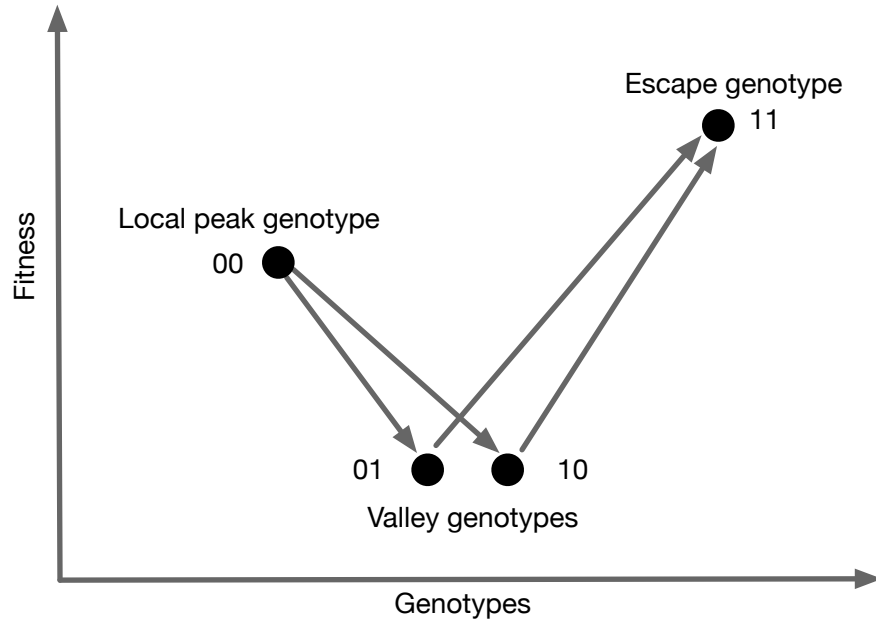


Figure 6.2: **Fitness Valley.** Here, we illustrate how the fitness interaction between loci, known as epistasis, can give rise to multiple fitness peaks. We consider two biallelic loci where each locus can be in one of two states, 0 or 1. In our example, starting from the local peak genotype 00, a mutation at any locus has a deleterious fitness effect. Consequently, the genotypes 01 and 10 are termed valley genotypes. It is only when the second mutation arises on a valley genotype the fitness effects are beneficials. The resulting genotype 11, known as the escape genotype, exhibits an even higher fitness than the local peak genotype.

vant framework to study evolutionary dynamics in such cases is evolutionary game theory. A commonly explored problem within this framework is the evolution of cooperation, often studied by computing the fixation probability of a cooperator ( $C$ ) introduced into a population of defectors ( $D$ ) [19].

In evolutionary game theory, individuals play games with their neighbors, and the resulting payoffs gives the fitness of each individual. A common choice to study evolution of cooperation is the game of prisoner's dilemma

[47] with payoff matrix given by

$$\begin{array}{c} C \quad D \\ \begin{array}{cc} C & D \\ D \end{array} \end{array} \begin{pmatrix} b-c & -c \\ b & 0 \end{pmatrix}. \quad (6.1)$$

In this game,  $b > c > 0$ , where a cooperator incurs a cost,  $c$ , to benefit others by  $b$  units. Conversely, a defector neither pays a cost nor provides any benefit.

In well-mixed populations, regardless of the update rule the cooperation fails to spread for large population sizes. However, spatial structures facilitate the evolution of cooperation by enabling the formation of cooperators clusters, thereby increasing the fitness of cooperators [112]. Previous research by Ohtsuki et al. demonstrated that under dB updating, natural selection favors cooperation on regular graphs if the benefit-to-cost ratio  $b/c > k$ , where  $k$  is the average mean degree [42].

In the initial phase of the fixation dynamics, cooperators generally face a fitness disadvantage and thus, fails to establish. Given our finding that under constant selection, temperature-initialised dB updating ( $\text{dB}^p$ ) increases the probability of fixation for deleterious mutants, it is expected that the same holds true for cooperators under frequency dependent selection. That is, under  $\text{dB}^p$ , it is anticipated that cooperators have a higher probability of fixation on a spatial structure than with other updating schemes. This prediction, however, requires further verification. Additionally, long-term evolution with non-local mutations and frequency-dependent selection on graphs [113] presents an intriguing research question for future exploration. To summarise, the ability to fix of deleterious mutants opens door for new possibilities.

Amplifiers of selection (*AoS*), known for their potential to accelerate evolution, have been in the limelight EGT. In Ref. [36], it was demonstrated that nearly any structure can be transformed into an *AoS* by introducing self-loops and manipulating link weights. Because of their ability to efficiently fix beneficial mutants, *AoS* attain higher fitness than the well-mixed population for the low mutation rate dynamics. However, in chapter 4 we found that beyond the low mutation rates self-looped *AoS* can attain lower fitness not just compared to the well-mixed population, but also the suppressors of selection (*SoS*). Therefore, structures that attain higher fitness for sequential long-term dynamics need not perform better than the complete

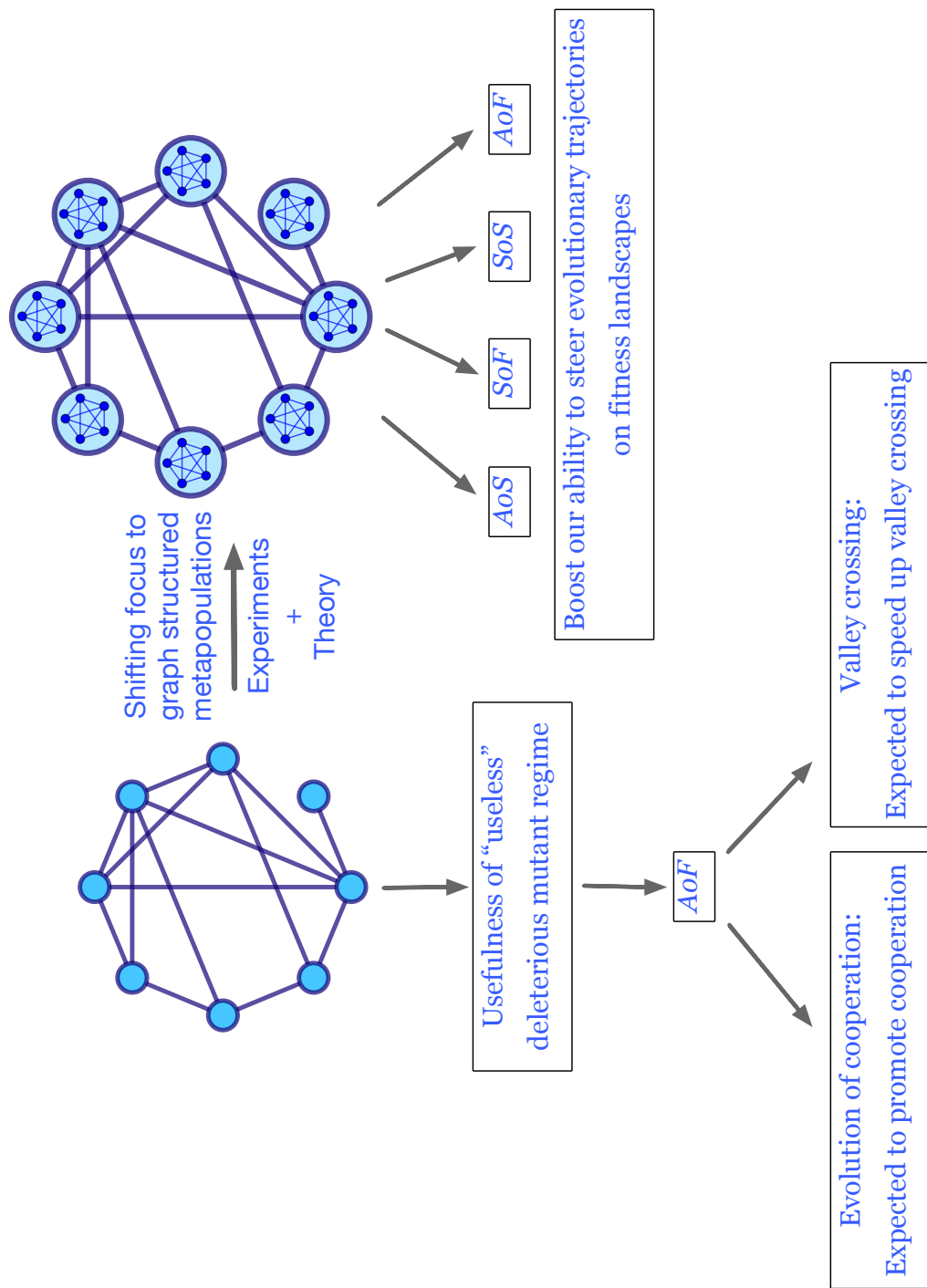


Figure 6.3: **Outlook.** Here, we present a list of some immediate problems along with their respective motivations that are of particular interest to us.

graph for higher mutation rates. Whereas, less famous *SoF* can maintain higher fitness both within and outside the weak mutation rates. Overall, it could be worthwhile to sometimes shift focus from the mainstream amplifiers of selection.

The majority of research in EGT is driven by theorists. Only very recently, experimental studies have started to emerge [88]. To facilitate EGT research in experimental evolution, the proposal is to replace each node with a well-mixed population, creating a network-structured metapopulation, see Fig. 6.3. However, it is crucial to recognise that the findings from classical one-node-one-individual research cannot be directly extrapolated to the metapopulation level. Therefore, it is imperative to pursue a parallel development of the theoretical framework, focusing on network-structured metapopulations. References such as [114, 89, 90, 115] represent some initial efforts in this direction. Drawing from the experiences of the one-node-one-individual theory, where the choice of update rules strongly influences the outcomes, it remains to be seen to what extent the choice of update rules presented in chapter 5 impact structured metapopulation dynamics.

While we have already mentioned quite a few future directions, other important problems to be explored are following:

- The first is to move beyond the assumption of a constant population size. Studying spatially structured growing populations not only holds its own biological relevance [55] but can also enhance the robustness of the evolutionary outcomes regarding the choice of update rules. The update rules for a growing population differs from the traditional constant population size birth-death updates in the sense that birth and death need not occur in equal proportions. Branching processes [116, 117] provide a natural starting point for addressing growing populations on spatial structures with empty sites [118].
- Secondly, mutation rates often do not adhere to the weak mutation rate approximation for a population. Typically, multiple beneficial mutants are competing with each other to fix in the population, leading to the regime of clonal interference [119, 120]. Consequently, studying clonal interference on graphs becomes an important area of research.
- Third is to examine long-term evolution in network-structured metapopulations. This approach would enable the experimental validation of the results obtained in this thesis.

Another line of research could be the study of weighted Erdős-Rényi graph structured metapopulations with demes of different sizes occupying nodes. One motivation behind this study is to understand the modifications required to transform a random Erdős-Rényi graph into one of the following structures: an *AoS*, a *SoS*, an *AoF*, or a *SoF*. These modifications would then provide insights into designing spatial structures with desired fixation probabilities for mutants in the laboratory settings. This would enhance our ability to steer evolutionary dynamics on fitness landscapes.

Exciting times for EGT lie ahead!



# Author contributions

## Author initials

AT Arne Traulsen JK Joachim Krug  
SD Suman Das SY Sedigheh Yagoobi  
NS Nikhil Sharma

## Contributor Roles Taxonomy (CRediT, <https://credit.niso.org>)

[C] Conceptualisation, [D] Data curation, [A] Formal Analysis, [I] Investigation, [M] Methodology, [S] Software, [U] Supervision, [V] Validation, [N] Visualisation, [O] Writing-original draft, and [E] Writing-review and editing.

## Contributions per author

	Author	C	D	A	I	M	S	U	V	N	O	E
<b>Chapter 2</b>	NS	x	x	x	x	x	x		x	x	x	x
	AT	x			x			x	x	x		x
<b>Chapter 3</b>	NS	x	x	x	x	x	x		x	x	x	x
	AT	x			x			x	x	x		x
	SD			x					x			x
	JK	x			x			x	x	x		x
<b>Chapter 4</b>	NS	x	x	x	x	x	x		x	x	x	x
	AT	x						x	x	x		x
	SY			x					x			x
<b>Chapter 5</b>	NS								x	x		x
	AT	x						x	x	x		x
	SY	x	x	x	x	x	x		x	x	x	x

---

Nikhil Sharma

# Acknowledgements

I feel extremely lucky to have work with Arne Traulsen for my doctoral studies. He is an excellent supervisor. He gave me the perfect amount of freedom to conduct scientific research and was always available, even during his USA sabbatical, when I needed his inputs. I now feel more confident to design and carry out a research project. Thank you, Arne. He also taught me to be empathetic while writing a research article, taking both the present and future experts into consideration. In his words, “think of the master thesis student who would want to understand and build upon your work.”

I am grateful to Sören Christensen, Tal Dagan and Regina Scherließ for agreeing to be the part defense committee. I am also thankful to my thesis advisory committee— Julien Dutheil, Sören, Arne, and Andy Farr, for their timely suggestions. Special thanks to Angela Donner, Ursula Krützfeldt, Martin Ganter, and Derk Wachsmuth for helping with the bureaucracy and IT related issues. Your assistance saved my time and energy. Thanks to Michael Sieber and Christian Hilbe for assisting with the English-German translation of the thesis abstract.

At MPI Plön, I had the privilege of meeting some inspiring people: Christian Hilbe, Emil Mallmin, Guilhem Doucier, Román Zapién-Campos, Jun Ishigohoka, and Sedigheh Yagoobi. You all have shown me how honesty, curiosity and courage, supplemented with a little hard work, leads to a joyful pursuit. Thanks to generous Max Planck society, that I could discuss my work with scientists from different parts of the world at MPI Plön: Helen Alexander, Arjan De Visser, Yuriy Pichugin, Daniel Fisher, Dmitri Petrov, Hye Jin Park, Jacob Scott, and Jasmine Foo.

I am thankful to Arne for supporting the research visit to IBP Cologne where I could work with my friend Suman G. Das, and my hero, Joachim Krug. I am grateful to Joachim’s group members— Sakshi Pahujani, Rotem Gross, Muna Turki, Suman, Muhittin Mungan— for being welcoming and

making me part of their group. Thanks to Joachim for suggesting MPI Plön in the first place for PhD studies, and dear Chaitanya Gokhale for letting me spend some initial months in his research group as an intern.

Besides work, I had the pleasure to meet a great international group of people: Xiaowen Zhong, Charlotte Rossetti, Alejandra Ramírez, Ernesto Berríos, Amanda de Azevedo, Emil, Iqra Kasu, Amor II Damatac, Marta Couto, Ian Dewan, Saptarshi Pal, Lavisha Parab, Jun, Sedigheh (collaborator), Roman, Estela JM, Puneeth Deraje, Gaurav Athreya, Dharanish Rajendra, Dana Lauenroth, Prateek Verma, Saumil Shah, Guilhem, Florence Bansept, and Qianci Yang. You all have made last few years a memorable one. Special mention for Charlotte for always volunteering to organise social events, and arranging a meeting with Didier Queloz. I am also thankful to my school and college friends for keeping in touch despite long-distance: Pankaj Chaudhary, Shantun Sharma, Oinam Singh Nepolian, Tiente Rengneichuong Koirang, Saurabh Kumar, and Mohammad Atif Javed. Thank you all for inspiring and tolerating me.

Above all, thank you golu, mummy, and daddy for your constant unconditional support!

# Declaration

I hereby declare,

- i that apart from the supervisor's guidance, the content and design of the thesis is all the candidate's own work;
- ii that the thesis has not been submitted either partially or wholly as part of a doctoral degree to another examining body and whether it has been published or submitted for publication than indicated in the thesis;
- iii that the thesis has been prepared with regard to the Rules of Good Scientific Practice of the German Research Foundation;
- iv that prior to this thesis, I have not attempted and failed to obtain a doctoral degree.

---

Nikhil Sharma

---

Plön 2023

# Bibliography

- [1] J. Cairns. Mutation selection and the natural history of cancer. *Nature*, 255:197–200, 1975.
- [2] M. A. Nowak, F. Michor, and Y. Iwasa. The linear process of somatic evolution. *Proceedings of the National Academy of Sciences USA*, 100:14966–14969, 2003.
- [3] Laura Hindersin, Benjamin Werner, David Dingli, and Arne Traulsen. Should tissue structure suppress or amplify selection to minimize cancer risk? *Biology Direct*, 11(1):41, 2016.
- [4] Hans-Curt Flemming, Jost Wingender, Ulrich Szewzyk, Peter Steinberg, Scott A Rice, and Staffan Kjelleberg. Biofilms: an emergent form of bacterial life. *Nature Reviews Microbiology*, 14(9):563–575, 2016.
- [5] Simon van Vliet, Christoph Hauert, Kyle Fridberg, Martin Ackermann, and Alma Dal Co. Global dynamics of microbial communities emerge from local interaction rules. *PLOS Computational Biology*, 18(3):e1009877, 2022.
- [6] L. Vermeulen, E. Morrissey, M. van der Heijden, A. M. Nicholson, A. Sottoriva, S. Buczacki, R. Kemp, S. Tavaré, and D. Winton. Defining stem cell dynamics in models of intestinal tumor initiation. *Science*, 342:995–998, 2013.
- [7] L. Vermeulen and H. J. Snippert. Stem cell dynamics in homeostasis and cancer of the intestine. *Nature Reviews Cancer*, 14:468–480, 2014.
- [8] Ran Nathan and Helene C Muller-Landau. Spatial patterns of seed dispersal, their determinants and consequences for recruitment. *Trends in ecology & evolution*, 15(7):278–285, 2000.

- [9] Uri Alon. *An introduction to systems biology: design principles of biological circuits*. CRC press, 2019.
- [10] Mark Newman. *Networks*. Oxford university press, 2018.
- [11] J. H. Gillespie. *Population Genetics : A Concise Guide*. The Johns Hopkins University Press, 2004 (2nd edition).
- [12] Edward Pollak. On the survival of a gene in a subdivided population. *Journal of Applied Probability*, 3(1):142–155, 1966.
- [13] Takeo Maruyama. On the fixation probability of mutant genes in a subdivided population. *Genetics Research*, 15(2):221–225, 1970.
- [14] Takeo Maruyama. A simple proof that certain quantities are independent of the geographical structure of population. *Theoretical Population Biology*, 5:148–154, 1974.
- [15] R. Lande. Effective deme sizes during long term evolution estimated from rates of chromosomal rearrangements. *Evolution*, 33:234–251, 1979.
- [16] M. Slatkin. Fixation probabilities and fixation times in a subdivided population. *Evolution*, 35:477–488, 1981.
- [17] Hidenori Tachida and Masaru Iizuka. Fixation probability in spatially changing environments. *Genetics Research*, 58(3):243–251, 1991.
- [18] E. Lieberman, C. Hauert, and M. A. Nowak. Evolutionary dynamics on graphs. *Nature*, 433:312–316, 2005.
- [19] Martin A Nowak. *Evolutionary dynamics: Exploring the equations of life*. Harvard University Press, 2006.
- [20] Mark. Broom and Jan Rychtář. *Game-Theoretical Models in Biology*. Chapman and Hall/CRC, 2013.
- [21] Karan Pattni, Mark Broom, Jan Rychtář, and Lara J Silvers. Evolutionary graph theory revisited: when is an evolutionary process equivalent to the moran process? *Proceedings of the Royal Society A: Mathematical, Physical and Engineering Sciences*, 471(2182):20150334, 2015.

- [22] M. Möller, L. Hindersin, and A. Traulsen. Exploring and mapping the universe of evolutionary graphs identifies structural properties affecting fixation probability and time. *Communications Biology*, 2(137), 2019.
- [23] Roberto Livi and Paolo Politi. *Nonequilibrium statistical physics: a modern perspective*. Cambridge University Press, 2017.
- [24] Simon A Levin and Robert T Paine. Disturbance, patch formation, and community structure. *Proceedings of the National Academy of Sciences*, 71(7):2744–2747, 1974.
- [25] Robert T Paine and Simon A Levin. Intertidal landscapes: disturbance and the dynamics of pattern. *Ecological monographs*, 51(2):145–178, 1981.
- [26] Richard Durrett and Simon A Levin. The importance of being discrete (and spatial). *Theoretical Population Biology*, 46:363–394, Aug 1994.
- [27] T. Antal, S. Redner, and V. Sood. Evolutionary dynamics on degree-heterogeneous graphs. *Physical Review Letters*, 96(18):188104, 2006.
- [28] Ben Adlam, Krishnendu Chatterjee, and Martin A. Nowak. Amplifiers of selection. *Proceedings of the Royal Society A*, 471(2181):20150114, 2015.
- [29] W. J. Ewens. *Mathematical Population Genetics. I. Theoretical Introduction*. Springer, New York, 2004.
- [30] A. Traulsen and C. Hauert. Stochastic evolutionary game dynamics. In Heinz Georg Schuster, editor, *Reviews of Nonlinear Dynamics and Complexity*, volume II, pages 25–61. Wiley-VCH, Weinheim, 2009.
- [31] M. Kimura. On the probability of fixation of mutant genes in a population. *Genetics*, 47:713–719, 1962.
- [32] David M McCandlish, Charles L Epstein, and Joshua B Plotkin. Formal properties of the probability of fixation: identities, inequalities and approximations. *Theoretical population biology*, 99:98–113, 2015.
- [33] Josep Díaz, Leslie Ann Goldberg, George B. Mertzios, David Richerby, Maria Serna, and Paul G. Spirakis. On the fixation probability of

- superstars. *Proceedings of the Royal Society A*, 469(2156):20120193, 2013.
- [34] A. Jamieson-Lane and C. Hauert. Fixation probabilities on superstars, revisited and revised. *Journal of Theoretical Biology*, 382:44–56, 2015.
  - [35] Andreas Galanis, Andreas Göbel, Leslie Ann Goldberg, John Lapinskas, and David Richerby. Amplifiers for the moran process. *Journal of the ACM (JACM)*, 64(1):1–90, 2017.
  - [36] Andreas Pavlogiannis, Josef Tkadlec, Krishnendu Chatterjee, and Martin A. Nowak. Construction of arbitrarily strong amplifiers of natural selection using evolutionary graph theory. *Communications Biology*, 1(78), 2018.
  - [37] L. Hindersin and A. Traulsen. Most undirected random graphs are amplifiers of selection for Birth-death dynamics, but suppressors of selection for death-Birth dynamics. *PLoS Computational Biology*, 11:e1004437, 2015.
  - [38] M. Kimura. Evolutionary rate at the molecular level. *Nature*, 217:624–626, 1968.
  - [39] M. Frean, P. Rainey, and A. Traulsen. The effect of population structure on the rate of evolution. *Proceedings of the Royal Society B*, 280:20130211, 2013.
  - [40] Josef Tkadlec, Andreas Pavlogiannis, Krishnendu Chatterjee, and Martin A Nowak. Population structure determines the tradeoff between fixation probability and fixation time. *Communications biology*, 2(1):1–8, 2019.
  - [41] Josef Tkadlec, Andreas Pavlogiannis, Krishnendu Chatterjee, and Martin A Nowak. Fast and strong amplifiers of natural selection. *Nature Communications*, 12:4009, 2021.
  - [42] H. Ohtsuki, C. Hauert, E. Lieberman, and M. A. Nowak. A simple rule for the evolution of cooperation on graphs. *Nature*, 441:502–505, 2006.
  - [43] Benjamin Allen, Gabor Lipper, Yu-Ting Chen, Babak Fotouhi, Martin A Nowak, and Shing-Tung Yau. Evolutionary dynamics on any population structure. *Nature*, 544:227–230, 2017.



- [44] H. Ohtsuki and M. A. Nowak. The replicator equation on graphs. *Journal of Theoretical Biology*, 243:86–97, 2006.
- [45] Alex McAvoy, Andrew Rao, and Christoph Hauert. Intriguing effects of selection intensity on the evolution of prosocial behaviors. *PLoS Computational Biology*, 17(11):e1009611, 2021.
- [46] Qi Su, Benjamin Allen, and Joshua B Plotkin. Evolution of cooperation with asymmetric social interactions. *Proceedings of the National Academy of Sciences*, 119(1):e2113468118, 2022.
- [47] M. A. Nowak, C. E. Tarnita, and T. Antal. Evolutionary dynamics in structured populations. *Philosophical Transactions of the Royal Society B*, 365:19–30, 2010.
- [48] Sedigheh Yagoobi, Hosna Yousefi, and Keivan Aghababaei Samani. Mutation-selection stationary distribution in structured populations. *Physical Review E*, 98(4):042301, 2018.
- [49] M. Broom and J. Rychtář. An analysis of the fixation probability of a mutant on special classes of non-directed graphs. *Proceedings of the Royal Society A*, 464:2609–2627, 2008.
- [50] C. Hadjichrysanthou, Mark Broom, and J. Rychtář. Evolutionary games on star graphs under various updating rules. *Dynamic Games and Applications*, 1(3):386–407, 2011.
- [51] T. Monk, P. Green, and Paulin M. Martingales and fixation probabilities of evolutionary graphs. *Proceedings of the Royal Society A*, 470:20130730, 2014.
- [52] M. Broom, J. Rychtář, and B. T. Stadler. Evolutionary dynamics on graphs – the effect of graph structure and initial placement on mutant spread. *Journal of Statistical Theory and Practice*, 5(3):369–381, 2011.
- [53] Nikhil Sharma and Arne Traulsen. Suppressors of fixation can increase average fitness beyond amplifiers of selection. *Proceedings of the National Academy of Sciences*, 119(37):e2205424119, 2022.
- [54] Josef Tkadlec, Andreas Pavlogiannis, Krishnendu Chatterjee, and Martin A Nowak. Limits on amplifiers of natural selection under death-birth updating. *PLoS computational biology*, 16(1):e1007494, 2020.

- [55] Manja Saebelfeld, Suman G Das, Arno Hagenbeek, Joachim Krug, and J Arjan GM de Visser. Stochastic establishment of  $\beta$ -lactam-resistant escherichia coli mutants reveals conditions for collective resistance. *Proceedings of the Royal Society B*, 289(1974):20212486, 2022.
- [56] Z Patwa and Lindi M Wahl. The fixation probability of beneficial mutations. *Journal of The Royal Society Interface*, 5:1279–1289, 2008.
- [57] H Uecker and J Hermisson. On the Fixation Process of a Beneficial Mutation in a Variable Environment. *Genetics*, 188(4):915–930, 2011.
- [58] W. J. Ewens. *Mathematical Population Genetics*. Springer, Berlin, 1979.
- [59] T. Antal and István Scheuring. Fixation of strategies for an evolutionary game in finite populations. *Bulletin of Mathematical Biology*, 68:1923–1944, 2006.
- [60] Peter Czuppon and Arne Traulsen. Understanding evolutionary and ecological dynamics using a continuum limit. *Ecology and Evolution*, 11:5857–5873, 2021.
- [61] N.S. Goel and N. Richter-Dyn. *Stochastic Models in Biology*. Academic Press, New York, 1974.
- [62] Su-Chan Park, Damien Simon, and Joachim Krug. The speed of evolution in large asexual populations. *Journal of Statistical Physics*, 138(1):381–410, 2010.
- [63] Naoki Masuda and Hisashi Ohtsuki. Evolutionary dynamics and fixation probabilities in directed networks. *New Journal of Physics*, 11(033012), 2009.
- [64] Sedigheh Yagoobi, Nikhil Sharma, and Arne Traulsen. Categorizing update mechanisms for graph-structured metapopulations. *Journal of the Royal Society Interface*, 20(200):20220769, 2023.
- [65] K. Kaveh, N. L. Komarova, and M. Kohandel. The duality of spatial death-birth and birth-death processes and limitations of the isothermal theorem. *Royal Society Open Science*, 2(140465), 2015.

- [66] Alex McAvoy, Ben Adlam, Benjamin Allen, and Martin A Nowak. Stationary frequencies and mixing times for neutral drift processes with spatial structure. *Proceedings of the Royal Society A: Mathematical, Physical and Engineering Sciences*, 474(2218):20180238, 2018.
- [67] Bertrand Ottino-Loffler, Jacob G Scott, and Steven H Strogatz. Evolutionary dynamics of incubation periods. *ELife*, 6:e30212, 2017.
- [68] Natalia L Komarova, Anirvan Sengupta, and Martin A Nowak. Mutation-selection networks of cancer initiation: tumor suppressor genes and chromosomal instability. *J Theor Biol*, 223(4):433–450, Aug 2003.
- [69] P. Erdős and A. Rényi. On the evolution of random graphs. *Publications of the Mathematical Institute of the Hungarian Academy of Sciences, Series B*, 5:17–61, 1960.
- [70] E. N. Gilbert. Random graphs. *Annals of Mathematical Statistics*, 30(4):1141–1144, 1959.
- [71] Benjamin Allen, Christine Sample, Yulia Dementieva, Ruben C. Medeiros, Christopher Paoletti, and Martin A. Nowak. The molecular clock of neutral evolution can be accelerated or slowed by asymmetric spatial structure. *PLoS Computational Biology*, 11(2):e1004108, 2015.
- [72] David M McCandlish, Charles L Epstein, and Joshua B Plotkin. The inevitability of unconditionally deleterious substitutions during adaptation. *Evolution*, 68(5):1351–1364, 2014.
- [73] Sergey Kryazhimskiy, Gašper Tkačik, and Joshua B Plotkin. The dynamics of adaptation on correlated fitness landscapes. *Proceedings of the National Academy of Sciences*, 106(44):18638–18643, 2009.
- [74] David M McCandlish and Arlin Stoltzfus. Modeling evolution using the probability of fixation: history and implications. *The Quarterly review of biology*, 89(3):225–252, 2014.
- [75] N. G. van Kampen. *Stochastic Processes in Physics and Chemistry*. Elsevier, Amsterdam, 2 edition, 1997.

- [76] C. W. Gardiner. *Handbook of Stochastic Methods*. Springer, NY, Berlin, third edition, 2004.
- [77] Michael Manhart, Allan Haldane, and Alexandre V Morozov. A universal scaling law determines time reversibility and steady state of substitutions under selection. *Theoretical population biology*, 82(1):66–76, 2012.
- [78] John FC Kingman. A simple model for the balance between selection and mutation. *Journal of Applied Probability*, 15(1):1–12, 1978.
- [79] G. Sella and A. E. Hirsh. The application of statistical physics to evolutionary biology. *Proceedings of the National Academy of Sciences USA*, 102(27):9541–9546, 2005.
- [80] Yoh Iwasa. Free fitness that always increases in evolution. *Journal of Theoretical Biology*, 135(3):265–281, 1988.
- [81] Johannes Berg, Stana Willmann, and Michael Lässig. Adaptive evolution of transcription factor binding sites. *BMC evolutionary biology*, 4(1):1–12, 2004.
- [82] Nicholas H Barton and JB2973150 Coe. On the application of statistical physics to evolutionary biology. *Journal of theoretical biology*, 259(2):317–324, 2009.
- [83] David M McCandlish. Long-term evolution on complex fitness landscapes when mutation is weak. *Heredity*, 121(5):449–465, 2018.
- [84] Brian Charlesworth. Effective population size and patterns of molecular evolution and variation. *Nature Reviews Genetics*, 10(3):195–205, 2009. 10.1038/nrg2526.
- [85] S. Giaimo, J. Arranz, and A. Traulsen. Invasion and effective size of graph-structured populations. *PLoS Computational Biology*, 14:e1006559, 2018.
- [86] Benjamin Allen, Christine Sample, Robert Jencks, James Withers, Patricia Steinhagen, Lori Brizuela, Joshua Kolodny, Darren Parke, Gabor Lippner, and Yulia A Dementieva. Transient amplifiers of selection and reducers of fixation for death-birth updating on graphs. *PLoS computational biology*, 16(1):e1007529, 2020.

- [87] Benjamin Allen, Christine Sample, Patricia Steinhagen, Julia Shapiro, Matthew King, Timothy Hedspeth, and Megan Goncalves. Fixation probabilities in graph-structured populations under weak selection. *PLoS computational biology*, 17(2):e1008695, 2021.
- [88] Partha Pratim Chakraborty, Louis R Nemzer, and Rees Kassen. Experimental evidence that network topology can accelerate the spread of beneficial mutations. *Evolution Letters*, page grad047, 2023.
- [89] Sedigheh Yagoobi and Arne Traulsen. Fixation probabilities in network structured meta-populations. *Scientific Reports*, 11(1):1–9, 2021.
- [90] Loïc Marrec, Irene Lamberti, and Anne-Florence Bitbol. Toward a universal model for spatially structured populations. *Physical Review Letters*, 127(21):218102, 2021.
- [91] L. Hindersin, M. Moeller, A. Traulsen, and B. Bauer. Exact numerical calculation of fixation probability and time on graphs. *BioSystems*, 150:87–91, 2016.
- [92] Charles Miller Grinstead and James Laurie Snell. *Introduction to probability*. American Mathematical Soc., Providence, RI, 2012.
- [93] L. Hindersin and A. Traulsen. Counterintuitive properties of the fixation time in network-structured populations. *Journal of The Royal Society Interface*, 11:20140606, 2014.
- [94] Frank P Kelly. *Reversibility and stochastic networks*. Cambridge University Press, 2011.
- [95] S. P. Otto and T. Day. *A Biologist’s Guide to Mathematical Modeling in Ecology and Evolution*. Princeton University Press, Princeton, New Jersey, 2007.
- [96] Nikhil Sharma, Sedigheh Yagoobi, and Arne Traulsen. Self-loops in evolutionary graph theory: Friends or foes? *PLoS Computational Biology*, 19(9):e1011387, 09 2023.
- [97] B. Adlam and M. A. Nowak. Universality of fixation probabilities in randomly structured populations. *Scientific Reports*, 4(6692), 2014.

- [98] Andreas Pavlogiannis, Josef Tkadlec, Krishnendu Chatterjee, and Martin A. Nowak. Amplification on undirected population structures: Comets beat stars. *Scientific Reports*, 7(82), 2017.
- [99] T. Monk. Martingales and the fixation probability of high-dimensional evolutionary graphs. *Journal of Theoretical Biology*, 451:10–18, 2018.
- [100] Alex McAvoy and Benjamin Allen. Fixation probabilities in evolutionary dynamics under weak selection. *Journal of Mathematical Biology*, 82(3):1–41, 2021.
- [101] Yang Ping Kuo, Cesar Nombela-Arrieta, and Oana Carja. A theory of evolutionary dynamics on any complex spatial structure. *bioRxiv*, 2021.
- [102] D.M. Weinreich, N.F. Delaney, M.A. DePristo, and D.L. Hartl. Darwinian evolution can follow only very few mutational paths to fitter proteins. *Science*, 312:111–114, 2006.
- [103] Kristina Crona, Devin Greene, and Miriam Barlow. The peaks and geometry of fitness landscapes. *Journal of theoretical biology*, 317:1–10, 2013.
- [104] J Arjan Gm De Visser and Joachim Krug. Empirical fitness landscapes and the predictability of evolution. *Nature Reviews Genetics*, 15(7):480–490, 2014.
- [105] Y. Iwasa, F. Michor, and M. A. Nowak. Stochastic tunnels in evolutionary dynamics. *Genetics*, 166:1571–1579, 2004.
- [106] C. S. Gokhale, Y. Iwasa, M. A. Nowak, and A. Traulsen. The pace of evolution across fitness valleys. *Journal of Theoretical Biology*, 259:613–620, 2009.
- [107] Daniel B Weissman, Michael M Desai, Daniel S Fisher, and M. W Feldman. The rate at which asexual populations cross fitness valleys. *Theoretical Population Biology*, 75(4):286–300, 2009.
- [108] Natalia L Komarova, Leili Shahriyari, and Dominik Wodarz. Complex role of space in the crossing of fitness valleys by asexual populations. *Journal of The Royal Society Interface*, 11(95):20140014, Jun 2014.

- [109] D. M. Weinreich and L. Chao. Rapid evolutionary escape by large populations from local fitness peaks is likely in nature. *Evolution*, 59:1175–1182, 2005.
- [110] M. Kimura. The role of compensatory neutral mutations in molecular evolution. *Journal of Genetics*, 64:7–19, 1985.
- [111] Wolfgang Stephan. The rate of compensatory evolution. *Genetics*, 144(1):419–426, 1996.
- [112] M. A. Nowak. Five rules for the evolution of cooperation. *Science*, 314:1560–1563, 2006.
- [113] Christoph Hauert and Michael Doebeli. Spatial social dilemmas promote diversity. *Proceedings of the National Academy of Sciences*, 118(42):e2105252118, 2021.
- [114] Bahram Houchmandzadeh and Marcel Vallade. The fixation probability of a beneficial mutation in a geographically structured population. *New Journal of Physics*, 13(7):073020, 2011.
- [115] Alia Abbara and Anne-Florence Bitbol. Frequent asymmetric migrations suppress natural selection in spatially structured populations. *bioRxiv*, pages 2023–06, 2023.
- [116] K. B. Athreya and P. E. Ney. *Branching Processes*. Springer, Berlin, 1972.
- [117] Hildegard Uecker, Sarah P. Otto, and Joachim Hermisson. Evolutionary rescue in structured populations. *The American Naturalist*, 183(1):E17 – E35, jan 2014.
- [118] Hye Jin Park, Christian Hilbe, Martin A Nowak, Beom Jun Kim, and Hyeong-Chai Jeong. Vacancies in growing habitats promote the evolution of cooperation. *Journal of Theoretical Biology*, page 111629, 2023.
- [119] P J Gerrish and R E Lenski. The fate of competing beneficial mutations in an asexual population. *Genetica*, 102-103:127–144, 1998.

- [120] S.-C. Park and J. Krug. Clonal interference in large populations. *Proceedings of the National Academy of Sciences USA*, 104(46):18135–18140, 2007.



# Nikhil Sharma

---

## Personal data

Date of birth    October 30th, 1996  
Place of birth    Una, Himachal Pradesh, India  
Nationality    Indian

---

## Education and scientific career

09/2020–    **Doctoral researcher**, Department of Theoretical Biology, Max-Planck Institute for Evolutionary Biology, Plön, Germany.  
Supervisor: Prof. Arne Traulsen

03/2020–    **Research Intern**, Eco-Evolutionary dynamics research group, Max-Planck Institute  
08/2020    for Evolutionary Biology, Plön, Germany.  
Internship supervisor: Prof. Chaitanya Gokhale

10/2018–    **Teaching assistant**, Institute for Theoretical Physics, University of Cologne.  
10/2019

10/2017–    **M.Sc. Physics**, Bonn- Cologne Graduate school of Physics and Astronomy, University  
12/2019    of Cologne, Germany.  
Thesis supervisor: Prof. Sebastian Diehl

08/2014–    **B.Sc. Physics**, St. Stephen's College, University of Delhi, India.  
05/2017

---

## Publications

- [1] N. Sharma and A. Traulsen, "Suppressors of fixation can increase average fitness beyond amplifiers of selection," *Proceedings of the National Academy of Sciences*, vol. 119, no. 37, p. e2205424119, 2022.
- [2] S. Yagoobi, N. Sharma, and A. Traulsen, "Categorizing update mechanisms for graph-structured metapopulations," *Journal of the Royal Society Interface*, vol. 20, no. 200, p. 20220769, 2023.
- [3] C. S. Gokhale and N. Sharma, "Optimizing crop rotations via Parrondo's paradox for sustainable agriculture," *Royal Society Open Science*, vol. 10, no. 5, p. 221401, 2023.
- [4] N. Sharma, S. Yagoobi, and A. Traulsen, "Self-loops in evolutionary graph theory: Friends or foes?," *PLoS Computational Biology*, vol. 19, pp. 1–32, 09 2023.